Understanding past and future changes in northern Fennoscandian snow cover.

Rebecca Marianne Vignols
Newnham College

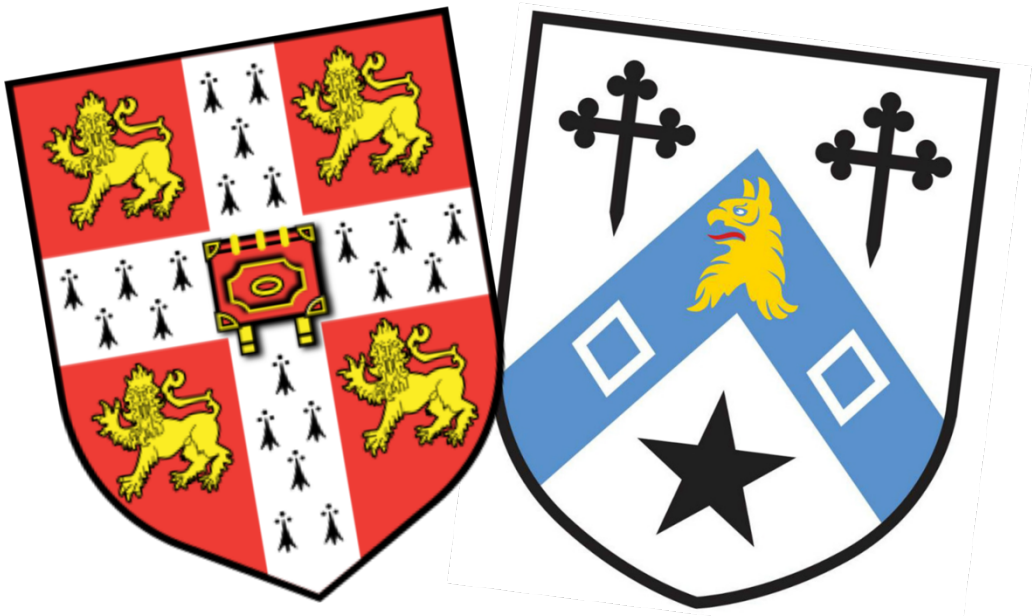

British Antarctic Survey
NATURAL ENVIRONMENT RESEARCH COUNCIL

November 2019

This thesis is submitted for the degree of Doctor of Philosophy

Preface

This dissertation is the result of my own work and includes nothing which is the outcome of work done in collaboration except as declared in the Preface and specified in the text.

It is not substantially the same as any that I have submitted, or, is being concurrently submitted for a degree or diploma or other qualification at the University of Cambridge or any other University or similar institution except as declared in the Preface and specified in the text. I further state that no substantial part of my dissertation has already been submitted, or, is being concurrently submitted for any such degree, diploma or other qualification at the University of Cambridge or any other University or similar institution except as declared in the Preface and specified in the text.

It does not exceed the prescribed page limit for the relevant Degree Committee.

Understanding past and future changes in northern Fennoscandian snow cover.

Rebecca Marianne Vignols

Abstract

In this project, a combination of field measurements, remote sensing data and regional climate model outputs were used to study recent and projected future changes in Northern Fennoscandian snow cover. The research questions considered in this thesis are: What are the uncertainties in remote sensing and climate modelling datasets used in snow studies? How has snow cover been changing since the 1960s and how will it change over the next century, at a regional level over Northern Fennoscandia?

Field measurements were made over two field seasons in the Khibiny Mountains in Arctic Russia. This ground data was used to gain an understanding of snow cover behaviour in the Western Mountain Regions (WMR) of the Kola Peninsula and to ground-truth 500 m resolution satellite data (MODIS: Moderate Resolution Imaging Spectroradiometer) snow products. The overall root mean square error (RMSE) for both MODIS instruments was found to be less than 10 %. The ground-truthed MODIS snow product was then used with station data to analyse past changes in snow cover in the WMR over the past 16 years. Though there is high inter-annual and spatial variability in the long-term snow cover trends in the WMR, overall, the duration of the snow cover season has increased at lower elevations and decreased at higher elevations.

Field measurements and MODIS data were used in the sensitivity analysis of the Weather Research and Forecasting (WRF) regional climate model. Twelve experiments with different physics parameterisations were run over the first field season, and a statistical scores evaluation was undertaken to determine the optimised parameter setup for modelling snow in the region. Three CMIP5 (Coupled Model Intercomparison Project 5) models were used to force WRF in historical (1990 - 1999) and two future climate (2090 - 2099) emission scenarios over Northern Fennoscandia. Outputs from the historical runs were compared to data from 10 stations across Northern Fennoscandia in order to further validate WRF. WRF makes excellent temperature estimates, with a mean bias in the yearly mean temperature outputs of the runs of -1.89 °C. The precipitation outputs are less accurate with values often higher than observations, especially for extreme precipitation events (CMIP5 ‘ensemble’ mean RMSE of 24.0 mm for 20 + mm precipitation events).

Finally, the future runs were compared to historical runs to study projected future changes in temperature, precipitation, snowfall and snow cover. The three models give a range of different future predictions for regional climate change over Northern Fennoscandia. However, all CMIP5 models agree that in both emission scenarios mean snow cover duration will be lower over 2090 to 2099 than it was between 1990 and 1999. Importantly, changes in temperature, precipitation and snowfall are all higher, and snow cover is most impacted, in the higher emission scenario. RCP 8.5 consistently sees a higher decrease in solid precipitation than RCP 4.5 at all stations, and for all models and seasons, for example. Thus, aiming to reduce greenhouse gas emissions is still crucial to reducing anthropogenic impact on Northern Fennoscandian snow.

Acknowledgements

I would like to thank my supervisors, the Gareths, for their help during my PhD; Tony Phillips for his guidance with some of the more complex python coding; Dan Bannister for his support when I started using WRF. Thank you also to Yulia Zaika and Olga Tutubalina from Moscow State University for their help organising fieldwork, providing data, and overall enabling me to have the pleasure of studying a remote Russian region; and to Ilona Blinova for providing snow data and giving me a tour of the Polar-Alpine Botanical Garden institute. I'm also very grateful to Liz Harper for her continued support throughout my entire higher education and being an excellent mentor during these past four years. Finally, I would like to thank my amazing parents, sister Clarisse, and partner Harriet, for their unwavering support and believing in me the most.

Table of contents

Chapter 1
Introduction

1.1 Overview

The overall aim of my dissertation is to study changes in snow cover over Northern Fennoscandia (Fig. 1.1). Both past and future snow cover in the region are investigated by using a combination of field-collected data, meteorological station data, remote sensing and climate model outputs.

The main research questions I aim to answer in my dissertation are:

1. What are the uncertainties in remote sensing and climate modelling datasets used in snow studies?
2. How has snow cover been changing since the 1960s and how will it change over the next century, at a regional level over Northern Fennoscandia?

Figure 1.1: Map showing the position of Northern Fennoscandia (outlined in red).

1.2 Context and rationale for the project

There is no doubt that the Earth's climate is changing (e.g. Field et al., 2014). Temperatures are rising fastest over the Arctic (e.g. Overland et al., 2014; Serreze and Francis, 2006), and as a result snow cover is changing over these higher latitudes (e.g. Armstrong and Brodzick, 2011; Kitaev et al., 2010).

Northern Fennoscandia (which includes Northern Finland, Norway, Russia and Sweden) is an Arctic to sub-Arctic region and, as such, is undergoing these major climatic changes (e.g. Dankers and Christensen, 2005; Høgda et al, 2001; Kilpeläinen et al., 2010). Snow cover is extremely important through its impacts on the climate as a whole and on people (e.g. Armstrong and Brun, 2008; Robinson et al., 1993; Storvold et al., 2006). At a regional level, snow cover has a very important role within local communities in Northern Fennoscandia impacting transport, energy, winter tourism and indigenous communities reliant on reindeer herding for example (e.g. Rasmus et al., 2016). As a result, it is crucial to study how snow has been changing and model how it will change over the next century. In this section, some of the gaps in the current literature studying Northern Hemisphere snow cover are detailed and the steps taken in order to address these gaps are specified.

As one of the few mountain ranges in the Kola Peninsula (the Russian part of Northern Fennoscandia), the Khibiny Mountains are a very interesting region in terms of snow cover, but snow studies there are rare, and the great majority are published in Russian (e.g. Glazovskaya, 2000; Vikulina, 2009; Zaika et al., 2013). This is due to the limited access to the region for non-Russian citizens and is also partially a result of the local avalanche service being privately owned, which makes data-sharing more difficult. Having the opportunity to undertake two field seasons there meant that more valuable data could be collected for the analysis of snow in the region, and scientific collaborations were both prolonged (with Moscow State University) and initiated (with the Polar-Alpine Botanical Garden-Institute), permitting data-sharing.

Past studies of snow and climate in the Kola Peninsula have also focussed primarily on using field and station data (e.g. Zaika et al., 2013, Blinova and Chmielewski, 2014; Marshall et al., 2016). Though using these types of datasets is very valuable, combining them with remote sensing data or reanalysis data adds a spatial continuity to the analysis, which broadens the conclusions that can be reached. In my project, I use high-resolution (500 m) remote sensing data over part of the Kola Peninsula in order to study past changes in snow cover within a small mountainous region. Both the development of new field datasets and the use of remote sensing to study trends in snow cover over mountains are important pieces of work. Indeed, Bormann et al. (2018) in their review of work to be done studying snow from space identify both of these as major gaps in snow research.

Bokhorst et al. (2016) identified gaps in the study of changes in Arctic snow cover specifically. One of the needs that they pinpointed is a better understanding of the detailed timing of changes in snow cover, including snow build-up and spring snow melt. In this dissertation, I aim to address this gap by studying the timing (which includes the snow cover start, end and duration) of the snow cover season over the Western Mountains Region (WMR) using remote sensing data from the past two decades and over the entirety of Northern Fennoscandia using regional climate model outputs covering the last decade of the 21st century.

Finally, there is considerable uncertainty in many snow studies, regarding the reliability of datasets used. Recently for example, Mudryk et al. (2017) have demonstrated the limitations of the National Oceanic and Atmospheric Administration (NOAA) climate data record (NCDR) which they find returns anomalous trends in snow cover extent over four months of the year. In this dissertation, a great emphasis is placed on validating the remote sensing dataset and climate model parameterisation used. The validation of the remote sensing dataset used was a particularly valuable contribution to snow research using satellite data, as it tested the effectiveness of a particular remote sensing instrument in a novel region with a lack of openly accessible ground data.

1.3 Thesis organisation

The organisation of this dissertation is as follows. This introductory chapter is followed by a literature review (Chapter 2). As a result of the breadth of the research methods used for this project, I chose not to include a methods chapter, but rather to include a methods section in each data chapter instead. My dissertation contains four data chapters (Chapters 3 to 6). I begin each of these with a short summary of what is included in the chapter and end each one with a 'fit within thesis' section in which I discuss the links between the data chapters and how results from each chapter are used in the next. Each chapter is otherwise divided into a standard publication structure: introduction, methods, results, discussion, conclusions and references. The main findings of my four data chapters are revisited in my conclusions chapter (Chapter 7).

1.4 Chapter aims

In the following paragraphs, the outline of the dissertation is given, and the main aims of each chapter are detailed. Chapter Two constitutes my literature review, the aim of which is to summarise the current understanding of snow research. In this chapter, the importance of studying snow in general and the role snow performs within the climate system are explained. A background review of the three aspects of snow research used in this dissertation is provided: modelling, remote sensing and field measurements, going from the larger scale to the smaller scale. I finish this chapter with a summary of the current understanding of past changes in snow cover over the Northern Hemisphere including over Northern Fennoscandia.

Chapter 3 is the first data chapter. In this chapter, I present the results of two seasons of fieldwork in the Khibiny Mountains, Arctic Russia, which I undertook in the first two years of my PhD. The results presented can be broadly divided into two parts. First, the dataset that I collected in the field is presented, questioning the relationships between different snow parameters, and thus investigating the behaviour of snow in these mountains in Northern Fennoscandia. In the second part of the chapter, the albedo measurements made in the field are used to ground truth the MODerate resolution Imaging Spectroradiometer (MODIS) snow dataset, which is later used in the dissertation. It must be noted that,

due to the limited time spent in the field, very little error analysis was undertaken on the field measurements themselves. The main aims of this chapter are to present the dataset collected, to interrogate the data to gain a better understanding of snow in the region, and to test the reliability of the data used later in the dissertation to study past changes in regional snow cover.

The aim of Chapter 4 is to study past changes in snow cover over the region surrounding the Khibiny Mountains in the Kola Peninsula. This new region was defined as part of this work to include all low mountain ranges near the Khibiny Mountains and to include the surrounding plains; it is referred to as the WMR. In this chapter, recent changes in the timing and duration of the snow cover season are investigated for the first time in the WMR using MODIS data, as well as station data. In addition, I try to reconcile opposing trends in the literature concerning snow cover season duration in the Kola Peninsula.

In Chapter 5, I use the Weather Research and Forecasting (WRF) regional climate model. Parameter optimisation can be undertaken with this model to meet the requirements of the analysis or study area. The research question I aimed to answer was: How well can WRF model the climate in Northern Fennoscandia and, in particular, the snow cover extent and duration? In the first half of this chapter, I undertake a sensitivity analysis of WRF, running 12 experiments to find the optimised parameterisation for the five most important physics options. The experimentally-found optimised physics setup for WRF over the WMR is then used for all following climate model runs. In the second half of this chapter, historical (1990 - 1999) runs are performed over Northern Fennoscandia and their temperature and precipitation outputs are validated using data from ten meteorological stations distributed across the study region.

Chapter 6 is the final data chapter of this dissertation. For this chapter, I ran WRF forced by data from three different CMIP5 (Coupled Model Intercomparison Project) models over the final decade of the 21st century. This dynamical downscaling process is explained in both chapters 2 and 5. The regional climate model outputs are analysed over Northern Fennoscandia for this 2090 - 2099 period. The research question I look to answer in this chapter is: What are the likely changes in snow cover over Northern Fennoscandia by the end of the 21st century?

Finally, in Chapter 7, my dissertation aims are revisited, addressing to what extent I have met them. I also summarise the main conclusions of my dissertation and consider future research directions that could be undertaken to expand on my work.

1.5 References

Armstrong, R.L. and Brodzik, M.J., 2001. Recent Northern Hemisphere snow extent: A comparison of data derived from visible and microwave satellite sensors. Geophysical Research Letters, 28(19), pp.3673-3676. https://doi.org/10.1029/2000GL012556

Armstrong, R.L. and Brun, E. eds., 2008. Snow and climate: physical processes, surface energy exchange and modeling. Cambridge University Press.

Blinova, I. and Chmielewski, F.M., 2014. Climatic warming above the Arctic Circle: are there trends in timing and length of the thermal growing season in Murmansk Region (Russia) between 1951 and 2012? International journal of biometeorology, 59(6), pp.693-705. https://doi.org/10.1007/s00484-014-0880-y

Bokhorst, S., Pedersen, S.H., Brucker, L., Anisimov, O., Bjerke, J.W., Brown, R.D., Ehrich, D., Essery, R.L., Heilig, A., Ingvander, S. and Johansson, C., 2016. Changing Arctic snow cover: A review of recent developments and assessment of future needs for observations, modelling, and impacts. Ambio, 45(5), pp.516-537. https://doi.org/10.1007/s13280-016-0770-0

Bormann, K.J., Brown, R.D., Derksen, C. and Painter, T.H., 2018. Estimating snow-cover trends from space. *Nature Climate Change*, *8*(11), p.924. https://doi.org/10.1038/s41558-018-0318-3

Dankers, R. and Christensen, O.B., 2005. Climate change impact on snow coverage, evaporation and river discharge in the sub-arctic Tana Basin, Northern Fennoscandia. Climatic Change, 69(2-3), pp.367-392. https://doi.org/10.1007/s10584-005-2533-y

Field, C.B., Barros, V.R., Dokken, D.J., Mach, K.J., Mastrandrea, M.D., Bilir, T.E., Chatterjee, M., Ebi, K.L., Estrada, Y.O., Genova, R.C. and Girma, B., 2014. Climate Change 2014: Impacts, Adaptation, and Vulnerability. Part A: Global and Sectoral Aspects. Contribution of Working Group II to the Fifth Assessment Report of the Intergovernmental Panel on Climate Change, CB Field and others (eds.), Cambridge, Cambridge University Press.

Glazovskaya T.G., 2000. Possible changes in snow and avalanche activity due to projected global warming. MGI materials of glaciological research, Iss. No. 88, pp. 70-73. (in Russian)

Høgda, K.A., Karlsen, S.R. and Solheim, I., 2001. Climatic change impact on growing season in Fennoscandia studied by a time series of NOAA AVHRR NDVI data. In IGARSS 2001. Scanning the Present and Resolving the Future. Proceedings. IEEE 2001 International Geoscience and Remote Sensing Symposium (Cat. No. 01CH37217) (Vol. 3, pp. 1338-1340). IEEE. https://doi.org/10.1109/IGARSS.2001.976837

Kilpeläinen, A., Gregow, H., Strandman, H., Kellomäki, S., Venäläinen, A. and Peltola, H., 2010. Impacts of climate change on the risk of snow-induced forest damage in Finland. Climatic Change, 99(1-2), pp.193-209. https://doi.org/10.1007/s10584-009-9655-6

Kitaev, L., Førland, E., Razuvaev, V., Tveito, O.E. and Krueger, O., 2005. Distribution of snow cover over Northern Eurasia. Hydrology Research, 36(4-5), pp.311-319. https://doi.org/10.2166/nh.2005.0024

Marshall, G.J., Vignols, R.M. and Rees, W.G., 2016. Climate change in the Kola Peninsula, Arctic Russia, during the last 50 years from meteorological observations. Journal of Climate, 29(18), pp.6823-6840. https://doi.org/10.1175/JCLI-D-16-0179.1

Mudryk, L.R., Kushner, P.J., Derksen, C. and Thackeray, C., 2017. Snow cover response to temperature in observational and climate model ensembles. Geophysical Research Letters, 44(2), pp.919-926. https://doi.org/10.1002/2016GL071789

Overland, J.E., Wang, M., Walsh, J.E. and Stroeve, J.C., 2014. Future Arctic climate changes: Adaptation and mitigation time scales. Earth's Future, 2(2), pp.68-74. https://doi.org/10.1002/2013EF000162

Rasmus, S., Kivinen, S., Bavay, M. and Heiskanen, J., 2016. Local and regional variability in snow conditions in northern Finland: A reindeer herding perspective. Ambio, 45(4), pp.398-414. https://doi.org/10.1007/s13280-015-0762-5

Robinson, D.A., Dewey, K.F. and Heim Jr, R.R., 1993. Global snow cover monitoring: An update. Bulletin of the American Meteorological Society, 74(9), pp.1689-1696. https://doi.org/10.1175/1520-0477(1993)074<1689:GSCMAU>2.0.CO;2

Serreze, M.C. and Francis, J.A., 2006. The Arctic amplification debate. Climatic change, 76(3-4), pp.241-264.

Storvold, R., Malnes, E., Larsen, Y., Høgda, K.A., Hamran, S.E., Mueller, K. and Langley, K.A., 2006. SAR remote sensing of snow parameters in norwegian areas—Current status and future perspective. Journal of Electromagnetic Waves and Applications, 20(13), pp.1751-1759.

Vikulina M.A., 2009. Assessment of avalanche activity, hazard and risk (with the Khibiny Mountains as an example). In Glaciology in the Beginning of the 21st Century (Proceedings of the International Scientific Conference). Moscow State University Publication: ed., University Book, p.260. (in Russian)

Zaika Yu.V., Vikulina M.A., Chernous P.A., 2013. Long-term dynamics of nival processes in the Khibiny. (in Russian)

Chapter 2
Literature Review

2.1 Why study snow?

Snow is one of the most important variables on the Earth's surface for many reasons. The presence or absence of snow impacts human societies on multiple levels. Snow cover also has a large influence on physical, chemical and biological processes (Gray and Prowse, 1993), including on the Earth's climate, vegetation, atmosphere and oceans.

2.1.1 The importance of snow cover on people

Snow cover has a direct impact on human life in many parts of the world. It affects hydrology, engineering, farming, travel, recreation, and affects safety through floods and avalanches (Robinson et al., 1993; Tedesco, 2015).

One of the most important impacts of snow on society is through its role in water resources and hydrology. The amount of winter snowfall, timing of snow melt and the fate of this melt water (Gray and Prowse, 1993) all have a large effect on the availability of the world's water resources. More than half of the world's drinking water is provided by rivers, which are sensitive to changes in snow melt (Barnett et al., 2005). As of 2008, it was estimated that over one billion people relied on snow accumulation for water resources worldwide (Armstrong and Brun, 2008). For example, 90 % of the annual water supply in the Colorado Rockies results from snowfall (Singh and Gan, 2000). Additionally, 1.4 billion people rely on water supply from Himalayan rivers, themselves sustained by glacier and seasonal snow melt (Immerzeel et al., 2010). Hydrology also links with the role of snow in engineering. In 2006, 98 % of Norwegian electricity was produced by hydropower and about 50 % of that water comes from melted snow (Storvold et al., 2006). Further engineering and infrastructure impacts include the loading of snow on the roofs of buildings, costs of road clearance and the general vulnerability of human activities (e.g. air travel) as a result of extreme snow events (Kivinen et al., 2017). Additionally, snow plays a role in urban emissions and urban pollution, with fuel consumption in urban areas estimated to increase by 50 % for as little as 5 cm of snowfall (Armstrong and Brun, 2008).

The important role of snow in water management also has an impact on different types of farming. Crop-farming can be affected by both low snowfall years in semi-arid regions where lack of water may lead to crop failure, and high snowfall years in regions with higher water-supply whereby floods may be caused by high snowmelt, thus drowning crops (Armstrong and Brun, 2008). Extreme snow events can also have direct negative impacts on agriculture, with the 2008 snow storm in Southern China for example, which negatively impacted crops, forestry, animal husbandry as well as fisheries (Dawei et al., 2008). In Arctic regions, reindeer herding, a highly important and traditional livelihood, is highly dependent on winter conditions. Difficult snow years with extreme snowfall and snow storm

events have been shown to have long-term negative impacts on reindeer and caribou populations (Langlois et al., 2017), thus influencing the viability of indigenous populations (Rasmus et al., 2016).

Aspects of human recreation and travel are also snow-dependant. Northern economies are reliant on tourism and, similar to reindeer herding, this snow tourism is very vulnerable to extreme winter conditions (Kietäväinen and Tuulentie, 2013). Lack of snow is obviously negative for ski resorts (Jÿlha et al., 2008) and high amounts of snow may hinder travel to and within snowy regions. There are also many risks associated with winter tourism activities caused by snow, such as avalanches in mountainous regions. Snow absence can also cause important hazards with, for example, the higher risk of forest fires associated with low snow years in semi-arid regions (Armstrong and Brun, 2008).

2.1.2 The importance of snow cover on climate

Another way in which snow is extremely important is through its role in the climate system. Snow is one of the fastest changing surface variables on Earth, with the proportion of snow-covered land ranging from 7 to 40 % over a year (Singh and Gan, 2000). Snow is also the largest component of the terrestrial cryosphere by area (e.g. Lemke et al., 2007) and 98 % of seasonal snow is located in the Northern Hemisphere (Armstrong and Brodzik, 2001). Over the Northern Hemisphere in winter, the average maximum terrestrial snow cover is approximately 47×10^6 km^2 (Robinson et al., 1993) of approximately 100×10^6 km^2 land area.

This large seasonal variation combined with the physical characteristics of snow results in snow having a large impact on the Earth's energy balance (e.g. Flanner et al., 2011; Qu and Hall, 2014; Thackeray and Fletcher, 2016). Snow has a high albedo, high emissivity and low thermal conductivity. Importantly, snow's high albedo leads to a feedback loop (e.g. Thackeray and Fletcher, 2016). Indeed, snow reflects radiation back out to space and thus contributes to keeping a cool Earth surface. As the atmosphere warms, snow melts, which means more radiation can be absorbed by the surface. This effect on the Earth's albedo leads to further warming and so more snow melt: this is a positive albedo feedback loop. Snow albedo is the third most important climate feedback after water-vapour and cloud feedbacks (e.g. Bony et al., 2006). This snow-albedo feedback effect is strongest in spring (April and May), as this is when incoming solar radiation is strongest over snow-covered areas (Groisman et al., 1994).

This positive feedback mechanism for climate change, caused by the large contrast between snow-covered and snow-free land, is not the only feedback due to changes in snow cover. Armstrong and Brun (2008) emphasized two other important feedbacks. Firstly, snow has a strong impact on the Earth's energy balance by altering the energy flux between the atmosphere and the material beneath the snow (e.g. Walland and Simmonds, 1997; Fields et al., 2014). A negative feedback is caused by the presence of snow cover, as the land surface temperature becomes limited to 0 °C, in turn limiting the outgoing longwave radiation. This has been shown in observation- (Dewey, 1977) and modelling-based studies (Vavrus, 2007). Secondly, the 'warming – snow cover decrease – increased warming' feedback is overly simplified. Indeed, some cold regions, where snowfall is currently limited by moisture supply

rather than temperature, are expected to undergo increases in snow cover rather than decreases as a result of warming (Armstrong and Brun, 2008).

Seasonal snow has been shown to be responsible for the largest annual and interannual variability in albedo (Armstrong and Brodzik, 2001; Atlaskina et al., 2015; Thackeray and Fletcher, 2016), however, other things like snow age and pollution are also important (e.g. Painter et al., 2010; Dumont et al., 2014; Skiles et al., 2018). The albedo of fresh snow, for example, ranges between 0.9 to 0.95 whereas older snow can have an albedo as low as 0.5 (Wuttke et al., 2006). Hansen and Nazarenko (2004) suggested that as much as 25 % of the warming observed over the Northern Hemisphere between 1880 and 2000 was caused by the presence of soot on snow and ice.

Snow also has very important effects on other components of the cryosphere. Fresh snow has a thermal conductivity of approximately 0.1 $W.m^{-1}K^{-1}$, 10 to 20 times lower than the thermal conductivity of wet soil or ice. With this low thermal conductivity, snow also effectively insulates the underlying soil, thus only near-surface ground freezes and deep water draining can continue uninterrupted (Lynch-Stieglitz, 1994). This means that snow also affects the extent of permafrost (Zhang, 2005; Lawrence and Slater, 2010; Gouttevin et al., 2012). All of these links between snow and climate mean that studying snow cover is crucial for climate modelling and cryosphere-climate feedback studies (Brown and Robinson, 2011).

2.1.3 Importance of snow and vegetation interactions

Making predictions for future changes in the planet's albedo clearly requires an understanding of snow cover, but also an understanding of future temperature, vegetation and precipitation (Atlaskina et al., 2015). For example, Qu and Hall (2014) suggested that uncertainties in vegetation changes may be responsible for the large inter-model spread in CMIP5 in the estimates of the snow-albedo feedback. Indeed, another important aspect of snow are its interactions with vegetation.

Snow affects mountainous ecosystems and plant survival (e.g. Keller et al., 2005). Snowmelt is often the source of water that enables the survival and governs the productivity of vegetation (Fagre et al., 2003; Trujillo et al., 2012). Additionally, the thermal barrier caused by thick snow cover may reduce or even prevent soil frost, thus protecting plants during winter (Vajda et al., 2006). However, too much snow in spring will tend to negatively affect plants by reducing the growing season length.

Conversely, vegetation itself may also have an impact on snow cover (Broxton et al., 2015). From the 1930s to 2010, changes in forest cover explained 72 % and 57 % of the variance of relative changes in snow accumulation and ablation over Northern Europe and America, respectively (Varhola et al., 2010). Tree canopies can intercept significant amounts of falling snow in forested environments. This snow may then sublimate before reaching the snowpack on the ground (Essery et al., 2003; Molotch et al., 2007). In contrast, forests with lower canopy cover (Lundquist et al., 2013) and increased shrub vegetation (Myers-Smith et al., 2011) capture and hold more snow, thus lengthening the snow-covered period and extending the supply of melt-water (Vajda et al., 2006). Arctic “shrubification”, which is the

expansion of shrubs in some Arctic regions (Pearson et al., 2013; Urban et al., 2014), may thus have an important effect on snow distribution.

Another impact of vegetation on snow accumulation patterns is through the interactions of trees and wind (e.g. Winstral et al., 2002). Indeed, as snow is scoured from highly exposed areas, it is deposited in more sheltered areas such as immediately downwind of trees (Broxton et al., 2015). Similarly, changes in vegetation patterns from forest fires or forest harvesting have been shown to influence the spatial variation of snow in northern Finland via winds (Vajda et al., 2006). Snow drifting occurs more on the open tundra from the altered surface roughness and associated increased wind velocity. This increase in drift leads to a 30 cm thinner snowpack and with almost 50 % lower snow water equivalent (SWE) than forest snowpacks (Vajda et al., 2006).

Finally, complex interactions in surface albedo occur where snow and vegetation interact. In areas of short vegetation, light snow can easily submerge the dark plants, thus greatly increasing the albedo of the surface and also affecting surface roughness. However, in areas of dense forest, trees will typically only successfully intercept low amounts of snow, thus retain low albedos even when snow covered (Viterbo and Betts, 1999).

As a result of these complex interactions, models can sometimes struggle to accurately represent snow in regions with different normalized difference vegetation indexes (NDVIs; indicator used to quantify vegetation in remote sensing). Research shows that surface models have issues simulating mid-winter snow ablation in forests (Slater et al., 2001) and snow models perform less consistently in forested areas than in open ones (Essery et al., 2009; Rutter et al., 2009).

2.1.4 Links between snow and atmospheric processes

Snow cover is understood to have considerable effects on the atmosphere. By insulating the underlying surface, snow is able to modify the turbulent transfer of heat and moisture into the atmosphere above (Barry, 2002). Atmospheric thickness is expected to decrease as a result of reduction in air temperature itself caused by the presence of snow on the ground (e.g. Lamb, 1955; Davies, 1994). This results in a feedback loop with the change in atmospheric thickness influencing the steering of cyclones, which itself can modify the occurrence of snowfall (Williams, 1978; Barry, 2002).

Larger-scale links between snow and atmospheric processes have also been demonstrated. Walland and Simmonds (1997) showed a link between snow cover variability in North America and Europe. The authors suggested that this could be due to teleconnections, i.e. when the climate system demonstrates covariance over large distances. Eurasian snow cover extent was shown to modify the downstream planetary wave structure, which in turn impacted the climate over the North Pacific and western North America (Clark and Serreze, 2000). Many, more recent, studies have linked large-scale atmospheric effects with snow cover changes (Bokhorst et al., 2016) and a better understanding of these teleconnections may help elucidate the causes of Arctic Amplification (see Section 2.5.1).

The North Atlantic Oscillation (NAO) and Arctic Oscillation (AO), in particular, have been associated with snow cover changes (e.g. Zhong et al., 2018). The NAO is defined by the difference in

sea-level pressure between the Subtropical (Azores) High and the Icelandic Low. A positive NAO is characterised by below-normal pressure across the high latitudes of the North Atlantic and above-normal heights and pressure over the central North Atlantic, the eastern United States and western Europe. The AO is a climate pattern characterized by circumpolar winds circulating around the Arctic at around 55°N latitude. A ring of stronger than average winds circulates around the North Pole and confines colder air across polar regions in a positive AO. In a negative AO, these colder winds are able to reach further South (NOAA Teleconnections, 2016). Cohen et al. (2007) proposed a relationship between snow cover extent and the AO, whereby increased Eurasian snow cover extent during autumn leads to a negative AO-like response in the following winter through the enhanced upward propagation of planetary waves.

More positive NAO and AO mean the colder circulation patterns do not reach as far south into the Northern Hemisphere; this has been linked with decreases in snow cover extent in March and April (Watanabe and Nitta, 1999; Overland et al., 1999). Brown and Robinson (2011) argued that the start of reductions in snow cover in the 1980s was linked with changes in atmospheric circulation associated with a positive NAO as well as the Scandinavia pattern (semi-permanent ridge of winter high pressure over Scandinavia and Northern Europe). Tedesco and Monaghan (2009) demonstrated that variability in the AO can explain 50 % of the melt onset variability in Europe and 10 % in North America.

The extent of the influence of AO on Eurasian snow cover extent was studied by Yeo et al. (2017). They showed that the AO and Eurasian warming are differently and independently responsible for snow cover extent changes at different times of the year. In January, the correlation coefficient of snow cover extent with AO is 0.57, and 0.07 with the Eurasian warming. And in October, the correlation is 0.20 for the AO, and 0.67 for the warming. Overall, the snow cover extent variability over Europe during winter seems to be primarily related to AO variability.

More recently, negative AO trends have been associated with Arctic winter cooling despite predictions of warming. Cohen et al. (2012) explained that summer and autumn warming led to higher moisture, which in turn has been causing an increase in snow cover. They argued that this has been causing the more negative AO trends, an example of how the AO can influence and be influenced by snow cover.

Another atmospheric anomaly pattern associated with arctic snow cover is the Siberian High. This high-pressure centre is caused by temperature anomalies controlled by snow cover variability in Siberia: an anomalously high snow cover forces increased sea-level pressure (Cohen and Entekhabi, 2001). Marshall et al. (2016) demonstrated that a positive Siberian High results in a colder and drier Kola Peninsula, which is the equivalent of a negative NAO.

Therefore, snow cover is both strongly influenced and strongly influences atmospheric processes through many different climatic teleconnections.

2.1.5 Links between snow and ocean processes

Finally, snow indirectly influences some ocean processes. Snow impacts oceanic processes in coastal zones through its role in freshwater supply (Frei et al., 2012). The freshwater flux caused by melting

snow is particularly important in the Arctic Ocean. As a result, the timing of Arctic snowmelt and the magnitude of the resulting freshwater flux has an impact on biological and thermodynamic processes in this ocean. This in turn can have worldwide impacts through the role of cold freshwater in North Atlantic Deep Water (NADW) formation (Rahmstorf, 2000; Frei et al., 2012). NADW is a crucial driver of the ocean thermohaline circulation, which is key in the transport of nutrients and the storing of carbon in the oceans (e.g. Broecker et al., 1990). Very large freshwater influxes into the northern Atlantic Ocean have been shown to reduce or halt the formation of NADW formation in the past, by significantly decreasing surface water density (Rahmstorf, 2000).

Additionally, snow affects sea-ice through loading (Field et al., 2014). A heavy snow load can push the sea ice surface below sea level which will speed up the transformation from snow to ice. Snow can also slow ice formation through its influences on heat flow through ice (sea-ice but also river and lake ice). The flux of heat through thin ice remains high until the ice reaches a thickness of 30 to 40 cm. The heat flux through thin ice will be greatly reduced with even just a thin layer of snow deposited on top. Therefore, a small amount of snowfall will greatly slow down the rate of ice growth (Armstrong and Brun, 2008). Conversely, snow will retard ice melt in the melt period by slowing down warming, as a large amount of energy is needed to melt ice (Armstrong and Brun, 2008).

For these many reasons, snowfall timing and snow cover persistence are very important. And it is crucial for us to have a good understanding of how snow has been changing over the past decades and how it is likely to change over the next century.

2.2 Modelling of snow

Many different types of model can be used to model snow on the ground. At a basic level, hydrological models can be used to model snow. For example, electricity consumption estimates are dependent on predicted runoff from hydrological models, which relies on predictions of snow onset, snow cover extent, snow wetness and SWE.

Snow models are specialised numerical models that have been developed to represent snowpacks to a high standard. These models simulate snowpacks as homogenous, infinite area layers, which are parallel to the ground surface. These range from simple models, which model the snowpack as a single layer, intermediate models, which include several layers representing different types of snow at different depths, and very detailed, complex, snow-physics models, which deal with a larger number of layers of variable thickness. This accuracy in the latter models is needed in order to simulate the many physical processes at the snow surface and within the snowpack realistically (e.g. Brun et al., 1997). These are very high-resolution models and are not typically used for studies over large regions.

For climate modelling, scientists usually rely on climate models to derive projections of future snow. The simulated response of the climate system to future emission scenarios, derived using climate models, is referred to as a climate projection (IPCC, 2013). Climate models can reproduce basic properties of snow well, such as snow cover extent, depth or SWE (e.g. Wang et al., 2009) and fit these

within the climate system. For this reason, climate models are used to predict future changes in snow cover. In this dissertation, outputs from General Circulation Models are used as input to a Regional Climate Model; therefore, for the rest of this section, I will focus on these two types of climate models.

Future projections are typically made for the four main emission scenarios developed by the IPCC (Intergovernmental Panel on Climate Change); these are called the RCP (Representative Concentration Pathways) scenarios and represent a range of possible future anthropogenic greenhouse gas emission scenarios (van Vuuren et al., 2011). These range between radiative forcings of 2.6 to 8.5 $W.m^{-2}$ by the end of the 21st century. RCP 8.5 is the scenario that follows current emissions most closely (Peters et al., 2012) though, in the Arctic, observed warming trends are already greater than those predicted by climate models forced using this RCP scenario (Overland et al., 2014). In this section, two older emission scenarios are also discussed. These are the A2 and B2 scenarios, used by the IPCC until the Fourth Assessment Report (2007). To simplify, A2 refers to a world with higher population growth and higher emissions than B2 (Nakicenovic and Swart, 2000).

2.2.1 General Circulation Models and the Coupled Model Intercomparison Project

General Circulation Models (GCMs) are advanced numerical models that depict physical processes in the atmosphere, ocean, cryosphere and land surface. GCMs are highly advanced tools, which enable the simulation of global climate with both geographically and physically consistent estimates of climate change. These models are crucial to the scientific community in order to advise policy makers to mitigate and prepare for climate change. GCMs have a coarse horizontal resolution (between 100 and 600 km) and represent climate using a three dimensional grid over the planet. Vertically, GCMs usually include 10 to 20 layers in the atmosphere and up to 30 layers in the oceans (ipcc-data.org). One of the main sources of uncertainty in GCM simulations is a result of mismatched scales. Physical processes that occur at smaller scales cannot be properly represented by these models. These include cloud processes, which play key roles in the climate system. In addition to this, certain feedback mechanisms are also poorly represented in GCMs, such as water vapour and warming, clouds and radiation, ocean circulation and ice and snow albedo (ipcc-data.org).

The Coupled Model Intercomparison Project (CMIP) multimodel ensembles, developed by the IPCC, are collections of different models that are used in combination to make projections in an attempt to simulate the climate system. Indeed, an ensemble is useful in that it enables the questioning of why different models have different outcomes when they are forced in the same way (Taylor et al., 2012). This is explained by climate noise (natural variation in the climate system which has little to no structure) and the differences in model parameterisations and model resolutions. To separate signal from noise, it is possible to run all the members of the ensemble using the same conditions but with different initial conditions. Multiple versions of the CMIP ensemble have been created: CMIP5 is discussed in this chapter and used in this dissertation.

CMIP5 aims to make climate projections on decadal timescales. Taylor et al. (2012) emphasized that correcting these runs for climate drift and bias is very complicated. The authors recommend that

users focus on the following variables in near-term decadal projections, as these have been bias corrected by the modelling groups: near-surface air temperature, surface temperature, precipitation rate, and sea level pressure. CMIP5 models collect 14 variables for land ice and snow (Taylor, 2012) and have been used to make projections of future snow cover (e.g. Brutel-Vuilmet et al., 2013). The grid cells of CMIP5 models range from just under 100 to over 200 km across. These scales make comparison of outputs to observations difficult and are too large for regional studies. The CMIP5 model ensemble and its individual GCMs are nevertheless used for a range of global climate analyses. Some results are presented in section 2.2.4.

2.2.2 Regional Climate Models

Finer spatial resolution (than the scale of hundreds of kilometres of GCMs) is crucial when studying the impact of climate change at a local level. Regional climate models (RCMs) are usually used for these high-resolution simulations, as RCMs are designed to be higher resolution, limited area, counterparts to GCMs (metoffice.gov.uk).

2.2.2.1 Dynamical downscaling

Dynamical downscaling is a method of studying climate change at a higher resolution (Gao et al., 2012). This technique uses GCM outputs to provide the initial and boundary conditions for RCMs, enabling these to project globally consistent high-resolution local climate conditions (Caldwell et al., 2009). Dynamical downscaling is usually preferred to its alternative method, statistical downscaling, as climate is dependent on physical processes with the method chosen, as opposed to statistical correlations, and there is no need for an assumption of climate stationarity (Fowler et al., 2007).

The use of downscaling increases the amount of information that can be gained about regional- and local-scale processes, which can't be captured using the coarse GCM resolutions (Mayer et al., 2015), such as the representation of winds over complex orography (Barstad et al., 2012). A higher resolution is also necessary for climate studies of extreme weather events and their impacts (Gao et al., 2012). Scales of the order of 10 km and lower are needed to study the impacts of extreme precipitation events and their associated floods for example (Mayer et al., 2015). Indeed, scales below 4 km are needed in order to represent convective processes (Weisman et al., 1997). The coarse resolution of GCMs can cause their climate extreme outputs to exhibit large errors, especially in mountain ranges (Lader et al., 2017). Indeed, high resolution topography is needed for accurate climate projections and, as such, dynamical downscaling is particularly useful for regions with complex terrain such as mountainous areas or coastlines (Mayer et al., 2015). Bates et al. (2008), in the IPCC Climate Change and Water report, emphasized that improved modelling resolution through dynamical downscaling is particularly needed in studies looking at the effects of climate change on all aspects of the hydrological cycle, including the cryosphere. Finally, in addition to its use for improved resolution, dynamical downscaling of GCMs using regional climate models can provide outputs, such as wave or storm surge, that would usually not be simulated using GCMs (Marcos et al., 2011; Perez et al., 2014).

2.2.2.2 The Weather Research and Forecasting model

The regional climate model used for the climate projections in this dissertation is the Weather Research and Forecasting model (WRF). WRF is a next-generation mesoscale forecasting model and assimilation system, which was developed by the National Centre for Atmospheric Research (NCAR) and multiple National Oceanic and Atmospheric Administration (NOAA) and U.S. Department of Defence partners. It was created for studying mesoscale precipitation systems to further our understanding and improve the prediction of these (Skamarock et al., 2008). This model has been applied in a wide variety of studies, from "idealized research to operational forecasting, with an emphasis on a horizontal grid in the range of 1-10 km" (Shi et al., 2010, pp2249). It is possible to choose the physics parameterisation of the WRF model and it can thus be finely tuned to best fit the needs of each study. A specialised version of the model, Polar WRF, exists to better model the energy balance over sea-ice at very high latitudes. In this project, 'regular' WRF was used as part of Northern Fennoscandia is sub-Arctic. WRF has successfully been used in many dynamical downscaling studies; some key examples are described here.

Lader et al. (2017) dynamically downscaled the CMIP5 GFDL-CM3 model using WRF with spectral nudging in order to make projections of end-century temperature and precipitation extremes over Alaska. Spectral nudging is a way of feeding data into a model at the initial conditions and during the, usually long, model run, not only at the lateral boundaries but also over the entire domain in order to guarantee that the model develops realistic climate features. Climate extremes were studied at 20 km resolution and across 49 vertical levels. The authors found that cold extremes warm faster than warm extremes and that the greatest change is likely to occur in winter.

Regarding snow, WRF has been used previously to model solid precipitation at a high resolution. Shi et al. (2010) used WRF at cloud-resolving resolution (≈ 1 km) for the first time at high latitudes to study two snowfall events. This very fine scale is needed to reproduce realistically the evolution of cold-cloud systems and requires very high computational resources. The authors looked at whether WRF can properly simulate the cloud systems and snowfall associated with high-latitude snow events occurring in continental environments. They tested this by comparing the model outputs to snowfall datasets from ground, aircraft and satellite high-frequency radiometer measurements and found a reasonably good fit. Wang et al. (2011) studied snowfall events at 15 km resolution over northeast China using WRF and found that the model does a good job at reproducing snowfall and both large-scale and regional circulation anomalies. They concluded that WRF is effective at modelling extreme weather events. Skofronick-Jackson et al. (2013) took this high-resolution snowfall modelling further and studied the threshold of snowfall detection of multiple remote sensing sensors by comparing their retrievals to WRF predictions at 1 km resolution. They found that surface type has a large effect on the threshold of detection of snow, with the lowest detection values being over lakes.

2.2.3 Validating model outputs against observations

It is crucial to validate modelling work by comparing hindcast model outputs to observation datasets. This relies on the premise that, if a model is able to accurately model past or present-day climate

conditions, its results for future climate should be dependable. Additionally, such validation efforts make it possible to identify potential systematic biases within the models (Jacob et al., 2007).

CMIP5 models are consistently tested and validated as part of the broader CMIP ensemble project. By validating them, model outputs and thus climate projections can be improved. Some examples of this broad validation effort follow. Several publications describe the performance of subsets of CMIP5 models for important climate variables (temperature, precipitation, sea-level pressure etc), for example: Nikulin et al. (2010) simulated results for maximum and minimum temperature and precipitation over Europe; Yin et al. (2012) studied precipitation over South America; Brands et al. (2013) analysed several variables in Europe and Africa, and Su et al. (2013) studied precipitation and temperature over the Tibetan Plateau. Perez et al. (2014) validated the skill of CMIP5 GCMs to model sea-level pressure over the north-east Atlantic region, which covers a small part of Scandinavia. The authors tested three aspects of the GCMs: their ability to reproduce synoptic situations, their ability to reproduce the historical inter-annual variability and the consistency of GCM experiments in the 21st century projections. All of these publications specified which CMIP5 model studied best represents the analysed variables over their respective study regions.

Of particular relevance to my work, CMIP5 and other GCM model outputs have also been tested for their accuracy at modelling various aspects of snow cover. Brutel-Vuilmet et al. (2013) used field data (from Brown and Robinson, 2012) and a snowfall dataset (from Weedon et al., 2011) to test the accuracy of the modelling of recent snow cover extent using a CMIP5 model ensemble. The models were found to reproduce observed SCE well, though the 1979 - 2005 reduction in spring snow cover was underestimated in the model outputs, which is a key conclusion from this paper. A similar issue was found in the CMIP3 model simulations (Roesch, 2006). Mudryk et al. (2017) compared the observed (seven observational datasets) and modelled (25 CMIP models) relationship between land surface temperature and snow cover in the 1981 - 2010 interval. The authors concluded that observed snow cover extent sensitivity to temperature estimates over Arctic regions are consistent with simulated values, though modelled sensitivity to temperature is weaker than observed in mid-latitude and alpine regions. They found that the spread in modelled snow cover trends reflects roughly equal contributions from inter-model variability and from natural variability. Comparing modelled and observed snow cover extent trends is made difficult because of this natural variability. Indeed, for the same model and forcing, different trends in temperature and snow cover extent can be driven as a result of the natural variability (Mudryk et al., 2017). One way of tackling this issue is using large model ensembles as these will account for most natural variability. The authors also found that using multiple observation-based estimates of snow cover extent trends improves the agreement with simulated snow cover trends.

Other studies have validated outputs from RCMs, including WRF. One example of RCM validation is Jylhä et al. (2008). The authors applied observational data to examine the model performance of eight RCMs forced by eight GCMs and found that, over northern European land areas, the snow cover duration was reasonably well simulated by the multi-model average. WRF is the RCM used in this dissertation and so only validation studies of this RCM are discussed further. Lader et al.

(2017) tested WRF performance at modelling extreme temperature and precipitation events over Alaska. They found that the ERA-Interim (ERA-I) reanalysis consistently has a lower root mean square error (RMSE) than the model outputs when compared to observations. This is not surprising as ERA-I assimilates station and satellite observations. Nevertheless, as a result of this validation, the authors were able to bias-adjust the WRF outputs used in their subsequent analysis. In other validation studies, WRF is sometimes shown to improve on reanalysis datasets. Jiménez et al. (2012) found that WRF model outputs at 2 km horizontal resolution were able to reproduce the observed spatio-temporal wind variability over the study area (Iberia), showing a clear added value with respect to the initial and boundary data they used (ERA-40).

In the final example, Mayer et al. (2015) undertook a detailed validation study to identify the added value of high-resolution modelling over Scandinavia. The authors used two regional climate models, including WRF, and ran two 8 km resolution experiments (1990 - 2010) using ERA-I as initial conditions and forcing data. Due to the relevance of this publication for this dissertation in terms of the study region and model used, I focus on this publication more. This analysis was done by undertaking a 'perfect boundary experiment' (as defined by Rummukainen, 2010), which relies on the use of global reanalysis datasets as initial and lateral boundary data for RCMs. The authors used gridded observational and station data as ground truth and compared these datasets to daily mean, minimum, and maximum temperature and mean precipitation model outputs. They used skill score performance as a metric to evaluate the effectiveness of the models at reproducing observations. The results indicate systematic cold and wet biases on seasonal time scales for both models, with the largest precipitation bias being in the winter season (up to 100 % wet bias). However, the skill scores testing returned good results in terms of variability of daily temperature and precipitation. With the exception of a mountainous region with limited station data, both models studied returned values within the observational uncertainty for temperature (± 2 standard error). Like Jiménez et al. (2012), Mayer et al. (2015) found an improvement in the WRF outputs over the reanalysis in terms of wind speed representation, here over the North and Norwegian Seas. The authors also demonstrated improvements in terms of extreme precipitation (timing, intensity and location) over specific areas.

2.2.4 Previous studies modelling future global and regional snow

Terrestrial snow cover has been decreasing for the past few decades and this trend is expected to continue over the next century. Future changes in snow can be, and are, simulated using a range of climate models in order to make predictions. Many different studies have been published, focussing on various aspects of future changes in snow and many rely on predictions of precipitation changes.

2.2.4.1 Precipitation

One of the main challenges in modelling snow results from the difficulty of modelling solid precipitation (Bokhorst et al., 2016). Though recent progress has been made (Marks et al., 2013; Mizukami et al., 2013), accurately partitioning precipitation into rain and snow remains a difficulty. As a result,

confidence in the quantitative estimates of future changes is lower for precipitation than for temperature (e.g. Nikulin et al., 2010).

Climate change is projected to result in an increase in global mean evaporation and precipitation by approximately 1 to 3 % per 1 K increase in global temperature (Roeckner et al., 1999; Sun et al., 2007; Shiogama et al., 2010). Precipitation over high latitude regions is mostly expected to increase, both in summer and winter (Houghton et al., 2001). GCMs suggest a global increase in the intensity of precipitation extremes, even over regions with a projected decrease in mean precipitation (Kharin et al., 2007; Kharin et al., 2013).

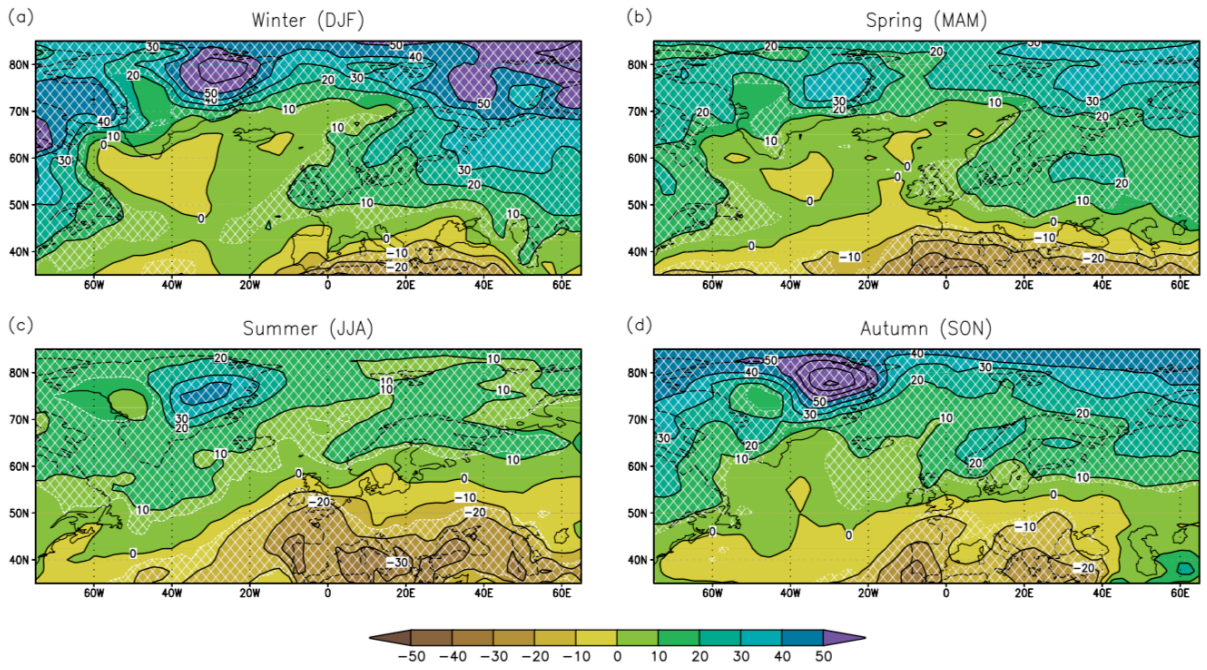

Figure 2.1: Key figure from Lehtonen et al., (2014). Projected multi-model mean change (%) in mean precipitation from 1971 - 2000 to 2081 - 2100 in (a) winter, (b) spring, (c) summer and (d) autumn under the A1B scenario. Hatched areas are significant to 95%.

At a more regional level, Dankers et al. (2005) found that by the end of the century, mean annual precipitation in Northern Fennoscandia is also expected to increase, by 10 - 40 %. This is also predicted for Northern Europe, where mean precipitation and extreme short-term precipitation events are very likely to increase over the 21st century, particularly in winter (Christensen et al., 2007; Lehtonen et al., 2014). Indeed, Lehtonen et al. (2014) analysed projected changes in European extreme precipitation indices from ten global and five regional climate model ensembles. Though the scatter in the simulations was overall much smaller for the RCM than for the GCM, the authors found no fundamental differences between the GCM and RCM projections. Indeed, both indicated a more extreme precipitation climate, characterized by increases both in indices representing wet conditions and also dry conditions (Figure 2.1). Nikulin et al. (2010) analysed future projections of precipitation over Europe in an ensemble of regional climate simulations driven by six different global climate models. The simulated future changes in European precipitation extremes have a distinct seasonal pattern. In winter, the authors found an intensification of precipitation extremes over most of Europe consistent across the six models. The

recurrence time of intense precipitation reduces from 20 year in the control period to 6 - 10 year over northern and central Europe in summer and to 2 - 4 year in Scandinavia in winter.

2.2.4.2 Snow cover

Many studies have investigated what these futures changes in precipitation, as well as projected temperature changes, mean for changes in snow cover patterns. In the RCP 8.5 emission scenario, global spring snow cover is projected to decrease by 25 % by the end of the century (Collins et al., 2013).

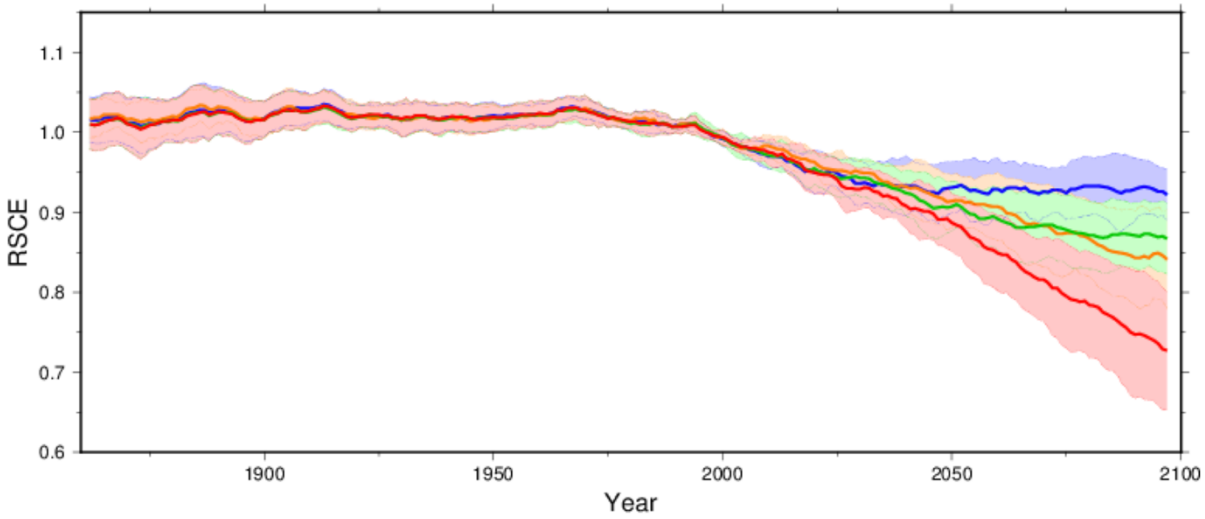

Figure 2.2: Key figure from Brutel-Vuilmet et al. (2013). Relative snow cover extent (RSCE; relative to 1986 – 2005 reference period) in Northern Hemisphere until the end of the century as modelled by CMIP5 ensemble in the four RCP scenarios (blue: RCP 2.6; green: RCP 4.5; yellow: RCP 6.0; red: RCP 8.5).

Brutel-Vuilmet et al. (2013) used the CMIP5 ensemble to model present and future snow cover extent. The interannual variability was only calculated from one of the models in the ensemble, as using the average between all of them would lead to an underestimate of the interannual variability. As discussed in Section 2.2.3, in spite of these precautions, the authors found that the models underestimate the interannual variability of Northern Hemisphere snow cover extent. They found that the lowest latitudes with seasonal snow cover will be the most affected, as the warming there will "immediately lead to a replacement of solid by liquid precipitation and to earlier melt" (Brutel-Vuilmet et al., 2013, pp74). In all emission scenarios, the authors found that the observed and simulated spring snow cover extent and the spring surface air temperatures are strongly and linearly correlated. They hence suggested that it may be possible to study future snow cover extent solely by predicting the annual global mean temperature. Figure 2.2 shows the results of the CMIP5 modelling of Northern Hemisphere snow cover extent: snow cover extent is predicted to decrease over the next century for all four RCPs.

Further validating this argument, Mudryk et al. (2017) found that simulated snow cover extent trends are principally, though not exclusively, controlled by the temperature response on both hemispheric and regional scales. The temperature response explains between 40 % and 85 % of the snow cover extent trend variability. The fraction of Arctic snow cover extent trend variability explained by Arctic temperature trends is higher during the spring (April–May) compared to the autumn (September–

November). This is due to the fact that snow onset will be more weakly coupled to temperature trends since variability in both regional precipitation and temperature have a role in initiating snow cover.

Regional climate simulations of the Nordic regions found that by the end of this century the mean annual temperature in Northern Fennoscandia may rise by 3 - 4 °C, which would lead to an extension of the growing season (number of days with daily mean temperature above 5 °C) by 30 - 60 days and a shortening of the snow season by 50 days (SMHI, 1998) despite a predicted increase in precipitation. Dankers et al. (2005) studied the impact of climate change on snow coverage in the sub-arctic Tana Basin in Finland and Norway, Northern Fennoscandia. They looked at spatial patterns using a distributed water balance model coupled to an RCM in order to study the former under the future conditions of the A2 scenario. The simulations were made for the 2071 - 2100 interval, as well as a 30-year control run that corresponds to a greenhouse gas forcing of 1961. Results showed a much shorter snow season with decreased sublimation, an increase in evapotranspiration and a shift in annual runoff peak. As the snow free season is extended, the amount of solar radiation received during this period increases significantly: +16 %.

Another study, simulating future changes in frost and snow in Europe used seven RCMs all forced by the same GCM, mainly in the A2 and B2 IPCC scenarios (Jylhä et al., 2008). By comparing the outputs of the RCMs, they were aiming to evaluate the confidence that can be placed in individual RCM model projections. In all model simulations and irrespective of the forcing scenario, the results showed fewer days with frost and snow, shorter frost seasons, a smaller liquid water equivalent of snow, and reduced sea ice. In spite of different sources of uncertainties, all models agreed about substantial decreases in snow cover duration (SCD) ranging from 5 to 15 % (Jylhä et al., 2008). Differences in the simulations were a result of different RCM design, uncertainties in future emissions and random effects of climate variability. Decreases of more than 60 snow cover days were projected to occur around the northern Baltic Sea, on the western slope of the Scandinavian mountains and in the Alps. In the sub-domain of northern Europe, the projected seasonal mean decreases (in days) in SCD were almost as large in autumn and winter as in spring. The decrease in the SCD, despite a predicted increase in precipitation for the end of the century in Northern and central Europe, is explained by the authors as being caused by the coincident decrease in the occurrence of frost days. Finally, the authors emphasized that exceptions to the decreasing SCD trend, with negligible tendencies or trends of the opposite sign, have mainly been observed in mountains (Scherrer et al. 2004) and in cold areas with abundant snow (e.g., Hyvärinen 2003; Moberg and Jones, 2005).

2.2.4.3 Snow water equivalent

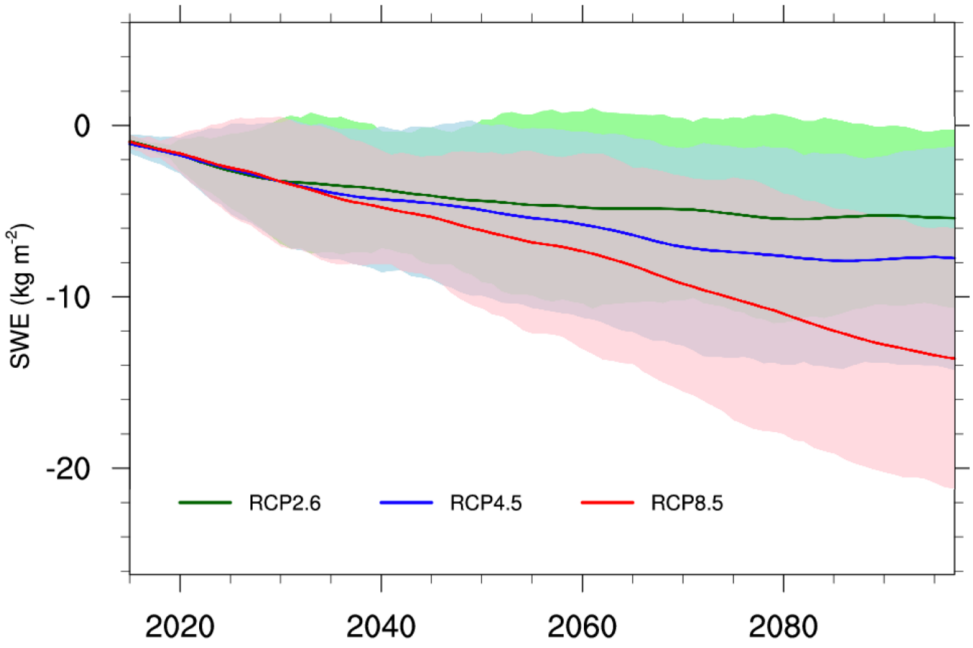

Figure 2.3: Key figure from Shi and Wang (2015). Predicted changes in Northern Hemisphere snow water equivalent (SWE) until the end of the century as modelled by CMIP5 ensemble for three IPCC RCP scenarios.

Modelling studies of future SWE have also been undertaken. It is likely that SWE will change over the next century as it responds both to precipitation and air temperature, both of which are projected to have positive trends (Collins et al., 2013). Shi and Wang (2015) investigated the changes in SWE in the Northern Hemisphere in three intervals of the 21st century: early (2016 - 2035), middle (2046 - 2065) and late (2080 - 2099) using 20 models from the CMIP5 ensemble (Fig. 2.3). The reliability of the results was tested by comparing model outputs with GlobSnow, a field and station measurement dataset (Luojus et al., 2010). Despite some uncertainty in the models, Shi and Wang (2015) found that it is clear that SWE will decrease over the next century in all three emission scenarios considered (Fig. 2.3). The differences between the scenarios increase with time and become clearer later, from mid-century. The authors found that the largest reductions in SWE will occur at lower latitudes and during spring. Eastern Siberia is the only exception to the SWE reduction with a predicted increase in SWE as high as + 60 % for the end of the century in the highest emission scenario.

These findings agree with work from Räisänen (2008), who found that over the next century SWE will mostly decrease, but that increasing SWE will be observed in very cold regions. Indeed, Räisänen (2008) found that the sign of projected changes of SWE is spatially variable as it depends on the present local climate conditions. Maloney et al. (2014) found that the largest decreases in SWE will occur at low altitudes. Finally, Shi and Wang (2015) demonstrated that the predicted decrease in Northern Hemisphere SWE is mainly due to the projected decrease in snowfall resulting from warming.

It has also been shown that the seasonal percentage reductions were smaller for SCD than for SWE (Putkonen and Roe, 2003), especially in northern Europe (Rasmus et al., 2004; Jylhä et al., 2008).

A possible explanation for this is that rain-on-snow events and the partial melting of snow will become more common, leading to a larger proportion of days with only a thin snow cover (Jylhä et al., 2008).

2.2.4.4 Other variables

Multiple studies focus on modelling projections of snowfall in Scandinavia because of the potential impacts of snow loading on forests. One example, Kilpelainen et al. (2010), studied the impacts of snow cover change on forest damage in Finland, by looking at the number of days with high-risk amounts of snow (exceeding 20 $kg.m^2$). Over the whole country, the mean annual number of risk days decreased by 11 %, 23 % and 56 % in the first (1991 - 2020), second (2021 - 2050) and third (2070 - 2099) 30-year period, respectively, compared to the baseline period (1961 - 1990). This suggests a large decrease in extreme snowfall over the next century.

2.3 Remote sensing of snow

In this section, the use of remote sensing in snow cover studies is discussed. The sensor used in this dissertation is considered in detail and a brief summary of the literature of using remotely sensed data to study snow is given.

	Visible and Near-IR	Passive microwave	Active microwave	LiDAR	Gamma Radiation	Gravity data
Extent	■	■	■	■	■	■
Grain size	■		■			
Albedo	■					
Pollution	■					
Depth		■	■	■		
SWE		■	■		■	■
Wetness		■	■			

Table 2.1: The different snow parameters that can be retrieved by different available remote sensing sensors (Guneriussen, 2000; Tedesco, 2015; Engen et al., 2004).

It is possible to map snow extent using remote sensing as it has a unique and spectrally varying reflectance (Nolin, 2010). Using remote sensing is a way of obtaining data over inaccessible areas, on local or global scales (Nolin, 2010; Tedesco and Miller 2007). It also provides regular measurements, which means snow cover trends can be studied. Another advantage of using remote sensing to study snow cover variation is that there is now an archive of this data that extends over multiple decades. Some of the main difficulties in the use of satellite data are in combining sensors with different scales, vegetation and scaling issues (Nolin, 2010). The snow parameters that can be investigated using

remotely sensed data are given in Table 2.1. Different types of sensors can be used to obtain information about discrete snow parameters by using different parts of the electromagnetic spectrum (Fig. 2.4). In this project, I only use Visible and Near-Infrared (VNIR) data.

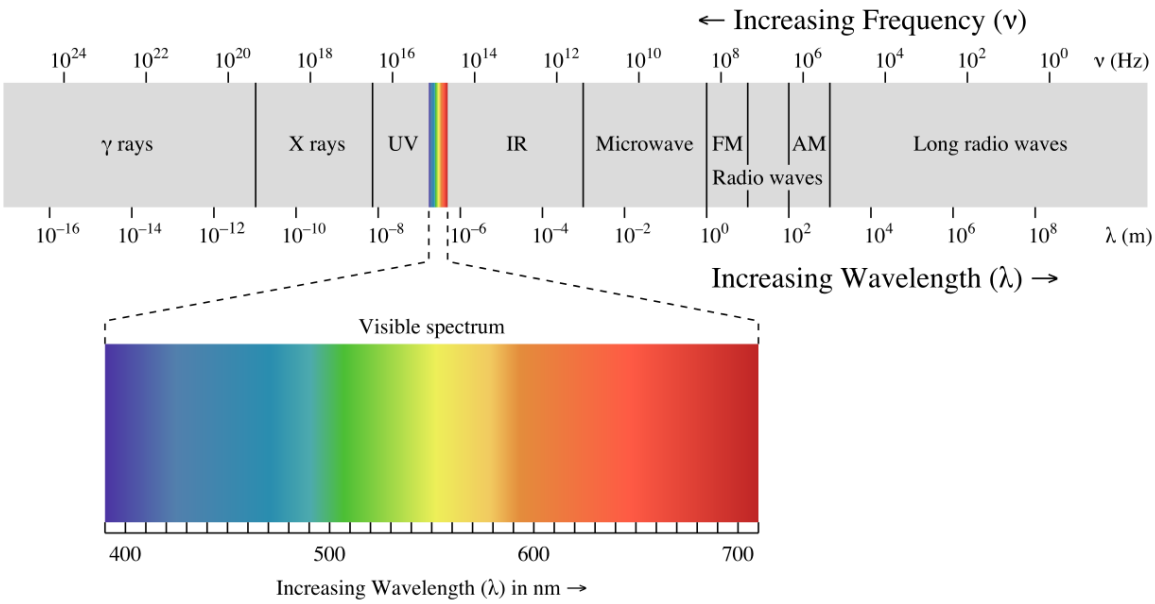

Figure 2.4: The electromagnetic spectrum (https://www.kullabs.com/classes/subjects/units/lessons/notes/note-detail/1823).

2.3.1 Visible and near infrared: MODIS

VNIR sensors use the portion of the electromagnetic spectrum between 400 and 1400 nm wavelength to image the Earth's surface. The main advantage of this data is its high spatial resolution (e.g. Tedesco and Miller, 2007), however, it also has limitations. The optical data is only useful in daylight and in the absence of clouds. Clouds not only block the view of the surface below, but they add an extra difficulty due to their resemblance to surface snow (e.g. Hall et al., 2010). VNIR remote sensing only gives information on the snowpack surface and usually ignores surface inhomogeneity (Tedesco, 2015). This is especially problematic in the case of sastrugi (wave-like ridges on the snow surface). If the incoming sunlight is perpendicular to these, then the snow albedo will decrease; this may be falsely interpreted as an increase in grain size or in the amount of soot in the snow (Zuravleva and Kokhanovsky, 2011). Mountain slopes, blowing snow and forested areas also impact the accuracy of snow data derived from remote sensing. The latter is an important source of uncertainty in the use of remote sensing over the Northern Hemisphere. Indeed, boreal forests are found in almost 1/5 of the seasonally snow-covered land in the Northern Hemisphere (Rutter et al., 2009) and thus snow retrievals over these parts have greater errors as snow is less well represented under trees.

Snow maps from visible imagery have been available since the 1960s in the form of the NOAA Climate Data Record maps (Robinson et al., 1993). However, these maps are not global and had to be "fine-tuned" by analysts, so it is not a purely objective data-set (Hall et al., 2002). Additionally, these snow maps are weekly and have very low resolution with cells ranging from 16 000 to 42 000 km^2 as

of 1993 (Robinson et al., 1993) and only reaching ~580 km^2 from 1997. The sensors on the Landsat satellites have an excellent spatial resolution with 80 m for Landsat 1 (Rango and Martinec, 1979) and as fine as 15 m for Landsat 8 (2013). However, the Landsat repeat pass intervals are of 16 to 18 days. In this project, a high temporal resolution was needed for my analysis. Therefore, the Moderate-Resolution Imaging Spectroradiometer, MODIS, was preferred despite its 500 m resolution (Hall et al., 2002) because although it has the same orbital repeat period as Landsat, its much larger swath width means that daily snow cover extent maps are available (Hall et al., 2002).

MODIS instruments operate onboard both the NASA Earth Observing System (EOS) Terra and Aqua satellites and collect Earth observations in 36 spectral bands ranging from 0.4 - 14.4 μm at spatial resolutions of 250 - 1000 m (Barnes et al., 1998). MODIS data are available from December 1999 for Terra and May 2002 for Aqua and data from both Aqua and Terra satellites are often combined in studies to maximise the number of pixels without cloud cover. When a pixel is cloud covered in the product of one satellite, but not the other, the pixel data of the latter can be used (Dietz et al., 2012; Foppa and Seiz, 2012; Hüsler et al., 2014; Malnes et al., 2016). MODIS calibrations are updated periodically to reflect new understanding of instrument changes, with the entire data record reprocessed as a new 'Collection'.

The version of the data used in this project is Collection 6 (C6), described in Sayer et al. (2015). C6 contains significant revisions of the calibration and aims to address the long-term drift in the calibration of the MODIS instruments, which is most pronounced on the Terra sensor (e.g. Franz et al., 2008; Wang et al., 2012; Lyapustin et al., 2014). The impact of this sensor calibration update was analysed by Casey et al. (2017). They studied the MODIS products over the period 2001 - 2016 and found that the C6 data products reduce the magnitude of the surface reflectance and albedo decline trends obtained from previous MODIS data. Overall, this new calibration was shown to be successful and C6 was found to be "suitable for quantitative scientific analyses" (Sayer et al., 2015, pp157).

2.3.1.1 Snow cover extent

Both binary snow/no-snow or fractional snow cover maps can be derived from MODIS data. The latter provide more information, especially regarding areas of patchy snow and so are usually preferred (Nolin, 2010). The fractional snow cover classification is still imperfect. Fractional snow cover will still be underestimated in forested areas for example, where only part of the snow is visible (Nolin, 2010; Rutter et al., 2009). This is an important uncertainty in this thesis as a great proportion of Northern Fennoscandia is covered in boreal forest. Painter et al. (2003, 2009) developed a method for fractional snow-cover mapping. This method, entitled MODIS Snow Covered-Area and Grain size retrieval algorithm (MODSCAG), assumes that the spectral reflectance of the snow end-member varies with surface grain size. More recently, MODIS outputs include Normalised Difference Snow Index (NDSI). This is a snow cover index that is directly related to the presence of snow in a pixel and is a more accurate description of snow detection compared to fractional snow cover products (Riggs et al., 2016).

2.3.1.2 Snow grain size

MODIS also generates grain size data (e.g. Zege et al., 2011). In remote sensing, the snow grain size measured is the optical-equivalent grain size and is related to the Specific Surface Area (SSA) (see section 2.4.6), which is the surface area to volume ratio of a snow grain (Wiscombe and Warren, 1980; Grenfell and Warren, 1999). The grain size value represents the particle size distribution of grain sizes in the surface layer of the snow (Nolin, 2010).

Snow reflectance is hardly influenced by the grain size in the UV-visible region of the electromagnetic spectrum (Tedesco, 2015). However, in the near-infrared, the relative importance of grain size increases as larger grain sizes result in enhanced scattering. This means that by measuring reflectance, grain size can be determined (e.g. Stamnes et al., 2007; Zege et al., 2011). Aoki et al. (2007) found a good fit between satellite derived grain size and ground measurements. Painter et al. (2009) used a radiative transfer model to map snow grain size in MODIS images, thus creating the MODSCAG dataset. This dataset was not used in this project as a result of its limited cover and lack of accessible albedo product. Finally, it is possible to use different wavelength channels to penetrate to various depths in order to obtain information on grain size within the top few layers of the snowpack (Tedesco, 2015).

2.3.1.3 Albedo

The MODIS instruments also provide snow albedo data. A snow albedo algorithm was developed to determine daily snow albedo for cloud-free pixels mapped as snow by the MODIS snow-mapping algorithm (Klein and Hall, 1999; Klein et al., 2000). Importantly, the albedo measured in multispectral remote sensing is not the broadband albedo, but the narrowband albedo. This is the albedo integrated over the spectral range of a single channel, which then needs to be integrated over the entire solar spectrum to give the broadband albedo that is of interest (Nolin, 2010). It is important to note that albedo also depends on the solar zenith angle and the relative proportions of direct beam and diffuse solar irradiance (Nolin, 2010). For this reason, Schaaf et al. (2002) produced the MODIS Bidirectional Reflectance Distribution Function/Albedo Product. This is a 16-day composite, which results in the acquisition of reflectances at multiple viewing angles and, through model inversion, produces surface albedo. This 16-day composite is not used in this project, as daily data was needed.

2.3.1.4 Ground truthing

Ground truthing or validation of MODIS grain size, albedo and impurities retrievals has been performed in various studies (e.g. Nolin and Dozier, 2000; Stroeve et al., 2005; Aoki et al., 2007). Most of the albedo analyses are not specific to snow products and find high correlation coefficients between ground albedo and the MODIS product (Liang et al., 2005; Liu et al., 2009). For example, a comparison of MODIS albedo data to ground data from Greenland found that the difference was less than 2 % (Stroeve et al., 2005) and Stroeve et al. (2013) performed a direct validation of the MODIS snow albedo product

and found an RMSE of 0.067. The authors found that using both Terra and Aqua albedo products in combination increases the potential for retrieval of high-quality albedo (Stroeve et al., 2013).

2.3.2 Previous remote sensing studies of snow

In this section, a selection of remote sensing studies of snow are described to demonstrate some of the key snow parameters that can be obtained using satellite data.

Firstly, examples of the use of VNIR data in snow studies are considered. Atlaskina et al. (2015) looked at Northern Hemisphere snow albedo changes in spring using MODIS data. The Northern Hemisphere was divided into six smaller areas based on their climate and geographical position. Snow cover extent was shown to be the parameter with the strongest influence on albedo. Snow cover extent itself is often studied using VNIR data, commonly NOAA maps (e.g. Armstrong and Brodzick, 2001; Brown and Robinson, 2011; Derksen and Brown, 2012; Estilow et al., 2015) or MODIS (e.g. Brown et al., 2010; Maskey et al., 2011). Brown and Robinson (2011), for example, looked at Northern Hemisphere snow cover extent variability between 1922 - 2010, using station data from 1922 onwards and NOAA data over the 1966 - 2010 interval. They included an uncertainty assessment and found a 95 % confidence in the NOAA data used.

VNIR data can also be used to study snow climatology. The following examples all use MODIS datasets in their analyses. Saavedra et al. (2016) studied the snow climatology of the Andes using the MODIS 8-day maximum binary snow cover product. This dataset provides the maximum snow cover and minimum cloud cover during that 8-day period from the daily time step product. The authors used data for the 2000 to 2014 interval to identify regions with similar snow patterns, i.e. where snow accumulates at similar elevations and times of the year and to identify snow persistence zones within these regions. Their definition of the snow regions is based on the following three parameters: minimum elevation of snow cover, rate of change of snow persistence with elevation and timing of the minimum elevation snow cover. To evaluate annual snow patterns, they used snow zones (as defined in Moore et al., 2015): little or no snow, intermittent, transitional and persistent snow zones.

Studies of the timing and duration of the snow cover seasons have also been undertaken using VNIR remote sensing datasets (e.g. Wang and Xie, 2009; Dietz et al., 2012; Malnes et al., 2016). The two most recent of these papers extracted the first and last snow-free day over the entirety of Europe (2000 - 2011) and the boreal Arctic transition of Northern Norway (2000 - 2010), respectively. Dietz et al. (2012) used a combination of both Terra and Aqua data and applied a temporal cloud filter. By doing so, the authors were able to reduce the combined cloud percentage from 47.7 % to 39.9 %. Malnes et al. (2016) used a similar method though they only used MODIS data from the Terra satellite. From this processed dataset, both studies derived the start and end of the snow season for their regions of interest, though neither publication investigated trends as a result of the short period of analysis.

It is not uncommon for snow studies using one type of remote sensing data to rely on another as ground truth. The sensor used to validate the other remote sensing instrument usually has a much higher spatial resolution. Singh and Gan (2000) retrieved SWE data using Passive Microwave (PM)

brightness temperature products. In 2000, most of the retrieval algorithms were statistically rather than physically based due to a lack of snow field data. In this paper, the authors used airborne gamma-ray measurements of SWE as the ground truth. Similarly, Che et al. (2008) used PM data from the Scanning Multichannel Microwave Radiometer (SMMR) and the Special Sensor Microwave/Imager (SSM/I) to study snow depth in China and modified a pre-existing algorithm by including vegetation and water body distribution maps of China. This algorithm was validated using meteorological observations as well as MODIS data. MODIS was considered as the "truth" here as it has a higher spatial resolution and a more comprehensive snow-cover algorithm (Che et al., 2008). The authors found a good agreement between PM and MODIS snow cover extent for a definition of snow-covered ground as 2 cm depth for PM and more than 50 % snow fraction for MODIS retrievals.

Researchers also often assimilate other datasets, such as observations, in order to improve snow parameters extracted from remote sensing datasets. Takala et al. (2011) assimilated weather station data into satellite PM data to help deal with the problem of multiple solutions fitting a single brightness temperature value and found an improvement compared to using only PM data. Brown et al. (2010) used MODIS along with nine other datasets (including observations and other remote sensing types) to study Arctic monthly snow cover extent in the May–June melt period for 1967 to 2008. In their subsequent publication, the authors showed there can be large differences in retrievals made by different sensors depending on "spatial resolution, cloud cover and wavelength specific interactions with the atmosphere, snowpack, terrain and land cover" (Brown et al., 2011, pp219). It is hence useful to combine data from different sensors in order to improve the retrieval. For example, Tedesco and Miller (2007) studied snow depth in the Northern Hemisphere between 1999 and 2004 using a combination of active and passive microwave systems for high temporal resolution and large spatial scale. The satellite data was ground-truthed using station data and the authors found that using a combination of active and passive data improved the snow depth retrievals.

Hallikainen et al. (2003) also found that combining active and passive data improves the retrieval accuracy of using only PM data. However, they also emphasized that combining those two methods is problematic for two reasons. Firstly, they have very different spatial resolutions, with active microwave instruments having a resolution three orders of magnitude higher. Secondly, the two sensors are not spatially and temporarily coincident. Armstrong and Brodzick (2001) compared the use of visible (NOAA weekly maps) and passive microwave (SMMR) remote sensing in the study of snow cover extent. The sensors yield similar trends, though the passive microwave data consistently undermeasure during autumn, with improved agreement during winter and spring. The authors explained this by arguing that, as the winter season progresses, the amount of area covered by deeper snow increases, which facilitates the detection of snow by the PM algorithm. They thus argued that it is useful to combine VNIR and PM data. An example of this is described by Huang et al. (2016), who looked at trends in snow in the 2000 to 2014 interval in all areas of China in a similar manner to Dietz et al (2012) and Malnes et al (2016)**.** However, in this study, the authors used the MODIS daily snow cover product alongside PM snow depth data to produce a daily cloudless snow cover area product and a downscaled

snow depth product with a 500 m spatial resolution. They then combined these two products to extract the dates of the snow season over China.

2.4 Field measurements of snow

As discussed in the Section 2.3.1.4, remote sensing data needs to be ground truthed in order to calibrate algorithms and validate the output data (Tedesco, 2015). Furthermore, it is important to use ground measurements to gain an understanding of the variability at a spatial scale below that of the remote sensing sensor. This requires the measurement of the snow parameters of interest in the field. In-situ measurements give the most reliable data but are very time consuming, usually expensive and destructive. For these reasons, these will often be restricted to small areas and short periods of time (Tedesco, 2015). Denoth et al. (1984) emphasized that in the case of snow, measurements must be made quickly and, where possible, non-destructively as the snowpack will change fast when disturbed. Most snow parameters are collected in snow pits. These are often dug to the ground and measurements are made along the wall facing away from the sun, which is thus in the shade.

2.4.1 Snow depth

Snow depth can be measured using probes, up to approximately 10 m depth (Schaffhauser et al., 2008). Stake arrays are also used at some stations, whereby graduated stakes are left in place and snow depth is recorded manually (Tedesco, 2015). Another method is to use an ultrasonic depth sensor which enables the measurement to be continuous at a fixed point (DeWalle and Rango, 2008; Schaffhauser et al., 2008). The time it takes for an ultrasonic pulse to reach the ground and return to the surface is used to calculate the snow depth. This method is much more expensive, but longer-term datasets can be obtained more easily.

2.4.2 Snow density

The main method for measuring snow density in the field is straightforward: a sample of a known volume of snow is weighed in a cutter and the density can then be calculated. The size of the cutters can vary between 100 to 1000 cm^3 (Tedesco, 2015), with the larger cutters being used to sample the average density and the smaller one for more precise structural density measurements. In some cases, density is measured on a larger scale using small coring instruments which are typically 0.5 m long (Fig. 2.5).

Older instruments for measuring snow wetness and density were developed in the 1980s with the Denothmeter (Denoth et al., 1984) and the Snowfork (Sihvola and Tivri, 1986). Stähli et al. (2004) proposed a new technique for measuring snow density and SWE using an in-situ dielectric sensor which measures the transmission of radio frequencies in the snow. Though this technique was found to agree well with traditional snowpack measurements, it was not adopted by the snow science community. Proksch et al. 2015 wrote that "we still lack a convenient retrieval of density" (pp247) and that there are no objective methods of measuring this parameter yet.

Figure 2.5: Use of a density coring instrument, Khibiny Mountains, 2017 (Photo credit: Ilona Blinova).

2.4.3 Snow water equivalent

SWE is calculated using the snow density and depth measurements. When an average SWE measurement is needed for an area, as snow depth is often more spatially variable than density, many depth measurements are used with a few density measurement (Tedesco, 2015).

$$SWE = \int_{ground}^{surface} \frac{\rho(z)}{\rho_w} dz \quad (2.1)$$

with $\rho(z)$ the snow density, ρ_w the density of water, z the direction normal to the surface.

2.4.4 Snow temperature

Measuring the temperature of the snow surface and within the snowpack is important as it is an indication of whether the snow is melting. It also provides information on the emitted radiation, as temperature is its main control (Tedesco, 2015). Snow temperature is easily measured in the field using a thermometer, usually by making temperature measurements every 5 or 10 cm down the wall of a snow-pit.

2.4.5 Snow albedo

Albedo is the ratio of outgoing to incoming solar radiation. As such, there is a range of instruments available for its measurement; radiometers, both broadband and narrowband, can be used. The former are often used in automated weather stations as they measure downwelling and upwelling radiative fluxes directly. Narrowband radiometers on the other hand measure these in specific frequency bands, which can be directly compared to satellite data or the data can be converted to the broadband albedo. Spectrometers can also be used: their advantage is that they are hand-held and measure a wide spectrum

of electromagnetic reflectance (Tedesco, 2015). These instruments are calibrated in the field using standards with known albedos.

2.4.6 Snow grain size

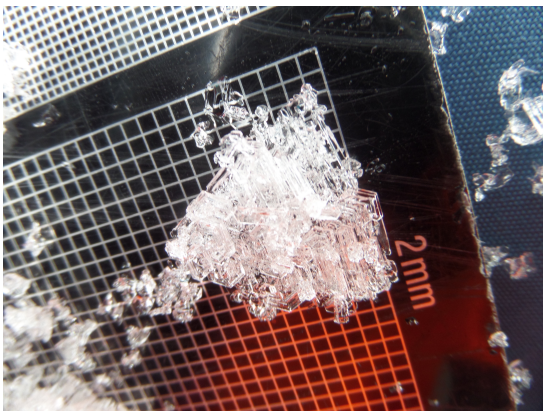

Figure 2.6: Measuring snow grain size on a measurement card with a 2 mm grid. Here, depth hoar grains are measured at Davos, Switzerland.

Grain size has been shown to be the most sensitive parameter of all the physical snow properties in microwave radiative transfer models (Montpetit et al., 2012; Sandells et al., 2017). The traditional method for measuring grain size is very simple: snow is placed on a measurement card with a millimetre grid (Fig. 2.6). The grain size is then estimated by looking at the snow grains relative to the spacing of the grid lines (Fierz et al., 2009). The average size and the maximum size are often recorded, though the snow grain size is usually taken as the largest size recorded, D_{max} (Fierz et al., 2009). It can be difficult to identify individual grains as the boundaries are not often clear (Domine et al., 2008). This means that this method of grain size measurement is very subjective (Painter et al., 2007).

Thus, many techniques have been suggested to measure an objective grain size in the field. Furthermore, the grain size given by remote sensing sensors is the optical-equivalent grain size (OGS) and not the grain size measured by traditional measurements (Fierz et al., 2009). To a first approximation, OGS can be estimated from the branch width of dendrites, the thickness of either thin plates or dendrites, the diameter of needles, or the shell thickness of hollow crystals (Mätzler, 2002; Aoki et al., 2003). Traditional measurements of the grain size and SSA cannot be directly compared to these measurements of OGS (Seidel et al., 2016). However, a conversion has been derived by Gallet et al. (2009) and Leppänen et al. (2015):

$$OGS = \frac{3}{SSA \times \rho_{ice}} \tag{2.2}$$

where ρ_{ice} is the density of ice (917 kg. m^{-3}).

OGS and SSA have been estimated using many different non-traditional methods: spectroscopy (Nolin and Dozier, 2000; Painter et al., 2003; Painter et al., 2007), stereology (Matzl and Schneebeli, 2010), shortwave-infrared (SWIR) photography (Matzl and Schneebeli, 2006; Montpetit et al., 2012),

SWIR reflectance (Gallet et al., 2009) etc. Proksch et al. (2015), for example, developed a high-resolution penetrometer, to extract SSA information from the snowpack at a millimetre resolution in less than one minute. This technique measures SSA with a 23.1 % error; though this is not as accurate as other methods, this technique offers the advantage of speed as it does not require the digging of a snow-pit. All of these non-traditional techniques however rely on the use of very expensive instruments, often unique, built by the researchers themselves.

2.4.7 Field measurement campaigns

Many major campaigns of data collection have been undertaken in recent years, oftentimes as part of larger remote sensing of snow studies. One such data collection campaign is the Cold Land Processes Field Experiment (CLPX; Elder and Goodbody, 2004). A high-quality observational dataset was collected in a series of nested domains from 1 ha to 160,000 km^2 in the central Rocky Mountains, Colorado. Snow density, temperature, stratigraphy, grain size and SWE were measured at a total of ~2000 snow pits. Snow wetness and surface roughness were also measured at some of these snow pits. The CLPX project also includes meteorological observations such as air temperature, relative humidity, radiation, wind speed and direction, solar and longwave radiations, soil temperature, and soil moisture. The measurements were made under varied topography and vegetation coverage (alpine tundra, boreal forest, coniferous forest). These snowpack measurements, which cover a wide area but at a high resolution, are crucial to monitoring spatial and temporal variations in the growth and melting of the snowpack over this region. This dataset has been used in many studies with, for example, Feng et al. (2008) using this observational dataset to test the skill of five snow models with varying levels of complexity.

A more recent campaign is the Nordic Snow Radar Experiment (NoSREx) which covers four seasons from 2009 to 2013 (Lemmetyinen et al., 2016). As the name suggest, the purpose of this project was to study snow cover radar products in the Nordic region using frequent in situ observations to support this work (e.g. Lemmetyinen et al., 2014). The main site of the NoSREx study was in Sodankyla in northern Finland and is representative of snow in boreal forest/taiga environments. Weekly snow pit measurements were undertaken in a forest clearing within 10-20 m of the radiometers. Snow depth and density profiles were collected, from which SWE was calculated. Temperature profiles of the snow were also made and snow grain size and shape were recorded using macro-photography. In addition to manual snow data, automated snow data was also collected. These automated measurements focussed on snow microstructure including grain size, with SSA measurements undertaken using near infrared photography (Matzl and Schneebeli, 2006) and snow micropenetrometry (Proksch et al., 2015). A similar project is SnowPEx, funded by the European Space Agency. The aim of this campaign is to determine and quantify the uncertainty in existing snow cover extent (Metsämäki et al., 2016) and SWE (Luojus et al., 2016) products (e.g. GlobSnow and SSM/I). Ground measurements of snow made in the former Soviet Union, Russia and Finland are used as “truth” for this uncertainty assessment campaign.

2.5 Changes in snow cover in the Northern Hemisphere over the past century

Now that the wide range of methods for studying snow cover have been discussed, past changes in snow over the past century are presented. Studying Arctic snow is especially difficult due to its high spatial variability (Liston, 2004) and the rarity of long-term ground measurements. As snowpack thickness and 'behaviour' varies greatly in relation to terrain, orography and wind (Serreze and Barry, 2014), a high spatial coverage of data is needed to study regional trends in snow cover. However, lack of good coverage of ground measurements and issues with accessibility and accuracy of other datasets limit the amount of data available. Arctic precipitation specifically is difficult to assess, and this impacts our understanding of Arctic snowfall and associated snow cover. Some of the major issues of measuring mean precipitation totals over the Arctic are described in Serreze and Barry (2014). Firstly, measurement gauges and practices vary greatly between countries and hinder the interpretation of precipitation recordings, specifically those of solid precipitation which are often underestimated by gauge measurements. Secondly, the network of stations in the Arctic is very limited as a result of access difficulties. And finally, satellite-based and reanalysis-based precipitation estimates are subject to large biases (e.g. Marshall et al., 2018).

Arctic snow has nevertheless been the subject of many studies, which have used a range of observational and remote sensing data, as well as combinations of both. In this section, the literature that focusses on the trends in snow cover over the past century will be discussed. The focus of this section is on the results of these studies rather than methods used.

2.5.1 Why study past changes in snow cover?

Arctic amplification is the name given to the fact that Northern Hemisphere high-latitudes have undergone a much larger magnitude and more rapid warming than the globe as a whole (e.g. Serreze and Francis, 2006). In fact, the Arctic is warming at twice the rate of the Northern Hemisphere (Bekryaev et al., 2010; Pithan and Mauritsen, 2014). Defining the particular causes of Arctic amplification is difficult (Crook et al., 2011), but it has been suggested that declining terrestrial spring snow cover in the Arctic is contributing to Arctic amplification (Serreze and Barry, 2011; Matsumura et al., 2014). Other processes contributing to this amplification are: reductions in sea-ice extent, changes in atmospheric circulation that lead to atmospheric heat flux convergence, changes in clouds and water vapour, decreases in snow albedo as a result of soot deposition and increases in black carbon aerosols (Serreze and Barry, 2011; Serreze and Barry, 2014).

For the Arctic, the interval between October 2015 and September 2016 was the warmest year on record since 1900 (Lader et al., 2017). There is variation in the magnitude and patterns of warming and changes in associated precipitation across polar and circumpolar regions, but the rise in temperatures over Northern Europe including Northern Fennoscandia is expected to continue to be much larger than the global mean (Kivinen et al., 2017). Therefore, it is important to understand how snow has been changing over the past few decades in order to better predict how it will respond to climate change over the next century.

2.5.2 Large-scale snow cover changes

Many studies analysing changes in snow over the past century have focussed on the trends in snow cover extent. These trends have been negative in the Northern Hemisphere for the past few decades (e.g. Dye, 2002; Déry and Brown, 2007; Lemke et al., 2007), especially in spring (Brown and Robinson, 2011; Peng et al., 2013). Scientists have been aware of these negative trends for some time; Robinson et al. (1993) used NOAA snow cover maps to study trends in snow cover extent and noted the reduction in the 1988 to 1993 interval. More recently these trends have been quantified: Brown and Robinson (2011) showed that, in the 1979 to 2005 interval, there has been a decrease in the average snow cover extent of March and April of –3.4 ± 1.1 % per decade. The longer trend since 1922 is weaker: –1.0 ± 0.3% per decade. Flanner et al. (2011) showed that terrestrial snow cover feedbacks are strongest in April and May. Brown and Robinson's (2011) findings support this as they found a larger decrease in April than in March with a decrease in snow cover extent of 2.00×10^6 km^2 and 1.44×10^6 km^2, respectively, for each 1 °C of warming in the Northern Hemisphere. Tedesco and Monaghan (2009) found that, in the 1979 to 2008 interval, the duration of the melt season in the Northern Hemisphere has been shortening by 0.6 days/year. The inter-year variability is mostly due to fluctuations over relatively small areas (Robinson and Frei, 2000). The annual extent of snow cover over the Northern Hemisphere has declined by nearly 10 % during the period 1972 - 2003 (Diaz et al. 2003; Walsh et al. 2005), accompanied by lower springtime SWE (Mote et al. 2005),

Some studies look at the timing and duration of the snow season. One example, Peng et al. (2013), found a decrease in the overall snow cover duration in the Northern Hemisphere over the turn of the century (1980 to 2006). They found that the snow cover start date has become increasingly later in both North America and Northern Europe, but that the snow season end has stayed stable over North America and has become earlier in Northern Europe. The snow cover season has thus shortened more over Northern Europe than over North America. The duration of the snow cover season is also indirectly represented in studies focusing on the duration of the growing season. The thermal potential growing season has lengthened by about 10.5 days (1982 – 2011), with the overall lengthening being stronger and more significant in Eurasia (12.6 days, $p < 0.01$) than North America (6.2 days, $p > 0.05$) (Barichivich et al., 2013), which supports the results found by Peng et al. (2013).

Changes in snow cover have also been investigated using changes in albedo. Li et al. (2018) studied trends in albedo to understand snow and vegetation changes between 2002 and 2016 over the entire Northern Hemisphere. They found that albedo has widely decreased over the high latitudes of the Northern Hemisphere and regression analysis identified a greening trend over the northern Eurasian continent. These are both partially explained by an observed decrease in snow cover in the Arctic as a result of warming climate (e.g. Bintanja & Krikken, 2016; Lutz et al., 2016).

Finally, changes in snow depth over Eurasia between 1966 and 2012 were investigated by Zhong et al. (2018). The authors used a very large observational dataset in order to avoid the limitations of low-resolution remote sensing instruments (passive microwave) and numerical models. They used daily or 10-day interval ground-based measurements of snow depth from 1814 stations across Eurasia.

At a seasonal level, they found that snow depth increased in both winter and spring but decreased slightly in autumn. However, overall results show that both annual mean and maximum snow depth increased by 0.2 and 0.6 cm/decade respectively with the highest increases in snow depth occurring in regions north of 50 ºN.

2.5.3 Regional snow cover changes

The previous section summarises the large-scale trends across the Northern Hemisphere. At a smaller regional scale, the snow cover trends are not uniform. Snow cover duration has been found to be increasing in many areas in Eurasia (Bulygina et al., 2009; Shmakin, 2010). Ye and Ellison (2003) found a slight increase in the duration of the snow cover season over northern Eurasia between 1937 and 1994. A similar increase in snow season duration has occurred between 1936 and 2000 over Northern Europe (particularly Scandinavia and the north eastern European plains), caused by increases in precipitation (Kitaev et al., 2006). Ye and Ellison (2003) identified an increasingly early end to the snow cover season in northern European Russia and found that the length of continuous snow cover has nevertheless increased slightly over this area, as well as western Siberia. They explained this increase in duration by the much earlier onset of snow cover. Kitaev et al., (2004) also found an overall increase in snow cover duration between 1966 and 1990 throughout most of Northern Eurasia. This trend is also explained by an increasingly early start of the snow season over this period.

Using phenology (the study of the cycle of plants), Kozlov and Berlina (2002) found that the length of the summer in the Kola Peninsula decreased by 15 to 20 days in the 1930 to 1998 interval. Here, the plant growth season is used as a proxy for the snow season. Indeed, plants will start growing as the snow start to melt thus providing water and eventually sunlight to the plants below. This is not a direct and exact proxy but is a useful indication of the duration of the snow season and has been used in previous phenological studies (e.g. Jönsson et al., 2010). The decrease in the length of the plant growth season identified by Kozlov and Berlina (2002) thus implies an extension of the duration of snow season over this time period. This is supported by the 44 % increase in winter precipitation recorded over the Northern taiga forests in the Kola Peninsula (Høgda et al., 2001).

However, Bulygina et al. (2009) found high spatial variability over Russia in the number of days per year with more than 1 cm snow cover (Fig. 2.7). The snow cover duration has been decreasing in north-west and southern Russia since 1966 reaching -6 days/decade. Additionally, the Russian Arctic coast and northern (65 - 85°N) islands in Eurasia (Kitaev et al., 2004) and the southern Scandinavian Peninsula (Kitaev et al., 2006) have also been found to have undergone weak decreases in snow cover duration between 1966 and 1990. Finally, the only region with a decrease in snow cover duration between 1937 and 1994 is southern Siberia (Ye and Ellison, 2003). Thus, trends in snow cover in Eurasia are both regionally and temporally variable.

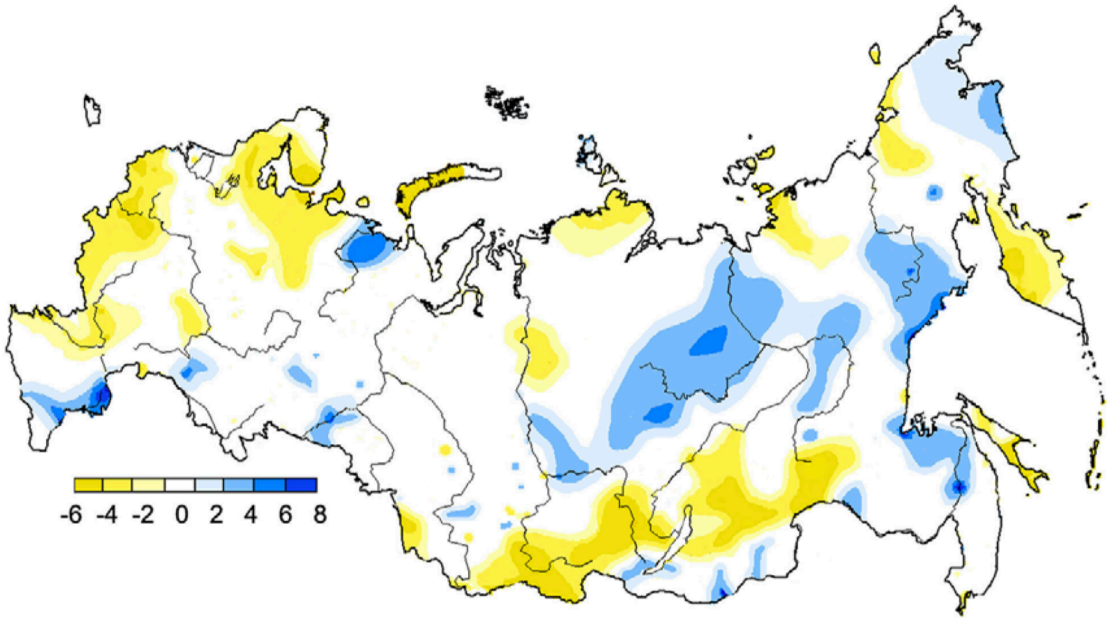

Figure 2.7: Spatial distribution of linear trend coefficients (days/decade; 1 - 5 % significance level) showing the number of days with snow cover exceeding 1 cm for 1966 - 2007, from Bulygina et al. (2009).

Concerning snow depth, mean and maximum winter snow depth have been increasing in Eurasia in the 1966 to 1996 period (Bulygina et al., 2007). Many studies on snow depth have focused on local and regional scales over Russia (Ye et al., 1998; Brasnett, 1999; Kitaev et al., 2005; Bulygina et al., 2009; Bulygina et al., 2011; Zhong et al., 2018). Bulygina et al. (2011) looked at snow duration and snow depth over 1966 to 2010 by using a very large dataset of 1000 stations distributed over the Russian territory. One aspect of snow studied is the number of days in winter with more than 20 cm snow depth. They find that across the Russian territory the number of days exceeding this depth has increased between 1966 and 2010, the exception being over southern- and western-European Russia. Overall, mean snow depth in Russia has increased over the past century. Ye et al. (1998) and Zhong et al. (2018) found a significant increase in snow depth over Russia in the 1936 - 1986 and 1966 - 2012 intervals respectively. Zhong et al. (2018) explained that the main cause of this increase is increased precipitation, rather than changes in air temperature. Mean SWE has also been shown to have increased in Russia, particularly over western Siberia, northern and eastern European Russia over the 1966 to 1996 period (Bulygina et al., 2010). Positive trends in maximum SWE (Krenke et al., 2001) have also been identified over this period, with the largest increases occurring over the Urals (1.9 $mm.yr^{-1}$) and the Far East (1.5 $mm.yr^{-1}$).

Kitaev et al. (2005) studied the distribution of snow cover over the entirety of Northern Eurasia but analysed results within six sub-regions. Over the 1936 to 2000 interval, for the whole region of Northern Eurasia, the analysis indicated positive trends of both snow depth (+0.91 cm/decade), snow cover duration (+1.19 days/decade in number of days with ≥ 50 % snow cover) and winter air temperature (+0.15 °C/decade). At a regional level, Kazakhstan has the highest increase in temperature +0.44 °C/decade and the only recorded decrease in the number of snow-covered days (-1.91 days/decade) between 1936 and 2000. Eastern Siberia has the lowest change in temperature with no

change recorded (0.00 °C/decade), but an increase in snow covered days of +1.43 days/decade. The smallest change in number of snow-covered days is in the Russian Far East with +0.94 days/decade. Finally, they identified a low increase in winter air temperature (+0.05 °C/decade) in Fennoscandia and an increase in the snow cover duration of +1.45 days/decade. They found that across the northern part of Northern Fennoscandia, the long-term increase in snow cover duration is higher over the eastern parts. This is linked with decreasing autumn temperatures and increasing winter precipitation from West to East (Kitaev et al., 2005).

In the second half of the 20th century, the number of thaw days in winter increased by 35 % (1.2 days/decade) in Fennoscandia as a whole (Groisman et al., 2011). Venäläinen et al. (2005) studied Finnish climate and found that the average temperature in Finland in the 1991 - 2000 interval has increased by 0.5 °C relative to the 1960 - 2000 interval; the monthly mean precipitation also increased in this time by +13 to +36 % and winds have weakened over this period (Venäläinen et al. 2005; Gregow et al., 2008). As a result, extreme snow events and the associated risk of heavier snow loads in Finland have increased over the 1961 - 2000 interval.

Finally, two publications focus on climatic changes in Northern Fennoscandia: Kivinen et al. (2017), who used data from nine stations to study climate trends over this entire region between 1914 and 2013 and Marshall et al. (2016) who studied meteorological data (surface air temperature, precipitation and sea level pressure) from 10 stations between 1966 and 2015 over the Kola Peninsula, the Russian part of Northern Fennoscandia. Both publications found that the most significant changes in all variables occurred in spring and autumn. Kivinen et al. (2017) found that temperatures in these two seasons and, to a lesser extent, in summer increased significantly in the study region, with the greatest increase affecting daily minimum temperatures. The warming trend was largest in spring with a significant increase in mean maximum air temperature by 0.4 °C/decade between 1950 and 1995. The authors suggested that the warming over north-eastern Fennoscandia is likely driven by reductions in sea-ice of the Barents and White seas. Over the Kola Peninsula, Marshall et al. (2016) found that yearly surface air temperature has increased by 2.3 ± 1.0°C over the past 50 years (0.46 °C/decade). Seasonally, statistically significant warming has taken place in spring (+0.54 °C/decade) and autumn (+0.47 °C/decade) with large increases in winter also (+0.54 °C/decade). Precipitation was shown to increase over Northern Fennoscandia as a whole in Kivinen et al. (2017), and extreme high precipitation events were shown to become more extreme (higher precipitation) towards the end of the study period. The authors also found significant declines in extreme cold climate events in all seasons and increases in extreme warm events, in spring and autumn. Marshall et al. (2016) found that, although there has been no significant change in annual PPN, spring has become significantly wetter (+1.0 mm/decade) and autumn drier (-1.6 mm/decade) over the Kola Peninsula between 1966 and 2015. Of the two studies, only Kivinen et al. (2017) considered changes in snow cover. Their results indicated that the snow season duration in Northern Fennoscandia has decreased over the past hundred years. The authors explained this change in snow cover with the increases in temperature and precipitation. Indeed, spring and autumn are transitional periods of melting and formation of continuous seasonal snow in Northern

Fennoscandia respectively. Therefore, increases in temperature in these two seasons will lead to a later start and earlier end to the snow cover season. In addition to this, the combined increases in precipitation and in temperature are likely to result in increases in rainfall and decreases in snowfall (Kivinen et al., 2017).

In conclusion, though most snow cover characteristics (snow cover duration, depth and SWE) have been increasing over northern Eurasia and Russia as a whole, trends are not so uniform regionally (e.g. Fig.2.7 from Bulygina et al., 2009) and there is high spatial variability in these characteristics. Of relevance to this dissertation, Northern Fennoscandia has undergone decreases in snow cover duration between 1914 and 2013 (Kivinen et al., 2017) and increases between 1936 and 2000 (Kitaev et al., 2005). Thus, high temporal variability also affects snow in this study region.

2.6 References

Aoki, T., Hachikubo, A. and Hori, M., 2003. Effects of snow physical parameters on shortwave broadband albedos. Journal of Geophysical Research: Atmospheres, 108(D19). https://doi.org/10.1029/2003JD003506

Aoki, T., Hori, M., Motoyoshi, H., Tanikawa, T., Hachikubo, A., Sugiura, K., Yasunari, T.J., Storvold, R., Eide, H.A., Stamnes, K. and Li, W., 2007. ADEOS-II/GLI snow/ice products—Part II: Validation results using GLI and MODIS data. Remote Sensing of Environment, 111(2-3), pp.274-290. https://doi.org/10.1016/j.rse.2007.02.035

Armstrong, R.L. and Brodzik, M.J., 2001. Recent Northern Hemisphere snow extent: A comparison of data derived from visible and microwave satellite sensors. Geophysical Research Letters, 28(19), pp.3673-3676. https://doi.org/10.1029/2000GL012556

Armstrong, R.L. and Brun, E. eds., 2008. Snow and climate: physical processes, surface energy exchange and modeling. Cambridge University Press.

Atlaskina, K., Berninger, F. and De Leeuw, G., 2015. Satellite observations of changes in snow-covered land surface albedo during spring in the Northern Hemisphere. Cryosphere. https://doi.org/10.5194/tc-9-1879-2015

Barnes, W.L., Pagano, T.S. and Salomonson, V.V., 1998. Prelaunch characteristics of the moderate resolution imaging spectroradiometer (MODIS) on EOS-AM1. IEEE Transactions on Geoscience and Remote Sensing, 36(4), pp.1088-1100. https://doi.org/10.1109/36.700993

Barnett, T.P., Adam, J.C. and Lettenmaier, D.P., 2005. Potential impacts of a warming climate on water availability in snow-dominated regions. Nature, 438(7066), p.303. https://doi.org/10.1038/nature04141

Barstad, I., Sorteberg, A. and Mesquita, M.D.S., 2012. Present and future offshore wind power potential in northern Europe based on downscaled global climate runs with adjusted SST and sea ice cover. Renewable Energy, 44, pp.398-405. https://doi.org/10.1016/j.renene.2012.02.008

Barry, R.G., 2002. The role of snow and ice in the global climate system: a review. Polar Geography, 26(3), pp.235-246. https://doi.org/10.1080/789610195

Bartelt, P. and Lehning, M., 2002. A physical SNOWPACK model for the Swiss avalanche warning: Part I: numerical model. Cold Regions Science and Technology, 35(3), pp.123-145. https://doi.org/10.1016/S0165-232X(02)00074-5

Bates, B., Kundzewicz, Z. and Wu, S., 2008. Climate change and water. Intergovernmental Panel on Climate Change Secretariat.

Bekryaev, R.V., Polyakov, I.V. and Alexeev, V.A., 2010. Role of polar amplification in long-term surface air temperature variations and modern Arctic warming. Journal of Climate, 23(14), pp.3888-3906. https://doi.org/10.1175/2010JCLI3297.1

Bintanja, R. and Krikken, F., 2016. Magnitude and pattern of Arctic warming governed by the seasonality of radiative forcing. Scientific reports, 6, p.38287. https://doi.org/10.1038/srep38287

Bokhorst, S., Pedersen, S.H., Brucker, L., Anisimov, O., Bjerke, J.W., Brown, R.D., Ehrich, D., Essery, R.L., Heilig, A., Ingvander, S. and Johansson, C., 2016. Changing Arctic snow cover: A review of recent developments and assessment of future needs for observations, modelling, and impacts. Ambio, 45(5), pp.516-537. https://doi.org/10.1007/s13280-016-0770-0

Bony, S., Colman, R., Kattsov, V.M., Allan, R.P., Bretherton, C.S., Dufresne, J.L., Hall, A., Hallegatte, S., Holland, M.M., Ingram, W. and Randall, D.A., 2006. How well do we understand and evaluate climate change feedback processes?. Journal of Climate, 19(15), pp.3445-3482. https://doi.org/10.1175/JCLI3819.1

Brands, S., Herrera, S., Fernández, J. and Gutiérrez, J.M., 2013. How well do CMIP5 Earth System Models simulate present climate conditions in Europe and Africa?. Climate dynamics, 41(3-4), pp.803-817. https://doi.org/10.1007/s00382-013-1742-8

Brasnett, B., 1999. A global analysis of snow depth for numerical weather prediction. Journal of Applied Meteorology, 38(6), pp.726-740. https://doi.org/10.1175/1520-0450(1999)038<0726:AGAOSD>2.0.CO;2

Broecker, W.S., Peng, T.H., Jouzel, J. and Russell, G., 1990. The magnitude of global fresh-water transports of importance to ocean circulation. Climate Dynamics, 4(2), pp.73-79. https://doi.org/10.1007/BF00208902

Brown, R., Derksen, C. and Wang, L., 2010. A multi-data set analysis of variability and change in Arctic spring snow cover extent, 1967–2008. Journal of Geophysical Research: Atmospheres, 115(D16). https://doi.org/10.1029/2010JD013975

Brown, R.D. and Robinson, D.A., 2011. Northern Hemisphere spring snow cover variability and change over 1922–2010 including an assessment of uncertainty. The Cryosphere, 5(1), pp.219-229. https://doi.org/10.5194/tc-5-219-2011

Broxton, P.D., Harpold, A.A., Biederman, J.A., Troch, P.A., Molotch, N.P. and Brooks, P.D., 2015. Quantifying the effects of vegetation structure on snow accumulation and ablation in mixed-conifer forests. Ecohydrology, 8(6), pp.1073-1094. https://doi.org/10.1002/eco.1565

Brun, E., Martin, E. and Spiridonov, V., 1997. Coupling a multi-layered snow model with a GCM. Annals of Glaciology, 25, pp.66-72. https://doi.org/10.3189/S0260305500013811

Brutel-Vuilmet, C., Ménégoz, M. and Krinner, G., 2013. An analysis of present and future seasonal northern hemisphere land snow cover simulated by CMIP5 coupled climate models. Cryosphere, 7(1). https://doi.org/10.5194/tc-7-67-2013

Bulygina, O.N., Groisman, P.Y., Razuvaev, V.N. and Korshunova, N.N., 2011. Changes in snow cover characteristics over Northern Eurasia since 1966. Environmental Research Letters, 6(4), p.045204. https://doi.org/10.1088/1748-9326/6/4/045204

Bulygina, O. N., Korshunova, N. N. and Razuvaev V. N., 2007. Changes in snow cover characteristics in recent decades. Proc. RIHMI-WDC, vol 173, pp 54–66. (in Russian)

Bulygina, O. N., Korshunova, N. N. and Razuvaev V. N., 2010. Climatic conditions over the territory of Russia. Online Information Provided by the All-Russian Research Institute of Hydrometeorological Information of Federal Service for Hydrometeorology and Environmental Monitoring. (in Russian)

Bulygina, O.N., Razuvaev, V.N. and Korshunova, N.N., 2009. Changes in snow cover over Northern Eurasia in the last few decades. Environmental Research Letters, 4(4), p.045026. https://doi.org/10.1088/1748-9326/4/4/045026

Caldwell, P., Chin, H.N.S., Bader, D.C. and Bala, G., 2009. Evaluation of a WRF dynamical downscaling simulation over California. *Climatic change*, *95*(3-4), pp.499-521. https://doi.org/10.1007/s10584-009-9583-5

Casey, K.A., Polashenski, C.M., Chen, J. and Tedesco, M., 2017. Impact of MODIS sensor calibration updates on Greenland Ice Sheet surface reflectance and albedo trends. The Cryosphere, 11(4), pp.1781-1795. https://doi.org/10.5194/tc-11-1781-2017

Che, T., Li, X., Jin, R., Armstrong, R. and Zhang, T., 2008. Snow depth derived from passive microwave remote-sensing data in China. Annals of Glaciology, 49, pp.145-154. https://doi.org/10.3189/172756408787814690

Christensen, J.H., Hewitson, B., Busuioc, A., Chen, A., Gao, X., Held, R., Jones, R., Kolli, R.K., Kwon, W.K., Laprise, R. and Magaña Rueda, V., 2007. Regional climate projections. In Climate Change, 2007: The Physical Science Basis. Contribution of Working group I to the Fourth Assessment Report of the Intergovernmental Panel on Climate Change, University Press, Cambridge, Chapter 11 (pp. 847-940).

Clark, M.P. and Serreze, M.C., 2000. Effects of variations in East Asian snow cover on modulating atmospheric circulation over the North Pacific Ocean. Journal of Climate, 13(20), pp.3700-3710. https://doi.org/10.1175/1520-0442(2000)013<3700:EOVIEA>2.0.CO;2

Cohen, J., Barlow, M., Kushner, P.J. and Saito, K., 2007. Stratosphere–troposphere coupling and links with Eurasian land surface variability. Journal of Climate, 20(21), pp.5335-5343. https://doi.org/10.1175/2007JCLI1725.1

Cohen, J. and Entekhabi, D., 2001. The influence of snow cover on Northern Hemisphere climate variability. Atmosphere-Ocean, 39(1), pp.35-53. https://doi.org/10.1080/07055900.2001.9649665

Cohen, J.L., Furtado, J.C., Barlow, M.A., Alexeev, V.A. and Cherry, J.E., 2012. Arctic warming, increasing snow cover and widespread boreal winter cooling. Environmental Research Letters, 7(1), p.014007. https://doi.org/10.1088/1748-9326/7/1/014007

Collins, M., R. Knutti, J. Arblaster, J.-L. Dufresne, T. Fichefet, P. Friedlingstein, X. Gao, W.J. Gutowski, T. Johns, G. Krinner, M. Shongwe, C. Tebaldi, A.J. Weaver and M. Wehner, 2013: Long-term Climate Change: Projections, Com- mitments and Irreversibility. In: Climate Change 2013: The

Physical Science Basis. Contribution of Working Group I to the Fifth Assessment Report of the Intergovernmental Panel on Climate Change [Stocker, T.F., D. Qin, G.-K. Plattner, M. Tignor, S.K. Allen, J. Boschung, A. Nauels, Y. Xia, V. Bex and P.M. Midgley (eds.)]. Cambridge University Press, Cambridge, United Kingdom and New York, NY, USA.

Crook, J.A., Forster, P.M. and Stuber, N., 2011. Spatial patterns of modeled climate feedback and contributions to temperature response and polar amplification. Journal of Climate, 24(14), pp.3575-3592. https://doi.org/10.1175/2011JCLI3863.1

Dankers, R. and Christensen, O.B., 2005. Climate change impact on snow coverage, evaporation and river discharge in the sub-arctic Tana Basin, Northern Fennoscandia. Climatic Change, 69(2-3), pp.367-392. https://doi.org/10.1007/s10584-005-2533-y

Davies, T.D., 1994. Snow cover-atmosphere interactions. IAHS Publications-Series of Proceedings and Reports-Intern Assoc Hydrological Sciences, 223, pp.3-14.

Dawei, Z., Maosong, L. and Zhiguo, H., 2008. Effects of 2008 Snow Disaster in Southern China on Agriculture and Countermeasures [J]. Journal of Institute of Disaster-Prevention Science and Technology, 2.

Denoth, A., Foglar, A., Weiland, P., Mätzler, C., Aebischer, H., Tiuri, M. and Sihvola, A., 1984. A comparative study of instruments for measuring the liquid water content of snow. Journal of Applied Physics, 56(7), pp.2154-2160. https://doi.org/10.1063/1.334215

Derksen, C. and Brown, R., 2012. Spring snow cover extent reductions in the 2008–2012 period exceeding climate model projections. Geophysical Research Letters, 39(19). https://doi.org/10.1029/2012GL053387

Déry, S.J. and Brown, R.D., 2007. Recent Northern Hemisphere snow cover extent trends and implications for the snow-albedo feedback. Geophysical Research Letters, 34(22). https://doi.org/10.1029/2007GL031474

DeWalle, D.R. and Rango, A., 2008. Principles of snow hydrology. Cambridge University Press.

Dewey, K.F., 1977. Daily maximum and minimum temperature forecasts and the influence of snow cover. Monthly Weather Review, 105(12), pp.1594-1597. https://doi.org/10.1175/1520-0493(1977)105<1594:DMAMTF>2.0.CO;2

Diaz, H.F., Eischeid, J.K., Duncan, C. and Bradley, R.S., 2003. Variability of freezing levels, melting season indicators, and snow cover for selected high-elevation and continental regions in the last 50 years. In Climate Variability and Change in High Elevation Regions: Past, Present & Future (pp. 33-52). Springer, Dordrecht. https://doi.org/10.1007/978-94-015-1252-7_3

Dietz, A.J., Wohner, C. and Kuenzer, C., 2012. European snow cover characteristics between 2000 and 2011 derived from improved MODIS daily snow cover products. Remote Sensing, 4(8), pp.2432-2454. https://doi.org/10.3390/rs4082432

Domine, F., Albert, M., Huthwelker, T., Jacobi, H.W., Kokhanovsky, A.A., Lehning, M., Picard, G. and Simpson, W.R., 2008. Snow physics as relevant to snow photochemistry. Atmospheric chemistry and physics, 8(2), pp.171-208. https://doi.org/10.5194/acp-8-171-2008

Dumont, M., Brun, E., Picard, G., Michou, M., Libois, Q., Petit, J.R., Geyer, M., Morin, S. and Josse, B., 2014. Contribution of light-absorbing impurities in snow to Greenland's darkening since 2009. Nature Geoscience, 7(7), p.509. https://doi.org/10.1038/ngeo2180

Dye, D.G., 2002. Variability and trends in the annual snow-cover cycle in Northern Hemisphere land areas, 1972–2000. Hydrological Processes, 16(15), pp.3065-3077. https://doi.org/10.1002/hyp.1089

Elder, K. and Goodbody, A., 2004. CLPX-Ground: ISA main meteorological data. National Snow and Ice Data Center, Boulder, CO, digital media. [Available online at http://nsidc.org/data/docs/daac/nsidc0172_clpx_mainmet/.].

Engen, G., Guneriussen, T. and Overrein, Y., 2004. Delta-K interferometric SAR technique for snow water equivalent (SWE) retrieval. IEEE Geoscience and remote sensing letters, 1(2), pp.57-61. https://doi.org/10.1109/LGRS.2003.822880

Essery, R., Pomeroy, J., Parviainen, J. and Storck, P., 2003. Sublimation of snow from coniferous forests in a climate model. Journal of Climate, 16(11), pp.1855-1864. https://doi.org/10.1175/1520-0442(2003)016<1855:SOSFCF>2.0.CO;2

Essery, R., Rutter, N., Pomeroy, J., Baxter, R., Stähli, M., Gustafsson, D., Barr, A., Bartlett, P. and Elder, K., 2009. SNOWMIP2: An evaluation of forest snow process simulations. Bulletin of the American Meteorological Society, 90(8), pp.1120-1136. https://doi.org/10.1175/2009BAMS2629.1

Estilow, T.W., Young, A.H. and Robinson, D.A., 2015. A long-term Northern Hemisphere snow cover extent data record for climate studies and monitoring. Earth System Science Data, 7(1), pp.137-142. https://doi.org/10.5194/essd-7-137-2015

Fagre, D.B., Peterson, D.L. and Hessl, A.E., 2003. Taking the pulse of mountains: ecosystem responses to climatic variability. Climatic Change, 59(1-2), pp.263-282. https://doi.org/10.1023/A:1024427803359

Field, C.B., Barros, V.R., Dokken, D.J., Mach, K.J., Mastrandrea, M.D., Bilir, T.E., Chatterjee, M., Ebi, K.L., Estrada, Y.O., Genova, R.C. and Girma, B., 2014. Climate Change 2014: Impacts, Adaptation, and Vulnerability. Part A: Global and Sectoral Aspects. Contribution of Working Group II to the Fifth Assessment Report of the Intergovernmental Panel on Climate Change, CB Field and others (eds.), Cambridge, Cambridge University Press.

Fierz, C.R.L.A., 8. others (2009) The international classification for seasonal snow on the ground. IHP-VII Tech. Doc. Hyrdol. No. 83, IACS Contrib. No. 1, UNESCO-IHP, Paris.

Flanner, M.G., Shell, K.M., Barlage, M., Perovich, D.K. and Tschudi, M.A., 2011. Radiative forcing and albedo feedback from the Northern Hemisphere cryosphere between 1979 and 2008. Nature Geoscience, 4(3), p.151. https://doi.org/10.1038/ngeo1062

Foppa, N. and Seiz, G., 2012. Inter-annual variations of snow days over Switzerland from 2000–2010 derived from MODIS satellite data. The Cryosphere, 6(2), pp.331-342. https://doi.org/10.5194/tc-6-331-2012

Fowler, H.J., Blenkinsop, S. and Tebaldi, C., 2007. Linking climate change modelling to impacts studies: recent advances in downscaling techniques for hydrological modelling. *International journal of climatology*, *27*(12), pp.1547-1578. https://doi.org/10.1002/joc.1556

Franz, B.A., Kwiatowska, E.J., Meister, G. and McClain, C.R., 2008. Moderate Resolution Imaging Spectroradiometer on Terra: limitations for ocean color applications. Journal of Applied Remote Sensing, 2(1), p.023525.

Frei, A., Tedesco, M., Lee, S., Foster, J., Hall, D.K., Kelly, R. and Robinson, D.A., 2012. A review of global satellite-derived snow products. Advances in Space Research, 50(8), pp.1007-1029. https://doi.org/10.1016/j.asr.2011.12.021

Gallet, J.C., Domine, F., Zender, C.S. and Picard, G., 2009. Measurement of the specific surface area of snow using infrared reflectance in an integrating sphere at 1310 and 1550 nm. https://doi.org/10.5194/tc-3-167-2009

Gao, Y., Fu, J.S., Drake, J.B., Liu, Y. and Lamarque, J.F., 2012. Projected changes of extreme weather events in the eastern United States based on a high resolution climate modeling system. Environmental Research Letters, 7(4), p.044025. https://doi.org/10.1088/1748-9326/7/4/044025

Gouttevin, I., Menegoz, M., Dominé, F., Krinner, G., Koven, C., Ciais, P., Tarnocai, C. and Boike, J., 2012. How the insulating properties of snow affect soil carbon distribution in the continental pan-Arctic area. Journal of Geophysical Research: Biogeosciences, 117(G2). https://doi.org/10.1029/2011JG001916

Gray, D.M. and Prowse, T.D., 1993. Snow and floating ice (Vol. 7, pp. 7-1). McGraw-Hill: New York.

Gregow, H., Puranen, U., Venäläinen, A., Peltola, H., Kellomäki, S. and Schultz, D., 2008. Temporal and spatial occurrence of strong winds and large snow load amounts in Finland during 1961–2000. Silva Fennica, 42(4), pp.515-534.

Grenfell, T.C. and Warren, S.G., 1999. Representation of a nonspherical ice particle by a collection of independent spheres for scattering and absorption of radiation. Journal of Geophysical Research: Atmospheres, 104(D24), pp.31697-31709. https://doi.org/10.1029/1999JD900496

Groisman, P.Y., Karl, T.R. and Knight, R.W., 1994. Observed impact of snow cover on the heat balance and the rise of continental spring temperatures. Science, 263(5144), pp.198-200. https://doi.org/10.1126/science.263.5144.198

Groisman, P., Gutman, G. and Reissell, A., 2010. Introduction: Climate and land-cover changes in the Arctic. In Eurasian Arctic Land Cover and Land Use in a Changing Climate (pp. 1-8). Springer, Dordrecht.

Guneriussen, T. ed., 2000. Research and Development of Remote Sensing Methods for Snow Hydrology: SnowTools Final Report. NORUT Informasjonsteknologi as.

Hall, D.K., Riggs, G.A., Salomonson, V.V., DiGirolamo, N.E. and Bayr, K.J., 2002. MODIS snow-cover products. Remote sensing of Environment, 83(1-2), pp.181-194. https://doi.org/10.1016/S0034-4257(02)00095-0

Hallikainen, M.T., Halme, P., Takala, M. and Pulliainen, J., 2003, July. Combined active and passive microwave remote sensing of snow in Finland. In IGARSS 2003. 2003 IEEE International Geoscience and Remote Sensing Symposium. Proceedings (IEEE Cat. No. 03CH37477) (Vol. 2, pp. 830-832). Ieee. https://doi.org/10.1109/IGARSS.2003.1293934

Hansen, J. and Nazarenko, L., 2004. Soot climate forcing via snow and ice albedos. Proceedings of the National Academy of Sciences, 101(2), pp.423-428. https://doi.org/10.1073/pnas.2237157100

Hogda, K.A., Karlsen, S.R. and Solheim, I., 2001. Climatic change impact on growing season in Fennoscandia studied by a time series of NOAA AVHRR NDVI data. In IGARSS 2001. Scanning the Present and Resolving the Future. Proceedings. IEEE 2001 International Geoscience and Remote Sensing Symposium (Cat. No. 01CH37217) (Vol. 3, pp. 1338-1340). IEEE. https://doi.org/10.1109/IGARSS.2001.976837

Houghton, J.T., Ding, Y.D.J.G., Griggs, D.J., Noguer, M., van der Linden, P.J., Dai, X., Maskell, K. and Johnson, C.A., 2001. Climate change 2001: the scientific basis. The Press Syndicate of the University of Cambridge.

Huang, X., Deng, J., Ma, X., Wang, Y., Feng, Q., Hao, X. and Liang, T., 2016. Spatiotemporal dynamics of snow cover based on multi-source remote sensing data in China. The Cryosphere, 10(5), p.2453. https://doi.org/10.5194/tc-10-2453-2016

Hüsler, F., Jonas, T., Riffler, M., Musial, J.P. and Wunderle, S., 2014. A satellite-based snow cover climatology (1985–2011) for the European Alps derived from AVHRR data. The Cryosphere, 8(1), pp.73-90. https://doi.org/10.5194/tc-8-73-2014

Hyvärinen, V., 2003. Trends and Characteristics of Hydrological Time Series in FinlandPaper presented at the 13th Northern Res. Basins/Workshop (Saariselkä, Finland and Murmansk, Russia-Aug. 19-24 2001). Hydrology Research, 34(1-2), pp.71-90. https://doi.org/10.2166/nh.2003.0029

Immerzeel, W.W., Van Beek, L.P. and Bierkens, M.F., 2010. Climate change will affect the Asian water towers. Science, 328(5984), pp.1382-1385. https://doi.org/10.1126/science.1183188

Jacob, D., Bärring, L., Christensen, O.B., Christensen, J.H., De Castro, M., Deque, M., Giorgi, F., Hagemann, S., Hirschi, M., Jones, R. and Kjellström, E., 2007. An inter-comparison of regional climate models for Europe: model performance in present-day climate. Climatic change, 81(1), pp.31-52. https://doi.org/10.1007/s10584-006-9213-4

Jiménez, P.A., González-Rouco, J.F., Montávez, J.P., García-Bustamante, E., Navarro, J. and Dudhia, J., 2013. Analysis of the long-term surface wind variability over complex terrain using a high spatial resolution WRF simulation. Climate dynamics, 40(7-8), pp.1643-1656. https://doi.org/10.1007/s00382-012-1326-z

Jönsson, A.M., Eklundh, L., Hellström, M., Bärring, L. and Jönsson, P., 2010. Annual changes in MODIS vegetation indices of Swedish coniferous forests in relation to snow dynamics and tree phenology. Remote Sensing of Environment, 114(11), pp.2719-2730. https://doi.org/10.1016/j.rse.2010.06.005

Jylhä, K., Fronzek, S., Tuomenvirta, H., Carter, T.R. and Ruosteenoja, K., 2008. Changes in frost, snow and Baltic sea ice by the end of the twenty-first century based on climate model projections for Europe. Climatic Change, 86(3-4), pp.441-462. https://doi.org/10.1007/s10584-007-9310-z

Keller, F., Goyette, S. and Beniston, M., 2005. Sensitivity analysis of snow cover to climate change scenarios and their impact on plant habitats in alpine terrain. Climatic Change, 72(3), pp.299-319. https://doi.org/10.1007/s10584-005-5360-2

Kharin, V.V., Zwiers, F.W., Zhang, X. and Hegerl, G.C., 2007. Changes in temperature and precipitation extremes in the IPCC ensemble of global coupled model simulations. Journal of Climate, 20(8), pp.1419-1444. https://doi.org/10.1175/JCLI4066.1

Kharin, V.V., Zwiers, F.W., Zhang, X. and Wehner, M., 2013. Changes in temperature and precipitation extremes in the CMIP5 ensemble. Climatic change, 119(2), pp.345-357.

Kietäväinen, A.; Tuulentie, S. Tourism strategies and climate change: Rhetoric at both strategic and grassroots levels about growth and sustainable development in Finland. J. Sustain. Tour. 2013, 21, 845–861.

Kilpeläinen, A., Gregow, H., Strandman, H., Kellomäki, S., Venäläinen, A. and Peltola, H., 2010. Impacts of climate change on the risk of snow-induced forest damage in Finland. Climatic Change, 99(1-2), pp.193-209. https://doi.org/10.1007/s10584-009-9655-6

Kitaev, L., Førland, E., Razuvaev, V., Tveito, O.E. and Krueger, O., 2005. Distribution of snow cover over Northern Eurasia. Hydrology Research, 36(4-5), pp.311-319. https://doi.org/10.2166/nh.2005.0024

Kitaev, L.M., Radionov, V.F., Forland, E., Razuvaev, V.N. and Martuganov, R.A., 2004. Duration of northern Eurasia snow cover under present climate change conditions. Russian Meteorology and Hydrology, (11), pp.46-51. (in Russian)

Kitaev, L.M., Razuvaev, V.N., Heino, R. and Forland, E., 2006. Snow cover period in northern Europe. Russian Meteorology and Hydrology, (3), pp.72-76. (in Russian)

Kivinen, S., Rasmus, S., Jylhä, K. and Laapas, M., 2017. Long-term climate trends and extreme events in Northern Fennoscandia (1914–2013). Climate, 5(1), p.16. https://doi.org/10.3390/cli5010016

Klein, A.G. and Hall, D.K., 1999, June. Snow albedo determination using the NASA MODIS instrument. In Proc. East. Snow Conf (pp. 2-4).

Klein, A.G., Hall, D.K. and Nolin, A.W., 2000, May. Development of a prototype snow albedo algorithm for the NASA MODIS instrument. In Proceedings of the 57th Eastern Snow Conference (pp. 15-17).

Kozlov, M.V. and Berlina, N.G., 2002. Decline in length of the summer season on the Kola Peninsula, Russia. Climatic Change, 54(4), pp.387-398. https://doi.org/10.1023/A:1016175101383

Krenke, A.N., Kitaev, L.M. and Turkov, D.V., 2001. Climatic role of snow cover changes in the period of warming. Izvestya Ross. Akad. Nauk, Seriya Geogr. Proc. of the Russian Academy of Sciences. Geographical Series, 4, pp.44-51. (in Russian)

ipcc-data.org http://www.ipcc-data.org/guidelines/pages/gcm_guide.html (visited on 14.11.18)

Lader, R., Walsh, J.E., Bhatt, U.S. and Bieniek, P.A., 2017. Projections of twenty-first-century climate extremes for alaska via dynamical downscaling and quantile mapping. Journal of Applied Meteorology and Climatology, 56(9), pp.2393-2409. https://doi.org/10.1175/JAMC-D-16-0415.1

Lamb, H.H., 1955. Two-way relationship between the snow or ice limit and 1,000–500 mb thicknesses in the overlying atmosphere. Quarterly Journal of the Royal Meteorological Society, 81(348), pp.172-189. https://doi.org/10.1002/qj.49708134805

Langlois, A., Johnson, C.A., Montpetit, B., Royer, A., Blukacz-Richards, E.A., Neave, E., Dolant, C., Roy, A., Arhonditsis, G., Kim, D.K. and Kaluskar, S., 2017. Detection of rain-on-snow (ROS) events and ice layer formation using passive microwave radiometry: A context for Peary caribou habitat in the

Canadian Arctic. Remote Sensing of Environment, 189, pp.84-95. https://doi.org/10.1016/j.rse.2016.11.006

Lawrence, D.M. and Slater, A.G., 2010. The contribution of snow condition trends to future ground climate. Climate dynamics, 34(7-8), pp.969-981. https://doi.org/10.1007/s00382-009-0537-4

Lehtonen, I., Hoppula, P., Pirinen, P. and Gregow, H., 2014. Modelling crown snow loads in Finland: a comparison of two methods. Silva Fennica, 48(3), pp.1-30. https://doi.org/10.14214/sf.1120

Lemke, P., Ren, J., Alley, R.B., Allison, I., Carrasco, J., Flato, G., Fujii, Y., Kaser, G., Mote, P., Thomas, R.H. and Zhang, T., 2007. Observations: changes in snow, ice and frozen ground. Climate Change 2007: The Physical Science Basis. Contribution of Working Group I to the Fourth Assessment Report of the Intergovernmental Panel on Climate Change.

Lemmetyinen, J., Kontu, A., Pulliainen, J., Vehviläinen, J., Rautiainen, K., Wiesmann, A., Mätzler, C., Werner, C., Rott, H., Nagler, T. and Schneebeli, M., 2016. Nordic snow radar experiment. Geoscientific Instrumentation, Methods and Data Systems, 5(2), pp.403-415. https://doi.org/10.5194/gi-5-403-2016

Lemmetyinen, J., Pulliainen, J., Kontu, A., Wiesmann, A., Maetzler, C., Rott, H., Voglmeier, K., Nagler, T., Meta, A., Coccia, A. and Schneebeli, M., 2014, June. Observations of seasonal snow cover at X and Ku bands during the NoSREx campaign. In EUSAR 2014; 10th European Conference on Synthetic Aperture Radar (pp. 1-4). VDE.

Leppänen, L., Kontu, A., Vehviläinen, J., Lemmetyinen, J. and Pulliainen, J., 2015. Comparison of traditional and optical grain-size field measurements with SNOWPACK simulations in a taiga snowpack. Journal of Glaciology, 61(225), pp.151-162. https://doi.org/10.3189/2015JoG14J026

Liang, S., Stroeve, J. and Box, J.E., 2005. Mapping daily snow/ice shortwave broadband albedo from Moderate Resolution Imaging Spectroradiometer (MODIS): The improved direct retrieval algorithm and validation with Greenland in situ measurement. Journal of Geophysical Research: Atmospheres, 110(D10). https://doi.org/10.1029/2004JD005493

Li, Q., Ma, M., Wu, X. and Yang, H., 2018. Snow Cover and Vegetation-Induced Decrease in Global Albedo From 2002 to 2016. Journal of Geophysical Research: Atmospheres, 123(1), pp.124-138. https://doi.org/10.1002/2017JD027010

Liston, G.E., 2004. Representing subgrid snow cover heterogeneities in regional and global models. Journal of climate, 17(6), pp.1381-1397. https://doi.org/10.1175/1520-0442(2004)017<1381:RSSCHI>2.0.CO;2

Liu, J., Schaaf, C., Strahler, A., Jiao, Z., Shuai, Y., Zhang, Q., Roman, M., Augustine, J.A. and Dutton, E.G., 2009. Validation of Moderate Resolution Imaging Spectroradiometer (MODIS) albedo retrieval algorithm: Dependence of albedo on solar zenith angle. Journal of Geophysical Research: Atmospheres, 114(D1). https://doi.org/10.1029/2008JD009969

Lundquist, J.D., Dickerson-Lange, S.E., Lutz, J.A. and Cristea, N.C., 2013. Lower forest density enhances snow retention in regions with warmer winters: A global framework developed from plot-scale observations and modeling. Water Resources Research, 49(10), pp.6356-6370. https://doi.org/10.1002/wrcr.20504

Luojus, K., Pulliainen, J., Takala, M., Derksen, C., Rott, H., Nagler, T., Solberg, R., Wiesmann, A., Metsamaki, S., Malnes, E. and Bojkov, B., 2010, July. Investigating the feasibility of the GlobSnow snow water equivalent data for climate research purposes. In 2010 IEEE International Geoscience and Remote Sensing Symposium (pp. 4851-4853). IEEE. https://doi.org/10.1109/IGARSS.2010.5741987

Luojus, K., Pulliainen, J., Cohen, J., Ikonen, J., Takala, M., Lemmetyinen, J., Smolander, T., Derksen, C., Nagler, T. and Bojkov, B., 2016, July. Assessing global satellite-based snow water equivalent datasets in ESA SnowPEx project. In 2016 IEEE International Geoscience and Remote Sensing Symposium (IGARSS) (pp. 5284-5287). IEEE. https://doi.org/10.1109/IGARSS.2016.7730376

Lutz, S., Anesio, A.M., Raiswell, R., Edwards, A., Newton, R.J., Gill, F. and Benning, L.G., 2016. The biogeography of red snow microbiomes and their role in melting arctic glaciers. Nature Communications, 7, p.11968. https://doi.org/10.1038/ncomms11968

Lyapustin, A., Tucker, J., Hall, F., Sellers, P., Wu, A., Angal, A., Wang, Y., Xiong, X., Meister, G., Platnick, S. and Levy, R., 2014. Scientific impact of MODIS C5 calibration degradation and C6+ improvements. Atmospheric Measurement Techniques, 7(12). https://doi.org/10.5194/amt-7-4353-2014

Lynch-Stieglitz, M., 1994. The development and validation of a simple snow model for the GISS GCM. Journal of Climate, 7(12), pp.1842-1855.

Malnes, E., Karlsen, S.R., Johansen, B., Bjerke, J.W. and Tømmervik, H., 2016. Snow season variability in a boreal-Arctic transition area monitored by MODIS data. Environmental Research Letters, 11(12), p.125005. https://doi.org/10.1088/1748-9326/11/12/125005

Maloney, E.D., Camargo, S.J., Chang, E., Colle, B., Fu, R., Geil, K.L., Hu, Q., Jiang, X., Johnson, N., Karnauskas, K.B. and Kinter, J., 2014. North American climate in CMIP5 experiments: Part III: Assessment of twenty-first-century projections. Journal of Climate, 27(6), pp.2230-2270. https://doi.org/10.1175/JCLI-D-13-00273.1

Marcos, M., Jordà, G., Gomis, D. and Pérez, B., 2011. Changes in storm surges in southern Europe from a regional model under climate change scenarios. Global and Planetary Change, 77(3-4), pp.116-128. https://doi.org/10.1016/j.gloplacha.2011.04.002

Marks, D., Winstral, A., Reba, M., Pomeroy, J. and Kumar, M., 2013. An evaluation of methods for determining during-storm precipitation phase and the rain/snow transition elevation at the surface in a mountain basin. Advances in Water Resources, 55, pp.98-110. https://doi.org/10.1016/j.advwatres.2012.11.012

Marshall, G.J., Vignols, R.M. and Rees, W.G., 2016. Climate change in the Kola Peninsula, Arctic Russia, during the last 50 years from meteorological observations. Journal of Climate, 29(18), pp.6823-6840. https://doi.org/10.1175/JCLI-D-16-0179.1

Maskey, S., Uhlenbrook, S. and Ojha, S., 2011. An analysis of snow cover changes in the Himalayan region using MODIS snow products and in-situ temperature data. Climatic Change, 108(1-2), p.391. https://doi.org/10.1007/s10584-011-0181-y

Matsumura, S., Zhang, X. and Yamazaki, K., 2014. Summer Arctic atmospheric circulation response to spring Eurasian snow cover and its possible linkage to accelerated sea ice decrease. Journal of Climate, 27(17), pp.6551-6558. https://doi.org/10.1175/JCLI-D-13-00549.1

Matzl, M. and Schneebeli, M., 2006. Measuring specific surface area of snow by near-infrared photography. Journal of Glaciology, 52(179), pp.558-564. https://doi.org/10.3189/172756506781828412

Matzl, M. and Schneebeli, M., 2010. Stereological measurement of the specific surface area of seasonal snow types: Comparison to other methods, and implications for mm-scale vertical profiling. Cold Regions Science and Technology, 64(1), pp.1-8. https://doi.org/10.1016/j.coldregions.2010.06.006

Mätzler, C., 2002. Relation between grain-size and correlation length of snow. Journal of Glaciology, 48(162), pp.461-466. https://doi.org/10.3189/172756502781831287

Mayer, S., Fox Maule, C., Sobolowski, S., Bøssing Christensen, O., Danielsen Sørup, H.J., Antonia Sunyer, M., Arnbjerg-Nielsen, K. and Barstad, I., 2015. Identifying added value in high-resolution climate simulations over Scandinavia. Tellus A: Dynamic Meteorology and Oceanography, 67(1), p.24941. https://doi.org/10.3402/tellusa.v67.24941

Metsämäki, S., Ripper, E., Mattila, O.P., Fernandes, R., Bippus, G., Luojus, K., Nagler, T. and Bojkov, B., 2016, July. Evaluation of Northern Hemisphere Snow Extent products within ESA SnowPEx-project. In 2016 IEEE International Geoscience and Remote Sensing Symposium (IGARSS) (pp. 5280-5283). IEEE. https://doi.org/10.1109/IGARSS.2016.7730375

Mizukami, N., Koren, V., Smith, M., Kingsmill, D., Zhang, Z., Cosgrove, B. and Cui, Z., 2013. The impact of precipitation type discrimination on hydrologic simulation: Rain–snow partitioning derived from HMT-West radar-detected brightband height versus surface temperature data. Journal of Hydrometeorology, 14(4), pp.1139-1158. https://doi.org/10.1175/JHM-D-12-035.1

Moberg, A. and Jones, P.D., 2004. Regional climate model simulations of daily maximum and minimum near-surface temperatures across Europe compared with observed station data 1961–1990. Climate Dynamics, 23(7-8), pp.695-715. https://doi.org/10.1007/s00382-004-0464-3

Montpetit, B., Royer, A., Langlois, A., Cliche, P., Roy, A., Champollion, N., Picard, G., Domine, F. and Obbard, R., 2012. New shortwave infrared albedo measurements for snow specific surface area retrieval. Journal of Glaciology, 58(211), pp.941-952. https://doi.org/10.3189/2012JoG11J248

Mote, P.W., Hamlet, A.F., Clark, M.P. and Lettenmaier, D.P., 2005. Declining mountain snowpack in western North America. Bulletin of the American meteorological Society, 86(1), pp.39-50. https://doi.org/10.1175/BAMS-86-1-39

Molotch, N.P., Blanken, P.D., Williams, M.W., Turnipseed, A.A., Monson, R.K. and Margulis, S.A., 2007. Estimating sublimation of intercepted and sub-canopy snow using eddy covariance systems. Hydrological Processes: An International Journal, 21(12), pp.1567-1575. https://doi.org/10.1002/hyp.6719

Moore, C., Kampf, S., Stone, B. and Richer, E., 2015. A GIS-based method for defining snow zones: application to the western United States. Geocarto International, 30(1), pp.62-81. https://doi.org/10.1080/10106049.2014.885089

Mudryk, L.R., Kushner, P.J., Derksen, C. and Thackeray, C., 2017. Snow cover response to temperature in observational and climate model ensembles. Geophysical Research Letters, 44(2), pp.919-926. https://doi.org/10.1002/2016GL071789

Myers-Smith, I.H., Forbes, B.C., Wilmking, M., Hallinger, M., Lantz, T., Blok, D., Tape, K.D., Macias-Fauria, M., Sass-Klaassen, U., Lévesque, E. and Boudreau, S., 2011. Shrub expansion in tundra ecosystems: dynamics, impacts and research priorities. Environmental Research Letters, 6(4), p.045509. https://doi.org/10.7939/R33K79

Nakicenovic, N. and Swart, R., 2000. Emissions scenarios. Special report of the Intergovernmental panel on climate change.

Nikulin, G., Kjellström, E., Hansson, U.L.F., Strandberg, G. and Ullerstig, A., 2011. Evaluation and future projections of temperature, precipitation and wind extremes over Europe in an ensemble of regional climate simulations. Tellus A: Dynamic Meteorology and Oceanography, 63(1), pp.41-55. https://doi.org/10.1111/j.1600-0870.2010.00466.x

Nolin, A.W., 2010. Recent advances in remote sensing of seasonal snow. Journal of Glaciology, 56(200), pp.1141-1150. https://doi.org/10.3189/002214311796406077

Nolin, A.W. and Dozier, J., 2000. A hyperspectral method for remotely sensing the grain size of snow. Remote sensing of Environment, 74(2), pp.207-216. https://doi.org/10.1016/S0034-4257(00)00111-5

Overland, J.E., Adams, J.M. and Bond, N.A., 1999. Decadal variability of the Aleutian low and its relation to high-latitude circulation. Journal of Climate, 12(5), pp.1542-1548. https://doi.org/10.1175/1520-0442(1999)012<1542:DVOTAL>2.0.CO;2

Overland, J.E., Wang, M., Walsh, J.E. and Stroeve, J.C., 2014. Future Arctic climate changes: Adaptation and mitigation time scales. Earth's Future, 2(2), pp.68-74. https://doi.org/10.1002/2013EF000162

Painter, T.H., Barrett, A.P., Landry, C.C., Neff, J.C., Cassidy, M.P., Lawrence, C.R., McBride, K.E. and Farmer, G.L., 2007. Impact of disturbed desert soils on duration of mountain snow cover. Geophysical Research Letters, 34(12). https://doi.org/10.1029/2007GL030284

Painter, T.H., Deems, J.S., Belnap, J., Hamlet, A.F., Landry, C.C. and Udall, B., 2010. Response of Colorado River runoff to dust radiative forcing in snow. Proceedings of the National Academy of Sciences, 107(40), pp.17125-17130. https://doi.org/10.1073/pnas.0913139107

Painter, T.H., Dozier, J., Roberts, D.A., Davis, R.E. and Green, R.O., 2003. Retrieval of subpixel snow-covered area and grain size from imaging spectrometer data. Remote Sensing of Environment, 85(1), pp.64-77. https://doi.org/10.1016/S0034-4257(02)00187-6

Painter, T.H., Rittger, K., McKenzie, C., Slaughter, P., Davis, R.E. and Dozier, J., 2009. Retrieval of subpixel snow covered area, grain size, and albedo from MODIS. Remote Sensing of Environment, 113(4), pp.868-879. https://doi.org/10.1016/j.rse.2009.01.001

Pearson, R.G., Phillips, S.J., Loranty, M.M., Beck, P.S., Damoulas, T., Knight, S.J. and Goetz, S.J., 2013. Shifts in Arctic vegetation and associated feedbacks under climate change. Nature Climate Change, 3(7), p.673. https://doi.org/10.1038/nclimate1858

Peng, S., Piao, S., Ciais, P., Friedlingstein, P., Zhou, L. and Wang, T., 2013. Change in snow phenology and its potential feedback to temperature in the Northern Hemisphere over the last three decades. Environmental Research Letters, 8(1), p.014008. https://doi.org/10.1088/1748-9326/8/1/014008

Perez, J., Menendez, M., Mendez, F.J. and Losada, I.J., 2014. Evaluating the performance of CMIP3 and CMIP5 global climate models over the north-east Atlantic region. Climate dynamics, 43(9-10), pp.2663-2680. https://doi.org/10.1007/s00382-014-2078-8

Peters, G.P., Andrew, R.M., Boden, T., Canadell, J.G., Ciais, P., Le Quéré, C., Marland, G., Raupach, M.R. and Wilson, C., 2012. The challenge to keep global warming below 2 C. Nature Climate Change, 3(1), p.4. https://doi.org/10.1038/nclimate1783

Pithan, F. and Mauritsen, T., 2014. Arctic amplification dominated by temperature feedbacks in contemporary climate models. Nature Geoscience, 7(3), p.181. https://doi.org/10.1038/ngeo2071

Proksch, M., Löwe, H. and Schneebeli, M., 2015. Density, specific surface area, and correlation length of snow measured by high-resolution penetrometry. Journal of Geophysical Research: Earth Surface, 120(2), pp.346-362. https://doi.org/10.1002/2014JF003266

Putkonen, J. and Roe, G., 2003. Rain-on-snow events impact soil temperatures and affect ungulate survival. Geophysical Research Letters, 30(4). https://doi.org/10.1029/2002GL016326

Qu, X. and Hall, A., 2014. On the persistent spread in snow-albedo feedback. Climate Dynamics, 42(1-2), pp.69-81. https://doi.org/10.1007/s00382-013-1774-0

Rahmstorf, S., 2000. The thermohaline ocean circulation: a system with dangerous thresholds?. Climatic Change, 46(3), pp.247-256. https://doi.org/10.1023/A:1005648404783

Räisänen, J., 2008. Warmer climate: less or more snow?. Climate Dynamics, 30(2-3), pp.307-319. https://doi.org/10.1007/s00382-007-0289-y

Rango, A. and Martinec, J., 1979. Application of a snowmelt-runoff model using Landsat data. Hydrology Research, 10(4), pp.225-238. https://doi.org/10.2166/nh.1979.0006

Rasmus, S., Kivinen, S., Bavay, M. and Heiskanen, J., 2016. Local and regional variability in snow conditions in northern Finland: A reindeer herding perspective. Ambio, 45(4), pp.398-414. https://doi.org/10.1007/s13280-015-0762-5

Rasmus, S., Räisänen, J. and Lehning, M., 2004. Estimating snow conditions in Finland in the late 21st century using the SNOWPACK model with regional climate scenario data as input. Annals of Glaciology, 38, pp.238-244. https://doi.org/10.3189/172756404781814843

Remote Sensing, 2016. https://cone.gollnerfire.com/remote-sensing/

Riggs, G.A., Hall, D.K. and Román, M.O., 2016. MODIS snow products collection 6 user guide. National Snow & Ice Data Center.

Robinson, D.A., Dewey, K.F. and Heim Jr, R.R., 1993. Global snow cover monitoring: An update. Bulletin of the American Meteorological Society, 74(9), pp.1689-1696. https://doi.org/10.1175/1520-0477(1993)074<1689:GSCMAU>2.0.CO;2

Robinson, D.A. and Frei, A., 2000. Seasonal variability of Northern Hemisphere snow extent using visible satellite data. The Professional Geographer, 52(2), pp.307-315. https://doi.org/10.1111/0033-0124.00226

Roeckner, E., Bengtsson, L., Feichter, J., Lelieveld, J. and Rodhe, H., 1999. Transient climate change simulations with a coupled atmosphere–ocean GCM including the tropospheric sulfur cycle. Journal of climate, 12(10), pp.3004-3032. https://doi.org/10.1175/1520-0442(1999)012%3C3004:TCCSWA%3E2.0.CO;2

Roesch, A., 2006. Evaluation of surface albedo and snow cover in AR4 coupled climate models. Journal of Geophysical Research: Atmospheres, 111(D15). https://doi.org/10.1029/2005JD006473

Rummukainen, M., 2010. State-of-the-art with regional climate models. Wiley Interdisciplinary Reviews: Climate Change, 1(1), pp.82-96. https://doi.org/10.1002/wcc.8

Rutter, N., Essery, R., Pomeroy, J., Altimir, N., Andreadis, K., Baker, I., Barr, A., Bartlett, P., Boone, A., Deng, H. and Douville, H., 2009. Evaluation of forest snow processes models (SnowMIP2). Journal of Geophysical Research: Atmospheres, 114(D6). https://doi.org/10.1029/2008JD011063

Saavedra, F.A., Kampf, S.K., Fassnacht, S.R. and Sibold, J.S., 2018. Changes in Andes snow cover from MODIS data, 2000–2016. The Cryosphere, 12(3), pp.1027-1046. https://doi.org/10.5194/tc-12-1027-2018

Sandells, M., Essery, R., Rutter, N., Wake, L., Leppänen, L. and Lemmetyinen, J., 2017. Microstructure representation of snow in coupled snowpack and microwave emission models. The Cryosphere, 11(1), pp.229-246. http://dx.doi.org/10.5194/tc-11-229-2017

Sayer, A.M., Hsu, N.C., Bettenhausen, C., Jeong, M.J. and Meister, G., 2015. Effect of MODIS Terra radiometric calibration improvements on Collection 6 Deep Blue aerosol products: Validation and Terra/Aqua consistency. Journal of Geophysical Research: Atmospheres, 120(23), pp.157-174. https://doi.org/10.1002/2015JD023878

Schaaf, C.B., Gao, F., Strahler, A.H., Lucht, W., Li, X., Tsang, T., Strugnell, N.C., Zhang, X., Jin, Y., Muller, J.P. and Lewis, P., 2002. First operational BRDF, albedo nadir reflectance products from MODIS. Remote sensing of Environment, 83(1-2), pp.135-148. https://doi.org/10.1016/S0034-4257(02)00091-3

Schaffhauser, A., Adams, M., Fromm, R., Jörg, P., Luzi, G., Noferini, L. and Sailer, R., 2008. Remote sensing based retrieval of snow cover properties. Cold Regions Science and Technology, 54(3), pp.164-175. https://doi.org/10.1016/j.coldregions.2008.07.007

Scherrer, S.C., Appenzeller, C. and Laternser, M., 2004. Trends in Swiss Alpine snow days: The role of local-and large-scale climate variability. Geophysical Research Letters, 31(13). https://doi.org/10.1029/2004GL020255

Seidel, F.C., Rittger, K., Skiles, S.M., Molotch, N.P. and Painter, T.H., 2016. Case study of spatial and temporal variability of snow cover, grain size, albedo and radiative forcing in the Sierra Nevada and Rocky Mountain snowpack derived from imaging spectroscopy. The Cryosphere, 10(3). https://doi.org/10.5194/tc-10-1229-2016

Serreze, M.C. and Barry, R.G., 2014. The Arctic climate system. Cambridge University Press.

Serreze, M.C. and Francis, J.A., 2006. The Arctic amplification debate. Climatic change, 76(3-4), pp.241-264.

Shi, H.X. and Wang, C.H., 2015. Projected 21st century changes in snow water equivalent over Northern Hemisphere landmasses from the CMIP5 model ensemble. The Cryosphere, 9(5), pp.1943-1953. https://doi.org/10.5194/tc-9-1943-2015

Shi, J.J., Tao, W.K., Matsui, T., Cifelli, R., Hou, A., Lang, S., Tokay, A., Wang, N.Y., Peters-Lidard, C., Skofronick-Jackson, G. and Rutledge, S., 2010. WRF simulations of the 20–22 January 2007 snow events over eastern Canada: Comparison with in situ and satellite observations. Journal of Applied Meteorology and Climatology, 49(11), pp.2246-2266. https://doi.org/10.1175/2010JAMC2282.1

Shiogama, H., Emori, S., Takahashi, K., Nagashima, T., Ogura, T., Nozawa, T. and Takemura, T., 2010. Emission scenario dependency of precipitation on global warming in the MIROC3. 2 model. Journal of Climate, 23(9), pp.2404-2417. https://doi.org/10.1175/2009JCLI3428.1

Shmakin, A.B., 2010. Climatic characteristics of snow cover over North Eurasia and their change during the last decades. Ice and Snow, 1(1), pp.43-57.

Sihvola, A. and Tiuri, M., 1986. Snow fork for field determination of the density and wetness profiles of a snow pack. IEEE Transactions on Geoscience and Remote Sensing, (5), pp.717-721. https://doi.org/10.1109/TGRS.1986.289619

Singh, P.R. and Gan, T.Y., 2000. Retrieval of snow water equivalent using passive microwave brightness temperature data. Remote Sensing of Environment, 74(2), pp.275-286. https://doi.org/10.1016/S0034-4257(00)00121-8

Skamarock, W.C., Klemp, J.B., Dudhia, J., Gill, D.O., Barker, D.M., Duda, M.G., Huang, X.Y., Wang, W. and Powers, J.G., 2008. A description of the advanced research WRF version 3, NCAR Technical Note. National Center for Atmospheric Research: Boulder, CO, USA.

Skiles, S.M., Flanner, M., Cook, J.M., Dumont, M. and Painter, T.H., 2018. Radiative forcing by light-absorbing particles in snow. Nature Climate Change, p.1. https://doi.org/10.1038/s41558-018-0296-5

Skofronick-Jackson, G.M., Johnson, B.T. and Munchak, S.J., 2013. Detection thresholds of falling snow from satellite-borne active and passive sensors. IEEE Transactions on Geoscience and Remote Sensing, 51(7), pp.4177-4189. https://doi.org/10.1109/TGRS.2012.2227763

Slater, A.G., Schlosser, C.A., Desborough, C.E., Pitman, A.J., Henderson-Sellers, A., Robock, A., Vinnikov, K.Y., Entin, J., Mitchell, K., Chen, F. and Boone, A., 2001. The representation of snow in land surface schemes: Results from PILPS 2 (d). Journal of Hydrometeorology, 2(1), pp.7-25. https://doi.org/10.1175/1525-7541(2001)002<0007:TROSIL>2.0.CO;2

Stähli, M., Stacheder, M., Gustafsson, D., Schlaeger, S., Schneebeli, M. and Brandelik, A., 2004. A new in situ sensor for large-scale snow-cover monitoring. Annals of Glaciology, 38, pp.273-278. https://doi.org/10.3189/172756404781814933

Stamnes, K., Li, W., Eide, H., Aoki, T., Hori, M. and Storvold, R., 2007. ADEOS-II/GLI snow/ice products—Part I: Scientific basis. Remote Sensing of Environment, 111(2-3), pp.258-273. https://doi.org/10.1016/j.rse.2007.03.023

Storvold, R., Malnes, E., Larsen, Y., Høgda, K.A., Hamran, S.E., Mueller, K. and Langley, K.A., 2006. SAR remote sensing of snow parameters in norwegian areas—Current status and future perspective. Journal of Electromagnetic Waves and Applications, 20(13), pp.1751-1759.

Stroeve, J., Box, J.E., Gao, F., Liang, S., Nolin, A. and Schaaf, C., 2005. Accuracy assessment of the MODIS 16-day albedo product for snow: comparisons with Greenland in situ measurements. Remote Sensing of Environment, 94(1), pp.46-60. https://doi.org/10.1016/j.rse.2004.09.001

Stroeve, J., Box, J.E., Wang, Z., Schaaf, C. and Barrett, A., 2013. Re-evaluation of MODIS MCD43 Greenland albedo accuracy and trends. Remote sensing of environment, 138, pp.199-214. https://doi.org/10.1016/j.rse.2013.07.023

Su, F., Duan, X., Chen, D., Hao, Z. and Cuo, L., 2013. Evaluation of the global climate models in the CMIP5 over the Tibetan Plateau. Journal of Climate, 26(10), pp.3187-3208. https://doi.org/10.1175/JCLI-D-12-00321.1

Sun, Y., Solomon, S., Dai, A. and Portmann, R.W., 2007. How often will it rain?. Journal of Climate, 20(19), pp.4801-4818. https://doi.org/10.1175/JCLI4263.1

Takala, M., Luojus, K., Pulliainen, J., Derksen, C., Lemmetyinen, J., Kärnä, J.P., Koskinen, J. and Bojkov, B., 2011. Estimating northern hemisphere snow water equivalent for climate research through assimilation of space-borne radiometer data and ground-based measurements. Remote Sensing of Environment, 115(12), pp.3517-3529. https://doi.org/10.1016/j.rse.2011.08.014

Taylor, K.E., Stouffer, R.J. and Meehl, G.A., 2012. An overview of CMIP5 and the experiment design. Bulletin of the American Meteorological Society, 93(4), pp.485-498. https://doi.org/10.1175/BAMS-D-11-00094.1

Tedesco, M., 2015. Remote sensing of the cryosphere. John Wiley & Sons.

Tedesco, M. and Miller, J., 2007. Observations and statistical analysis of combined active–passive microwave space-borne data and snow depth at large spatial scales. Remote Sensing of Environment, 111(2-3), pp.382-397. https://doi.org/10.1016/j.rse.2007.04.019

Tedesco, M. and Monaghan, A.J., 2009. An updated Antarctic melt record through 2009 and its linkages to high-latitude and tropical climate variability. Geophysical Research Letters, 36(18). https://doi.org/10.1029/2009GL039186

Thackeray, C.W. and Fletcher, C.G., 2016. Snow albedo feedback: Current knowledge, importance, outstanding issues and future directions. Progress in Physical Geography, 40(3), pp.392-408. https://doi.org/10.1177/0309133315620999

Trujillo, E., Molotch, N.P., Goulden, M.L., Kelly, A.E. and Bales, R.C., 2012. Elevation-dependent influence of snow accumulation on forest greening. Nature Geoscience, 5(10), p.705. https://doi.org/10.1038/ngeo1571

Urban, M., Forkel, M., Eberle, J., Hüttich, C., Schmullius, C. and Herold, M., 2014. Pan-Arctic climate and land cover trends derived from multi-variate and multi-scale analyses (1981–2012). Remote Sensing, 6(3), pp.2296-2316. https://doi.org/10.3390/rs6032296

Vajda, A., Venalainen, A., Hanninen, P. and Sutinen, R., 2006. Effect of vegetation on snow cover at the northern timberline: a case study in Finnish Lapland. Silva Fennica, 40(2), p.195. https://doi.org/10.14214/sf.338

Van Vuuren, D.P., Edmonds, J., Kainuma, M., Riahi, K., Thomson, A., Hibbard, K., Hurtt, G.C., Kram, T., Krey, V., Lamarque, J.F. and Masui, T., 2011. The representative concentration pathways: an overview. Climatic change, 109(1-2), p.5. https://doi.org/10.1007/s10584-011-0148-z

Varhola, A., Coops, N.C., Weiler, M. and Moore, R.D., 2010. Forest canopy effects on snow accumulation and ablation: An integrative review of empirical results. Journal of Hydrology, 392(3-4), pp.219-233. https://doi.org/10.1016/j.jhydrol.2010.08.009

Vavrus, S., 2007. The role of terrestrial snow cover in the climate system. Climate Dynamics, 29(1), pp.73-88. https://doi.org/10.1007/s00382-007-0226-0

Venäläinen, A., Salo, T. and Fortelius, C., 2005. The use of numerical weather forecast model predictions as a source of data for irrigation modelling. Meteorological Applications, 12(4), pp.307-318. https://doi.org/10.1017/S135048270500188X

Viterbo, P. and Betts, A.K., 1999. Impact on ECMWF forecasts of changes to the albedo of the boreal forests in the presence of snow. Journal of Geophysical Research: Atmospheres, 104(D22), pp.27803-27810. https://doi.org/10.1029/1998JD200076

Walland, D.J. and Simmonds, I., 1997. Association between modes of variability of January Northern Hemisphere snow cover and circulation. Theoretical and applied climatology, 58(3-4), pp.197-210. https://doi.org/10.1007/BF00865020

Walsh, J.E., Anisimov, O., Hagen, J.O.M., Jakobsson, T., Oerlemans, J., Prowse, T.D., Romanovsky, V., Savelieva, N., Serreze, M., Shiklomanov, I. and Solomon, S., 2005. Cryosphere and hydrology. Arctic Climate Impacts Assessment, ACIA, C. Symon, L. Arris and B. Heal, Eds.

Wang, D., Morton, D., Masek, J., Wu, A., Nagol, J., Xiong, X., Levy, R., Vermote, E. and Wolfe, R., 2012. Impact of sensor degradation on the MODIS NDVI time series. Remote Sensing of Environment, 119, pp.55-61. https://doi.org/10.1016/j.rse.2011.12.001

Wang, L., Koike, T., Yang, K., Jackson, T.J., Bindlish, R. and Yang, D., 2009. Development of a distributed biosphere hydrological model and its evaluation with the Southern Great Plains Experiments (SGP97 and SGP99). Journal of Geophysical Research: Atmospheres, 114(D8). https://doi.org/10.1029/2008JD010800

Wang, H., Yu, E. and Yang, S., 2011. An exceptionally heavy snowfall in Northeast China: Large-scale circulation anomalies and hindcast of the NCAR WRF model. Meteorology and Atmospheric Physics, 113(1-2), pp.11-25. https://doi.org/10.1007/s00703-011-0147-7

Wang, X. and Xie, H., 2009. New methods for studying the spatiotemporal variation of snow cover based on combination products of MODIS Terra and Aqua. Journal of hydrology, 371(1-4), pp.192-200. https://doi.org/10.1016/j.jhydrol.2009.03.028

Watanabe, M. and Nitta, T., 1999. Decadal changes in the atmospheric circulation and associated surface climate variations in the Northern Hemisphere winter. Journal of Climate, 12(2), pp.494-510. https://doi.org/10.1175/1520-0442(1999)012%3C0494:DCITAC%3E2.0.CO;2

Weedon, G.P., Gomes, S., Viterbo, P., Shuttleworth, W.J., Blyth, E., Österle, H., Adam, J.C., Bellouin, N., Boucher, O. and Best, M., 2011. Creation of the WATCH forcing data and its use to assess global and regional reference crop evaporation over land during the twentieth century. Journal of Hydrometeorology, 12(5), pp.823-848. https://doi.org/10.1175/2011JHM1369.1

Weisman, M.L., Skamarock, W.C. and Klemp, J.B., 1997. The resolution dependence of explicitly modeled convective systems. Monthly Weather Review, 125(4), pp.527-548. https://doi.org/10.1175/1520-0493(1997)125<0527:TRDOEM>2.0.CO;2

Williams, L.D., 1978. Ice-sheet initiation and climatic influences of expanded snow cover in Arctic Canada. Quaternary Research, 10(2), pp.141-149. https://doi.org/10.1016/0033-5894(78)90097-2

Winstral, A., Elder, K. and Davis, R.E., 2002. Spatial snow modeling of wind-redistributed snow using terrain-based parameters. Journal of hydrometeorology, 3(5), pp.524-538. https://doi.org/10.1175/1525-7541(2002)003%3C0524:SSMOWR%3E2.0.CO;2

Wiscombe, W.J. and Warren, S.G., 1980. A model for the spectral albedo of snow. I: Pure snow. Journal of the Atmospheric Sciences, 37(12), pp.2712-2733. https://doi.org/10.1175/1520-0469(1980)037<2712:AMFTSA>2.0.CO;2

Wuttke, S., Seckmeyer, G. and König-Langlo, G., 2006. Measurements of spectral snow albedo at Neumayer, Antarctica. Annales Geophysicae 24. https://doi.org/10.15488/62

Ye, H., Cho, H.R. and Gustafson, P.E., 1998. The changes in Russian winter snow accumulation during 1936–83 and its spatial patterns. Journal of Climate, 11(5), pp.856-863. https://doi.org/10.1175/1520-0442(1998)011%3C0856:TCIRWS%3E2.0.CO;2

Ye, H. and Ellison, M., 2003. Changes in transitional snowfall season length in northern Eurasia. Geophysical Research Letters, 30(5). https://doi.org/10.1029/2003GL016873

Yeo, S.R., Kim, W. and Kim, K.Y., 2017. Eurasian snow cover variability in relation to warming trend and Arctic Oscillation. Climate dynamics, 48(1-2), pp.499-511. https://doi.org/10.1007/s00382-016-3089-4

Yin, L., Fu, R., Shevliakova, E. and Dickinson, R.E., 2013. How well can CMIP5 simulate precipitation and its controlling processes over tropical South America?. Climate Dynamics, 41(11-12), pp.3127-3143. https://doi.org/10.1007/s00382-012-1582-y

Zege, E.P., Katsev, I.L., Malinka, A.V., Prikhach, A.S., Heygster, G. and Wiebe, H., 2011. Algorithm for retrieval of the effective snow grain size and pollution amount from satellite measurements. Remote Sensing of Environment, 115(10), pp.2674-2685. https://doi.org/10.1016/j.rse.2011.06.001

Zhang, M., Lai, Y., Liu, Z. and Gao, Z., 2005. Nonlinear analysis for the cooling effect of Qinghai-Tibetan railway embankment with different structures in permafrost regions. Cold Regions Science and Technology, 42(3), pp.237-249. https://doi.org/10.1016/j.coldregions.2005.02.003

Zhong, X., Zhang, T., Kang, S., Wang, K., Zheng, L., Hu, Y. and Wang, H., 2018. Spatiotemporal variability of snow depth across the Eurasian continent from 1966 to 2012. The Cryosphere, 12(1), p.227. https://doi.org/10.5194/tc-12-227-2018

Zhuravleva, T.B. and Kokhanovsky, A.A., 2011. Influence of surface roughness on the reflective properties of snow. Journal of Quantitative Spectroscopy and Radiative Transfer, 112(8), pp.1353-1368. https://doi.org/10.1016/j.jqsrt.2011.01.004

Chapter 3
Fieldwork results and MODIS validation

In this chapter, I discuss my two field seasons and present the results of my work in Arctic Russia. This chapter is divided into two parts. In the first part, the various snow parameters measured in the field are discussed, and the relationships between these different parameters are analysed. In the second part, field albedo measurements are used to ground truth the MODerate resolution Imaging Spectroradiometer (MODIS) snow products.

3.1 Introduction

Snow has a crucial impact on both human environments and natural ecosystems (Jones et al., 2001; Armstrong and Brun, 2008), and as a result the study of snow has been part of human culture for centuries. Biswas (1970) described some of the first known snow measurements, which were recorded in China in the 13th century using snow gauges made of bamboo. Measurements of different snow parameters did not become systematic until the late 19th century (Armstrong and Brun, 2008), with the first snow depth measurements in Russia being made in the 1870s (Barry et al., 1993). Today, snow and climate scientists have access to high-resolution remote sensing data and multi-layer physical snowpack models (e.g. Bartlett and Lehning, 2002). Therefore, in a chapter focussing on field measurements of snow, it is relevant to consider the place of ground measurements in modern snow science.

Ground measurements can be made directly by people or using intermediary instruments. As such, these measurements are subject to human and instrument error, in both calibration and recordings. Another limitation of field measurements is their low temporal and spatial coverage (e.g. Lundberg et al., 2010). Ground measurements, unless automated, can be time-consuming and costly to make and, as a result, the density of measurements in space and time is very low when compared to remote sensing datasets. The spatial density of ground measurements is also highly region-dependent. For example, a much greater number of snow pit data are available in the Swiss Alps than in an equivalent-sized area in the Arctic, as a result of the easier access and financial incentives provided by the tourism industry for measurements to aid the safety of skiers. Automated ground measurements usually have a much higher temporal coverage but must be maintained well in order to avoid increases in measurement errors over time. This maintenance is both costly and adds a constraint regarding where these instruments may be placed, as they must be accessible to technicians. The spatial coverage of automated instruments is further limited by cost, as they are usually left in one location and a large number of instruments must be purchased in order to increase the spatial coverage of available measurements. Due to these various constraints, the number of Arctic field stations is low and their presence has actually decreased since the 1990s (Serreze and Barry, 2014).

However, in spite of their limitations and the significant advances in remote sensing instruments and modelling over the past few decades, snow science still depends heavily on field measurements of snow. Indeed, though human and instrumentation errors do occur in the field, ground measurements are the closest values to "truth" that can be recorded. These errors are understood to be much lower than those of remote sensing instruments or model outputs. Another reason for the necessity of ground measurements is a result of the remaining limitations of remote sensing and modelling. Both of these techniques struggle to either record or model snow in forested areas for example. For this reason, snow studies in highly vegetated or forested environments still rely heavily on ground measurements of the snowpack under trees.

Finally, one of the main reasons why ground measurements are still key in cryospheric science is their role in the validation of remote sensing instruments. Indeed, in order to develop and improve remote sensing algorithms and then assess the accuracy and effectiveness of the associated remote sensing retrievals, "true" measurements on the ground must be made and compared to the remote sensing datasets. This "ground truthing" of remote sensing instruments is a necessary part of using satellite data and has previously been undertaken for the MODIS remote sensing instruments I use here. Importantly, not only snow products, but also general surface albedo, can be retrieved from MODIS data. And though ground truthing of the MODIS retrievals of grain size, albedo and impurities has been performed (e.g. Nolin and Dozier, 2000; Stroeve et al., 2005; Aoki et al., 2007), most of the albedo analyses are not specific to snow products (Liu et al., 2009; Liang et al., 2005). These ground-truthing studies find high correlation coefficients between ground albedo and the MODIS product. For example, studies have undertaken comparisons of MODIS albedo to ground data from Greenland; these found RMSEs of the MODIS albedo product of 0.07 (Stroeve et al., 2005), 0.04 (Liang et al., 2005) and, in a direct validation of the MODIS snow albedo product, 0.067 (Stroeve et al., 2013). However, many of the snow albedo product validation studies use areas with 100 % snow cover, i.e. homogenous pixels (e.g. Stroeve et al., 2013). This is the best way to test the accuracy of the MODIS albedo retrieval algorithm, as the measurements of snow albedo on the ground can be directly compared to the MODIS pixel values. However, in this thesis, MODIS is used to study heterogeneous areas, with less than 100 % snow cover, and so a heterogeneous validation of MODIS is necessary. This is particularly important as previous studies have shown that MODIS does less well with heterogeneous targets (Stroeve et al., 2013). In this project, the MODIS snow datasets were ground truthed over heterogeneous pixels using field measurements made over two field seasons in the Khibiny Mountains of the Kola Peninsula.

In this chapter, methods and results from my two field seasons are described. This is a comprehensive, experimental review of snow parameters in the region with the aim of giving an insight into the variability of snow in the region as well as adequately describing the dataset collected as part of this thesis. In section 3.2, details of the two field seasons undertaken for this project are given, as well as the methods used in the field to make snow parameter measurements, the processing of the albedo field measurements and the methods developed for the ground truthing of MODIS data over the Khibiny mountains. Section 3.3 will present the results of this work, showing both the behaviour of the range of

snow parameters measured over the course of the field seasons as well as the results of the ground truthing process.

3.2 Data collection and methods

3.2.1 Field seasons

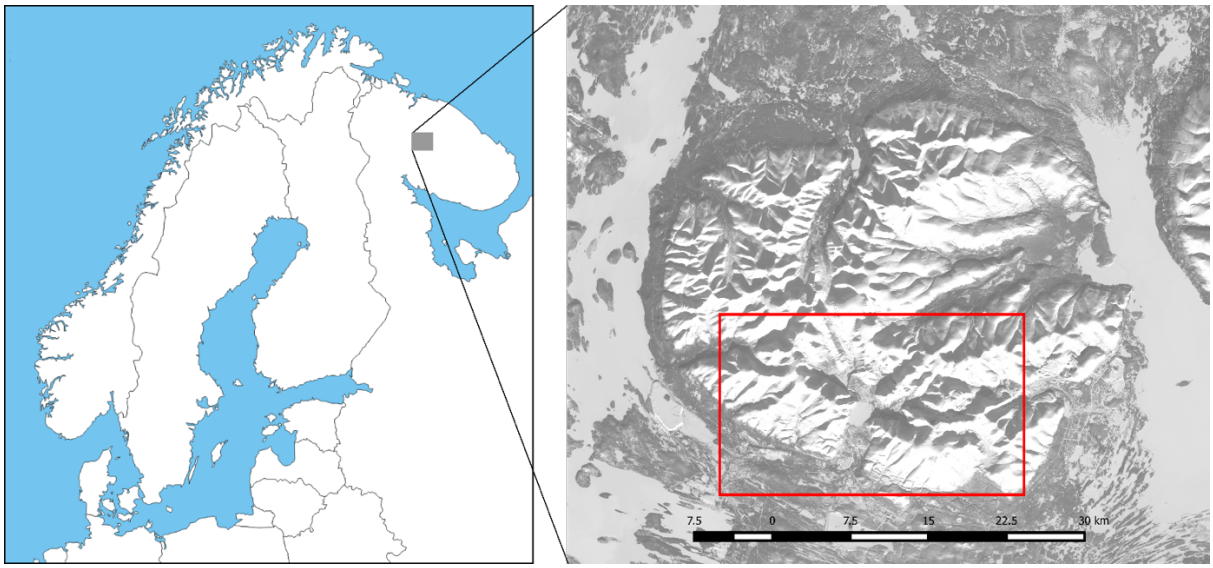

Figure 3.1: Location of the Khibiny Mountains in Russia; the red outline on the Landsat image shows the field research area.

Ground data were collected in the Khibiny Mountains of the Kola Peninsula (see Fig. 3.1), Arctic Russia, in 2016 and 2017. The two field seasons were undertaken in spring, in April and May of both years. The first data collection lasted 41 days and the second was 30 days long. I undertook this work with a field assistant from the British Antarctic Survey, Dr Iain Rudkin. We were based at the Khibiny Educational and Scientific Station of the Moscow State University Geography department. Dr Gareth Rees was present for the first two days of the 2016 expedition, during which we undertook the reconnaissance of the area in order to select the measurement areas (see Fig. 3.2). One of the main safety concerns of this fieldwork was the high avalanche risk in the mountains. We were nevertheless able to find many workable areas that could be accessed without avalanche risk. Some of these field areas were extended (B, F and G) and one abandoned (E) during the rest of the 2016 season, and a new area (H) was added in 2017 (Fig. 3.2). The structure of the work was the following: each day, Iain and I would hike out to make measurements in the mountains before returning to the station each night. Measurements were made in valleys, along slopes and on mountaintops in snow pits in the southern part of the Khibiny Mountains (see Fig. 3.1). The snow parameters measured were: snow cover, albedo, depth, density, surface grain-size and shape, as well as both air and snow temperature (surface and temperature profiles).

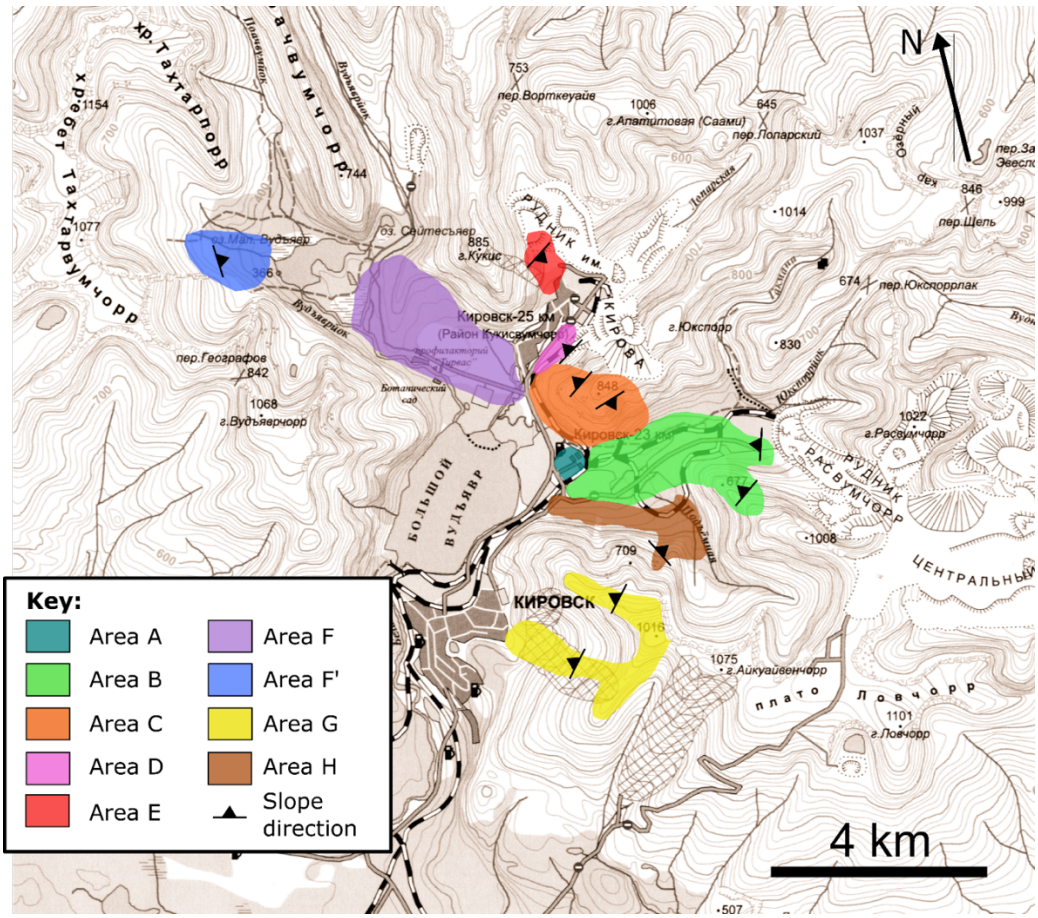

Figure 3.2: Distribution of the different areas visited in the field for measurement collection.

Area	Air Temperature		Albedo		Density		Depth		Grain size		Snow Temperature	
	S1	S2	S1	S2	S1	S2	S1	S2	S1	S2	S1	S2
A	32	29	24	5	32	30	32	30	32	30	32	30
B	34	31	30	12	36	21	36	31	36	31	34	31
C	20	12	16	0	20	9	21	13	20	13	20	13
D	5	4	3	0	5	2	5	4	5	4	5	4
E	13	0	10	0	13	0	13	0	13	0	13	0
F & F’	36	50	28	4	36	12	37	50	36	50	36	50
G	25	16	18	0	25	8	25	17	25	16	25	16
H	0	40	0	12	0	14	0	40	0	40	0	40

Table 3.1: Number of snow parameter measurements in regions A to H in the 2016 (season 1 – S1) and 2017 field seasons (season 2 – S2).

Table 3.1 shows the number of measurements of each snow parameter for each of the nine areas of measurement collection (Fig. 3.2). Timelines of the field seasons are included in the Appendix and show the frequency with which the areas were visited. The expeditions were a success in terms of the data collection, accessibility of the region and its weather; however, there were some limitations and issues that bear mentioning. I was only able to access a 1:100 000 map; anything at a higher resolution

was kept from us because of Russian secrecy law. Data for area E was only obtained for four weeks due to an access restriction imposed late in the 2016 season. Finally, two instruments were slightly damaged in the field: a thermometer in 2016 and a radiometer in 2017. Temperature measurements were not affected in 2016 as I had a back-up thermometer, but the issues with the radiometer in 2017 led to a lack of measurements for the period until a new measurement methodology was developed (see Section 3.2.1.2).

3.2.1.1 2016 field season

The 2016 field season was undertaken between 09/04 and 21/05. Despite some very low temperatures and many days warm enough for it to rain, the weather was always good enough for us to be able to work outside all day. Only two rest days were taken over the six weeks of data collection. In total, we were able to collect data at 169 snow pits, the deepest of which was 290 cm.

3.2.1.2 2017 field season

In 2017, field measurements were made between 16/04 and 15/5. The weather in 2017 was characterised by heavy snowfall for most of the season. This hindered albedo measurements quite significantly, due to the fact that the radiometer could not be used while it was snowing as it could be damaged. However, the weather was not sufficiently bad to prevent us making snow pit measurements, so we were still able to collect a large amount of data. We made measurements at 187 snow pits over 30 days, thus collecting more snow parameter data (excluding albedo) than in the 2016 season. This was a result of three factors. Firstly, having worked as a team before, Iain and I were able to divide the work to maximise productivity. We were making the same measurements as the previous year, so we had lots of practice which made for high efficiency during pit measurements. Secondly, as the weather was often bad in terms of visibility and very high winds at high altitudes, we ended up climbing a lot less than the previous year, which meant the time between measurement points was much shorter. Finally, on days when we were able to make albedo measurements, we did not dig all snow pits, favouring albedo readings over density measurements. This saved a lot of time and meant we were able to obtain data at more measurement points.

3.2.2 Snow parameters

Snow parameter measurements were made in snow pits. These were dug all the way to the ground with the clean edge kept facing away from the sun to avoid the temperature increasing rapidly during the measurements. Six different snow parameters were collected: depth, temperature, grain size, grain shape, density and albedo. These were selected as they are key snow characteristics and are commonly recorded in snow studies. A particular emphasis was placed on maximising the number of albedo measurements as these were to be used to ground truth MODIS (see Section 3.2.3).

3.2.2.1 Snow depth

Snow depth was initially measured using a probe. Approximate depth needed to be known in advance in order to evaluate how big the snow pit needed to be made and how many steps to build in. A more precise depth was then marked down once in the pit, using a graduated ruler (pits under 2 m depth) or avalanche probe (pits over 2 m depth). Depth was measured to the nearest centimetre.

3.2.2.2 Temperature

Multiple temperature measurements were made at each field site using a Traceable Waterproof Thermometer. First air temperature, and snow surface temperature were noted. A temperature profile was then recorded for the entirety of the snow pit wall. In 2016, temperature was measured every 5 cm for the top 20 to 30 cm, before moving to 10 cm increments. In 2017, all temperature measurements were made every 10 cm.

3.2.2.3 Snow surface grain size

Snow surface grain size was measured by placing snow grains on a granulometer and comparing their size against the millimetre grid using a hand-lens. In order for the grains not to change shape during the few seconds of observation, the card was pre-cooled by burying it in snow. The grain size was recorded by giving the range in size of the grains or, only when the shape was very uniform, giving the average grain size.

3.2.2.4 Surface grain shape

The grain shape of the snow surface was also recorded. The grain shape was analysed on a mm-gridded card using a hand-lens. The grain shape codes were taken from Fierz et al. (2009)'s classification for seasonal snow on the ground. These data were collected in the field but will not be presented in this chapter.

3.2.2.5 Snow density

Snow density measurements were made along the snow pit walls (see Fig. 3.3). Density was measured by cutting out a known volume of snow from the wall using a custom-made density cutter (96 cm^3 or 250 cm^3) and weighing this volume on an electronic balance, accurate to 0.1 g. In 2016, two density measurements were made for every 5 cm layer using a density cutter 3.5 cm thick (96 cm^3) for the majority of snow pits. For very deep snow pits, the 250 cm^3 cutter was occasionally used every 10 cm for the deepest parts of the pit in order to speed up the time needed for this part of the measurements. In 2017, all measurements were made for every 10 cm layer, with a 5 cm thick cutter (250 cm^3) and, as previously, two measurements were obtained for each layer. This decision was made to increase the speed of snow pit measurements in order to maximise the number of measurement sites.

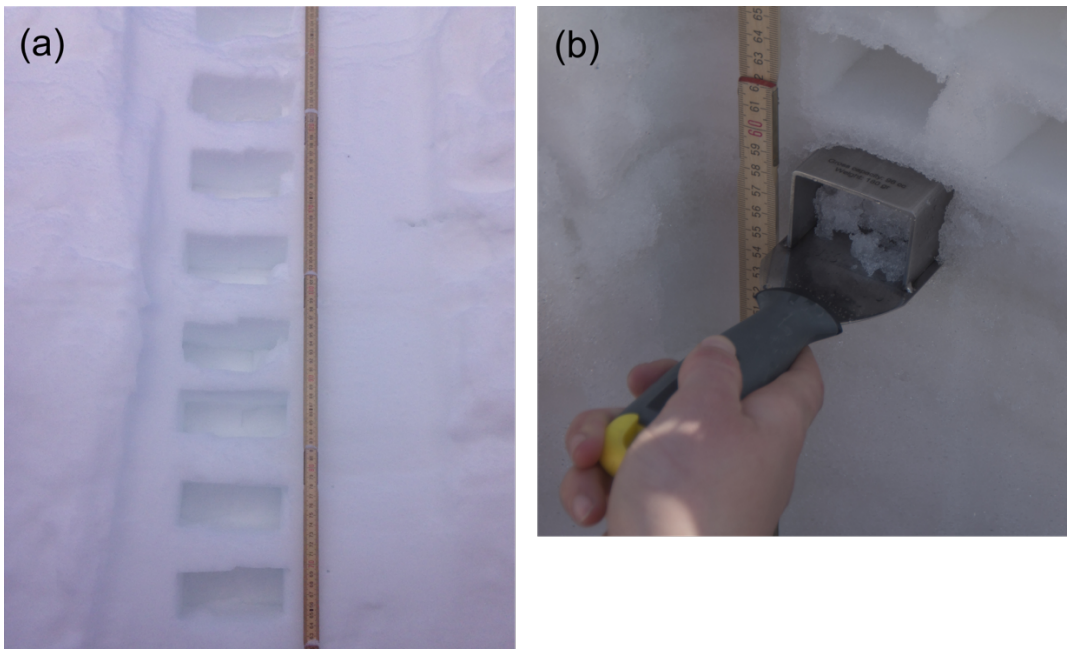

Figure 3.3: Technique for snow density measurements used in the field. (a) spacing of the density measurements in the snow pit wall, and (b) instrument used to extract known volumes of snow. Photo Credit (b): Iain Rudkin.

175

3.2.2.6 Snow surface albedo

Channel number	Band	Centre Wavelength (nm)	Bandwidth (nm)
1	Blue	481	52
2	Green	557	107
3	Red	682	64
4	Infra-Red	845	125

Table 3.2: Skye radiometer details of the four bands recording narrowband albedo.

180 Snow surface albedo measurements were made using a Skye radiometer, Spectrosense 2+ (SKL 910 /2) on a handheld pole lent to me by Dr Olga Tutubalina. This is an automatic data logger that measures incident and reflected radiation in four bands (see Table 3.2). A diffuser was applied to the upward-looking sensor (1 on Fig. 3.4), in order to measure the incident radiation coming from all angles. No diffuser was applied to the downward-looking sensor (2 on Fig. 3.4), in order to measure the radiation
185 reflected from a relatively small area (shown in Fig. 3.4). The narrowband albedo of the snow surface was then calculated from the ratio of these two measurements (see Section 3.2.3.2). The instrument could only be used in dry conditions (not snowing or raining), but measurements were made for all-sky conditions, not only blue-skies.

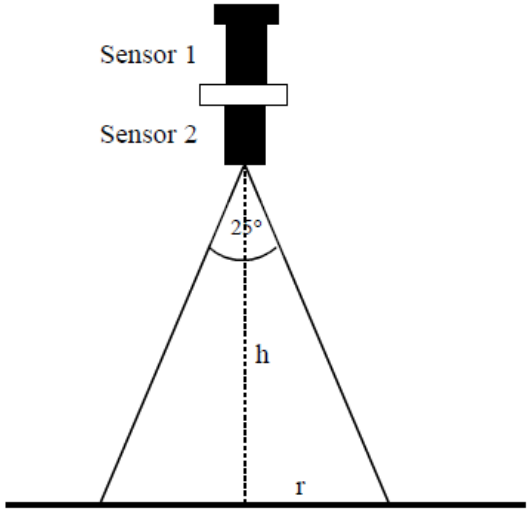

Figure 3.4: Simplified figure showing the two sensors and the angle of measurement on the downward facing sensor of the automatic data logger (from the Skye documentation).

The Skye radiometer was calibrated using a Spectralon reflectance standard before the fieldwork in 2016 and before and after the field season in 2017, by Dr Olga Tutubalina. The second calibration, carried out after the 2017 season, was necessary due to some issues using the radiometer in the field. Indeed, in the first week of the second field season, there was a failure in sensor 2 (Fig. 3.4). This led to a loss of data for the few days it was broken. There was no way to fix these measurements retrospectively. A new methodology was designed to be able to make some measurements over the rest of the season. Sensor 1 (see Figure 3.4) was used to make both the downwelling and upwelling radiation measurements, by physically swapping its position with sensor 2 and reconnecting the cables as required. This could only be done when illumination conditions were stable, because it relied on them staying the same for the 10 seconds it took to swap round the sensors. A combination of this equipment issue and the poor weather conditions led to no albedo measurements being recorded between 19/04/2017 and 08/05/2017.

Figure 3.5: Using the radiometer in the field. Photo Credit: Iain Rudkin.

3.2.3 MODIS ground truthing

3.2.3.1 MODIS data

The satellite data used in this study are the MODIS snow products from both satellites: Terra (MODIS/Terra Snow Cover Daily L3 Global 500m Grid, Version 6) and Aqua (MODIS/Aqua Snow Cover Daily L3 Global 500m Grid, Version 6). The datasets were downloaded from http://reverb.echo.nasa.gov/reverb on 21/02/17. Both the albedo and Normalised Difference Snow Index (NDSI) snow cover products were used for the ground truthing. The NDSI is a snow cover index that is directly related to the presence of snow in a pixel and is a more accurate description of snow detection compared to Fractional Snow Cover (FSC) products (Riggs et al., 2016). NDSI is calculated from MODIS Band 4 (B4) and Band 6 (B6) (see Table 3.3):

(3.1) $NDSI = (B4 - B6) / (B4 + B6)$

MODIS band number	MODIS Band	Centre Wavelength (nm)	Bandwidth (nm)
4	Green	555	20
1	Red	645	50
2	Infra-Red	856.5	37
6	Infra-Red	1640	24

Table 3.3: Band number and wavelength interval of MODIS instrument (from Greuell and Oerlemans, 2004).

Salomonson and Appel (2004) presented the three main equations relating NDSI and FSC, one of which (the Kauffman et al., 2002 equation) relies on corrected surface reflectance values and so cannot be tested with our field measurements. The other two are given in equations 3.2 (Barton et al., 2000) and 3.3 (Salomonson and Appel 2004):

(3.2) $FSC = 0.18 + 0.37 * NDSI + 0.26 * (NDSI)^2$

(3.3) $FSC = 0.06 + 1.21 * NDSI$

The relationships between NDSI and FSC as described by these two equations are presented in Figure 3.6. Since the span of these includes the simple 1:1 correspondence (FSC = NDSI) and because the average of the two equations over the NDSI values measured in the field is close to 1:1, we simply adopt the NDSI as a straightforward proxy for FSC.

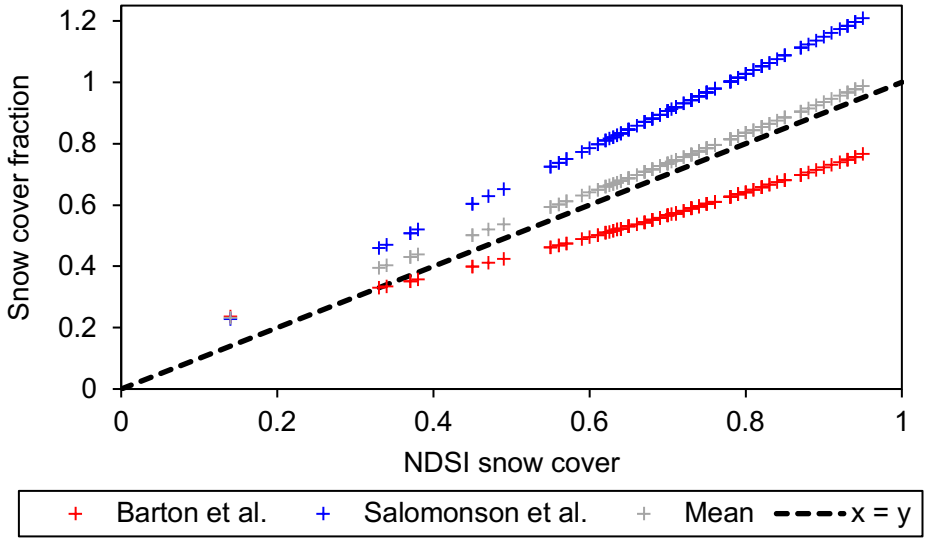

Figure 3.6: Relationship between the NDSI MODIS snow product and the snow cover fraction within the MODIS pixel, as defined by Barton et al. (2000), Salomonson et al. (2004) and the average of these two equations.

3.2.3.2 Narrowband to broadband conversion

MODIS is a remote sensing instrument that obtains data in the visible and near-infrared parts of the electromagnetic spectrum. The MODIS albedo product is given as broadband albedo (BB). The albedo measurements made in Russia were of the narrowband albedo (NB) of the snow in the four bands shown in Table 3.1. In order to ground truth the MODIS snow product, the ground albedo values need to be directly comparable to those recorded by the remote sensing instrument. The ground NB albedo was thus converted to BB. The equations used were from Greuell and Oerlemans (2004), who derived equations specifically for the NB to BB conversion for measurements of glacier ice and snow, based on modelling. These were preferred over those published by Liang (2000), as the latter were calculated to fit all surfaces, and so do not match snow as well as equations derived specifically for cryospheric applications. Two of the Greuell and Oerlemans (2004) equations are shown as equations 3.4 and 3.5. Both of these should give similar results for broadband albedo and the equation number to be used should be selected based on the bands of the NB measurement. The bands of the Skye radiometer matched those of Landsat TM and ETM+ sensors, and are thus slightly broader than the MODIS bands, but there is a good match between the two nevertheless. The equations for the NB to BB conversion that have been developed for MODIS (3.4 and 3.5) are hence applicable to the measurements made with the Skye radiometer.

(3.4) $$\alpha_{BB} = 0.734\ \alpha_{MODIS1} - 0.717\ \alpha^2_{MODIS1} + 0.428\ \alpha^2_{MODIS2} + 0.458\ \alpha^2_{MODIS4}$$

(3.5) $$\alpha_{BB} = 0.714\ \alpha_{MODIS1} - 0.110\ \alpha^2_{MODIS1} + 0.286\ \alpha^2_{MODIS2}$$

The snow BB was calculated for all sites with albedo measurements using both equations 3.4 and 3.5. For the 2016 values, the average difference between the BB albedos calculated using the two equations

is 0.88% and with a median of 0.71 %. This supports the use of the equations interchangeably as suggested by Greuell and Oerlemans (2004).

3.2.3.3 Ground truthing method developed

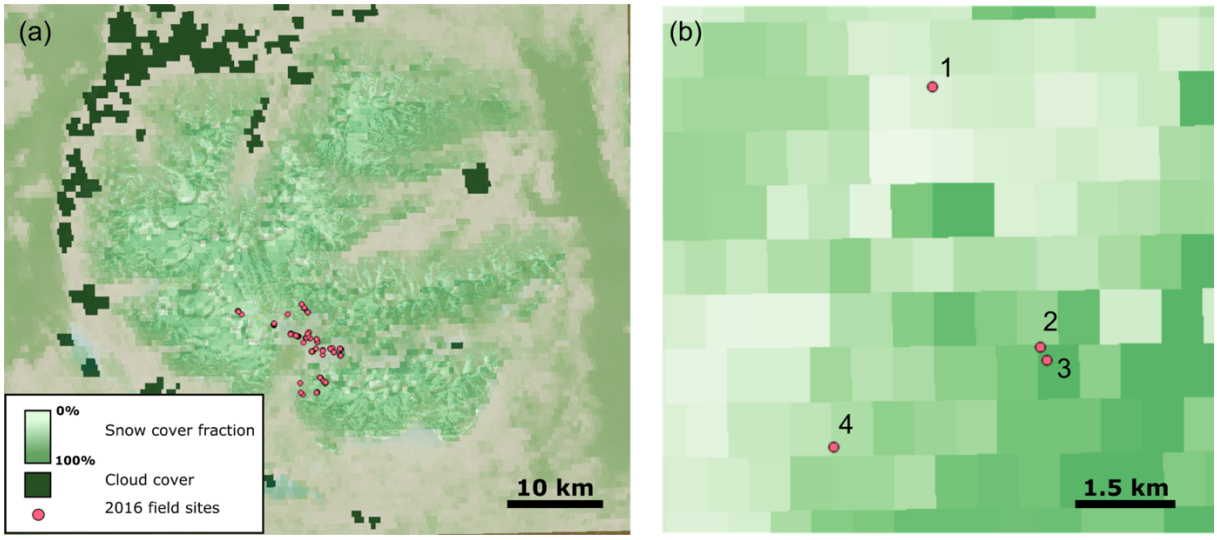

Figure 3.7: MODIS snow cover fraction product on April 15th 2016. (a) all 2016 measurement sites and (b) data points from April 15th 2016 i.e. those used in the ground truthing on this date. Points 1 and 3 are within a MODIS pixel, point 4 is between two pixels and point 2 is between three pixels.

The MODIS data were ground-truthed specifically for the region using the field data. Thus, the MODIS error is determined for the local topography and solar zenith angles typical of the spring season. Both the albedo and NDSI MODIS products were validated. The field measurement sites were overlaid on the appropriate daily MODIS products using the QGIS software (QGIS, 2017), and the albedo value and snow fraction (NDSI value) were then recorded for each site. When a measurement site was located exactly between two or three pixels, all values were noted and the mean of the two or three values was taken (see points 2 and 4 in Fig. 3.7b). When there was cloud cover over the pixel containing the measurement site, it was impossible to compare MODIS and the field data (see Fig.3.7a). This is a result of MODIS being a visible and near-infrared instrument and, as such, it does not "see" through clouds. Table 3.4 shows the total number of measurement sites at which albedo measurements were made and the total number of pixels that were ground truthed using this data. The difference between the two values is due to cloud cover.

All points with both a ground measurement of albedo and values in the MODIS snow products were used as part of the validation (Table 3.4). Stroeve et al. (2013) tested the effects of using clear-sky only ground measurements of albedo, as these are directly comparable to the MODIS products, and found that there is very little difference between the clear-sky and all-sky conditions in the recorded ground albedo. Because of this and in order to maximise the number of measurements, all albedo ground measurements were used for this study regardless of whether they were made in clear-sky or white-sky conditions.

	2016		2017	
Total number of measurement sites		169		187
Total Ground Albedo measurements		129		42
Ground measurements with non-cloudy	Aqua	Terra	Aqua	Terra
MODIS data	43	32	21	22

Table 3.4: Total number of measurement sites in the 2016 and 2017 field seasons; the number of sites at which ground albedo measurements were made, and the total number of Terra and Aqua pixels that could be ground truthed using the field albedo data.

The MODIS NDSI data, used as fractional snow cover data, provide the fraction of snow in a 500×500 m^2 pixel and the albedo product is a mean for the total pixel, not only of the snow. A method was designed to ground truth the MODIS snow products despite this mismatch of scales between the ground measurements and the data products. This combined ground-truthing is possible as the MODIS albedo product is calculated separately from the snow cover fraction product: the algorithms are completely independent (albedo algorithm: Klein and Stroeve, 2002).

Thus:

$$\alpha_{snow}F_{snow} + \alpha_{other}F_{other} = \alpha_{tot} \quad (3.6)$$

$$\alpha_{snow}F_{snow} + \alpha_{other}(1 - F_{snow}) = \alpha_{tot} \quad (3.7)$$

where α_{snow} is the snow albedo measured in the field, F_{snow} the MODIS NDSI product, α_{tot} the albedo of the entire pixel and α_{other} the albedo for non-snow (average of 43 field values).

The value of α_{other} used in this study is based on ground measurements. In the 2017 field season, a total of 43 albedo measurements were made on a variety of non-snow elements including trees, roads, rocks, water and infrastructure. An average of these was taken and used as α_{other}. By using a ground value for the snow and non-snow albedos (α_{snow} and α_{other}), and the fractional snow cover value given by the NDSI MODIS product, the snow albedo of the total pixel could be calculated and compared to the MODIS-derived total pixel albedo. The comparison of these values yields the error in the combined MODIS snow products. Using this method, it is not possible to identify whether the source of the error between the MODIS product and ground measurements was due to the albedo and/or snow cover fraction product. Nevertheless, it is a very useful indicator of how well the algorithms work on heterogeneous pixels.

3.3 Results and discussion

3.3.1 Snow parameter variability

	Mean	Standard deviation	Minimum	Maximum
Ait Temperature (°C)	1.3	3.9	-9.9	13.4
Albedo	0.65	0.15	0.40	0.99
Density (g.cm^{-3})	0.389	0.052	0.263	0.520
Depth (cm)	129	54	0	290
Elevation (m)	450	188	318	1080
Grain size (mm)	0.9	0.6	0.1	3
Snow temperature (°C)	-1.8	2.1	-10.8	0

Table 3.5: Summary of variability of field measurements (five snow parameters, air temperature and site elevation).

In this section, the various snow parameters measured in the field are discussed. Table 3.5 summarizes the variability of the five snow parameters measured in the field as well as the air temperature and elevation of the measurement sites. These demonstrate the high spatial variability of snow over the small (~8 x 10 km) field area. Additionally, due to the importance of the effects of air temperature on snowfall and on the snowpack, the air temperature measurements made over both the 2016 and 2017 field seasons are shown in Figure 3.8. The field seasons were very different and give a rough indication of annual variability in weather and timing of snow melt in the Khibiny Mountains. Thus, the field results indicate high spatial and temporal variability in snow over the mountains.

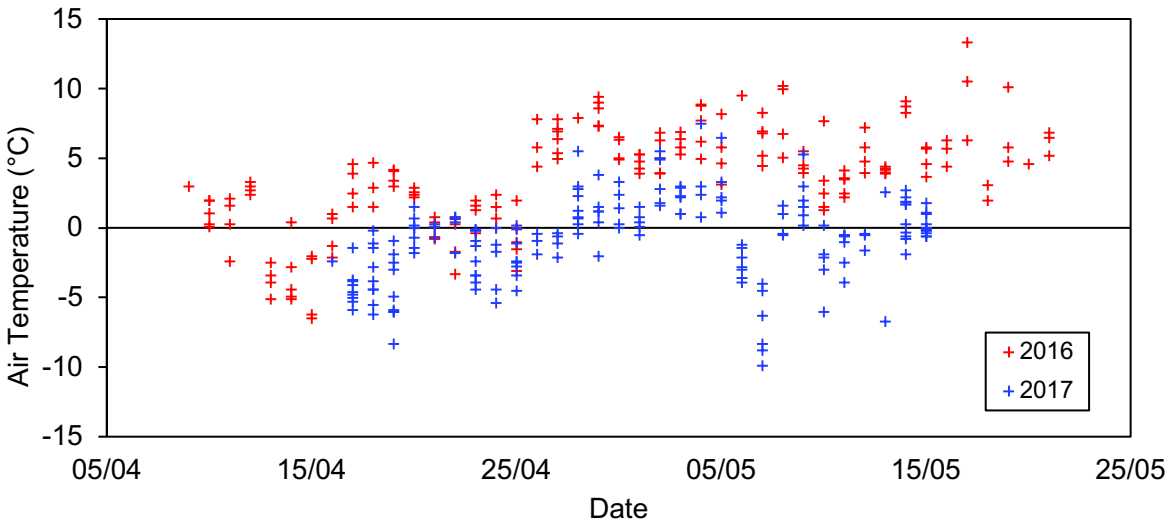

Figure 3.8: Air temperature measurements made over the course of the 2016 and 2017 field seasons.

3.3.2 Snow parameter correlations

Studying the interactions of different snow and weather parameters as well as topography provides an indication of what may promote variability in regional snow. This is useful to our broad understanding of snow in the Khibiny Mountains and will become particularly relevant in Chapter 4, in which past changes in snow in the Western Mountain Regions of the Kola Peninsula are studied. Additionally, two of these snow parameters (albedo and snow depth) are used in two different validation studies, that of MODIS (Section 3.3.4) and WRF (Chapter 5), in this thesis. Checking that these parameters follow expected trends with other variables is useful to gain an indication of the reliability of these observations being used as ground truth.

Spearman's Rank Correlation Test is used to quantify the degree of correlation of variables, by testing whether they are associated by a monotonic function. This test was chosen as it is one of the most basic statistical tests of relationship between variables. This test assumes a null hypothesis that the variables are uncorrelated and proceeds to either prove or disprove this assumption. Two samples are found to be correlated for p values of less than 0.05, equivalent to 95 % confidence that the null hypothesis was not erroneously rejected. A summary of the findings using the Spearman Test is given in Table 3.6 and these are discussed further in the text.

Data included	Snow parameter 1	Snow parameter 2	ρ
All values	Elevation	Snow depth	0.096
2016 only			0.411*
2017 only			-0.008
2017 only	Air Temperature	Snow Surface Temperature	0.717*
All values	Elevation	Snow Density	0.314*

Table 3.6: Results of Spearman's Rank Correlation test on all parameter relationships presented in section 3.3. Statistically significant results of the test are marked with an asterisks: * = $p < 0.5$.

3.3.2.1 Snow depth

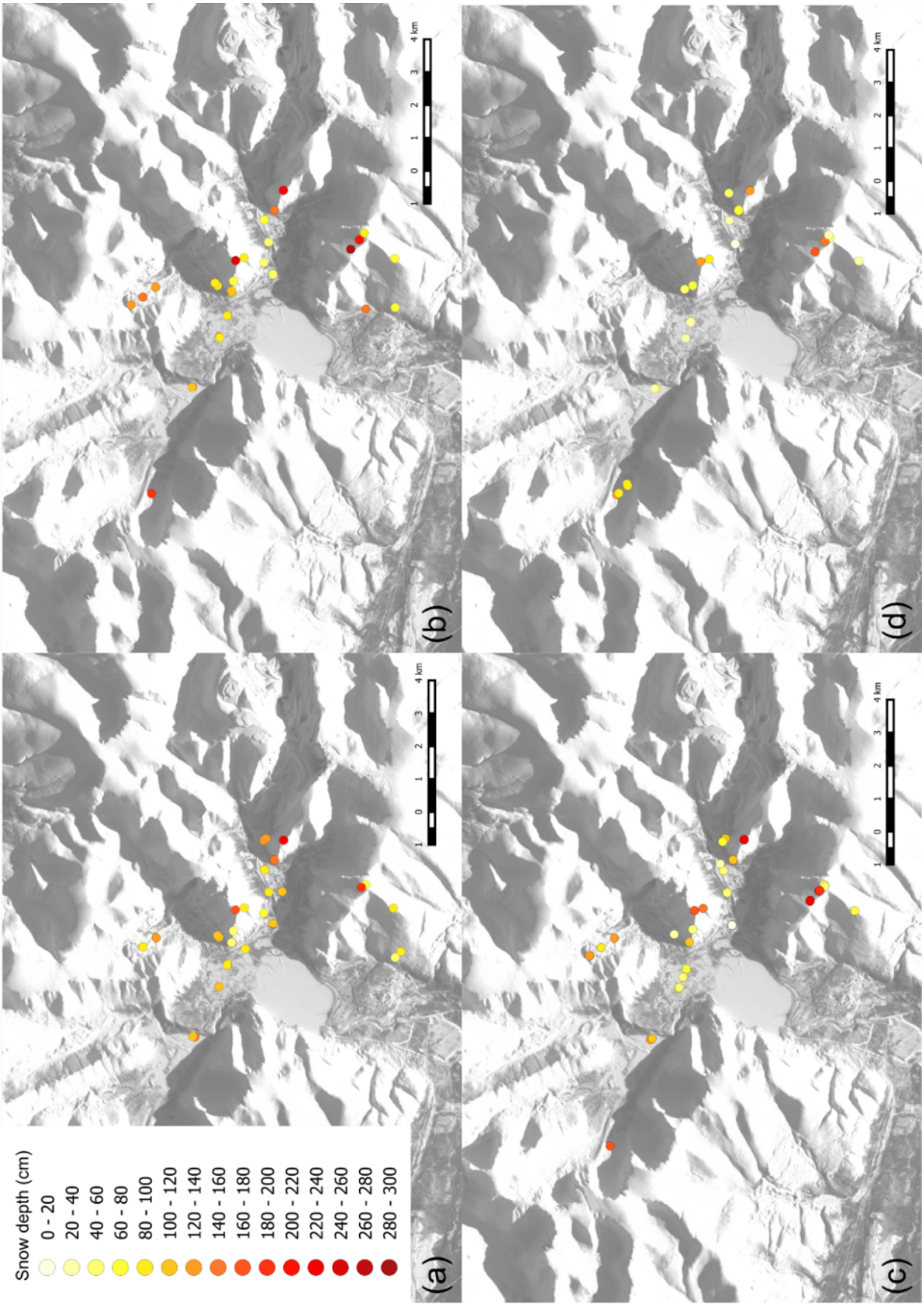

Figure 3.9: Spatial distribution of snow depth over the 2016 field season. Snow depth recorded between (a) April 9th and April 20th; (b) April 21st and April 30th; (c) May 1st and May 10th; (d) May 11th and May 21st.

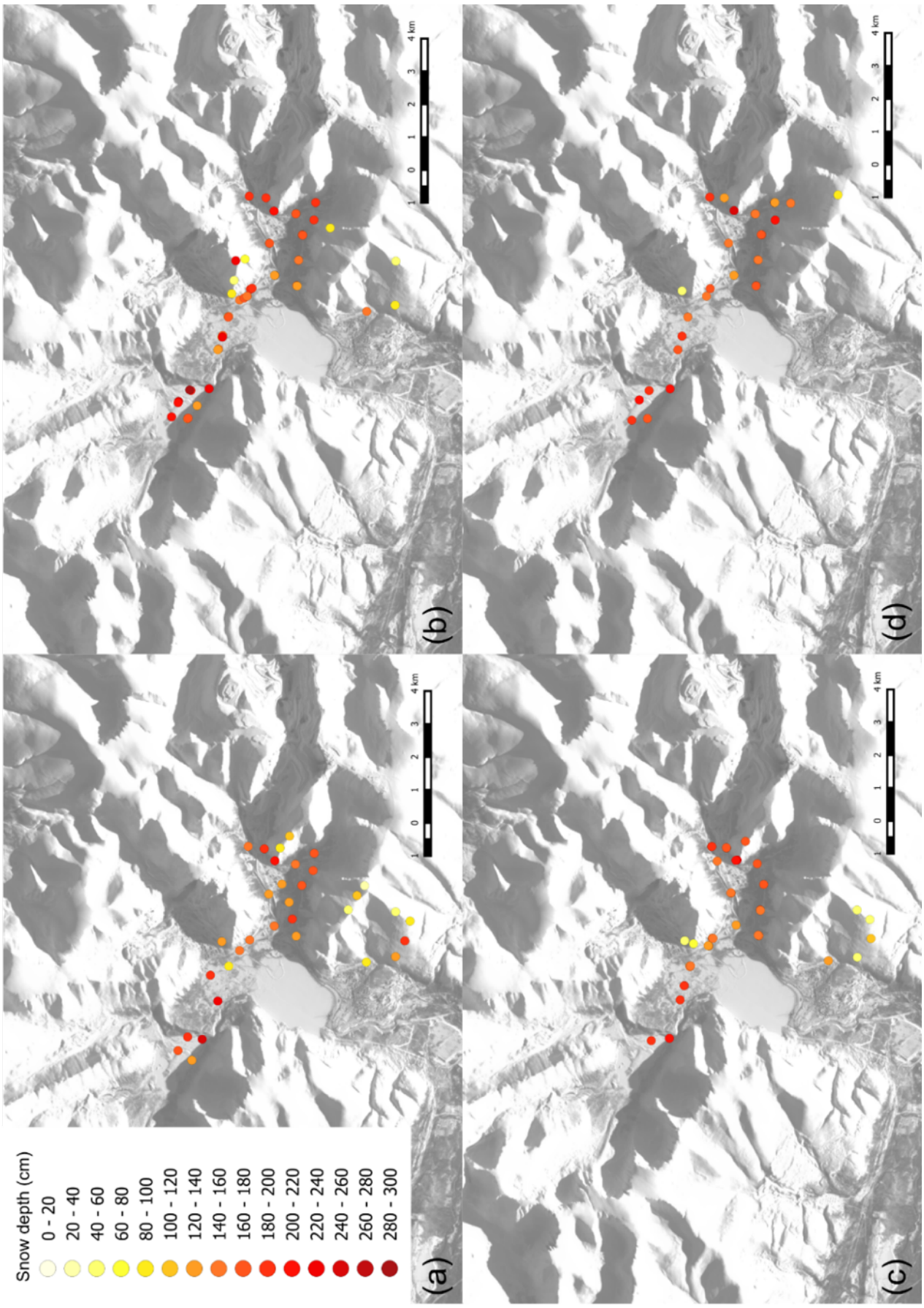

Figure 3.10: Spatial distribution of snow depth over the 2017 field season. Snow depth recorded between (a) April 9th and April 20th; (b) April 21st and April 30th; (c) May 1st and May 10th; (d) May 11th and May 21st.

Figures 3.9 and 3.10 show the distribution of snow depth in the field area over the duration of the two field seasons, with these divided into four time periods of similar lengths. By comparing the two figures, it is clear that overall the 2017 season had greater snow depth across the entire fieldwork area and duration, and that overall snow depth changed more during the 2016 season than in 2017.

Firstly, the changes in snow depth over time during the two field seasons are considered. The snow depth distribution over the field area is very similar across the four time periods of the 2017 season. Indeed, similar snow depths ($\geq$ 150 cm) can be seen in all four subplots in Figure 3.10 and the majority of measured snow depths across all time periods were greater than 100 cm. Overall, mean snow depth increased over the field season with a mean snow depth of 145 cm in the first quarter of the field season and of 162 cm in the final quarter. This is a result of the weather conditions not changing much over the weeks: the air temperatures remained low (see Fig. 3.8) and snowfall continued throughout the season. Contrastingly, the distribution of snow depth over the 2016 field season changes over time. The mean snow depth in the first quarter of the season (Figure 3.9a; 110 cm) is considerably higher than in the final quarter (Figure 3.9d; 86 cm). One clear example is on the sampled mountain furthest east (Area B in Fig. 3.2), with snow depths ranging from 120 cm to 240 cm in both Fig. 3.9a and 3.9b, from 60 to 240 cm in 3.9c and from 40 to 140 cm in the final quarter (May 11th to May 21st).

Typically, the largest snow accumulations are found in gullies and valleys and the lowest are on exposed mountain or hill tops (Woo et al., 1983). Over its entire duration, the 2017 measurements follow the expected trend of having shallower snow on exposed mountain-tops and deeper snow in the large valleys. However, the 2016 field season saw the opposite behaviour whereby ridges on the tops of mountains often represented the deepest snow depths on the maps. Another control on snow depth is the combined effects of slopes and ridge shapes (concave/convex) and wind conditions. Though topography shape was obviously identical between the two field seasons, wind conditions were not. Wind plays a key role in snow distribution in the Khibiny Mountains (Demin, personal communication). The closest station to my field area with wind measurement is Apatitovaya station (67.44 °N, 33.36 °E). This station recorded mean wind speeds of 6.0 m.s^{-1} over my 2016 season and 6.9 m.s^{-1} over my 2017 season. Hence, 2017 was a windier year and this could explain, in part, the difference in snow depths on exposed mountain tops between the two seasons. Another factor to consider when studying snow depth is vegetation, as tree canopies can significantly reduce snow depth by intercepting snowfall. For example, boreal forests may intercept up to 60 % of winter snowfall (Pomeroy and Schmidt, 1993). However, forests do not directly impact the snow depth measurements made in this case study as the measurement sites were selected carefully to be in non-covered areas in order to obtain good albedo measurements.

Finally, in figures 3.10b and 3.10c, the snow depths on south facing slopes appear to be lower than on slopes facing other directions. However, this is not seen across all time periods and in both seasons, so it is not clear whether slope orientation has a significant effect on snow depth.

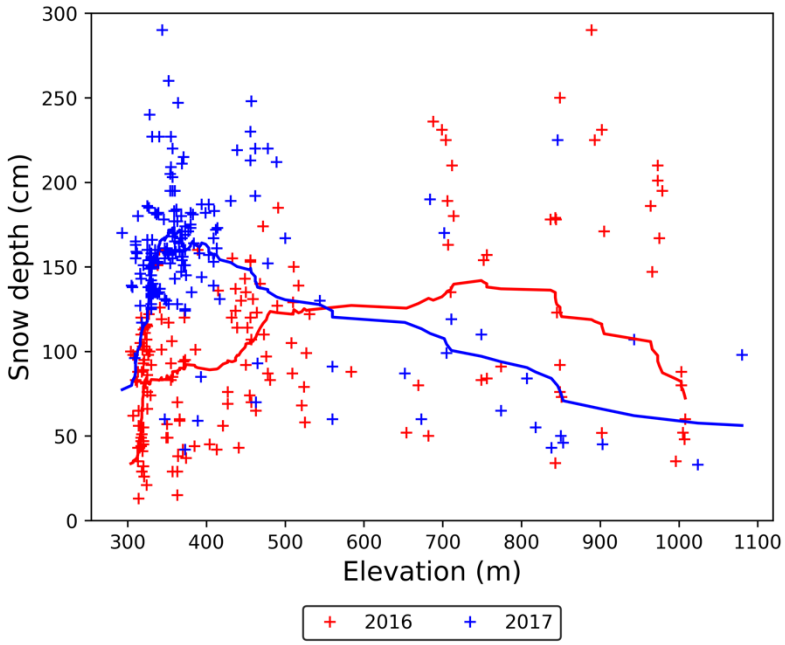

Figure 3.11: Snow depth as a function of elevation of the snow pit measurements of both the 2016 and 2017 field seasons.

Differing relationships between snow depth and elevation are observed in the 2016 and 2017 field seasons. When looking at the results from both field seasons together, snow depth and elevation are found to be uncorrelated ($\rho = 0.096$; p value > 0.05). However, the results from the 2016 season show statistically significant positive correlation between the two variables ($\rho = 0.411$; p value < 0.001). In this first field season, the spread in snow depths is much greater at high altitudes relative to the lower altitudes and snow also reaches much greater depths with increased elevation (Figure 3.11a). The results from the 2017 season indicate that the two variables are uncorrelated ($\rho = -0.008$; p value > 0.05). The weather conditions in 2017 were much worse than in 2016, with very high winds preventing us from making many high-altitude measurements. Thus, the 2017 season sees an underrepresentation of snow depth measurements at high elevations (Figure 3.11b).

Interestingly, the two field seasons have a very different range in snow depth at low elevations, reaching much higher values in 2017 than in 2016. This is a result of two factors. Firstly, 2017 saw a lot of late season snowfall, indeed snow kept falling for the entirety of the collection time. Secondly, the air temperature in the Khibiny Mountains in 2016 had already reached positive values at the start of the field season (see Figure 3.8). It is thus possible that some snow melt had already occurred before the start of the measurement collection in the first field season. Additionally, in 2016, snow depths as low as 0 to 50 cm were recorded. This is due to the fact that snow melted out entirely over the majority of the mountains in 2016, but did not start to melt at all in 2017. Indeed, in 2016, the six weeks of fieldwork coincided with the complete melt out from the lower altitudes and up to the higher altitudes. In contrast, no noticeable melting occurred during our four weeks of fieldwork in 2017.

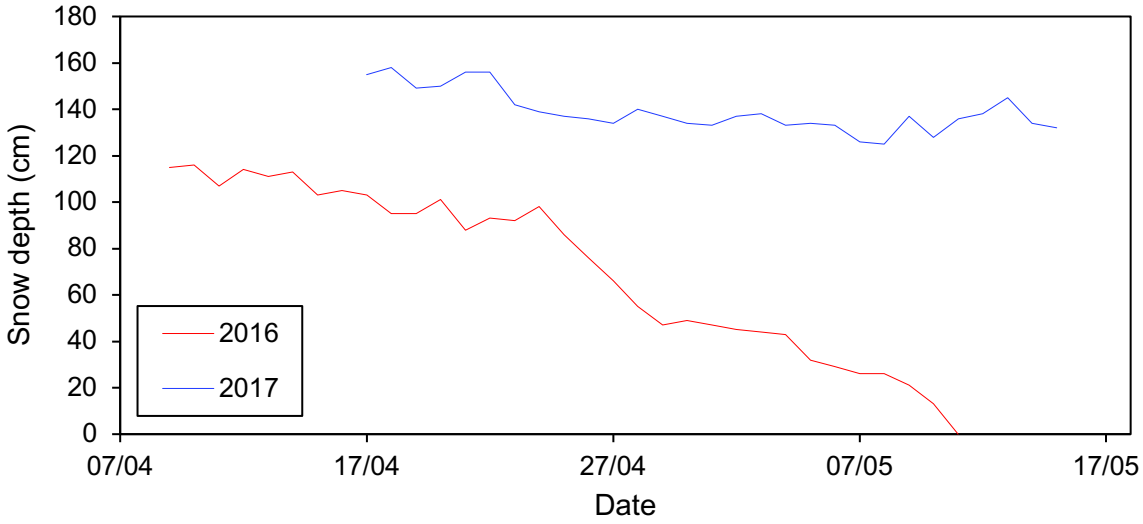

Figure 3.12: Snow depth as a function of time over the 2016 and 2017 field seasons at the MSU Khibiny field station (67.6376 °N, 33.7236 °E).

In both field seasons, measurements of all snow parameters were made at snow pits outside the MSU field station every day or until snow melted out. Figure 3.12 shows the evolution of snow depth there over April and May in the two field seasons. The measurements made in 2016 demonstrate how fast snowmelt occurs in the Khibiny Mountains. At the MSU station, complete meltout of the snowpack occurred over one month, at the longest. If the start of the melt season is taken as the tipping point seen on April 24th, then meltout may have occurred as fast as in 17 days. This fits well with the current understanding of Arctic snow melt wherein, typically, the snowmelt season is short in the Arctic Tundra, usually lasting less than two weeks (Weller et al., 1972). This is a result of the speed-up of snow melt once some bare ground becomes exposed, as this lowers the surface albedo, leading to the ground absorbing more heat, thus melting more snow (Serreze and Barry, 2014).

Figure 3.12 also clearly shows how high inter-annual variability can be in this region. Before the tipping point of the start of the melting on April 24th in the 2016 data, the snow depths of the 2017 snowpack were consistently 50 cm deeper at the same location. Furthermore, as previously discussed, no snow melt was seen in the 2017 field season which points to a minimum of 21 days of inter-annual difference in the start of the snow cover melting period.

3.3.2.2 Snow surface temperature

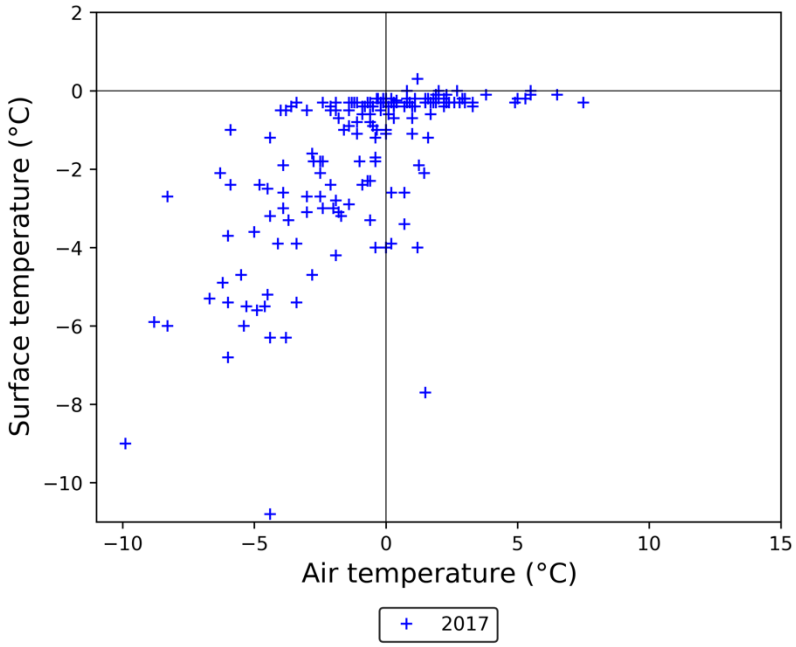

Figure 3.13: Dependence of snow surface temperature on air temperature measured at snow pit sites of the 2017 field season.

Figure 3.13 shows the correlated, positive ($\rho = 0.717$ and p value = < 0.001) relationship between air temperature and snow surface temperature. Only results from the 2017 field season are plotted here as 2016 results were affected by a positive temperature bias in the thermometer. Though the energy balance of an open snowpack is a complex system, these results clearly show that as air temperature increases, so does surface temperature. Here, it is worth considering whether these results fit within our understanding of snowpack systems. The details of the energy and mass balance of a snowpack can be found in Armstrong and Brun (2008). To simplify, radiation exchange dominates the heat exchange at the surface of the snowpack. Diffusion from still air has very little effect on snow surface temperature, however wind (warm or cold) can supply or draw sensible heat from the surface (Jamieson and Shirmer, 2016). This diffusion may explain the relationship between snow surface temperature and air temperature (Fig. 3.13). Thus, these results fit within the general understanding of the energy balance of snow.

3.3.2.3 Snow density

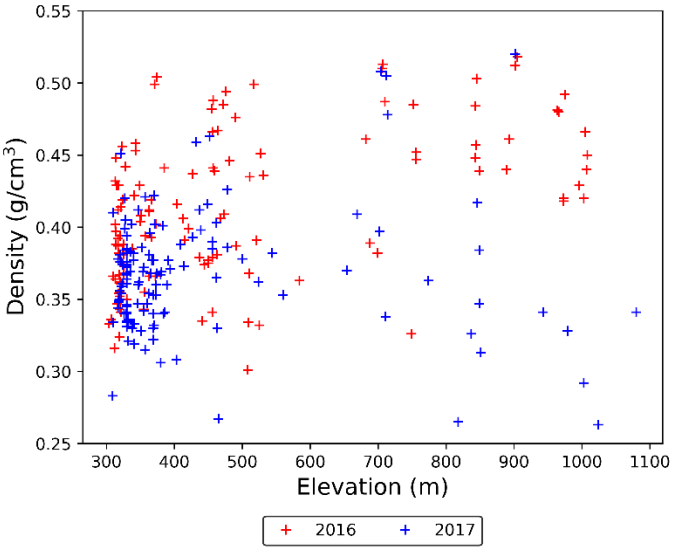

Figure 3.14: Snow density as a function of elevation measured at snow pit sites of both the 2016 and 2017 field seasons.

Figure 3.14 shows the relationship between average snowpack density and the elevation of the measurement site. Snow density and elevation are found to be correlated (p value = < 0.001) with a ρ of 0.314. However, both 2016 and 2017 field seasons sample different parts of the relationship. It appears that in 2016, higher elevations were associated with denser snow: however, in 2017 higher elevations saw a broader range of densities, with the majority of measurements representing lower densities than in 2016. Higher densities occur in warm, wet snow and wind-packed snow (Armstrong and Brun, 2008). The reason for the higher overall density in 2016 is likely a result of higher temperatures and associate snowmelt.

3.3.3 MODIS validation using field results

3.3.3.1 Effect of the value of non-snow albedo

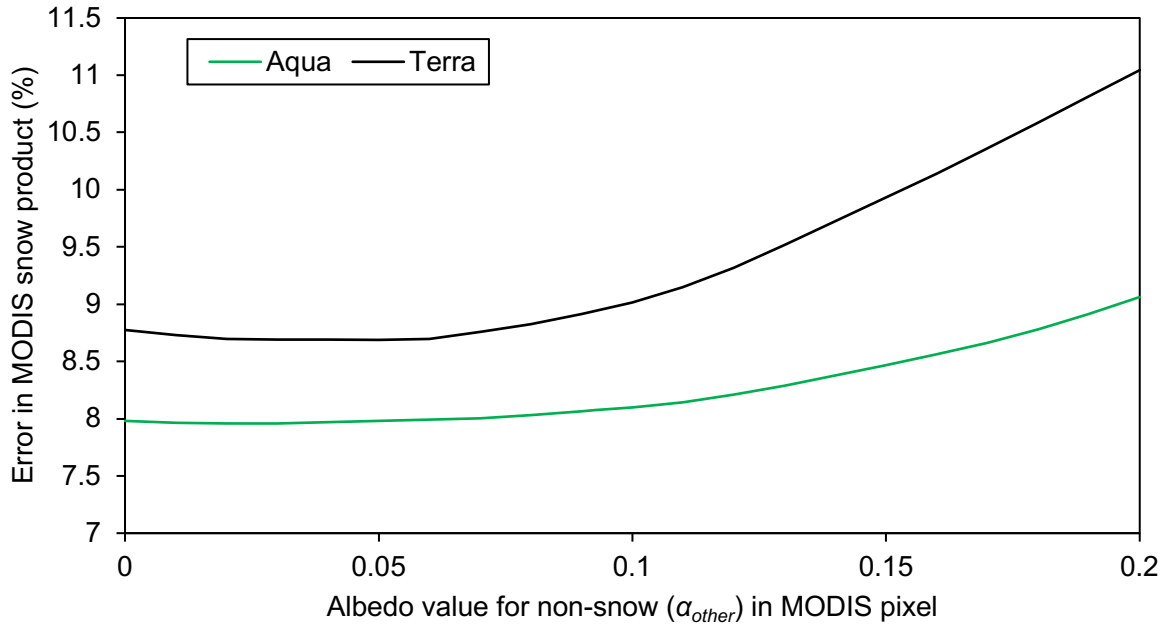

Figure 3.15: Error in the MODIS snow products as a function of the albedo values used for the non-snow component of the MODIS pixel. See equations 3.6 and 3.7.

As described in Section 3.2.3.3, the ground truthing of the MODIS snow data is dependent on a value for the albedo of the non-snow component (α_{other}) used in equation 3.7. In Figure 3.15, the effect of the value used for α_{other} is shown. Between 0 and 0.1 approximately, the value of the α_{other} makes very little difference in the overall error in the MODIS snow products. For values greater than 0.1, the greater the value of α_{other}, the greater the error in MODIS. As discussed in section 3.2.3.3, the non-snow albedo (α_{other}) value used for the calculation of the error in the MODIS snow products is based on ground measurements. The distribution of these measurements is shown in Fig. 3.16. They give an average value for non-snow albedo in the Khibiny region of 0.093. Though there is some spread in these measured values (the higher values reflecting the presence of some snow in the non-snow measurements), the fact that the majority of the values fall under 0.1 means that the values of α_{other} has little impact on the overall MODIS error calculated.

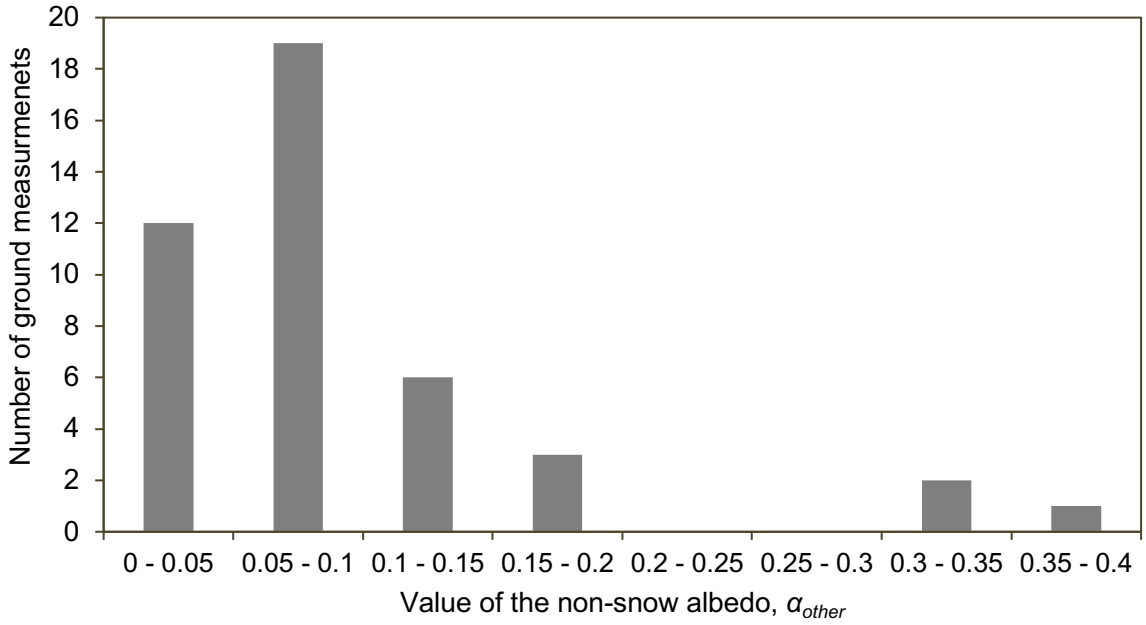

Figure 3.16: Distribution of non-snow albedo values from ground measurements made in 2017 field season.

3.3.3.2 Calculated MODIS error

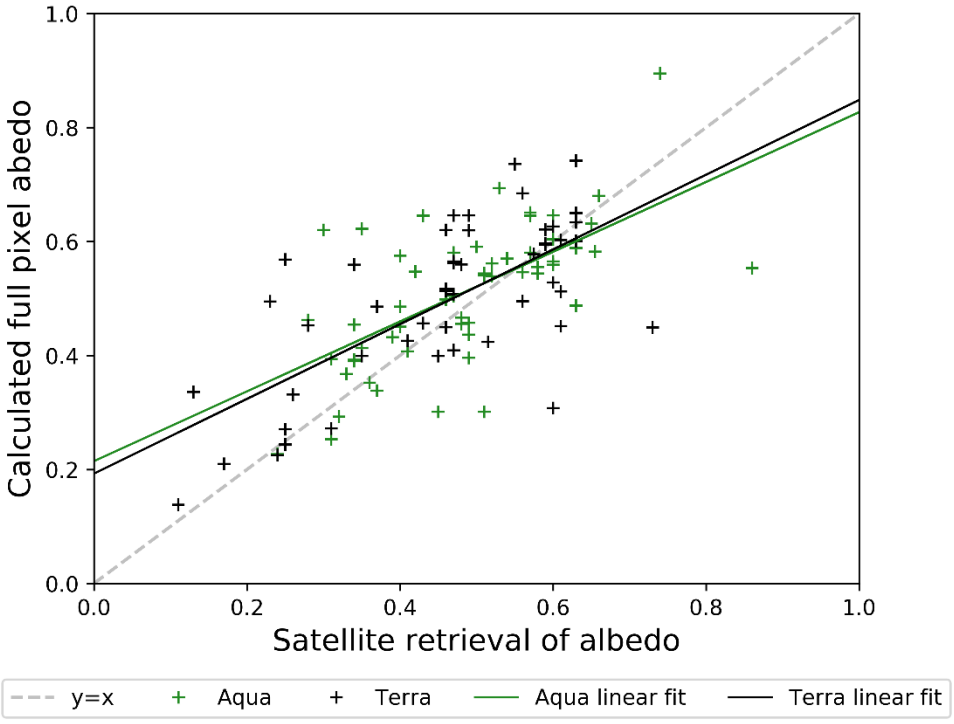

Figure 3.17: Correlation between the MODIS snow albedo product and the full pixel albedo calculated using field point measurements and the MODIS snow fraction dataset.

Using this average value for α_{other} and field values for α_{snow}, full pixel albedo values were calculated and the correlation between the MODIS snow albedo product and the calculated full pixel albedo was tested using linear regression analysis (Fig. 3.17). The Terra and Aqua regression lines have gradients of 0.66 and 0.61, respectively. MODIS tends to slightly underestimate albedo for low total-pixel albedos and

over-estimate albedos for high total-pixel albedos but, overall, the bias in the data is low (0.028 for Aqua and 0.037 for Terra). The RMSEs, determined in this analysis, in the MODIS retrievals from the instruments on the Aqua and Terra satellites are 0.081 and 0.089 respectively (see Table 3.7). These errors are of the same order of magnitude as those found in homogenous pixel studies (e.g. Stroeve et al., 2013). As the errors are low (less than 10 % on average), the MODIS snow products can be used reliably in the subsequent analysis of snow cover.

It is interesting to consider why the Terra MODIS retrievals consistently underperform compared to the Aqua retrievals in these results. Casey et al. (2017) found that since the MODIS calibration update in 2014, increasing Terra-Aqua discrepancies have appeared in the MODIS version 6 data. This more recent update was not able to sufficiently correct the calibration issues resulting from the large degradation of the solar diffuser (Lyapustin et al., 2014). This long-term drift in calibration, more pronounced in the Terra instrument, could explain the difference in errors between the Terra and Aqua satellite retrievals.

	Aqua	Terra
Total number of points ground truthed	62	43
RMSE – all values	0.0807	0.0894
RMSE - 2016 values	0.0702	0.0895
RMSE - 2017 values	0.0982	0.0894

Table 3.7: Number of data points used in the ground truthing, overall (2016 & 2017) RMSE and respective 2016 and 2017 RMSEs of the Aqua and Terra albedo retrievals.

3.3.3.3 Effects of solar zenith angle on albedo

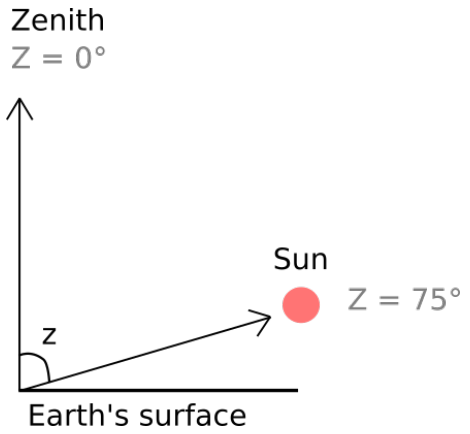

Figure 3.18: Schematic showing the definition of the Solar Zenith Angle (Z on the figure).

It is commonly agreed that the Solar Zenith Angle (SZA; see Fig. 3.18) at the time of measurement has a high impact on the reliability of albedo measurements. Higher SZAs impact albedo retrievals as a result of the associated decreases in solar radiation and signal-to-noise ratio. Many studies have shown

that with SZA higher than 70 - 75 º degrees, MODIS albedo products become unreliable (e.g. Stroeve et al., 2005). Wang and Zender (2010) found that the accuracy of the MODIS retrievals starts to deteriorate for SZA > 55 º and become physically unrealistic above 65 º. However, later studies directly addressed this paper (Schaaf et al., 2011; Stroeve et al., 2013) and demonstrated that Wang and Zender (2010) ignored quality flags in their analysis and their conclusions could not be applied to high-quality MODIS retrievals. Additionally, Stroeve et al. (2013) demonstrated realistic and accurate MODIS retrievals for SZA as high as 75 º at 17 stations in Greenland. For this reason, the error of the MODIS snow products should be calculated only for points with SZA less than 75 º.

As my field seasons took place in April and May, all the field measurements were made for SZA values under 70º, so all can be used in the validation of MODIS (Fig. 3.19). In this project, only testing the accuracy of MODIS at these lower angles is valid, as the main use of this MODIS data is to study the start and end dates of the snow season (see Chapter 4). These fall within the March to October interval which have lower solar zenith angles, so all the retrievals in this time will be of the accuracy found for SZA < 75 º. The effects of SZA on the error in the MODIS retrieval over the field season are shown in Fig. 3.20. There is no clear relationship between SZA and the accuracy of the MODIS retrievals; using Spearman's rank correlation test, it is shown that these samples are uncorrelated ($\rho = 0.105$; p value = > 0.05). However, my results support the work of Stroeve et al. (2013) and show that MODIS retrievals for SZA > 65 º are not physically unrealistic. Indeed, all but one measurement point for SZA > 65 º have errors of less than 9 % and one of the lowest individual retrieval errors of the entire field season (0.25 %) is for a measurement with 66.6 º SZA (Fig. 3.20).

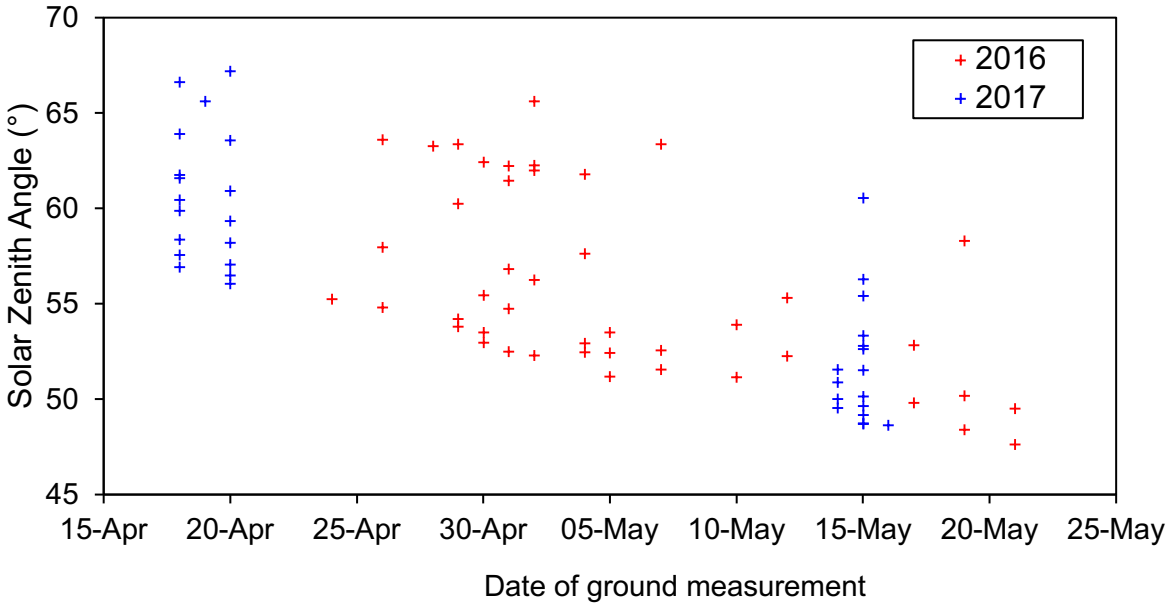

Figure 3.19: Solar Zenith Angles of all ground measurements used in ground truthing as a function of the date the ground measurement was made.

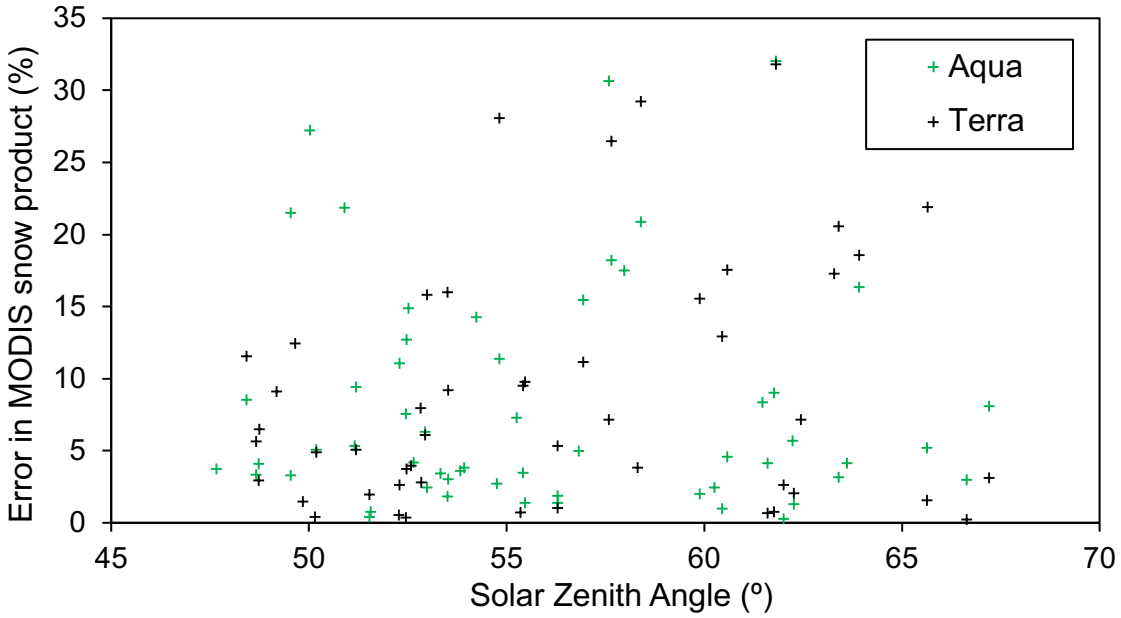

Figure 3.20: Error in the MODIS snow product as a function of Solar Zenith Angles.

3.3.3.4 Effects of elevation on MODIS retrieval accuracy

Previous studies have suggested that MODIS retrievals are less accurate at high elevations (Stroeve et al., 2005; Liang et al., 2005; Painter et al., 2009). Figures 3.21 and 3.22 suggest that errors in the MODIS snow products over the Khibiny Mountains are lower for higher elevations than for lower altitudes. Using Spearman's rank correlation test however, it is shown that elevation and MODIS error are uncorrelated ($\rho = 0.148$; p value = > 0.05). In the case of the Khibiny Mountains, lower elevations are associated with higher spatial heterogeneity in albedo. The lower measurement sites were indeed closer to roads, mining buildings and, in many cases, vegetation. Therefore, it is possible that MODIS retrievals are more accurate at higher altitudes in this case, as higher altitude pixels are also more homogenous. Finally, the range in elevation in the Khibiny Mountains is low (ranging from 300 m to 1005 m) and thus perhaps elevation is only an issue for retrievals at greater altitude ranges or purely at higher elevations. The example of high-elevation MODIS-retrieval bias in Painter et al. (2009) is the Himalayas, a very different region to the small Khibiny Mountains.

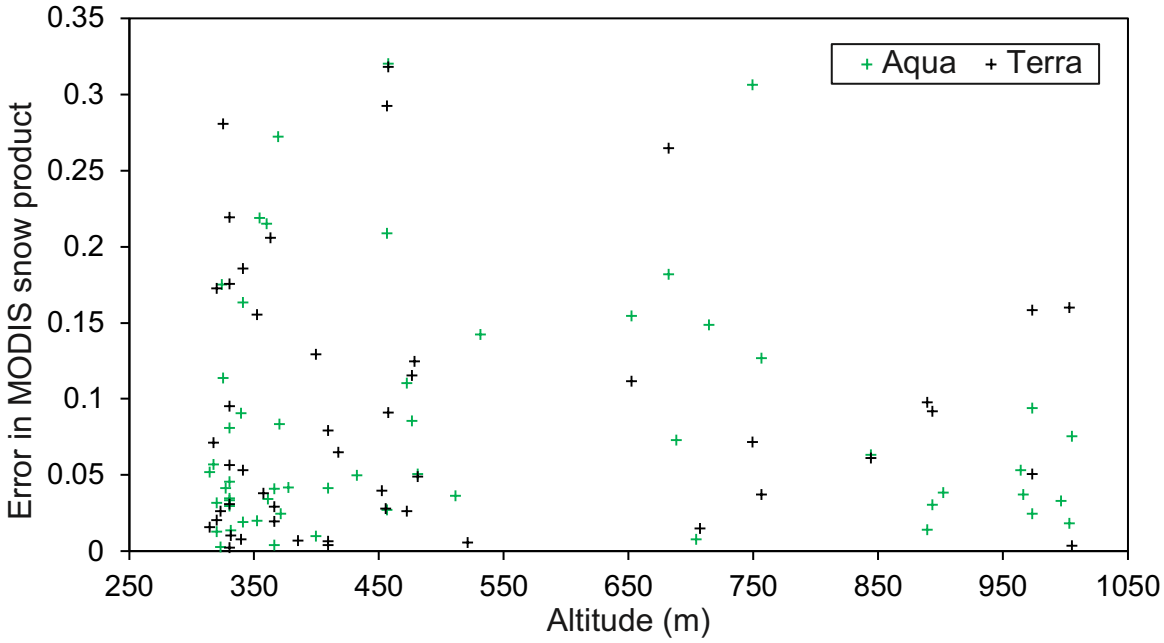

Figure 3.21: Error in the MODIS snow product as a function of altitude.

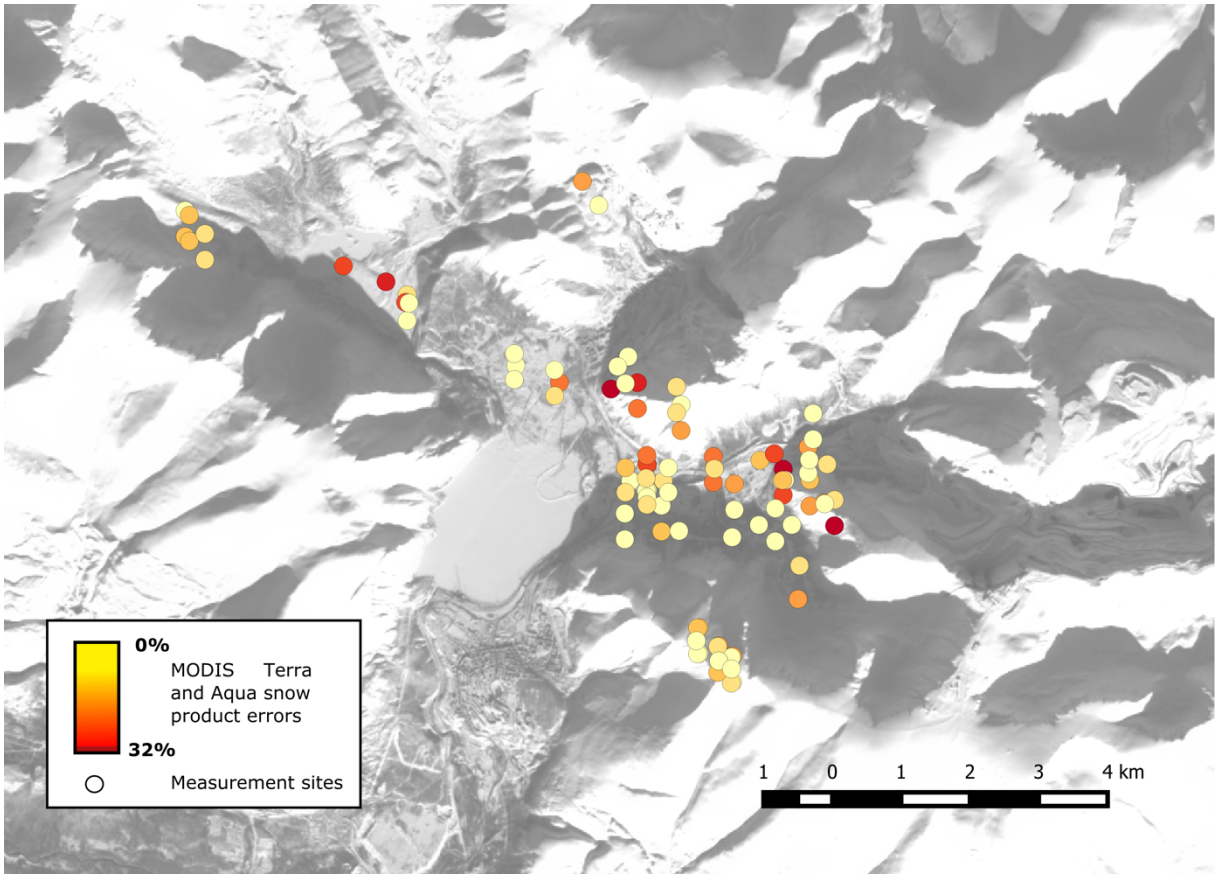

555 **Figure 3.22: Distribution of MODIS errors according to measurement site. The errors are from both the Aqua and Terra satellites and for both 2016 and 2017 field season. Points have been artificially separated to limit overlap.**

3.4 Conclusions

In this chapter, the fieldwork undertaken for this project was described and the results gained from this work were analysed.

- A large snow parameter dataset was collected over two field seasons in the southern Khibiny Mountains.
- From two field seasons in a remote-access area, it is clear that inter-annual differences can be very large in this region. The two seasons contrasted strongly in terms of weather, temperature and snow melt.
- The MODIS ground truthing effort was a success despite the significant high cloud cover limiting the number of pixels that could be ground truthed over the two field seasons. Overall 62 and 43 albedo measurements could be used for the Aqua and Terra snow datasets, respectively.
- The overall RMSE in the albedo retrievals was demonstrated to be less than 10% for both MODIS instruments, at 8.1 % and 8.9 % for Aqua and Terra, respectively.
- However, MODIS retrievals are demonstrated to be accurate up to SZA < 70 º, supporting work done by Stroeve et al. (2013), which demonstrated inaccuracies in the conclusions of Wang and Zender (2010).

3.5 Fit within thesis

The key result from this chapter is the low uncertainty in the MODIS snow products. This is crucial to this thesis as MODIS snow products are used in the following chapter to study past changes in snow cover over a small region surrounding the Khibiny Mountains. MODIS is also used in Chapter 5 as ground 'truth' for the sensitivity analysis of the Weather Research and Forecasting model. Thus, the clear relationship demonstrated between the MODIS imagery and the field-measured snow parameters gives confidence in its use for these studies. Additionally, the demonstrated high variability of snow at a sub-km scale is important in that it presents the difficulties in using point measurements to determine broader-scale patterns, such as the use of station data in chapters 4 and 5 to look at regional trends and validate model outputs respectively.

3.6 References

Aoki, T., Hori, M., Motoyoshi, H., Tanikawa, T., Hachikubo, A., Sugiura, K., Yasunari, T.J., Storvold, R., Eide, H.A., Stamnes, K. and Li, W., 2007. ADEOS-II/GLI snow/ice products—Part II: Validation results using GLI and MODIS data. Remote Sensing of Environment, 111(2), pp.274-290, https://doi.org/10.1016/j.rse.2007.02.035

Armstrong, R.L. and Brun, E. eds., 2008. Snow and climate: physical processes, surface energy exchange and modeling. Cambridge University Press.

Barry, R.G., Armstrong, R.L. and Krenke, A.N., 1993, June. An approach to assessing changes in snow cover, an example for the former Soviet Union. In Proc. Eastern Snow Conf., 50th Annual Meeting (pp. 25-33).

Bartlett, P. and Lehning, M., 2002. A physical SNOWPACK model for the Swiss avalanche warning: Part I: numerical model. Cold Regions Science and Technology, 35(3), pp.123-145. https://doi.org/10.1016/j.coldregions.2006.05.007

Barton, J.S., Hall, D.K. and Riggs, G.A., 2000, May. Remote sensing of fractional snow cover using Moderate Resolution Imaging Spectroradiometer (MODIS) data. In Proceedings of the 57th Eastern Snow Conference (pp. 171-183).

Biswas, A.K., 1970. History of hydrology. Elsevier Science Limited.

Casey, K.A., Kaspari, S.D., Skiles, S.M., Kreutz, K. and Handley, M.J., 2017. The spectral and chemical measurement of pollutants on snow near South Pole, Antarctica. Journal of Geophysical Research: Atmospheres, 122(12), pp.6592-6610. https://doi.org/10.1002/2016JD026418

Fierz, C.R.L.A., Armstrong, R.L., Durand, Y., Etchevers, P., Greene, E., McClung, D.M., Nishimura, K., Satyawali, P.K. and Sokratov, S.A., 2009. The International Classification for Seasonal Snow on the Ground (Vol. 5). UNESCO/IHP.

Gow, A.J., 1969. On the rates of growth of grains and crystals in South Polar firn. Journal of Glaciology, 8(53), pp.241-252. https://doi.org/10.3189/S0022143000031233

Green, R.O., Painter, T.H., Roberts, D.A. and Dozier, J., 2006. Measuring the expressed abundance of the three phases of water with an imaging spectrometer over melting snow. Water Resources Research, 42(10). https://doi.org/10.1029/2005WR004509

Greuell, W. and Oerlemans, J.: Narrowband-to-broadband albedo conversion for glacier ice and snow: equations based on modeling and ranges of validity of the equations. Remote Sensing of Environment, 89(1), pp.95-105, 2004. https://doi.org/10.1016/S0034-4257(02)00024-X

Jamieson, B. and Schirmer, M., 2016. MEASURING SNOW SURFACE TEMPERATURE: WHY, WHY NOT, AND HOW? Revised from Proceedings of the 2016 International Snow Science Workshop.

Jones, H.G., Pomeroy, J.W., Walker, D.A. and Hoham, R.W. eds., 2001. Snow ecology: an interdisciplinary examination of snow-covered ecosystems. Cambridge University Press.

Klein, A.G. and Stroeve, J., 2002. Development and validation of a snow albedo algorithm for the MODIS instrument. Annals of Glaciology, 34(1), pp.45-52. https://doi.org/10.3189/172756402781817662

Liang, S., Stroeve, J. and Box, J.E., 2005. Mapping daily snow/ice shortwave broadband albedo from Moderate Resolution Imaging Spectroradiometer (MODIS): The improved direct retrieval algorithm and validation with Greenland in situ measurement. Journal of Geophysical Research: Atmospheres, 110(D10). https://doi.org/10.1029/2004JD005493

Liu, J., Schaaf, C., Strahler, A., Jiao, Z., Shuai, Y., Zhang, Q., Roman, M., Augustine, J.A. and Dutton, E.G., 2009. Validation of Moderate Resolution Imaging Spectroradiometer (MODIS) albedo retrieval algorithm: Dependence of albedo on solar zenith angle. Journal of Geophysical Research: Atmospheres, 114(D1). https://doi.org/10.1029/2008JD009969

Lundberg, A., Granlund, N. and Gustafsson, D., 2010. Towards automated 'Ground truth'snow measurements—A review of operational and new measurement methods for Sweden, Norway, and Finland. Hydrological processes, 24(14), pp.1955-1970. https://doi.org/10.1002/hyp.7658

Lyapustin, A., Tucker, J., Hall, F., Sellers, P., Wu, A., Angal, A., Wang, Y., Xiong, X., Meister, G., Platnick, S. and Levy, R., 2014. Scientific impact of MODIS C5 calibration degradation and C6+ improvements. Atmospheric Measurement Techniques, 7(12). https://doi.org/10.5194/amt-7-4353-2014

Marshall, S. and Oglesby, R.J., 1994. An improved snow hydrology for GCMs. Part 1: Snow cover fraction, albedo, grain size, and age. Climate Dynamics, 10(1-2), pp.21-37. https://doi.org/10.1007/BF00210334

Nolin, A.W. and Dozier, J., 2000. A hyperspectral method for remotely sensing the grain size of snow. Remote sensing of Environment, 74(2), pp.207-216. https://doi.org/10.1016/S0034-4257(00)00111-5

Painter, T.H., Rittger, K., McKenzie, C., Slaughter, P., Davis, R.E. and Dozier, J., 2009. Retrieval of subpixel snow covered area, grain size, and albedo from MODIS. Remote Sensing of Environment, 113(4), pp.868-879. https://doi.org/10.1016/j.rse.2009.01.001

Pomeroy, J.W. and Schmidt, R.A., 1993. The use of fractal geometry in modelling intercepted snow accumulation and sublimation. In Proceedings of the Eastern Snow Conference (Vol. 50, pp. 1-10).

QGIS Development Team: QGIS Geographic Information System. Open source Geospatial Foundation Project. http://qgis.osgeo.org, 2017.

Riggs, G.A., Hall, D.K. and Román, M.O., 2016. MODIS snow products collection 6 user guide. National Snow & Ice Data Center.

Salomonson, V.V. and Appel, I., 2004. Estimating fractional snow cover from MODIS using the normalized difference snow index. Remote sensing of environment, 89(3), pp.351-360. https://doi.org/10.1016/j.rse.2003.10.016

Schaaf, C.B., Wang, Z. and Strahler, A.H., 2011. Commentary on Wang and Zender—MODIS snow albedo bias at high solar zenith angles relative to theory and to in situ observations in Greenland. Remote Sensing of Environment, 115(5), pp.1296-1300. https://doi.org/10.1016/j.rse.2011.01.002

Schneebeli, M., Coléou, C., Touvier, F. and Lesaffre, B., 1998. Measurement of density and wetness in snow using time-domain reflectometry. Annals of Glaciology, 26, pp.69-72. https://doi.org/10.3189/1998AoG26-1-69-72

Serreze, M.C. and Barry, R.G., 2014. The Arctic climate system. Cambridge University Press.

Stroeve, J., Box, J.E., Gao, F., Liang, S., Nolin, A. and Schaaf, C., 2005. Accuracy assessment of the MODIS 16-day albedo product for snow: comparisons with Greenland in situ measurements. Remote Sensing of Environment, 94(1), pp.46-60. https://doi.org/10.1016/j.rse.2004.09.001

Stroeve, J., Box, J.E., Wang, Z., Schaaf, C. and Barrett, A., 2013. Re-evaluation of MODIS MCD43 Greenland albedo accuracy and trends. Remote sensing of environment, 138, pp.199-214. https://doi.org/10.1016/j.rse.2013.07.023

Wang, X. and Zender, C.S., 2010. MODIS snow albedo bias at high solar zenith angles relative to theory and to in situ observations in Greenland. Remote Sensing of Environment, 114(3), pp.563-575. https://doi.org/10.1016/j.rse.2009.10.014

Weller, G., 1972. The tundra microclimate during snow-melt at Barrow, Alaska. Arctic, 25(4), pp.291-300. https://doi.org/10.14430/arctic2973

Woo, M.K., Heron, R., Marsh, P. and Steer, P., 1983. Comparison of weather station snowfall with winter snow accumulation in High Arctic basins. Atmosphere-Ocean, 21(3), pp.312-325. https://doi.org/10.1080/07055900.1983.9649171

Chapter 4
Assessing snow cover changes in the Kola Peninsula, Arctic Russia, using a synthesis of MODIS snow products and station observations.

In this chapter, I examine recent changes in snow cover (2000 - 2016) in the western mountain regions (hereinafter WMR) of the Kola Peninsula in Arctic Russia, an area that has undergone significant climate change in recent decades. For this analysis, a combination of meteorological observations and remote sensing data is used. This is the first time that remote sensing data have been used to assess snow cover in this region. These snow products were processed to maximise the number of cloud-free days. First and last days of snow cover were derived for each year from snow depth observations at meteorological stations. MODIS-derived snow cover dates were compared to these station-derived dates to look for systematic biases in the satellite data. These 'locally-calibrated' MODIS data were then used to determine the trends and variability in the duration of the snow season in the WMR between 2000 and 2016, and data from meteorological stations were used to extend the study to the past half century.

4.1 Introduction

Snow cover has a direct impact on human life and the natural environment in many parts of the world. It is the largest component of the terrestrial cryosphere by area (e.g. Lemke et al., 2007) and 98 % of seasonal snow is located in the Northern Hemisphere (NH) (Armstrong and Brodzik, 2001), with the proportion of snow-covered land ranging from 7 to 40 % over an annual cycle (Singh and Gan, 2000). Importantly, snow's albedo leads to a positive feedback loop. Fresh snow has a very high albedo, meaning it reflects solar radiation back out to space, thus maintaining a cool Earth's surface. As snow melts from a warming of the atmosphere, more radiation can be absorbed by the surface, leading to further warming and so more snow melt. Snow albedo is the third most important climate feedback after water-vapour and cloud feedbacks (e.g. Bony et al., 2006). Therefore, studying trends in snow cover in a warming climate is important. Studying arctic snow is problematic due to its high spatial variability (Liston, 2004) and the relative scarcity of ground-based measurements. As a result, remote sensing datasets are often used in Arctic snow studies as they provide spatially continuous information. However, these bring in new uncertainties with the difficulties of snow-mapping algorithms to distinguish snow from clouds (e.g. Hall et al., 2010) and to represent snow in forested areas (e.g. Rutter et al., 2009; Rittger et al., 2019).

Studies of changes in snow during the past century have focussed predominantly on the trends in snow cover extent. These trends have been negative across the NH as a whole for the past few decades (e.g. Dye, 2002; Lemke et al., 2007, Peng et al., 2013), especially in spring (Brown and Robinson, 2011). Tedesco and Monaghan (2009) noted that, in the 1979 to 2008 interval, the duration of the melt season

in the NH was shortening by 6.0 days/decade. However, these are the large-scale trends and at a smaller, regional, scale, snow cover trends are not uniform and have greater inter-annual variability (Robinson and Frei, 2000; Bormann et al., 2018). Here, I focus on the WMR of the Kola Peninsula in Arctic Russia (Fig. 4.1). These mountains are extremely rich in mineral resources and also make the WMR a popular winter sports tourist destination, making it a very economically valuable Russian region. Increases in the duration of the snow cover season may adversely impact the mineral extraction undertaken in the Khibiny Mountains and decreases in the snow season may result in a reduction in the local winter sports economy. Therefore, any changes in snow cover in this region will have a socio-economic impact. For this reason, the Kola Peninsula and parts of the WMR have been the focus of multiple Russian studies. Indeed, the work in this chapter follows on from a strong culture of Russian snow research in north-west Russia (e.g. Kitaev et al., 2007) and in the Khibiny Mountains (Glazovskaya, 2000; Sapunov et al 2006; Troshkina et al., 2005; Troshkina et al., 2009; Vikulina, 2009; Zyuzin et al., 2006), mainly focussing on snow microphysics and avalanche processes. This regional Russian snow research was summarised in 2013 with a comprehensive analysis of past changes in the Khibiny Mountains (Zaika et al., 2013). In addition to this, some chapters published in English have studied past climatic variations in the area (Kozlov and Berlina, 2002; Demin and Zyuzin, 2006; Demin and Zyuzin, 2009; Blinova and Chmielewski, 2014; Marshall et al., 2016) but none specifically focussed on snow cover. This work distinguishes itself by its wider spatial scope, comparing the snow cover in the mountains to the surrounding region, and, importantly, is the first to use remotely-sensed snow cover data to expand upon the availability of data from meteorological stations in the area. In this chapter, I focus on the rate of change of the snow season and its spatial variability in the WMR.

The Moderate Resolution Imaging Spectroradiometer (MODIS) snow cover product has been used to study snow cover changes in many regions (Zhang et al., 2010; Dietz et al., 2012; Huang et al., 2016; Malnes et al., 2016). Here, the MODIS Normalised Difference Snow Index (NDSI) snow cover data is employed to study snow cover in the WMR of the Kola Peninsula. The MODIS snow product lends itself well to snow cover studies within mountainous regions due to its high spatial (500 m) and temporal (daily) resolution (Bormann et al., 2018). We utilise a similar methodology to Malnes et al. (2016), demonstrate that it is applicable to WMR and extend it by analysing trends in the resultant 16-year long time series of regional snow cover data.

In section 4.2, I provide a brief introduction to the climate of the WMR, including a summary of the current understanding of the region's snow cover and opposing findings published in the literature. In section 4.3, the methods employed in this analysis are detailed, focussing on the validation of the MODIS data and the processing used to derive MODIS snow cover maps. In sections 4.4 and 4.5, the results are presented and discussed: trends in the snow cover start (SCS), snow cover end (SCE) and snow cover duration (SCD) are given for all of the available meteorological stations as well as SCS, SCE and SCD datasets of the entire WMR derived from MODIS data. Finally, section 4.6 comprises the conclusions.

4.2 Climate of the Western Mountain Regions (WMR)

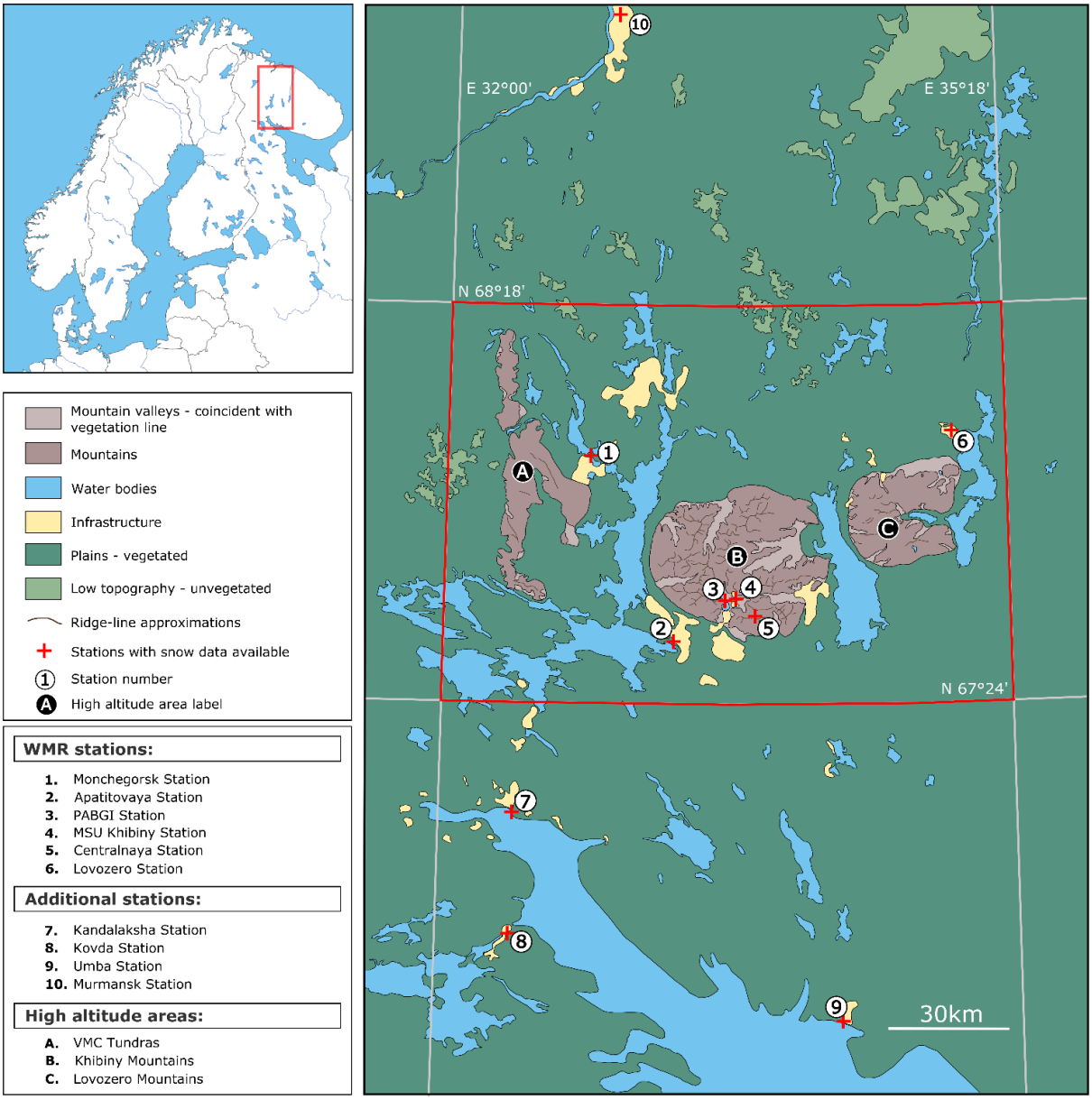

Figure 4.1: The WMR in relation to Fennoscandia. The WMR is the area delimited in red by the four grid lines. Red crosses show the locations of the ten meteorological stations with readily available snow data.

The WMR (see Fig. 4.1) is part of Murmansk Oblast (Region) (66 - 70° N), which essentially comprises the Kola Peninsula. The WMR, as defined for this chapter, contains both lower elevation plains and the highest orography of the Kola Peninsula. The definition of these high altitude areas is based on Blinova and Chmielewski (2014): three main high altitude areas are included in the WMR (see Fig. 4.1) and these are the Khibiny Mountains (1,191 m), the Lovozero Mountains (1,120 m) and the combined Volchji (955 m), Monche (965 m) and Chuna Tundras (1,114 m) hereafter the VMC Tundras (Blinova and Chmielewski, 2014). Almost all of the Murmansk Oblast is situated north of the Arctic Circle, but the Gulf Stream makes its climate milder than in nearby areas east of the Kola Peninsula (Blinova and Chmielewski, 2014). Temperatures in Russia are rising faster than average, especially in its northern Arctic regions (Olofinskaya et al., 2009). A number of chapters have analysed climatological trends in

the Kola Peninsula (Anisimov and Reneva, 2006; Demin, 2012; Demin et al., 2014; Demin et al., 2015; Blinova and Chmielewski, 2014; Marshall et al., 2016).

The Kola Peninsula is climatically heterogeneous. The regional mean annual air temperature is ~0 °C (Marshall et al 2016) and falls to −2 °C in the WMR (Blinova and Chmielewski, 2014) due to higher average altitude and the lack of warming oceanic influence. The snow cover period extends from the middle of October until the end of May, and the thermal growing season from early June until the middle of September (Koroleva, 1994; Blinova and Chmielewski, 2008; Blinova, 2011). Annual surface air temperature in the Kola Peninsula has increased by 2.3 ± 1.0 ºC over the past 50 years (Marshall et al., 2016). Seasonally, statistically significant warming has taken place in spring and autumn, although the largest trend has occurred in winter (Marshall et al., 2016). Spring has become significantly wetter and autumn drier, though annual precipitation has not undergone any significant change (Marshall et al., 2016). There has also been an overall trend towards stronger winds (Roshydromet, 2005). Within the WMR, at the highest altitudes of the Khibiny Mountains, air temperature increased in all the seasons by 0.22 to 0.54 °C per decade between 1965 and 2015 (Demin and Volkov, 2017).

Using phenology (the study of the seasonal development of plants), Kozlov and Berlina (2002) found that the length of the summer in the Kola Peninsula decreased by 15 to 20 days in the 1930 to 1998 interval. This is supported by the 44 % increase in winter precipitation recorded over the Northern taiga forests in the Kola Peninsula (Høgda et al., 2001). However, Bulygina et al. (2009) argued that snow cover duration has been decreasing in north-west Russia since 1966. Additionally, Blinova and Chmielewski (2014) demonstrated shifts in the timing of the growing season and its mean prolongation by 18.5 days in the 1951 to 2012 interval. In this period, the onset of the growing season advanced by 1.1 days/decade, while the end was extended by 1.8 days/decade. This matches the pattern observed in Fennoscandia, but it has not been detected in the rest of Europe (Karlsen et al., 2009; Høgda et al., 2013). These seemingly contradictory findings are investigated in section 4.4.1.2.2, in order to test whether these differing conclusions are a result of the different time intervals studied.

4.3 Data and methods

4.3.1 Station data

4.3.1.1 WMR stations

There are six meteorological stations with readily available snow data in the WMR (see Table 4.1), although only two of these stations have records that cover the entire period of MODIS availability (2000 - 2016). Data from the Khibiny Avalanche service is difficult to obtain and, as a result, I only use the maximum annual snow depth recorded at Centralnaya between 1962 and 2005, as used by Zaika et al. (2013). It is worth noting throughout this study that snow depth measurements from the stations within higher altitude areas (MSU Khibiny and PABGI Khibiny) are likely affected by false precipitation issues as a result of wind-blown snow (Demin, personal communication). However, as

this chapter focuses on spatial and temporal changes in snow distribution rather than snow depth, this markedly lessens the impact of such errors on our findings.

Station Name	Number on Fig. 4.1	Latitude (°N)	Longitude (°E)	Elevation (m)	Dates	Data used in this study
Apatitovaya	2	67.55	33.36	135	2010 - present	Daily snow depth.
Centralnaya	5	67.63	33.88	1050	1962 - 2005	Yearly maximum snow depth.
Lovozero	6	68.00	35.03	162	1992 - present	Daily snow depth.
Monchegorsk	1	67.97	32.88	131	2005 - present	Daily snow depth.
Moscow State University (MSU) Khibiny Research and Education	4	67.64	33.72	330	1984 - 2016	Monthly average and maximum snow depth. Snow cover start and end dates.
Polar-Alpine Botanical Garden Institute (PABGI) - Khibiny	3	67.64	33.67	310	1991 - 2014	Monthly snow depth.

Table 4.1: Description of the WMR stations and available snow depth data.

4.3.1.2 Western Murmansk Oblast stations

Snow depth data from additional stations with longer records in the western Murmansk Oblast (Table 4.2) are used for the validation of the MODIS data (Sect. 4.3.3.2) and for a wider understanding of snow cover changes in the western Kola Peninsula.

Station Name	Number on Fig. 4.1	Latitude (°N)	Longitude (°E)	Elevation (m)	Dates	Data used in this study
Kandalaksha	7	67.13	32.43	40	1936 - present	Daily snow depth.
Kovda	8	66.70	32.88	18	2005 - present	Daily snow depth.
Murmansk	10	68.98	33.09	96	1945 - present	Daily snow depth.
Umba	9	66.68	34.35	1	1966 - present	Daily snow depth.

Table 4.2: Description and available snow depth data of the four additional stations used in this study, the western Murmansk Oblast stations.

Station observations were checked for gross errors simply by plotting the data. Potentially incorrect values in the 21st century were cross-checked against other available sources (e.g. https://rp5.ru) and changed if confirmed as incorrect. Earlier likely incorrect values and recent values

where a more likely alternative could not be located were considered to be missing data. However, very few values were removed in this process so it will not have significantly impacted the calculated trends. Snow depth observations at the stations were made to the nearest centimetre.

4.3.1.3 Station data processing

Only one station (MSU Khibiny) recorded the start and end dates of the snow cover season (see Table 4.1), so a method of extracting SCS and SCE dates from snow depth data was used for the other stations. This method was based on that used to extract these dates from the MODIS data (see Section 4.3.2.2). SCS (/SCE) was defined as the first day with more than 5 (/10) days in a row with snow cover depth higher(/lower) than 1 cm at a station.

4.3.2 MODIS

4.3.2.1 General information

The satellite data used in this study comprise the MODIS snow product from both satellites (Terra and Aqua). These data were used from their earliest availability, 2000 for Terra and 2002 for Aqua, until August 31st 2016, taken as the end of the 2015/2016 snow cover season. The specific dataset used in this study is the NDSI snow cover dataset and, as discussed in Chapter 3 (section 3.2.3.1), this product is used as a straightforward proxy for FSC.

4.3.2.2 Data processing

The MODIS data were processed for long-term trend analysis. Before any data processing, the Aqua and Terra data comprised 52.6 % and 50.97 % cloud cover respectively. Merging both datasets together is the first step to replacing cloudy pixels with snow cover data (Dietz et al., 2012, Foppa and Seiz, 2012; Husler et al., 2014; Malnes et al., 2016). As the satellites have slightly different overpass times, a cloudy pixel in the data of one of the satellites may contain valid NDSI data in the other. For each pixel, each day, if there existed an NDSI value in one of the Aqua or Terra data sets, then this value was inserted. If a value existed in both satellite data sets then the average of the two was used. When a pixel had no value in either Aqua or Terra, a weighted average of the two nearest values within the previous five and following five days from either satellite was used to determine an NDSI value. If only one value could be found pre- or post- empty pixel, then this value was applied. Using this technique, over half of missing NDSI data were filled and the resulting combined dataset comprises only 23 % missing data as a result of cloud cover.

The first and last snow-free days for each year in the 2000 to 2016 interval were calculated following the method used by Malnes et al. (2016). A cutoff value for the NDSI data of 50 (equivalent to 50 % pixel FSC) was taken to evaluate the start and end of the snow cover. The SCS is defined as the first day when an NDSI value reached at least 50 for more than 5 days in a row. The SCE is defined as the first snow-free day when an NDSI value falls below 50 for more than 10 days in a row. This

difference in cutoff time is due to the high cloud cover in autumn which hinders MODIS' snow cover retrieval ability over longer periods of time than in spring.

Earliest and latest SCS and SCE dates were set for the analysis (Malnes et al., 2016). These dates were selected based on snow cover start and end dates at stations and on the dates of the Polar night in the region (Dec 2nd to January 10th) to avoid problems due to low solar angles. The SCS was set as being able to occur between September 1st and November 17th. The SCE was set as being able to occur between March 15th and August 31st. The SCD is the number of days with snow cover and the MODIS SCD was calculated from the SCS and SCE maps, following equation 4.2, with DiY being the number of days in the year (365 or 366).

(4.1) SCD = (DiY – SCS) + (SCE – 1) (as the end of snow cover is the first day with no snow)

4.3.3 Statistical methodology

Trends were calculated using standard least squares methodology. These trends were tested for statistical significance using the standard t-test and p values were extracted. Three degrees of significance are used: $p < 0.1$, $p < 0.05$, $p < 0.01$.

4.4 Results

4.4.1 Station data

4.4.1.1 Snow cover depth

Figure 4.2 shows plots of daily snow depth at the Apatitovaya, Lovozero and Monchegorsk stations located in the WMR for the entirety of their available record (see Table 4.3). The inter-annual range in snow depth at these three stations is considerable, especially for the two latter stations, with longer records. The largest inter-annual differences in snow depth can be seen at the end of the snow season. For example, in some years, such as 2016/17, the snow depth was at its highest peak or only just starting to melt out at the median time of disappearance of snow (Fig. 4.2). Thus, at Lovozero station, the highest inter-annual depth range can be seen in late April when the snow depth ranges from 0 to 88 cm. However, at Apatitovaya and Monchegorsk stations the maximum inter-annual difference is observed in early May, where the range is just over and just under 80 cm, respectively. Note that late season snowfall can be observed at Lovozero station, where a renewed snow depth peak appears at the end of the snow season. This is not seen at the other two stations but is likely to be simply a result of the longer record at Lovozero station, as all late season snowfall on record there occurred between 1996 and 2001.

The inter-annual difference in the dates of the appearance of the snow (> 0 cm depth) and the disappearance of the snow (= 0 cm depth) dates at these three stations is also clearly seen in these figures and is summarized in Table 4.3.

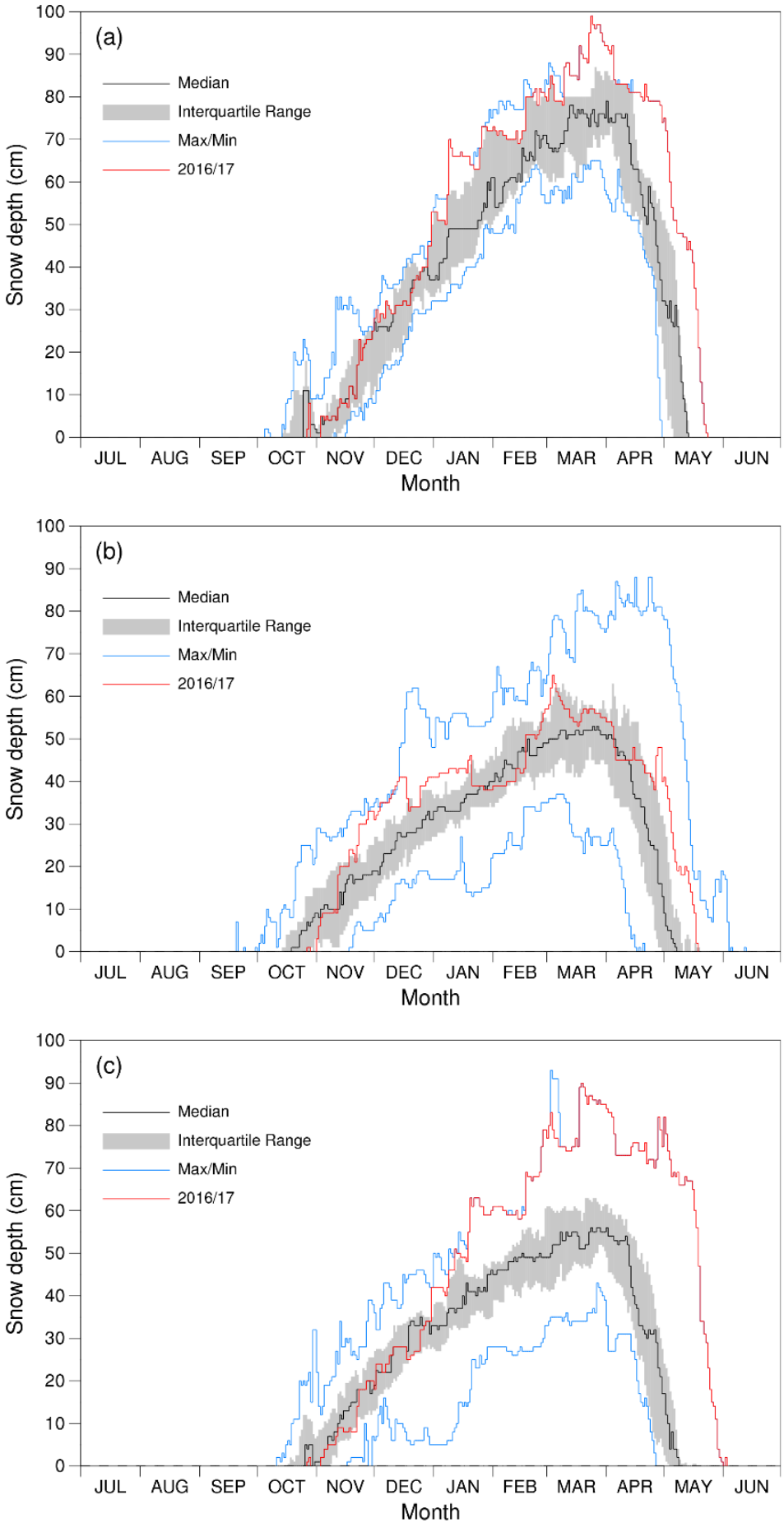

Figure 4.2: Snow depth range at (a) Apatitovaya station, (b) Lovozero station, (c) Monchegorsk station.

Station	Dates of available data	Range in the date of appearance of snow	Range in the date of disappearance of snow
Apatitovaya	2011 - 2017	October 13th - November 5th	April 30th - May 24th
Lovozero	1992 - 2017	October 1st - November 5th	April 22nd - June 6th
Monchegorsk	2005 - 2017	October 14th - November 16th	April 30th - June 4th

Table 4.3: Inter-annual differences in SCS and SCE dates at the Apatitovaya, Lovozero and Monchegorsk stations.

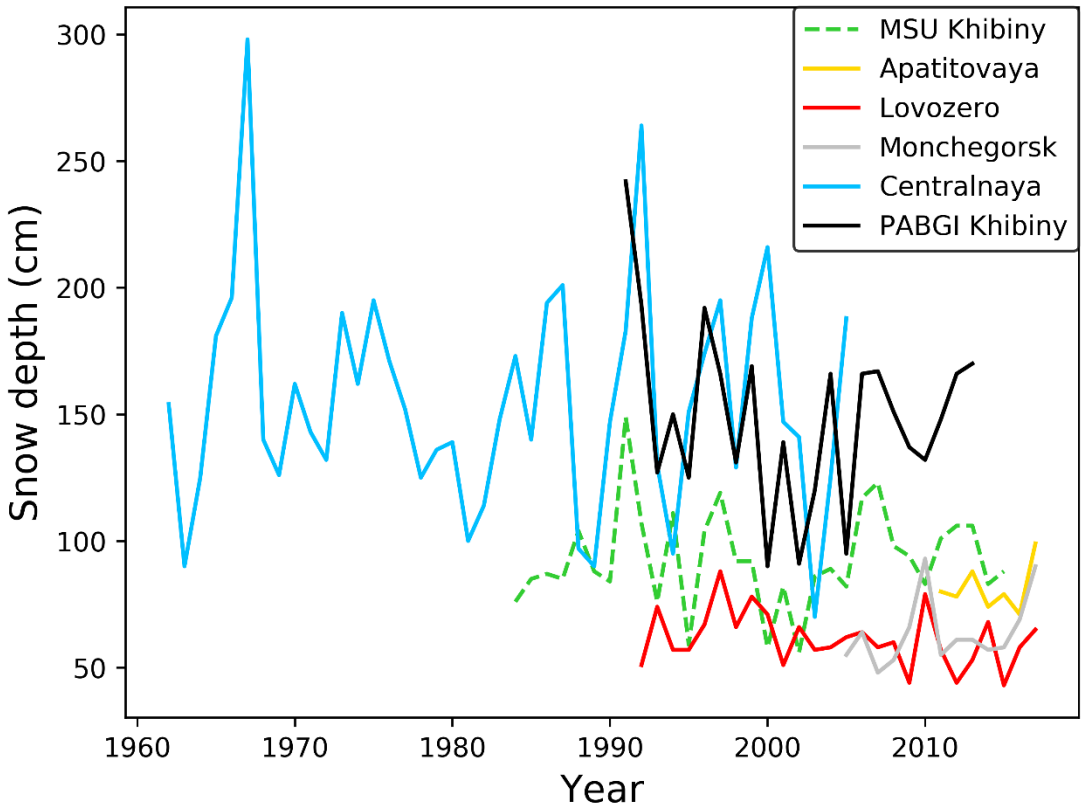

Figure 4.3: Maximum snow depth in centimetres at the Centralnaya station, MSU Khibiny station, PABGI Khibiny station, Lovozero station, Monchegorsk station and Apatitovaya station. The data from Centralnaya station was collected by the Khibiny avalanche service.

Figure 4.3 shows a comparison of yearly maximum snow depth at all six stations from the WMR used in this study. The maximum snow depth at the stations within the Khibiny Mountains (Centralnaya, PABGI Khibiny and MSU Khibiny stations) is on average higher than those in the surrounding plains (Apatitovaya, Lovozero and Monchegorsk stations). The station at the highest altitude, Centralnaya station, also has the greatest snow depth. Over the common period of 1991 to 2005, the Centralnaya yearly average maximum snow depth is 13.3 cm deeper than at PABGI Khibiny station. At Centralnaya station, maximum snow depth varies markedly, from 100 to 300 cm, between 1962 and 2005 but does not have a statistically significant trend over this long time period. The inter-annual variability in maximum snow depth is less for stations at lower altitudes, and there are no statistically significant trends here either.

It is interesting to compare the MSU Khibiny and PABGI Khibiny stations, as both are at similar altitudes in valleys within the Khibiny Mountains and are located only 2 km apart (see Fig. 4.1). Yearly

maximum snow depth is consistently much higher at PABGI Khibiny station than for MSU Khibiny station, by 56.5 cm on average.

4.4.1.2 Seasonal snow cover trends

4.4.1.2.1 Full time series

Station	Dates of available data	Parameter	Trend full time series (days/decade)
Apatitovaya	2011 - 2017	SCS	-1.7
		SCE	11.1
		SCD	11.4
Lovozero	1992 - 2017	SCS	3.8
		SCE	-4.4
		SCD	-9.4**
Monchegorsk	2005 - 2017	SCS	-5.1
		SCE	-3.6
		SCD	2.9
MSU Khibiny	1984 - 2016	SCS	-2.3
		SCE	2.4
		SCD	4.6
Kandalaksa	1936 - 2017	SCS	-1.0
		SCE	1.2***
		SCD	2.3***
Murmansk	1945 - 2017	SCS	-0.4
		SCE	1.8**
		SCD	2.9**
Umba	1966 - 2017	SCS	1.9
		SCE	-2.8***
		SCD	-5.4***

Table 4.4: Trends in days per decade, and their significance, of the Snow Cover Start (SCS), Snow Cover End (SCE) and Snow Cover Duration (SCD) at the WMR and the western Murmansk Oblast stations over their full available time-series. Statistically significant trends are marked with asterisks: * = p < 0.1, ** = p < 0.05, ***= p < 0.01.

From the daily snow depths recorded at the meteorological stations, I calculated the start, end and duration of each snow season. Least-squares linear regression was applied to estimate trends over time (see Table 4.4). It is important to note that the trends in SCS and SCE do not always add up to the trends in SCD. This is a result of missing years of data in the start or end of the snow cover, but not in the other. This means that the SCS and SCE trends contain more years of data than the SCD which will miss a year in any year missing SCS or SCE.

Over the 2005 to 2017 interval of data collected at Monchegorsk, the snow cover season has not undergone any statistically significant trends. Data from the MSU Khibiny station show a notable increase in the duration of the snow cover season since the start of the record in 1984, but none of the trends at MSU Khibiny are statistically significant. Finally, the Lovozero data show an increasingly late start and increasingly early end of the snow season over the past 25 years, but only the trend in its SCD is statistically significant ($p < 0.05$): the SCD has been shortening by 9.4 days/decade since 1992.

It is also interesting to look at trends at some of the longer datasets in the western Kola Peninsula in order to set the trends in the WMR in a longer temporal context (see Table 4.4). The daily snow depth dataset from Kandalaksha station is one of the longest available from the region and shows significant trends in SCE and SCD since 1936: overall the snow season has lengthened by 2.3 days/decade. At Murmansk station, the trends in the SCE and SCD are significant over the entire time-series. The snow cover season has been lengthening over the past 71 years at the rate of 2.9 days/decade. The SCS has changed very little over time (-0.4 days/decade; not statistically significant), so the extension of the snow cover season is primarily due to a much later end to the average snow cover season (1.8 days days/decade; significant at $p < 0.05$)., In contrast, at Umba station the snow cover season has been getting shorter over the past 39 years, at the rate of 5.4 days/decade. The delay in the start of the snow cover is not statistically significant, however the increasingly early end to the snow cover season (-2.8 days/decade) is ($p < 0.01$).

4.4.1.2.2 25-year common time series

Station	Parameter	25-year trend 1992-2016 (days/decade)
Kandalaksha	SCS	4.2
	SCE	-4.0**
	SCD	-8.2***
Lovozero	SCS	3.8
	SCE	-5.6
	SCD	-9.4**
MSU Khibiny	SCS	-2.6
	SCE	1.2
	SCD	3.8
Murmansk	SCS	6.2**
	SCE	-1.3
	SCD	-7.5*
Umba	SCS	3.1
	SCE	-4.2**
	SCD	-7.3**

Table 4.5: Trends in days per decade and their significance of the Snow Cover Start (SCS), Snow Cover End (SCE) and Snow Cover Duration (SCD) at the five stations with available data over the 25-year common interval (1992-2016). Statistically significant trends are marked with asterisks: * = p < 0.1, ** = p < 0.05, ***= p < 0.01.

By comparing changes in snow cover variability at the WMR stations to those in the wider western Murmansk Oblast over a common period, I can relate our findings to the broader regional spatial variability. Table 4.5 shows the trends (estimated by least-squares linear regression) in the SCS, SCE and SCD over a common 25-year time interval (1992 - 2016) for the five stations of both the WMR and the wider western Murmansk Oblast with available data for that time. Data at four of the five stations show a positive trend in the SCS (increasingly late start to the snow cover), a negative trend in the SCE (increasingly early end of the snow season) and an overall decrease in the duration of the snow cover season. The station showing opposite results is MSU Khibiny station, located within the Khibiny

Mountains and at a higher altitude than the other stations. Importantly, this opposite trend is also the only SCD trend that is not statistically significant. These results indicate a uniform regional signal of reduced SCD snow cover across the lower altitudes of the western Murmansk Oblast between 1992 and 2016. They also imply an opposite trend in the snow cover season at higher altitudes, although more long-term data in the mountainous areas are needed to make robust conclusions on these higher-altitude zones. To resolve the issue of spatial variability in station data, MODIS was used to obtain spatially continuous data over the WMR in order to identify the spatial variability of the snow there.

4.4.2 MODIS processed datasets

4.4.2.1 Missing data

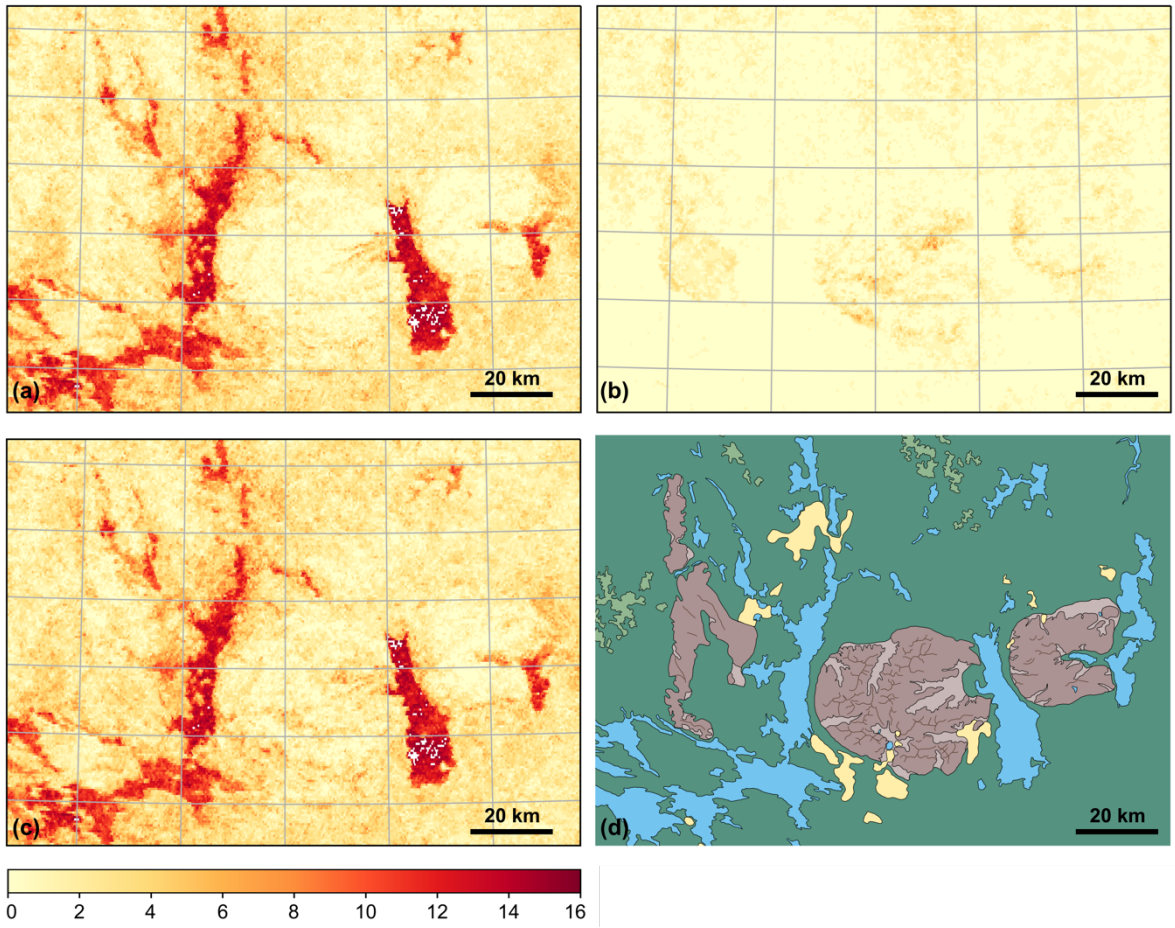

Figure 4.4: Number of years with missing a. SCS, b. SCE and c. SCD data over the 2000/2001 to 2015/2016 interval in the WMR. White pixels have 100 % missing data.

Despite processing efforts to minimise missing data described in section 4.3.2.2, cloud cover remained a hindrance to the extraction of SCS, SCE and SCD dates in the WMR. The number of missing years in each of the SCS, SCE and SCD datasets are shown in Fig. 4.4. Pixels of missing data make up 22.6 %, 5.9 % and 24.6 % of the SCS, SCE and SCD respectively. Water bodies (see Fig. 4.1) have missing data in the SCS datasets for 12 to 16 years out of a possible 16 years. This can be explained by the fact that these areas will only return a SCS date when they have frozen over and started accumulating snow on this surface. The freezing process is slow and usually does not occur in time for the ice to be covered in snow before November 17th. In the dry land section of the region, there is very little missing data in the

SCE dataset and more missing data in the SCS data, especially for the plains. This is a result of the increased cloud cover in the autumn associated with the high snowfall. SCD is calculated from SCS and SCE and, as a result, has a combination of the missing data in those two datasets.

4.4.2.2 Station validation

	SCS				SCE			
	Mean difference	Mean offset	Positive or negative offset	Number of missing years	Mean difference	Mean offset	Positive or negative offset	Number of missing years
Apatity	-3.5	3.5	Negative	2	4.4	4.4	Positive	0
Lovozero	-4.0	5.3	Both	4	11.1	11.1	Positive	1
Monchegorsk	0.7	10.4	Both	4	15.6	15.6	Positive	0
MSU Khibiny	7.9	12.4	Both	3	-1.6	6.2	Both	2
Murmansk	-3.6	10.5	Both	7	-5.9	12.9	Both	6
Kandalaksha				16	20.9	20.9	Positive	2
Kovda	7.4	10.4	Both	3	-8.0	8.0	Negative	0
Umba	-0.8	4.0	Both	7	-0.2	2.8	Both	0

Table 4.6: Summary statistics of the difference between dates determined from data collected at meteorological stations and from the MODIS processed datasets in the 2000/2001 to 2015/2016 interval for the SCS and SCE. This difference is taken as the station dates minus the MODIS dates, and the unit for the mean and mean offset columns are number of days.

The MODIS data processing algorithm was tested by comparing the derived SCS and SCE dates with those recorded at meteorological stations (Section 4.3.1.3). SCS and SCE dates were extracted from the SCS and SCE MODIS processed datasets for each of the following stations: Apatitovaya, Lovozero, Monchegorsk, MSU Khibiny, Murmansk, Kandalaksha, Kovda and Umba. The results of the comparison of these to the station data are shown in Table 4.6. The difference (in number of days) between the SCS and SCE end dates from station data and MODIS processing was calculated for all years at all stations. This difference is taken as the station dates minus the MODIS dates and the results are shown in Table 4.6. The offset represents the magnitude of this difference and the offset direction is presented (positive: MODIS is always early; negative: MODIS is always late). All annual 'maps' have missing data (see Fig. 4.4) and as a result, there is no MODIS data for some years at all stations. In one extreme case. No SCS dates could be extracted at all for Kandalaksha (Table 4.6).

On average, the difference is 8.6 and 10.4 days between the station and MODIS SCS and SCE dates, respectively. There is a slight bias in the MODIS dates with higher errors being positive, so finding an earlier date than the station data. On average the mean bias of the SCS and SCE dates are + 1.2 days and + 5.0 days respectively.

In the WMR, the MODIS dates are most representative of the Apatitovaya station data. The differences are uniform and quite low for the MSU Khibiny station for the SCE; however, errors are more inconsistent and reach higher values for the SCS. The Lovozero station is the opposite, with

consistent low differences in the SCS dates and higher more varied differences in the SCE dates. In the WMR, the deviation between station and MODIS dates is largest at the Monchegorsk station.

In the wider western Murmansk region, the MODIS dates best replicate Umba station data, where MODIS is neither consistently early nor late. At Kovda station, the deviation between MODIS and station data SCS is highly variable between years, reaching high values of over 30 days. The MODIS SCE dates there are all later than those recorded at the station (negative offset). Kandalaksha station values follow the opposite trend with the MODIS SCS dates being much earlier than the station values for all years (positive offset). The differences are highest for Kandalaksha station with an offset of up to 41 days.

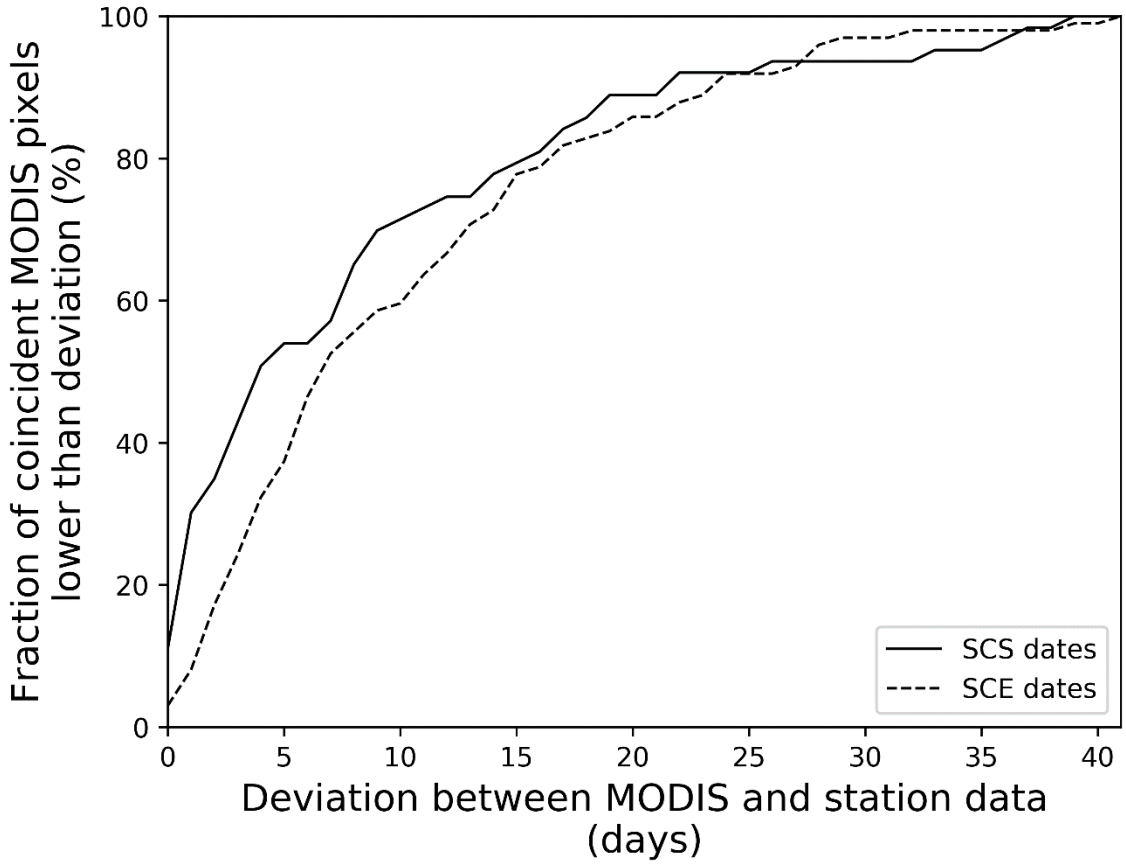

Figure 4.5: Graph showing the proportion of pixels with a deviation of lower than 0 to 41 days between the MODIS-derived and station data-derived SCS and SCE dates.

4.4.2.3 Mean SCS, SCE and SCD

Figure 4.6 shows the mean SCS, SCE and SCD dates over the entire MODIS period (2000 -2016) and illustrates the high spatial variability in the long-term snow cover distribution in the WMR.

Clear climatological differences between the mountainous areas (>400 m altitude) and the surrounding plains (<400 m altitude) can be seen (see Fig, 4.1 for topography of the region). The snow cover season starts much earlier in the mountains than in the plains and, as expected, it starts at the highest elevations first (around September 22nd on average) and then gradually moves to lower altitudes. For most years, the delay in the SCS in the mountain valleys is ~30 days later than the highest elevations. The snow cover season then begins in the north-east of the WMR as defined in this study before arriving

in the plains further south, surrounding the mountains. The SCS date for the plains surrounding the higher elevations of the WMR is usually similar to those of the larger valleys within the mountains (~October 21st).

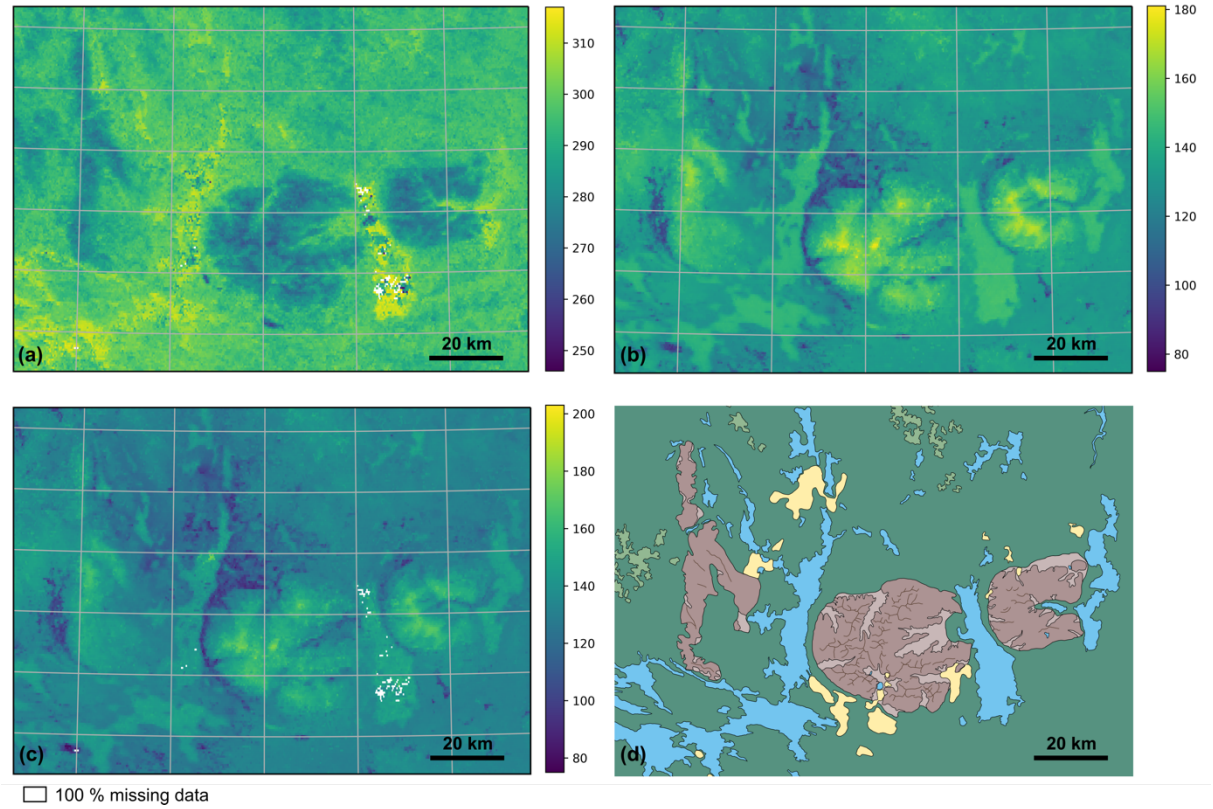

Figure 4.6: Three MODIS maps showing the (a) mean snow cover start, (b) mean snow cover end, and (c) mean snow cover duration of the WMR. Scales on (a) and (b) are the day of year, and for (c) the scale is of the number of days.

The SCS is slightly more uniform across the whole Khibiny and Lovozero mountains than the SCE, which is more gradual and follows altitude. The SCE is earliest at the lowest altitudes (~May 20th) while it occurs at the highest elevations around June 29th on average. This results in a very clear link between altitude and SCD, with the highest altitudes having the longest snow cover season in the entire area (~180 days) and the duration of the snow cover season decreasing with lower elevation. Thus, the snow season in the plains surrounding the mountains is much shorter than in the higher altitude areas (by approximately 50 days). Within the plains, the SCE is earliest on the western side of the two high mountain ranges and VMC Tundras. As a result, this area has the shortest snow cover season in the region, between 95 and 100 days long.

Finally, the water bodies have a very noticeable difference with the land around them, which sees them having a much later snow cover start than any other area in the region, but also have a later snow cover end. In 2015, the water bodies did not return snow cover end dates (see Fig. 4.A1o in the Appendix). In most other years, the water bodies which had frozen and were covered in snow, remained so until later in the year (~May 30th) than the surrounding plains (~May 15th). This is probably due to the snow on ice taking longer to melt out than the surrounding snow on top of ground, due to the higher heat capacity and reflectance of ice than soil.

4.4.2.4 SCS, SCE and SCD inter-annual variability

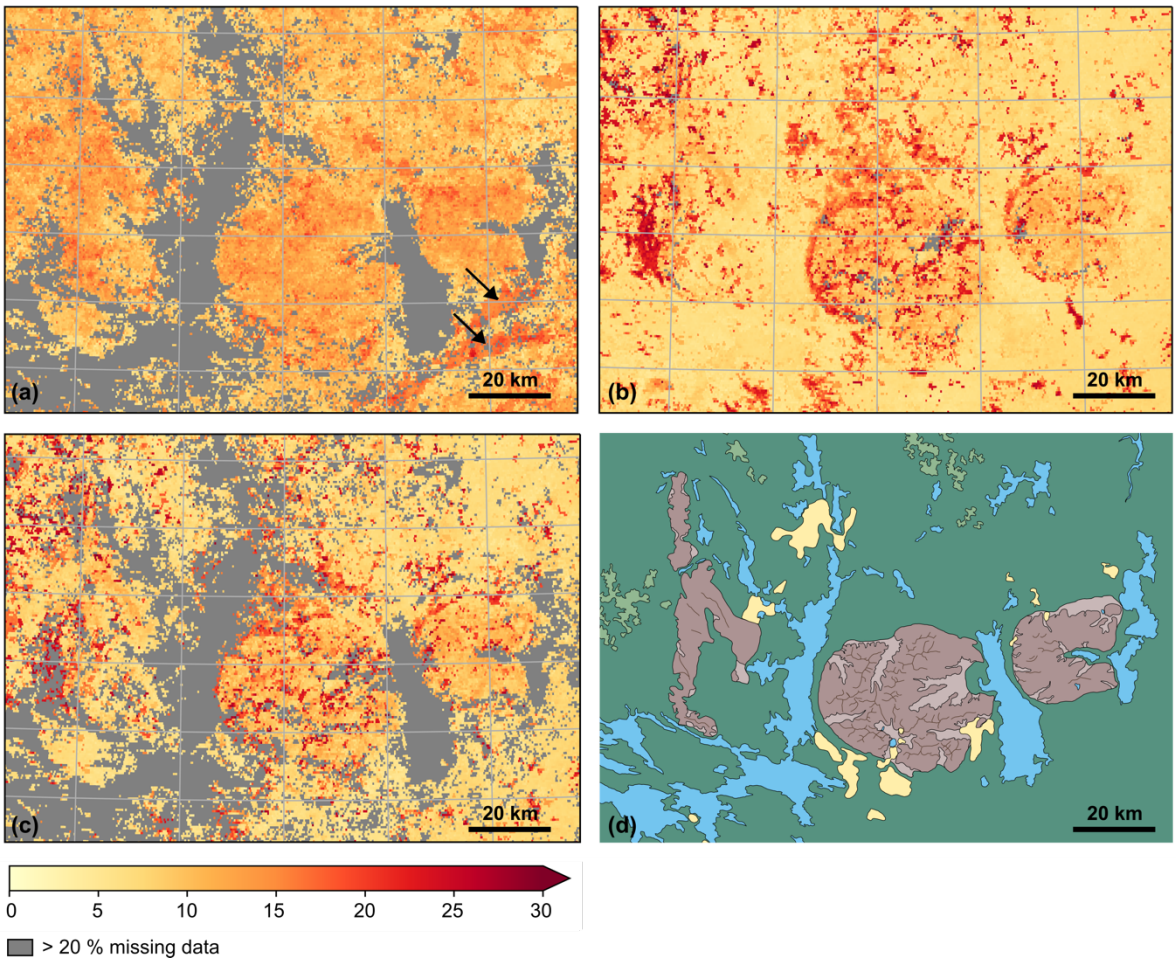

Figure 4.7: Standard deviation in days of the a. SCS, b. SCE and c. SCD over the 2000/2001 to 2015/2016 interval in the WMR.

Figure 4.7 shows the standard deviation from the mean in the SCS, SCE and SCD datasets. The two dark streaks south of the Khibiny Mountains in Fig. 4.7a (see arrows) are the result of a processing artefact in the original MODIS data in the year 2006 (see Fig. 4.A1g in the Appendix).

Most aspects of snow cover in the WMR have been characterised by high inter-annual variability over the past few decades. Figure 4.7 shows this particularly clearly where the standard deviation from the mean in SCS is consistently over 15 days across the region, and where the standard deviation reaches over 30 days in many pixels in the SCE and SCD datasets. Overall, for all three parameters the standard deviation is larger in the high-altitude areas, reaching over 30 days for SCE and SCD. The standard deviation is also high on the western edges to all topographical features in both the SCE and SCD, consistently reaching over 20 days. In the SCE and SCD parameters, the plains have very low standard deviations of under 10 days. At lower altitudes, the mean standard deviation is highest for the SCS. Indeed, the dates of SCS vary considerably from year to year, with a very noticeable difference between the consecutive years 2008 and 2009 for example, where the snow cover in the plains surrounding the mountains started on average 20 days later in 2009 than it did in 2008 (see Fig. 4.A1i and 4.A1j in the Appendix).

4.4.2.5 Trends in SCS, SCE and SCD

Station	Dates of common period with MODIS	Parameter	Trend Station data (days/decade)	Trend MODIS data (days/decade)
Lovozero	2000 - 2016	SCS	-4.1	-4.8
		SCE	-3.4	-1.4
		SCD	2.7	-2.8
Monchegorsk	2005 - 2016	SCS	-9.9	24.2
		SCE	-14.5***	-11.6*
		SCD	-5.4	-10.7
MSU Khibiny	2000 - 2016	SCS	-3.6	1.9
		SCE	5.3	-1.4
		SCD	8.7	2.6

Table 4.7: Trends in days per year and their significance of the Snow Cover Start (SCS), Snow Cover End (SCE) and Snow Cover Duration (SCD) at the four WMR stations from both data collected at those stations and from the MODIS processed dataset. Statistically significant trends are marked with asterisks: * = p < 0.1, ** = p < 0.05, ***= p < 0.01.

It is possible to investigate trends in the snow cover using the SCS, SCE and SCD dates extracted from the MODIS processed dataset. These can be compared to those recorded at the meteorological stations by calculating the trends over the common period of 2000 - 2016; Table 4.7 shows these trends. In section 4.4.1.2.1, I demonstrated that over the 2005 to 2017 interval of data collected at Monchegorsk, the snow cover season has not undergone any statistically significant trends. However, over the time period also covered by MODIS (2005 to 2016), a statistically significant trend is identified in the SCE ($p < 0.01$), wherein the snow cover season has been ending earlier at a rate of 14.5 days/decade. This is a result of the year 2017 being a very anomalous year (see Fig. 4.2), thus the inclusion of such an outlier year decreases the statistical significance of the trend. Importantly, the only statistically significant trend at a station location in the MODIS data is at Monchegorsk station, similar to the observations, where the snow cover season has been ending 11.6 days/decade earlier.

Figure 4.8 shows the high spatial variability of trends in snow cover in the WMR, as calculated from the MODIS processed dataset. Figure 4.9 shows the statistical significance of these trends, with statistically significant trends shown in colour, matching the direction of the trend.

The SCS trend figure (Fig. 4.8a) shows a clear orographic influence. The western side of the Khibiny Mountains has a positive SCS trend, in other words the SCS has been increasingly later in the year over the 2000 - 2016 period. Conversely, the eastern side of the mountains has a negative trend of less than 20 days/decade. The snow season in the Lovozero Mountains has also started later by 10 to 20 days/decade, as has the western edge of the VMC Tundras. The proportion of statistically significant trends in these two high-altitude (> 400 m) areas however is quite low (Fig. 4.9a). The plains do not show a consistent trend in Fig. 4.8a, but the majority of the statistically significant trends there (Fig. 4.9a) are negative.

In Fig. 4.8b, the plains have a consistent positive trend in SCE (of less than 10 days/decade). These positive trends are not so clear in Fig. 4.9b, as the majority of the trends in the plain are not

statistically significant. However, the main clusters of significant trends in the low altitude zones are negative over water bodies and are positive along the eastern edges of the mountain ranges (see Fig. 4.1 for topography). Trends in the SCE in the higher altitude areas are not so clear in Fig. 4.8b. Some of the high-altitude zones have had a delay in the end of the snow cover (positive trend) and others, such as the northern Khibiny and Lovozero Mountains, have had an increasingly early SCE (negative trend). The picture becomes clearer in Fig. 4.9b, where it is possible to see that parts of the northern Khibiny and Lovozero Mountains as well as the VMC Tundras are characterised by statistically significant negative trends, and that the only statistically significant positive trends in SCE at high elevations are in the southern and eastern Khibiny and Lovozero Mountains.

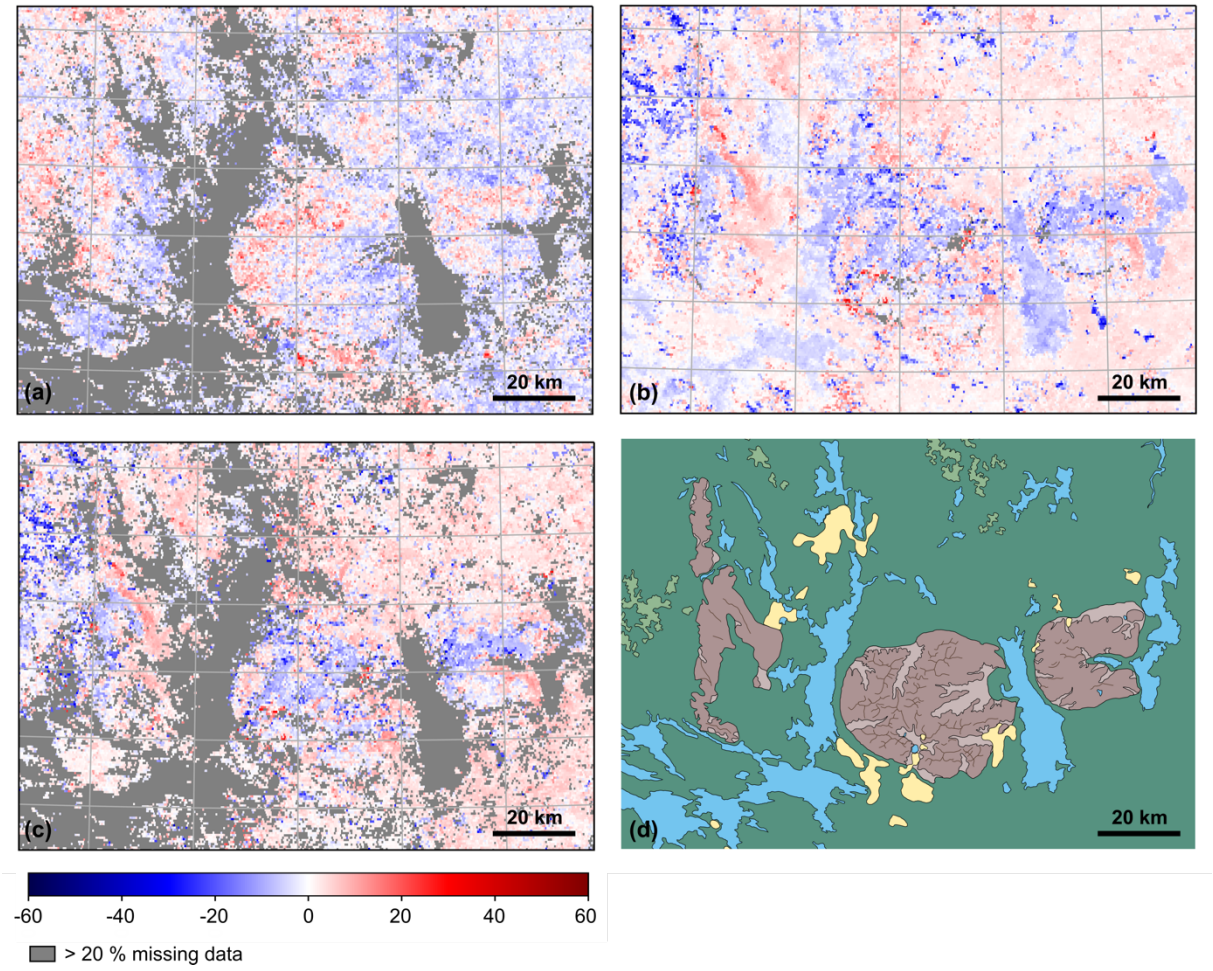

Figure 4.8: Trends in days per decade in the a. SCS, b. SCE and c. SCD over the 2000/2001 to 2015/2016 interval in the WMR.

The SCD has shortened statistically significantly by 10 to 20 days/decade within the mountains at the higher altitudes in the northern Khibiny, northern Lovozero Mountains as well as the lower elevation topography of the VMC Tundras. The very south-eastern areas of the Khibiny and Lovozero Mountains are the only regions of high elevation that have undergone statistically significant positive trends. Contrastingly, the SCD has undergone small, positive and statistically significant trends (less than 10 days/decade extension) in mountain valleys and widespread areas of the plains in the WMR. The plains to the north-west of the Khibiny Mountains are the only low elevation zone with an

increasingly short snow cover season, due to an earlier end of the snow season by approximately 20 days/decade.

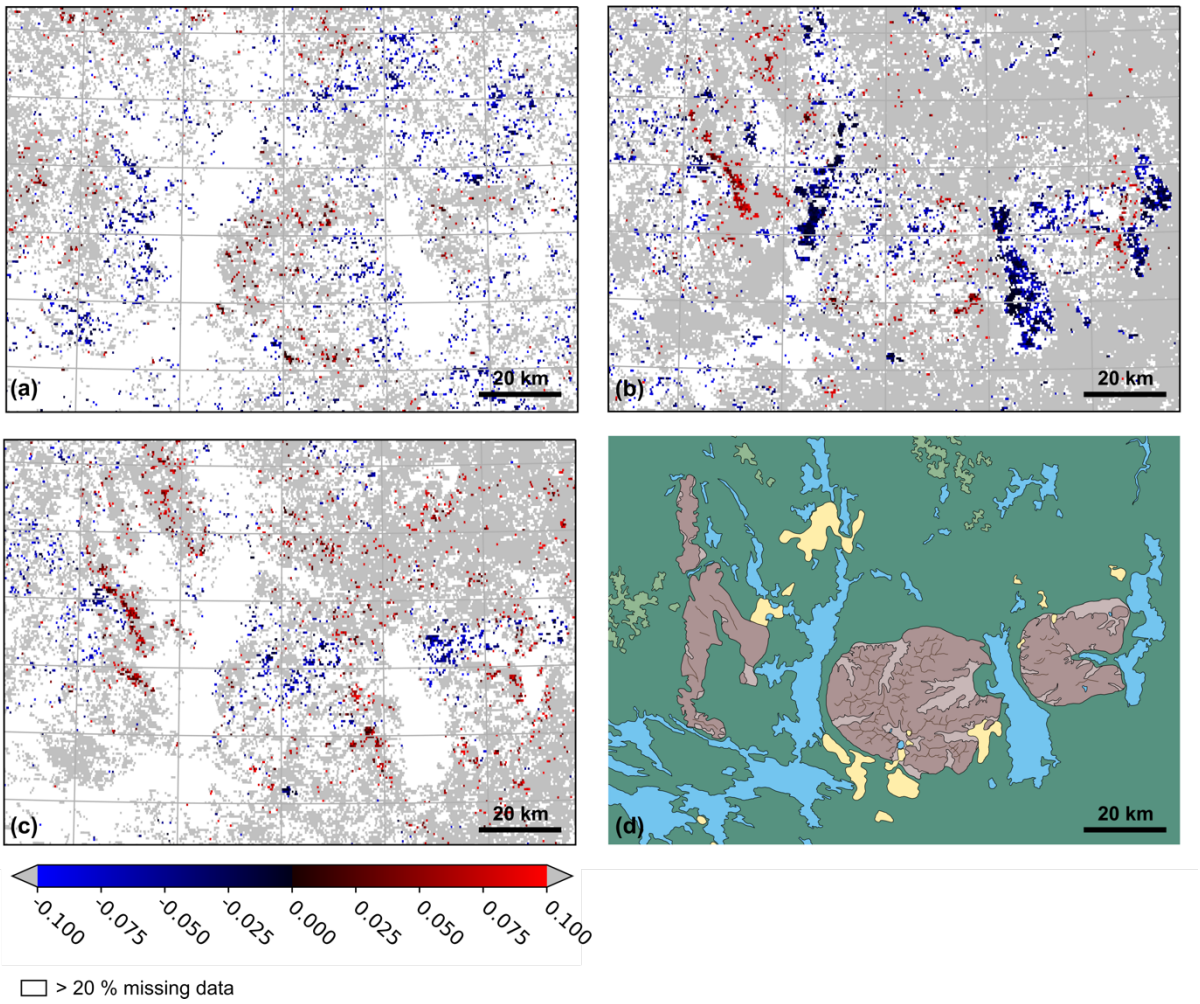

Figure 4.9: Statistical significance of positive (red) and negative (blue) trends in the a. SCS, b. SCE and c. SCD over the 2000/2001 to 2015/2016 interval in the WMR. Grey pixels show trends that are not statistically significant.

4.5 Discussion

4.5.1 Variability

In this section, the results presented in section 4.4 are discussed and placed in a broader context. As demonstrated in Chapter 3, there is large spatial variability in the Khibiny Mountains at a scale under 5 km^2 (fieldwork area). This spatial variability is also demonstrated in this chapter at the scale of the WMR. Mountains typically have large variations in climate zones (Beniston et al., 1997) and, consequently, snow (Immerzeel et al., 2009) as a result of the larger differences in elevation and slope aspects over small horizontal distances. Thus, snow cover is highly spatially variable in mountain ranges: e.g. in the Alps (Scherrer et al., 2013), Andes (Cornwell et al., 2016), Himalayas (Immerzeel et al., 2009), Pyrenees (López-Moreno and Vicente-Serrano, 2007; Buisan and López-Moreno, 2015) etc. This is seen in the result of this study, in particular, with the large differences in snow depth between two nearby stations (PABGI Khibiny and MSU Khibiny) within the Khibiny Mountains. This difference is likely explained by wind scouring. The MSU Khibiny station is situated at a highly exposed point in

the central-east valley, to the east of the largest lake in the mountains. In contrast to this, the PABGI Khibiny station is located on the lee side of the western Khibiny Mountains and has more cover from surrounding vegetation, and, as such, is shielded from the predominant westerly winds. This spatial variability in snow depth shows the importance of orography and other local factors in determining snow cover characteristics in the WMR. Additionally, it is important to be aware of how variable snow cover is, as it affects the scale needed to study changes in snow. In the modelling part of this thesis (Chapter 5 and 6), the resolution of the analysis is made as high as possible as a result of this high spatial variability.

As well as spatial variability, snow depth is shown to be variable at an inter-annual level in the WMR (see Fig. 4.2). This inter-annual variability in snow depth is likely explained by differences in air temperature, wind speed and solid precipitation (Demin, personal communication). The temporal variability of snow cover changes is also shown at a higher scale in the results of snow studies in the Kola Peninsula. Bulygina et al. (2009) found that snow cover duration has been decreasing in north-west Russia since 1966 and Blinova and Chmielewski (2014) demonstrated the mean growing season has been prolonged since 1951 in the Murmansk Oblast. Similar patterns have been found in Fennoscandia (Karlsen et al., 2009; Høgda et al., 2013). In contrast to these findings, using phenological evidence, Kozlov and Berlina (2002) found that the length of the summer in the Kola Peninsula decreased by 15 to 20 days in the 1930 to 1998 interval. Extracting the trends in the SCD at Kandalaksha station over comparable timescales to these two studies demonstrates that the contrasting conclusions of these previous studies can be explained by the different time periods analysed. Kandalaksha station shows a statistically significant lengthening of the snow cover season in the 1936 to 1998 interval of 4.5 days/decade, thus a decrease of the length of summer similar to Kozlov and Berlina (2002). In the 1966 to 2007 interval, a shortening of the snow cover season of 1.9 days/decade is found, though it is not statistically significant. This trend supports the conclusions of Bulygina et al. (2009).

Such temporal variability if typically found in mountainous regions. High temporal variability was found in Scherrer et al. (2013) in the Alps. In particular, they found high inter-decadal variability over a ~150-year data record. Immerzeel et al. (2009) found very high inter-annual, as well as seasonal, variability in snow coverage in the Himalayas. Another example of regional variability in the response of snow cover to climate change is an increase in the number of snow-covered days each year in China since 2000, where the average snow depth increased annually despite snow depth decreasing in all seasons but spring (Huang et al., 2016). This study also emphasized the significant regional differences in the variation of snow cover in China. Due to such high spatial and temporal variability in the response of snow cover to climate change, studying snow cover at a regional level is clearly essential.

4.5.2 Causes of observed changes

In this chapter, the causes of the identified trends in snow cover in the WMR were not studied as a result of the lack of available data. The most frequent causes of changes in snow cover (extent, timing and duration) can be divided into three. Firstly, changes in mean air temperature and precipitation

have a large impact on snowfall and snow melt and, thus, on snow cover (e.g. Alps – Beniston, 1997 and Scherrer et al., 2013; Himalayas – Immerzeel et al., 2009; Northern Hemisphere – Brown and Robinson, 2011; Russia – Bulygina et al., 2011). Secondly, the variability in snow depth and duration in the Arctic has also been associated with more localised features such as the characteristics of the underlying surface and the wind regime (e.g. Arctic – McBean et al., 2005 and Callaghan et al., 2011; Russia – Kopanev, 1971). Thirdly, as explained in Chapter 2 (section 2.1.4), atmospheric circulation changes can impact snow depth, extent and duration (e.g. Alps – Beniston, 1997; Andes – Rubio-Álvarez and McPhee, 2010; Pyrenees – Buisan and López-Moreno, 2015).

The main results regarding changes in snow cover start, end and duration are briefly considered in this section and their potential causes are discussed. In the WMR, the SCS trends show a clear orographic influence. The western side of the Khibiny Mountains has a positive SCS trend, in other words the SCS has been increasingly later in the year over the 2000 - 2016 period. The plains do not show a consistent SCS trend. The delay in the start of the snow season in the high altitudes is probably in part explained by the decrease in autumn precipitation in the Kola Peninsula (Marshall et al., 2016). The positive SCE trends found in the plains may be explained by the fact that spring has become increasingly wet (Marshall et al., 2016), so increased snowfall would delay the end of the snow season. The increasingly early end to the snow cover in the higher altitudes may be due, in part, to increased blowing snow (Demin, personal communication) as a result of the overall trend towards stronger winds in the Kola Peninsula (Roshydromet, 2005). This earlier end to the snow season at higher altitudes is a concerning trend in terms of water supply. Barnett et al. (2005) warned that even no changes liquid precipitation over spring and summer, earlier SCE in mountains leads to a shift in peak river runoff to winter and early spring, away from summer and autumn when water demand is highest.

In the plains, SCD is the most inter-annually uniform snow cover parameter. Station data suggests that this is a result of SCS and SCE moving in the same direction, and thus counter-balancing each other. The SCD has nevertheless shortened statistically significantly by 10 to 20 days/decade within the mountains at the higher altitudes in the northern Khibiny, northern Lovozero Mountains as well as the lower elevation topography of the VMC Tundras. Contrastingly, the SCD has undergone small, positive and statistically significant trends (less than 10 days/decade extension) in mountain valleys and widespread areas of the plains in the WMR. Farlaz (2004) found similar results over Poland in the 1948 - 1998 interval. Indeed, they found a decreasing trend in SCD over the majority of the country, but found that snow duration has increased over mountain ranges. These changes are cause by the increased frequency of western advection over Poland, as well as changes in air temperature, though the changes in snow do not scale proportionally with temperature. Beniston (1997) similarly explained SCD changes over the Alps, with changes in mean air temperature as well as large-scale atmospheric variation (NAO).

4.5.3 Uncertainty

Finally, the uncertainty of the MODIS products and its impact on the results are discussed. The effects on the results of the boreal forest cover in the WMR are considered. As discussed in Chapter 2,

forests hinder the retrieval of snow using VNIR satellite products. The MODIS algorithm makes use of the Normalized Difference Vegetation Index (NDVI) over forested areas (Klein et al., 1998). "Using a threshold on the NDVI it is possible that a forested pixel is classified as snow even if the NDSI is lower than 0.4" (Immerzeel et al., 2009; p44); the MODIS algorithm thus addresses some of the issues VNIR instruments face regarding snow cover mapping in forests. Parajka et al. (2012) studied the snow cover mapping accuracy of MODIS in both open and forested sites in a small mountain catchment in Northern Slovakia. They found that the respective errors of the combined Terra and Aqua MODIS products in open and forested land are 1.7 % and 7.3 % respectively (Parajka et al., 2012). These results, along with those of the MODIS ground truthing undertaken in Chapter 3 in the partly forested Khibiny Mountains, indicate that, though MODIS has higher uncertainty in forested areas, it is still a reliable dataset to analyse snow cover changes in the WMR.

Furthermore, the uncertainty in the MODIS products and results extracted from those was tested throughout section 4.4. The offsets between the recorded SCS and SCE dates at stations and those extracted from the MODIS processed dataset are calculated in section 4.4.2.2. The offsets are high, but not unprecedented. Indeed, Dietz et al (2012) found that 10 % (/3 %) of their study area was characterised by 34 to 72 (/72+) days deviation between station data and MODIS SCD. In this analysis, I find that for 85.8 % of pixels investigated (SCS and SCE combined) the deviation in the MODIS-derived dates is less than 20 days, 9.9 % of pixels have a deviation between 20 to 30 days and only 4.3 % of pixels are characterised by a deviation between 30 and 41 days (Fig. 4.5). Thus, despite the large magnitude of some errors, the difference between the station data and MODIS-derived snow cover season dates are in fact lower than some previous studies. Additionally, though these errors are still high, the focus of this chapter was in analysing trends and patterns of change, thus these errors in exact dates of SCS and SCE are not debilitating.

Importantly, the only statistically significant trend found at a station location in the MODIS data is at Monchegorsk station, similar to the observations, where the snow cover season has been ending 11.6 days/decade earlier. This result, and the lack of spurious statistically significant trends at the other stations, provides further evidence that MODIS can be used to analyse snow-cover trends in the WMR with a high degree of confidence.

4.6 Conclusions

In this chapter, I have used a combination of remote sensing data and meteorological observations to analyse past changes in snow cover in the WMR of the Kola Peninsula, Arctic Russia. MODIS snow products were processed in order to create SCS, SCE and SCD datasets. Although for some areas and some years, the start and end of the snow season could not be detected due to long overcast periods (Fig. 4.4), this MODIS post-processing reduced the number of missing pixels by more than half.

- MODIS is able to provide a highly reliable snow parameter dataset in the WMR of the Kola Peninsula, Arctic Russia. We have validated it through a comparison of the timing and trends

of the snow cover season with station data. The average difference between the station data and MODIS processed dataset-derived SCS and SCE dates is 8.6 and 10.4 days respectively, both relatively low errors. In this analysis, I find that for 85.8 % of pixels investigated (SCS and SCE combined) the deviation in the MODIS-derived dates is less than 20 days.

- It is possible to extract realistic trends from the MODIS processed dataset. Indeed, MODIS-extracted trends are identical to observed station trends in that MODIS was able to identify the only statistically significant trend while not giving spuriously significant trends elsewhere.
- There is high inter-annual and spatial variability in the long-term snow cover trends in the WMR of the Kola Peninsula. Overall, between 2000 and 2016, the snow cover duration has been decreasing at higher altitudes and increasing at lower altitudes. The end of the snow cover season has become increasingly later in the plains that surround the WMR, but there is not such a clear trend in SCE in the higher altitude areas. Snow depth was also found to be highly spatially variable and the difference in maximum yearly snow depth was found to be over 50 cm between two stations (PABGI Khibiny and MSU Khibiny) only 2 km apart at very similar altitudes in valleys within the Khibiny Mountains. These differences in snow depth as well as some of the trends in the snow cover season are probably explained by wind scouring that occurs in the WMR.
- Three of four meteorological stations in the WMR with SCS and SCE data were found to have recorded an increasingly long snow cover season across their differing lengths, but the only statistically significant trend was negative. This spatial variability is also found to exist on larger scales over longer periods.
- A uniform, statistically significant, regional decrease in the duration of the snow cover season between 1992 and 2016 has occurred across the lower altitudes of the western Murmansk Oblast.

4.7 Fit within thesis

Following from Chapter 3 where all measured snow parameters were shown to be highly variable at a sub-fieldwork area scale, snow continues to be highly spatially variable at the scale of the WMR. This is important for Chapter 5 where point measurements are used to validate model outputs and must be considered in this highly spatially variable context. As well as having low (< 10%) overall errors as demonstrated in Chapter 3, MODIS processed outputs are demonstrated to have a reasonably low uncertainty in the timing of the snow season and to have good skill in extracting trends. In this chapter, trends in the timing and duration of the snow cover season in a warming climate have been extracted. These trends will be put in a broader context in Chapter 6 where century scale changes in snow cover will be investigated in an increasingly warmer climate.

4.8 References

Anisimov, O. and Reneva, S., 2006. Permafrost and changing climate: the Russian perspective. AMBIO: A Journal of the Human Environment, 35(4), pp.169-175, https://doi.org/10.1579/0044-7447(2006)35[169:PACCTR]2.0.CO;2

Armstrong, R.L. and Brodzik, M.J., 2001. Recent Northern Hemisphere snow extent: A comparison of data derived from visible and microwave satellite sensors. Geophysical Research Letters, 28(19), pp.3673-3676, https://doi.org/10.1029/2000GL012556

Atlaskina, K., Berninger, F. and de Leeuw, G., 2015. Satellite observations of changes in snow-covered land surface albedo during spring in the Northern Hemisphere, The Cryosphere, 9(5), pp.1879-1893, https://doi.org/10.5194/tc-9-1879-2015

Beniston, M., 1997. Variations of snow depth and duration in the Swiss Alps over the last 50 years: links to changes in large-scale climatic forcings. In Climatic change at high elevation sites (pp. 49-68). Springer, Dordrecht. https://doi.org/10.1007/978-94-015-8905-5_3

Blinova, I. and Chmielewski, F.M., 2008. Subarctic warming and its influence on the growth of orchid populations in the Extreme North-East of Europe (Murmansk Region). Journal Europäischer Orchideen, 40(4), p.663.

Blinova, I. and Chmielewski, F.M., 2014. Climatic warming above the Arctic Circle: are there trends in timing and length of the thermal growing season in Murmansk Region (Russia) between 1951 and 2012?. International journal of biometeorology, 59(6), pp.693-705, https://doi.org/10.1007/s00484-014-0880-y

Blinova, I., 2011. The traits of seasonal development of orchid species north of the Arctic Circle. Bot Zh, 96(3), pp.396-411. (in Russian)

Bony, S., Colman, R., Kattsov, V.M., Allan, R.P., Bretherton, C.S., Dufresne, J.L., Hall, A., Hallegatte, S., Holland, M.M., Ingram, W. and Randall, D.A., 2006. How well do I understand and evaluate climate change feedback processes?. Journal of Climate, 19(15), pp.3445-3482.

Bormann, K.J., Brown, R.D., Derksen, C. and Painter, T.H., 2018. Estimating snow-cover trends from space. Nature Climate Change, 8(11), p.924., https://doi.org/10.1038/s41558-018-0318-3

Brown, R.D. and Robinson, D.A., 2011. Northern Hemisphere spring snow cover variability and change over 1922–2010 including an assessment of uncertainty. The Cryosphere, 5(1), pp.219-229, https://doi.org/10.5194/tc-5-219-2011

Broxton, P.D., Harpold, A.A., Biederman, J.A., Troch, P.A., Molotch, N.P. and Brooks, P.D., 2014. Quantifying the effects of vegetation structure on snow accumulation and ablation in mixed-conifer forests. Ecohydrology, 8(6), pp.1073-1094, https://doi.org/10.1002/eco.1565

Buisan, S.T., Saz, M.A. and López-Moreno, J.I., 2015. Spatial and temporal variability of winter snow and precipitation days in the western and central Spanish Pyrenees. International Journal of Climatology, 35(2), pp.259-274. https://doi.org/10.1002/joc.3978

Bulygina, O.N., Groisman, P.Y., Razuvaev, V.N. and Korshunova, N.N., 2011. Changes in snow cover characteristics over Northern Eurasia since 1966. Environmental Research Letters, 6(4), p.045204.

Bulygina, O.N., Razuvaev, V.N. and Korshunova, N.N., 2009. Changes in snow cover over Northern Eurasia in the last few decades. Environmental Research Letters, 4(4), p.045026, https://doi.org/10.1088/1748-9326/4/4/045026

Callaghan, T.V., Johansson, M., Brown, R.D., Groisman, P.Y., Labba, N., Radionov, V., Bradley, R.S., Blangy, S., Bulygina, O.N., Christensen, T.R. and Colman, J.E., 2011. Multiple effects of changes in Arctic snow cover. Ambio, 40(1), pp.32-45. https://doi.org/10.1007/s13280-011-0213-x

Callaghan, T.V., Johansson, M., Brown, R.D., Groisman, P.Y., Labba, N., Radionov, V., Barry, R.G., Bulygina, O.N., Essery, R.L., Frolov, D.M. and Golubev, V.N., 2011. The changing face of Arctic snow cover: A synthesis of observed and projected changes. AMBIO: A Journal of the Human Environment, 40(sup 1), pp.17-31, https://doi.org/10.1007/s13280-011-0212-y

Cohen, J., Screen, J.A., Furtado, J.C., Barlow, M., Whittleston, D., Coumou, D., Francis, J., Dethloff, K., Entekhabi, D., Overland, J. and Jones, J., 2014. Recent Arctic amplification and extreme mid-latitude weather. Nature geoscience, 7(9), pp.627-637, https://doi.org/10.1038/ngeo2234

Cornwell, E., Molotch, N.P. and McPhee, J., 2016. Spatio-temporal variability of snow water equivalent in the extra-tropical Andes Cordillera from distributed energy balance modeling and remotely sensed snow cover. Hydrology and Earth System Sciences, 20(1). https://doi.org/10.5194/hess-20-411-2016

Demin V. I. and Volkov A.V., 2017. A comparison of air temperature trends in the Khibiny Mountains and over the surrounding plains. Fundamental and applied climatology, 3, pp.6-27. (in Russian)

Demin V.I., Antsyferova A.P., and Mokrotovarova O.I., 2015. Changes of the air temperature in Murmansk since the 19th century. Herald of the Kola Science Centre of the Russian Academy of Sciences, 20(1), pp.113-126. (in Russian)

Demin V.I., Sviashchennikov P.N., and Ivanov B.V., 2014. Long-Term Variations of Large-Scale Atmosphere Circulation and the modern climate warming at the Kola Peninsula. Herald of the Kola Science Centre of the Russian Academy of Sciences, 17(2), pp.101-106. (in Russian)

Demin, V.I. and Zyuzin, Y.L., 2006. On climatic changes in the Khibiny Mountains (Kola Peninsula, Russia). Physics of Auroral Phenomena, Proceedings of the XXIX Annual Seminar, Apatity, pp. 281-284.

Demin, V.I. and Zyuzin, Y.L., 2009. Detection of the mountain ecosystem dynamics in the Khibiny by technique of comparison of modern and old photographs and its relation with climate changes. Physics of Auroral Phenomena, 31(1), pp.189-191.

Demin, V.I., 2012. General climatic tendencies on the Kola Peninsula during the meteorological measurements period. Proc. Kola Sci. Cent., 1, pp.98–110. (in Russian)

Dewey, K.F., 1977. Daily maximum and minimum temperature forecasts and the influence of snow cover. Monthly Weather Review, 105(12), pp.1594-1597, https://doi.org/10.1175/1520-0493(1977)105<1594:DMAMTF>2.0.CO;2

Dietz, A.J., Wohner, C. and Kuenzer, C., 2012. European snow cover characteristics between 2000 and 2011 derived from improved MODIS daily snow cover products. Remote Sensing, 4(8), pp.2432-2454, https://doi.org/10.3390/rs4082432

Duguay, C.R., Flato, G.M., Jeffries, M.O., Ménard, P., Morris, K. and Rouse, W.R., 2003. Ice-cover variability on shallow lakes at high latitudes: model simulations and observations. Hydrological Processes, 17(17), pp.3465-3483, https://doi.org/10.1002/hyp.1394

Dye, D.G., 2002. Variability and trends in the annual snow-cover cycle in Northern Hemisphere land areas, 1972–2000. Hydrological processes, 16(15), pp.3065-3077, https://doi.org/10.1002/hyp.1089

Essery, R., Pomeroy, J., Parviainen, J. and Storck, P., 2003. Sublimation of snow from coniferous forests in a climate model. Journal of Climate, 16(11), pp.1855-1864, https://doi.org/10.1175/1520-0442(2003)016<1855:SOSFCF>2.0.CO;2

Fagre, D.B., Peterson, D.L. and Hessl, A.E., 2003. Taking the pulse of mountains: ecosystem responses to climatic variability. Climate Variability and Change in High Elevation Regions: Past, Present & Future. Springer, Dordrecht, pp.263-282, https://doi.org/10.1023/A:1024427803359

Falarz, M., 2004. Variability and trends in the duration and depth of snow cover in Poland in the 20th century. International Journal of Climatology: A Journal of the Royal Meteorological Society, 24(13), pp.1713-1727. https://doi.org/10.1002/joc.1093

Foppa, N. and Seiz, G., 2012. Inter-annual variations of snow days over Switzerland from 2000-2010 derived from MODIS satellite data. The Cryosphere, 6(2), p.331, https://doi.org/10.5194/tc-6-331-2012

Glazovskaya T.G., 2000. Possible changes in snow and avalanche activity due to projected global warming. MGI materials of glaciological research, Iss. No. 88, pp. 70-73. (in Russian)

Gouttevin, I., Menegoz, M., Domin, F., Krinner, G., Koven, C., Ciais, P., Tarnocai, C. and Boike, J., 2012. How the insulating properties of snow affect soil carbon distribution in the continental pan-Arctic area. Journal of Geophysical Research: Biogeosciences, 117(G2), https://doi.org/10.1029/2011JG001916

Gregow, H., Puranen, U., Venäläinen, A., Peltola, H., Kellomäki, S. and Schultz, D., 2008. Temporal and spatial occurrence of strong winds and large snow load amounts in Finland during 1961–2000. Silva Fennica, 42(4), pp.515-534.

Groisman, P.Y., Bogdanova, E.G., Alexeev, V.A., Cherry, J.E. and Bulygina, O.N., 2014. Impact of snowfall measurement deficiencies on quantification of precipitation and its trends over northern Eurasia. Lëd i Sneg, 54(2), pp.29-43, https://doi.org/10.15356/2076-6734-2014-2-29-43

Høgda, K.A., Karlsen, S.R. and Solheim, I., 2001. Climatic change impact on growing season in Fennoscandia studied by a time series of NOAA AVHRR NDVI data. In Geoscience and Remote Sensing Symposium, 2001, IGARSS'01, IEEE International, 3, pp. 1338-1340, https://doi.org/10.1109/IGARSS.2001.976837

Høgda, K.A., Tømmervik, H. and Karlsen, S.R., 2013. Trends in the start of the growing season in Fennoscandia 1982–2011. Remote Sensing, 5(9), pp.4304-4318, https://doi.org/10.3390/rs5094304

Huang, X., Deng, J., Ma, X., Wang, Y., Feng, Q., Hao, X. and Liang, T., 2016. Spatiotemporal dynamics of snow cover based on multi-source remote sensing data in China. The Cryosphere, 10(5), p.2453, https://doi.org/10.5194/tc-10-2453-2016

Hüsler, F., Jonas, T., Riffler, M. and Musial, J.P., 2014. A satellite-based snow cover climatology (1985-2011) for the European Alps derived from AVHRR data. The Cryosphere, 8(1), p.73, https://doi.org/10.5194/tc-8-73-2014

Immerzeel, W.W., Droogers, P., De Jong, S.M. and Bierkens, M.F.P., 2009. Large-scale monitoring of snow cover and runoff simulation in Himalayan river basins using remote sensing. Remote sensing of Environment, 113(1), pp.40-49. https://doi.org/10.1016/j.rse.2008.08.010

IPCC, 2014. Climate Change 2014: Impacts, Adaptation, and Vulnerability. Part A: Global and Sectoral Aspects. Contribution of Working Group II to the Fifth Assessment Report of the Intergovernmental Panel on Climate Change [Field, C.B., V.R. Barros, D.J. Dokken, K.J. Mach, M.D. Mastrandrea, T.E. Bilir, M. Chatterjee, K.L. Ebi, Y.O. Estrada, R.C. Genova, B. Girma, E.S. Kissel, A.N. Levy, S. MacCracken, P.R. Mastrandrea, and L.L. White (eds.)]. Cambridge University Press, Cambridge, United Kingdom and New York, NY, USA, pp 1132.

Karlsen, S.R., Høgda, K.A., Wielgolaski, F.E., Tolvanen, A., Tømmervik, H., Poikolainen, J. and Kubin, E., 2009. Growing-season trends in Fennoscandia 1982–2006, determined from satellite and phenology data. Climate Research, 39(3), pp.275-286, https://doi.org/10.3354/cr00828

Keller, F., Goyette, S. and Beniston, M., 2005. Sensitivity analysis of snow cover to climate change scenarios and their impact on plant habitats in alpine terrain. Climatic Change, 72(3), pp.299-319, https://doi.org/10.1007/s10584-005-5360-2

Kitaev L.M., Volodicheva N.A., and Oleynikov A.D., 2007. Long-term snow dynamics in the north-west of the Russian plain. The materials of glaciological research, 102, pp.65-72.

Klein, A.G., Hall, D.K. and Riggs, G.A., 1998. Improving snow cover mapping in forests through the use of a canopy reflectance model. Hydrological Processes, 12(10-11), pp.1723-1744. https://doi.org/10.1002/(SICI)1099-1085(199808/09)12:10/11<1723::AID-HYP691>3.0.CO;2-2

Kopanev I D 1971 Methods of Studying Snow Cover (Leningrad: Gidrometeoizdat) p 225 (in Russian)

Koroleva, N.E., 1994. Phytosociological survey of the tundra vegetation of the Kola Peninsula, Russia. Journal of Vegetation Science, 5(6), pp.803-812, https://doi.org/10.2307/3236195

Kozlov, M.V. and Berlina, N.G., 2002. Decline in length of the summer season on the Kola Peninsula, Russia. Climatic Change, 54(4), pp.387-398, https://doi.org/10.1023/A:1016175101383

Lawrence, D.M. and Slater, A.G., 2005. A projection of severe near-surface permafrost degradation during the 21st century. Geophysical Research Letters, 32(24), https://doi.org/10.1029/2005GL025080.

Lemke, P., Ren, J., Alley, R.B., Allison, I., Carrasco, J., Flato, G., Fujii, Y., Kaser, G., Mote, P., Thomas, R.H. and Zhang, T., 2007. Observations: changes in snow, ice and frozen ground. Climate Change 2007: The Physical Science Basis. Contribution of Working Group I to the Fourth Assessment Report of the Intergovernmental Panel on Climate Change. Cambridge University Press, Cambridge, United Kingdom and New York, NY, USA, pp 1132.

Liston, G.E., 2004. Representing subgrid snow cover heterogeneities in regional and global models. Journal of climate, 17(6), pp.1381-1397, https://doi.org/10.1175/1520-0442(2004)017<1381:RSSCHI>2.0.CO;2

López-Moreno, J.I. and Vicente-Serrano, S.M., 2007. Atmospheric circulation influence on the interannual variability of snow pack in the Spanish Pyrenees during the second half of the 20th century. Hydrology Research, 38(1), pp.33-44. https://doi.org/10.2166/nh.2007.030

Malnes, E., Karlsen, S.R., Johansen, B., Bjerke, J.W. and Tømmervik, H., 2016. Snow season variability in a boreal-Arctic transition area monitored by MODIS data. Environmental Research Letters, 11(12), p.125005, https://doi.org/10.1088/1748-9326/11/12/125005

Marshall, G.J., Vignols, R.M. and Rees, W.G., 2016. Climate change in the Kola Peninsula, Arctic Russia, during the last 50 years from meteorological observations. Journal of Climate, 29(18), pp.6823-6840, https://doi.org/10.1175/JCLI-D-16-0179.1

Maskey, S., Uhlenbrook, S. and Ojha, S., 2011. An analysis of snow cover changes in the Himalayan region using MODIS snow products and in-situ temperature data. Climatic Change, 108(1-2), p.391. https://doi.org/10.1007/s10584-011-0181-y

Matsumura, S., Zhang, X. and Yamazaki, K., 2014. Summer Arctic atmospheric circulation response to spring Eurasian snow cover and its possible linkage to accelerated sea ice decrease. Journal of Climate, 27(17), pp.6551-6558, https://doi.org/10.1175/JCLI-D-13-00549.1

McBean, G., Alekseev, G., Chen, D., Foerland, E., Fyfe, J., Groisman, P.Y., King, R., Melling, H., Vose, R. and Whitfield, P.H., 2005. Chapter 2: Arctic Climate: past and present. Arctic Climate Impact Assessment.[np].

Molotch, N.P., Blanken, P.D., Williams, M.W., Turnipseed, A.A., Monson, R.K. and Margulis, S.A., 2007. Estimating sublimation of intercepted and sub-canopy snow using eddy covariance systems. Hydrological Processes, 21(12), pp.1567-1575, https://doi.org/10.1002/hyp.6719

Olofinskaya, N., Dobrolyubova, J., Berdin, V., Gershinkova, D. and Masloboyev, V., 2009. Integrated Climate Change Strategies for Sustainable Development of Russia's Arctic Regions (Case Study for Murmansk oblast). Summary.

Parajka, J., Holko, L., Kostka, Z. and Blöschl, G., 2012. MODIS snow cover mapping accuracy in a small mountain catchment–comparison between open and forest sites. Hydrology and Earth System Sciences, 16(7), pp.2365-2377. https://doi.org/10.5194/hess-16-2365-2012

Peng, S., Piao, S., Ciais, P., Friedlingstein, P., Zhou, L. and Wang, T., 2013. Change in snow phenology and its potential feedback to temperature in the Northern Hemisphere over the last three decades. Environmental Research Letters, 8(1), p.014008, https://doi.org/10.1088/1748-9326/8/1/014008

Riggs, G.A., Hall, D.K. and Román, M.O., 2016. MODIS snow products collection 6 user guide. National Snow & Ice Data Center. https://doi.org/10.1029/2019WR024914

Rittger, K., Raleigh, M.S., Dozier, J., Hill, A.F., Lutz, J.A. and Painter, T.H., 2019. Canopy Adjustment and Improved Cloud Detection for Remotely Sensed Snow Cover Mapping. Water Resources Research.

Robinson, D.A. and Frei, A., 2000. Seasonal variability of Northern Hemisphere snow extent using visible satellite data. The Professional Geographer, 52(2), pp.307-315, https://doi.org/10.1111/0033-0124.00226

Robinson, D.A., Dewey, K.F. and Heim Jr, R.R., 1993. Global snow cover monitoring: An update. Bulletin of the American Meteorological Society, 74(9), pp.1689-1696, https://doi.org/10.1175/1520-0477(1993)074<1689:GSCMAU>2.0.CO;2

Roshydromet: Strategic forecast of climate changes in the Russian Federation for the period until 2010-2015 and their influence on Russian economic sectors. Moscow. Roshydromet, 2005. (the document is available at the Roshydromet web-site http://meteorf.ru)

Rubio-Álvarez, E. and McPhee, J., 2010. Patterns of spatial and temporal variability in streamflow records in south central Chile in the period 1952–2003. Water Resources Research, 46(5). https://doi.org/10.1029/2009WR007982

Rutter, N., Essery, R., Pomeroy, J., Altimir, N., Andreadis, K., Baker, I., Barr, A., Bartlett, P., Boone, A., Deng, H. and Douville, H., 2009. Evaluation of forest snow processes models (SnowMIP2). Journal of Geophysical Research: Atmospheres, 114(D6). https://doi.org/10.1029/2008jd011063

Salomonson, V.V. and Appel, I., 2004. Estimating fractional snow cover from MODIS using the normalized difference snow index. Remote sensing of environment, 89(3), pp.351-360, https://doi.org/10.1016/j.rse.2003.10.016

Sapunov VN, Seliverstov Yu.G., Troshkina E.S., Chernous P.A., 2006. Temperature regime of air in winter seasons and its influence on avalanche activity in the Khibiny. Cryosphere of the Earth, volume X., No. 4., pp.68-73. (in Russian)

Scherrer, S.C., Wüthrich, C., Croci-Maspoli, M., Weingartner, R. and Appenzeller, C., 2013. Snow variability in the Swiss Alps 1864–2009. International journal of climatology, 33(15), pp.3162-3173. https://doi.org/10.1002/joc.3653

Serreze, M.C. and Barry, R.G., 2011. Processes and impacts of Arctic amplification: A research synthesis. Global and Planetary Change, 77(1), pp.85-96, https://doi.org/10.1016/j.gloplacha.2011.03.004

Serreze, M.C., Barrett, A.P., Stroeve, J.C., Kindig, D.N. and Holland, M.M., 2009. The emergence of surface-based Arctic amplification. The Cryosphere, 3(1), p.11.

Shmakin, A.B., 2010. Climatic characteristics of snow cover over North Eurasia and their change during the last decades. Ice and Snow, 1(1), pp.43-57.

Singh, P.R. and Gan, T.Y., 2000. Retrieval of snow water equivalent using passive microwave brightness temperature data. Remote Sensing of Environment, 74(2), pp.275-286, https://doi.org/10.1016/S0034-4257(00)00121-8

Storvold, R., Malnes, E., Larsen, Y., Høgda, K.A., Hamran, S.E., Mueller, K. and Langley, K.A., 2006. SAR remote sensing of snow parameters in norwegian areas—Current status and future

perspective. Journal of Electromagnetic Waves and Applications, 20(13), pp.1751-1759, https://doi.org/10.1163/156939306779292192

Tedesco, M. and Monaghan, A.J., 2009. An updated Antarctic melt record through 2009 and its linkages to high-latitude and tropical climate variability. Geophysical Research Letters, 36(18), https://doi.org/10.1029/2009GL039186

Tedesco, M., 2015. Remote sensing of the cryosphere. John Wiley & Sons, https://doi.org/10.1002/9781118368909

Troshkina E.S., Sapunov VN, Seliverstov Yu.G., Chernous P.A., 2005. Dynamics of the snow cover in the Khibiny Mountains (1936-2002). MGIM Materials of glaciological research, 99, pp.112-115. (in Russian)

Troshkina E.S., Seliverstov Yu.G., Mokrov E.G., Sapunov V.N., Chernous P.A., Solovyev A.Yu., 2009. Influence of climatic conditions change on nival-glacial processes in the Khibiny Mountains. Bulletin of Moscow University, Series 5: Geography, pp.26-32. (in Russian)

Trujillo, E., Molotch, N.P., Goulden, M.L., Kelly, A.E. and Bales, R.C., 2012. Elevation-dependent influence of snow accumulation on forest greening. Nature Geoscience, 5(10), p.705, https://doi.org/10.1038/ngeo1571

Vajda, A., Venalainen, A., Hanninen, P. and Sutinen, R., 2006. Effect of vegetation on snow cover at the northern timberline: a case study in Finnish Lapland. Silva Fennica, 40(2), p.195. https://doi.org/10.14214/sf.338

Vavrus, S., 2007. The role of terrestrial snow cover in the climate system. Climate Dynamics, 29(1), pp.73-88, https://doi.org/10.1007/s00382-007-0226-0

Vikulina M.A., 2009. Assessment of avalanche activity, hazard and risk (with the Khibiny Mountains as an example). In Glaciology in the Beginning of the 21st Century (Proceedings of the International Scientific Conference). Moscow State University Publication: ed., University Book, p.260. (in Russian)

Walland, D.J. and Simmonds, I., 1997. North American and Eurasian snow cover co-variability. Tellus A, 49(4), pp.503-512, https://doi.org/10.1034/j.1600-0870.1997.t01-3-00007.x

Wuttke, S., Seckmeyer, G. and König-Langlo, G., 2006. Measurements of spectral snow albedo at Neumayer, Antarctica. Annales Geophysicae 24, Nr. 1, http://dx.doi.org/10.5194/angeo-24-7-2006

Yakovlev, B.A.: Climate of Murmansk region. Murmansk Knizhn Izd, Murmansk, 1961. (in Russian)

Zaika Yu.V., Vikulina M.A., Chernous P.A., 2013. Long-term dynamics of nival processes in the Khibiny. (in Russian)

Zhang, M., Lai, Y., Liu, Z. and Gao, Z., 2005. Nonlinear analysis for the cooling effect of Qinghai-Tibetan railway embankment with different structures in permafrost regions. Cold Regions Science and Technology, 42(3), pp.237-249, https://doi.org/10.1016/j.coldregions.2005.02.003

Zhang, Y., Yan, S. and Lu, Y., 2010. Snow cover monitoring using MODIS data in Liaoning Province, Northeastern China. Remote Sensing, 2(3), pp.777-793, https://doi.org/10.3390/rs2030777

Zyuzin Yu.L, 2006. The severe face of Khibiny, Murmansk. Advertising Polygraphy, pp.235. (in Russian)

4.9 Appendix

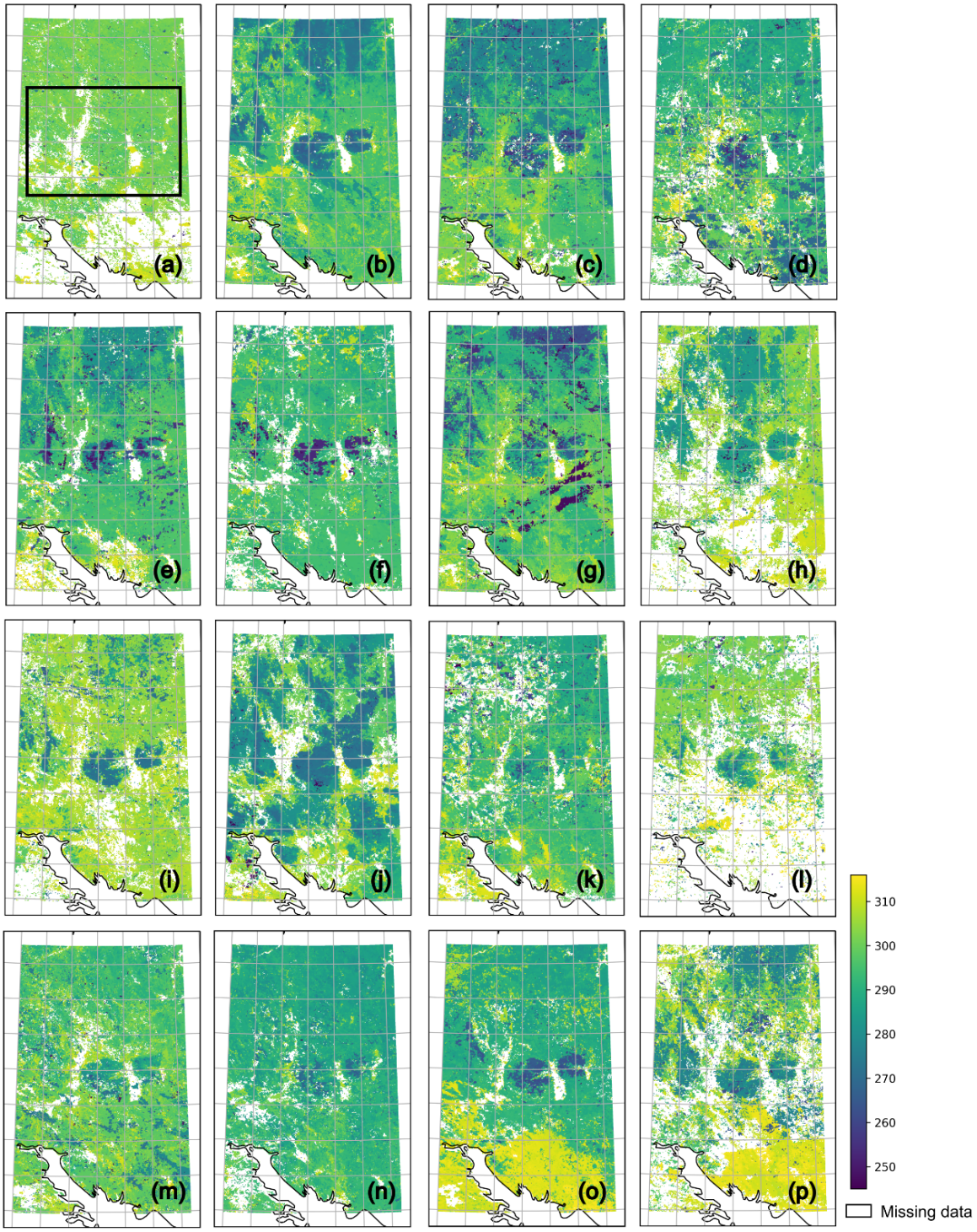

Figure 4.A1: SCS maps for the WMR showing the last day of the snow-free season from the year 2000 (a) to 2015 (p). The colourbar shows the day of the year. The WMR is outlined in (a) for scale.

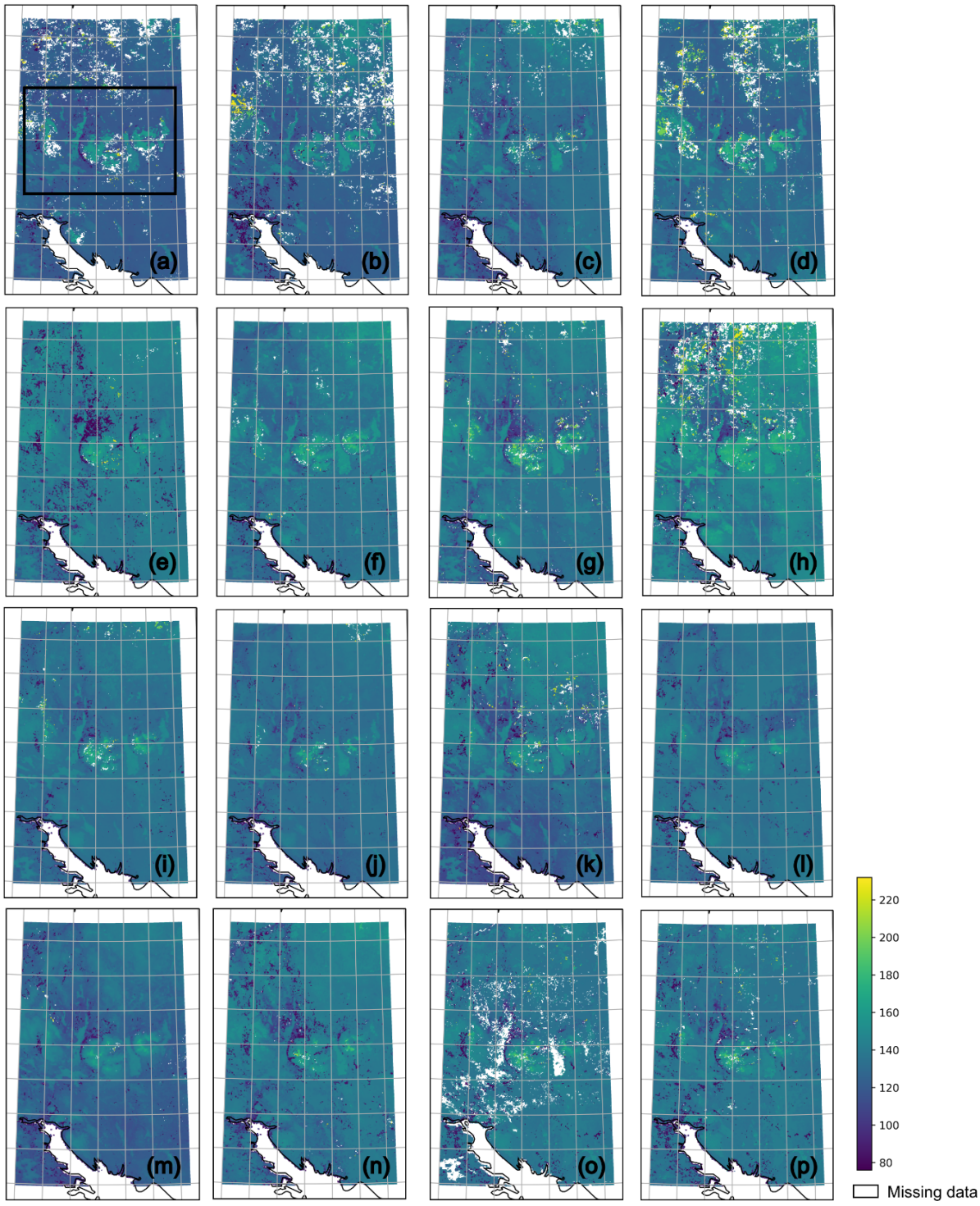

950

Figure 4.A2: SCE maps for the WMR showing the first day of the snow-free season from the year 2001 (a) to 2016 (p). The colourbar shows the day of the year. The WMR is outlined in (a) for scale.

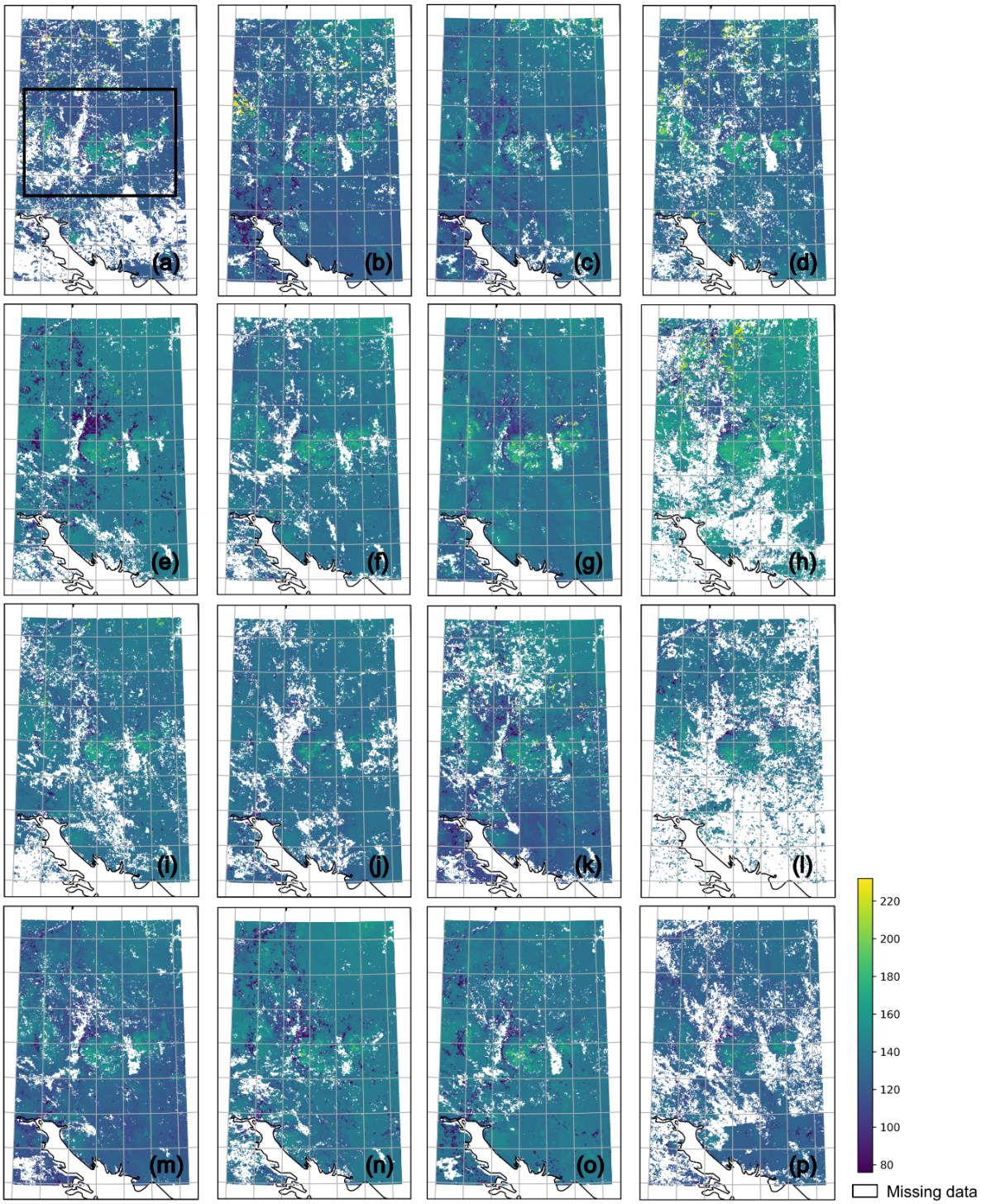

Figure 4.A3: SCD maps for the WMR showing the duration of the snow season from the snow year 2000/2001 (a) to 2015/2016 (p). The colourbar shows the number of days. The WMR is outlined in (a) for scale.

Chapter 5
Sensitivity study and validation of the Weather Research and Forecasting model

In the first part of this chapter, a sensitivity test of the Weather Research and Forecasting model is described. Different physics parameterisations of the model were tested by running it over the period of my first field season and comparing the outputs of the different parameterisations to both field measurements and remote sensing data. The optimal physics parameterisation was determined (i.e. the one for which the model best reproduced the observations) and used for all further WRF model runs. The second part of this chapter concerns the validation of the outputs of long historical runs made using WRF. The effectiveness of WRF at modelling temperature and precipitation over Northern Fennoscandia was tested and the different forcing datasets were compared.

5.1 Introduction

Downscaling is the process through which large-scale climate datasets are used to make projections at smaller scales. Two downscaling techniques exist: statistical and dynamical. Statistical downscaling relies on the application of statistical, observed and calibrated relationships between different variables at large scales on the same variables at smaller scales (Tang et al., 2016). One main limitation of statistical downscaling is its dependence on the assumption that relationships will remain the same in a changing climate system (Soares et al., 2012). Dynamical downscaling is the use of regional climate models (RCMs) forced by reanalysis or general circulation model (GCM) data to make high-resolution climate projections (Soares et al., 2012). RCMs require initial and boundary conditions in order to represent the system's relationship with its surroundings.

In this research, I used the Weather Research and Forecasting model (WRF; version 3.8.1) RCM to dynamically downscale both reanalysis and Coupled Model Intercomparison Project 5 (CMIP5) data in order to model snow cover over Northern Fennoscandia. The Advance Research WRF, developed as a collaboration between the National Center for Atmospheric Research (NCAR), the National Oceanic and Atmospheric Administration (NOAA), the National Center for Environmental Prediction (NCEP), and others, was used. WRF is a next-generation mesoscale, limited-area, non-hydrostatic, primitive-equation numerical weather prediction (NWP) model, with a range of options for various physical parameterisation schemes (Skamarock et al., 2008).

It is essential that models accurately describe the evolution of seasonal snow, because of the large effects of snow on land and atmospheric processes (Liston, 1999). Thus, it was crucial to test and optimise WRF outputs for my analysis. The effectiveness of WRF has often been tested in the literature. Heikkilä et al. (2011) downscaled ERA-40 using WRF over the complex terrain of Norway to 30 and 10 km resolution and assessed WRF's accuracy by comparing outputs to meteorological temperature,

wind and precipitation datasets. The authors found that WRF performs better than the mean and the individual RCMs at 25 km resolution used in the ENSEMBLES project (ENSEMBLES members, 2009). They also showed that WRF performs comparably well in terms of the quality of the modelled wind and precipitation. Soares et al. (2012) undertook a high-resolution dynamical downscaling of the ERA-Interim (ERA-I) reanalysis using WRF over Portugal over 20 years (1989 - 2008). Model outputs at 9 km resolution were compared with continuous records from 32 stations for temperature and 308 for precipitation. They found that, in all analysed variables, downscaled WRF outperformed the ERA-I reanalysis data, with good results in the representation of annual cycles as well as a considerable improvement in the representation of both extreme temperature and extreme precipitation. The authors emphasized that this improved modelling of extreme events is of major importance to policy makers in order to develop adequate mitigation and adaptation strategies.

However, there are limitations to regional climate modelling even at high resolutions. In mountainous regions, precipitation rates along windward slopes are often over-predicted and snowfall tends to be under-predicted. This effect is usually cited as orographic bias (Leung and Qian, 2003). It has also been shown that higher spatial resolution does not always improve model performance. Zängl (2007) showed that outside of mountainous regions, higher spatial resolution does not necessarily improve precipitation estimates. It is thus important to validate model outputs before using them, by both testing multiple physics settings in order to find the optimal model parameterisation and validating final model outputs in order to take model bias into account when interpreting model outputs.

Detailed sensitivity studies of the effectiveness of regional climate models in high-resolution modelling, specifically of snow cover, have previously been undertaken and the sensitivity study in this chapter was carried out in a similar manner to Maussion et al. (2011) and Shreshtha et al. (2011), themselves based on Yang and Tung (2003) and Rakesh et al (2007). Shrestha et al. (2012) validated the snow cover extent and snow depth outputs of a hydrological model (Wang et al., 2009) with improved snow physics (WEB-DHM-S; Shrestha et al. 2010) over the Dudhkoshi region of the Nepali Himalayas. Maussion et al (2011) assessed the effectiveness of WRF precipitation (rain and snow) simulations at 2 km resolution over the Tibetan Plateau over one month. The aim of these sensitivity analyses was to compare where snow had been simulated by the WRF model relative to observational data. Both of these studies used MODIS snow data as a validating dataset, as well as other ground data and used statistical evaluation scores to check the effectiveness of the NWP models using different physical parameters. In Shrestha et al. (2012), snow depth was evaluated at point-scale and snow extent was validated using a pixel-to-pixel comparison between model outputs and MODIS 8-day composite data. This snow extent validation showed that the hydrological model used agrees with the MODIS data to an accuracy of 90%. In their study, Maussion et al. (2011) carried out eight experiments, applying two of the commonly used physics schemes for each of the cumulus, microphysics, surface layer and planetary boundary layer parameterisation schemes. Though the results of this research show good accuracy in the simulated precipitation, they found that there is no fully optimal physics set-up for high-altitude modelling: compromise is always needed.

In this chapter, I detail the sensitivity study that was undertaken to optimise the WRF parameterisation for high resolution modelling of snow cover over the western mountain regions (WMR) in the Kola Peninsula. In the second part, I describe the in-depth validation of decadal WRF runs using the ERA-I reanalysis as well as CCSM4, GFLD-CM3 and CNRM-CM5 historical data, as forcing data.

5.2 Sensitivity study

5.2.1 Objectives

The main objective of the sensitivity study was to find the optimal physics parameterisation for modelling snow cover at a high spatio-temporal resolution in the WMR. Indeed, WRF has been designed as a highly 'tunable' model, with multiple potential physics setups. I therefore focused on optimising the snow depth and snow extent outputs of WRF forced by ERA-I, by comparing these model outputs to those derived from station and MODIS data, respectively. The secondary objective was to find out how well WRF performs in representing snow on the ground with this optimised setup.

5.2.2 Design of the sensitivity experiment

5.2.2.1 Domain and resolution selection

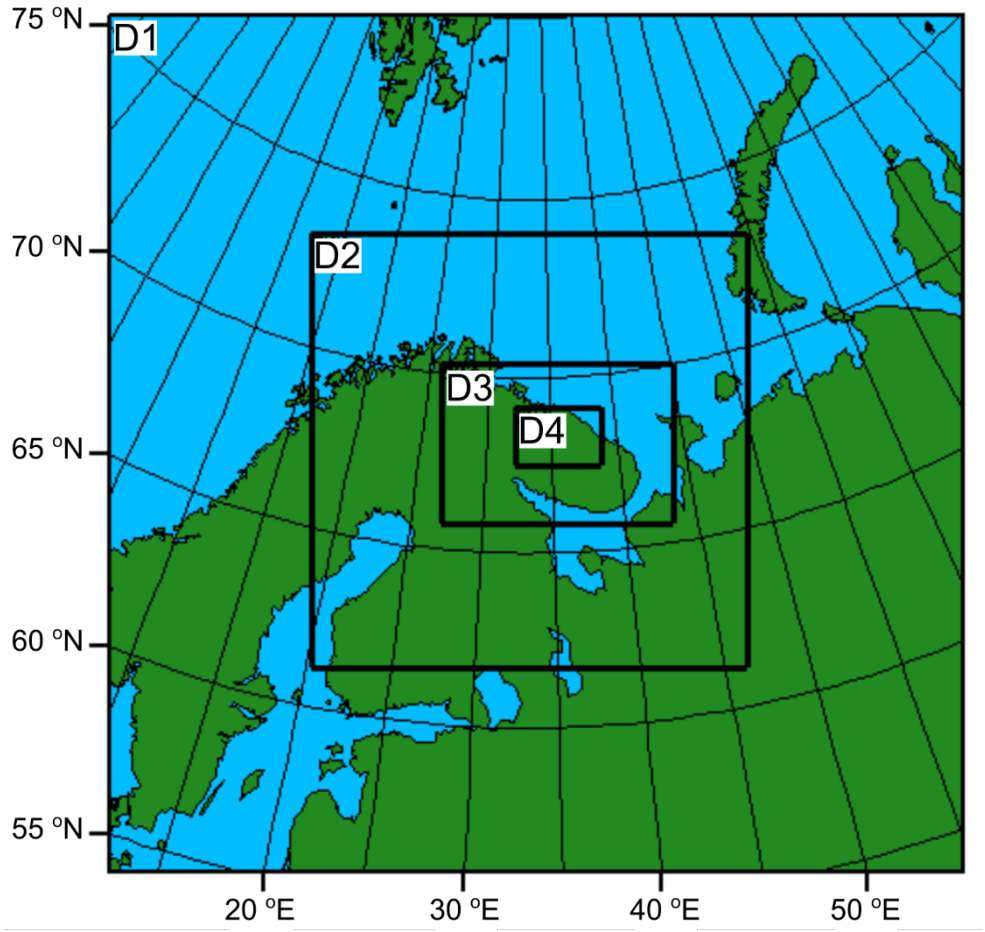

Figure 5.1: Nested domain setup of this study. Domain 1, the parent domain, makes up the entire figure with 45 km resolution. The nested domains 2, 3 and 4 have resolutions of 15, 5 and 1 km respectively.

The target of this study was to improve and assess the effectiveness of WRF downscaling over the WMR in the Kola Peninsula. A series of nested domains was used in the downscaling of ERA-I (see section 5.2.2.4) creating an inner domain over the WMR (Fig. 5.1). The ratio of the resolution of the parent domain to the nest has to be 1/3 or 1/5 for optimal results of downscaling. For this reason, four domains were used to downscale the ~70 km resolution ERA-I data to a 1 km resolution inner domain. The grid sizes were 45 km, 15 km, 5 km and 1 km for domains D1, D2, D3 and D4 respectively (Fig. 5.1). Due to the very high resolution of the inner domain, its size needed to be kept as low as possible in order to keep the model run-time low. For the boundary between the nest and mother domain, a minimum of 5 grid points is encouraged (Giorgi et al., 1994) and so, similarly to Gao et al. (2012), I used a minimum of 10 grid points to ensure a sufficient buffer zone. The detailed sensitivity analysis was performed primarily on D4, the domain with the highest resolution. Only a basic analysis is undertaken for D2 in this section, the domain with the resolution used for our long-term climate analysis (see chapter 6), as a detailed validation of runs at 15 km resolution is described in section 5.3.

5.2.2.2 Simulation period

A validation period of 5 weeks, with an additional 8 days of spin-up time was chosen for the sensitivity analysis. Spin-up is the time needed for the model to reach physical equilibrium after being forced by a set of initial conditions (see section 5.2.2.4). The model was run from 2016-04-02-12:00:00 (year-month-day-time) to 2016-05-23-12:00:00, with the analysis period starting on 2016-04-10-00:00:00 and ending 2016-05-23-00:00:00. This period was chosen to coincide with my 2016 field season, in order to add field measurements to the available observational dataset. Additionally, a validation performed for a period of over a month enabled the analysis of a range of weather conditions. When using MODIS as ground truth for snow extent, this is particularly important as analysing only a short period of time runs the risk of having the area covered by cloud for the entire time, thus making the validation impossible.

5.2.2.3 Experiment parameterisation

Pre-WRF steps were undertaken using the WRF Pre-processing System (WPS) on the ERA-I data in order to prepare it to be used as lateral boundary conditions by WRF (Skamarock et al., 2008). The ERA-I surface variables were horizontally interpolated in this step to the four spatial resolutions of the selected WRF domains. Model physics is not involved in this process and so the forcing data were identical for all the sensitivity runs. This data is used as initial boundary conditions for all four domains but, as WRF runs, each domain is driven at its boundaries by its parent domain. In total, ten model runs were created to test five different physics settings (see Tables 5.1 and 5.2). The different physics parameters were chosen to test the most commonly used WRF settings. The physics configurations with their respective codes are given in Table 5.1 as these details are often missing from publications, making reproducibility difficult. Runs 2 through 10 were compared to the initial baseline run with the basic WRF setup. These runs were analysed (see section 5.2.3) and, as a result, two more runs (11 and 12)

were created that combined different physics parameterisations with more accurate results than the Base Run (Table 5.2).

Physics	WRF Code	Configuration	Reference
Microphysics	3	WSM3	Hong, Dudhia and Chen (2004)
	8	Thompson	Thompson, Field, Rasmussen and Hall (2008)
	10	Morrison 2-mom	Morrison et al. (2009)
Planetary Boundary Layer (PBL)	1	YSU	Hong, Noh and Dudhia (2006)
	2	MYJ	Janjić (1994)
Surface Layer	1	YSU	
	2	MYJ	
Radiation	1	RRTM	Dudhia (1989)
	4	RRTMG	Iacono et al. (2008)
	5	New Goddard	Chou and Suarez (1999)
Cumulus	1	Kain-Fritsch	Kain (2004)
	2	Betts-Miller-Janjic	Janjić (1994; 2000)
	5	Grell 3D	Grell and Dévényi (2002)

Table 5.1: Description of the different physics options tested in the sensitivity analysis.

In addition to altering the model physics, the effect of changing the number of vertical levels was also tested. Usually, an increase in the number of vertical levels is associated with an improved performance of the model. Heikkilä et al. (2011) used 40 vertical levels to run WRF over Norway with its high orography and a domain that partly covered high northern latitudes like those of the Kola Peninsula. The use of 40 levels was tested in this sensitivity analysis in addition to the basic setup of 30 vertical levels. Given that the 60-day model-run took approximately 9 days to run with 30 levels (~0.28 model days per wall-clock hours) and approximately 13 days with 40 levels (~0.19 model days per wall-clock hours), a set-up of 49 vertical levels, as used in Bieniek et al. (2016) over Alaska, was not included in the interest of minimising model run time.

Finally, the effects of spectral nudging were investigated at 1 km and at 15 km resolution. Nudging is a way of feeding data into a model not only at the initial conditions but also during the, usually long, model run in order to guarantee that the model develops realistic climate features. Spectral nudging is a dynamic downscaling method that passes the nudging data, not only onto the lateral boundaries, but also into the interior of the regional domain of interest (Waldron et al., 1996). This method has been used in long-term analyses over the Arctic (Barstad et al., 2009; Heikkilä et al., 2011; Bieniek et al., 2016). The analysis in Chapter 6 required decade-long WRF runs and, as such, spectral

nudging was needed to keep the large-scale circulation of the regional model in phase with the global models.

While spectral nudging has clear positive impacts, such as to reduce the sensitivity to the chosen model domain or grid size (Alexandru et al., 2009; Miguez-Macho et al., 2004), the advantages of some other aspects of spectral nudging are less clear. For example, some studies suggested that it can affect extreme precipitation by artificially increasing intense precipitation (Radu et al., 2008) and limits internal variability (Alexandru et al., 2009). Conversely Heikkilä et al. (2011) found that, with their set-up, "nudging does not constrain the model's ability to develop small scale features" and nudged runs reproduce extreme precipitation better than free runs. I followed the nudging methods used in Heikkilä et al., (2011), itself based on Miguez-Macho et al. 2005 and Radu et al. (2008). Nudging was only applied to the outer domain in order to let the regional model create its own structures in the higher resolution nests. For the same reason, I applied nudging only on vertical levels above the boundary layer. The threshold for wavelengths over which atmospheric waves were nudged was 1,000 km. This means the model is nudged at the synoptic scale, in order to guarantee that the broad scale circulation is modelled correctly. The nudging was applied to u and v winds (zonal and meridional wind components respectively), temperature, geopotential height and humidity. Humidity is sometimes excluded from the nudging process (Heikkilä et al., 2011), but Radu et al. (2008) were able to remove the only detrimental impact of spectral nudging that they identified by nudging humidity. Thus I nudged humidity in this study.

		Run number											
		Base Run	2	3	4	5	6	7	8	9	10	11	12
Physics	Microphysics	3	10				10	10			8	8	8
	PBL	1			2							2	2
	Surface Layer	1			2							2	2
	Radiation	1				5	5	4				5	4
	Cumulus	1							2	5			
Grid	Vertical levels	30		40									

Table 5.2: Model parameterisations of all options which were changed from the basic WRF setup in the sensitivity analysis. The Base Run setup is detailed fully and, for all other runs, only the options modified from that Base Run are included. The numbers refer to the physics configuration codes (see Table 5.1).

5.2.2.4 Model boundary forcing data

ERA-I is a global reanalysis dataset with a horizontal resolution of approximately 70 km (Dee et al., 2011). This dataset is provided by the European Centre for Medium-Range Weather Forecasts (ECMWF). ERA-I was chosen as the forcing data for the initial boundary conditions. Marshall et al.

(2018) showed that this reanalysis is one of the best over Fennoscandia. Indeed, over 1979 - 2013 the correlation in monthly SAT between ERA-I and data from 32 stations across the region is 0.9970 and the Root Mean Square Error (RMSE) was found to be the lowest (1.17 °C) of the four reanalyses investigated. Equivalent values for monthly precipitation are 0.8355 and 22.61 mm, respectively. Additionally, ERA-I has previously been successfully used in combination with WRF as a tool for dynamical downscaling over many regions (e.g. Bieniek et al., 2016; Gao et al., 2015; Liu et al., 2014; Soares et al., 2012).

5.2.2.5 Case study validation datasets

5.2.2.5.1 MODIS snow fraction dataset

The processed MODIS Normalised Difference Snow Index (NDSI) dataset (see Chapter 4) was used in this analysis as ground truth for snow extent. The resolution of the original remote sensing dataset is 500 m, which was converted into 1 km^2 grids using the iris package in python (https://scitools.org.uk/iris/docs/latest/). Nearest neighbour analysis was used to regrid the MODIS data as in Maussion et al. (2011). For the validation, the processed MODIS data had to be converted into a binary (snow/no-snow) dataset. This transformation was done by setting any pixels above or equal to 50 % snow fraction (NDSI $\geq$ 0.5) to 1 (snow) and anything below 50 % snow fraction (NDSI $<$ 0.5) to 0 (no-snow), following the original MODIS binary algorithm (Hall et al., 2002; Rittger et al., 2013).

5.2.2.5.2 Meteorological station snow depth data

Three stations within the WMR record 6-hourly snow depth and were used for validating this parameter in WRF (Table 5.3). These are the Apatity, Lovozero and Monchegorsk stations. No processing was needed as these data could be directly compared to the snow depth outputs of the model runs.

Station Name	Data type	Latitude (°N)	Longitude (°E)	Elevation (m)
Apatitovaya	Met station	67.55	33.36	135
Lovozero	Met station	68.00	35.03	162
Monchegorsk	Met station	67.97	32.88	131
Moscow State University (MSU) Khibiny Research and Education	Field	67.64	33.72	330

Table 5.3: Details of the station data used to validate snow depth in the sensitivity study.

5.2.2.5.3 Field snow depth data

In addition to the station data in the WMR, one additional validation location was created using data collected in the field (Table 5.3). Daily snow parameter measurements (including depth measurements) were made in the grounds of the Moscow State University (MSU) Khibiny Research and Education station between April 16th and April 23rd 2016.

5.2.2.6 Case study validation method

In this sensitivity analysis, I used a combination of six statistical evaluation scores taken from Maussion et al. (2011) and Shrestha et al. (2012) to test the efficacy and bias of the model runs using different model parameterisations. Following these two studies, I used a two by two contingency table (Table 5.4) to compute these evaluation scores. Codes in this table define: A - a successful identification of snow by the model; B - an over prediction of snow by the model ('false alarm'); C - a 'miss' of the model; D - a successful prediction of a lack of snow. Six indices are derived from these four variables (total number of pixels of A, B, C or D), so they are not independent from each other. However, there are subtle differences between the indices and are thus all informative in different ways.

		MODIS data	
		Snow	No snow
WRF model output	Snow	A	B
	No snow	C	D

Table 5.4: Contingency table used to compute the evaluation scores (Shrestha et al., 2012).

The indices used in this study are the following:

- BIAS – bias in the modelling of snow. The closer to 1 the better.

$$BIAS = \frac{A + B}{A + C}$$

- FAR – false alarm rate, the fraction of predicted events that were not observed. The lower this score the better.

$$FAR = \frac{B}{A + B}$$

- POFD – probability of false detection of snow, the fraction of falsely predicted snow events relative to the total number of no-snow events. The lower this score the better.

$$POFD = \frac{B}{B + D}$$

- POD – probability of detection. The higher this score the better, though this should be compared to the POFD and FAR as many model runs hugely over predict snow, making the POD high, but making POFD extremely high also.

$$POD = \frac{A}{A + C}$$

- KSS – Hanssen-Kuipers skill score (Woodcock, 1976). This is the score combining the probability of detecting snow and the probability of detecting no snow. Thus the higher the score the better.

$$KSS = \frac{\mathrm{A}}{\mathrm{A}+\mathrm{C}} + \frac{\mathrm{D}}{\mathrm{B}+\mathrm{D}} - 1$$

- PC – proportion correct. This score assesses the overall accuracy of the model. The higher the score the better.

$$PC = \frac{\mathrm{A}+\mathrm{D}}{\mathrm{A}+\mathrm{B}+\mathrm{C}+\mathrm{D}}$$

5.2.3 Results of the sensitivity study

5.2.3.1 Fit with MODIS data

5.2.3.1.1 Statistical evaluation scores

WRF Run	Base	2	3	4	5	6	7	8	9	10	11	12
BIAS	1.726	1.710	1.721	1.683	1.159	1.289	1.107	1.764	1.797	1.777	1.280	1.165
FAR	0.421	0.415	0.419	0.406	0.165	0.240	0.145	0.433	0.444	0.437	0.233	0.173
POFD	0.910	0.890	0.903	0.855	0.239	0.387	0.201	0.922	0.931	0.877	0.373	0.252
POD	0.999	1.000	0.999	0.999	0.968	0.980	0.947	0.999	0.999	1.000	0.982	0.963
KSS	0.089	0.110	0.096	0.144	0.729	0.593	0.746	0.077	0.068	0.123	0.609	0.711
PC	0.596	0.605	0.598	0.620	0.876	0.817	0.881	0.582	0.570	0.588	0.824	0.868

Table 5.7: Statistical evaluation scores of all the different sensitivity runs. The optimal model parametisation for each index is highlighted in purple.

The results of the statistical evaluation are given in Table 5.7. Runs 5, 6 and 7 have much lower BIAS than the other physics setups. Of these three runs, Run 7 has the best BIAS score, which is very close to 1. These three runs also have the lowest POD. This means that they actually do not model snow in some of the instances in which MODIS retrieved snow cover. These POD scores, however, are still high, with the lowest POD being 0.947. Additionally, runs 5, 6 and 7 have considerably lower FAR and POFD scores than the other runs (Base run to Run 10). This means that runs 5, 6 and 7 do not over-predict snow as much as the other runs. The perfect or near-perfect POD in the lower performance runs (base, 2, 3, 4, 8, 9 and 10) is partly explained by their high POFD: these runs over-model snow cover which means they are more likely to successfully predict snow. Runs 5, 6 and 7 also have the highest KSS and PC scores, and thus are overall the more accurate model parameterisations. Run 6's KSS score is clearly

the lowest of the three and Run 7 has the best KSS and PC scores. Overall, Run 7 has the best combination of scores, with the best score in five of the six indices (Table 5.7).

These results show that the radiation scheme, tested in runs 5, 6 and 7 (see Table 5.2), has the highest impact on the skill of the model at modelling regional snow. These runs do the best at reproducing the snow cover over the study period. Radiation scheme 4 especially appears to improve the performance of WRF. Other runs do better than the Base Run overall, but by a much smaller margin than 5, 6 and 7. These are Run 4, which tested the PBL and Surface layer schemes, and Run 10, which tested the microphysics scheme. A combination of all these best physics options was tested in runs 11 and 12 to attempt to maximise the efficiency of WRF. Settings from runs 4, 5, 6, 7 and 10 were combined (see Table 5.2). Run 3's settings were not chosen for these 'optimised' setups, as increasing the number of vertical levels increased the model run-time and only very slightly improved the results relative to the Base Run. Runs 11 and 12 both perform better than the majority of the other runs, but do not do better overall than Run 7 (see Table 5.7). Thus, using the statistical evaluation scores, the physics parameterisation of Run 7 appears best.

5.2.3.1.2 Spatial comparison

In addition to using statistical evaluation scores, I used the spatial extent of snow cover to test the increased performance of Run 7 relative to the Base Run (see Fig. 5.2). The PC score of each weekly dataset was added onto Figure 5.2 as a quantitative measure of the overall accuracy of the model. In the first instance, both models perform identically and represent snow on the ground well (PC $\geq$ 0.93). The main difference with the MODIS data in the first three dates (April 10th, 17th and 24th) is a result of WRF modelling snow on the ground everywhere, whereas MODIS identifies a few areas of patchy non-snow where snow has started to melt out at the lowest altitudes.

The difference between the two model parameterisations (Base and 7) is much greater in the second half of the simulation period and coincides with the melting of the snow cover. The start of the melting season begins much too late in the WRF Base Run, only really commencing between May 15th and May 23rd compared to between April 24th and May 1st in the MODIS data. As a result, the PC number for the Base Run between May 1st and May 23rd is low (PC = 0.12 to 0.72). Interestingly, data from May 15th and May 23rd in the Base Run are very similar to those in the MODIS dataset on April 24th and May 1st. Thus, the rate of the melting in the Base Run is similar to the observed melt rate.

The lowest PC number for WRF Run 7 is for May 1st (0.72), when the snow has already started melting on the ground in the MODIS dataset, but not yet in the WRF 7 outputs. In WRF Run 7, melting started before May 1st only in the south-east corner of the region and a considerable amount of melting then occurs between May 1st and May 8th in Run 7. Most of the plains and the Khibiny Mountains, with the exception of the highest altitudes, are modelled to melt out in one week. From then, the MODIS and Run 7 binary maps look much more similar again, with the PC number rising back to 0.87. Snow melt occurs faster in Run 7 than in the MODIS dataset, and on May 15th and 23rd the sign of the difference between the two datasets is now opposite, with WRF modelling less snow on the ground than was

observed. However, overall WRF Run 7 does a much better job on those two weeks with PC numbers over 0.94.

Though actual snow melt rate is modelled more closely by the Base Run than Run 7, the outputs of the latter are seen as more successful as they match the timing of the snow melt considerably better, with a delay of one week compared to an approximately four-week delay in the Base Run. This fits with Maussion et al. (2011)'s conclusion that no physics setup can be perfectly optimal and that it is necessary to compromise.

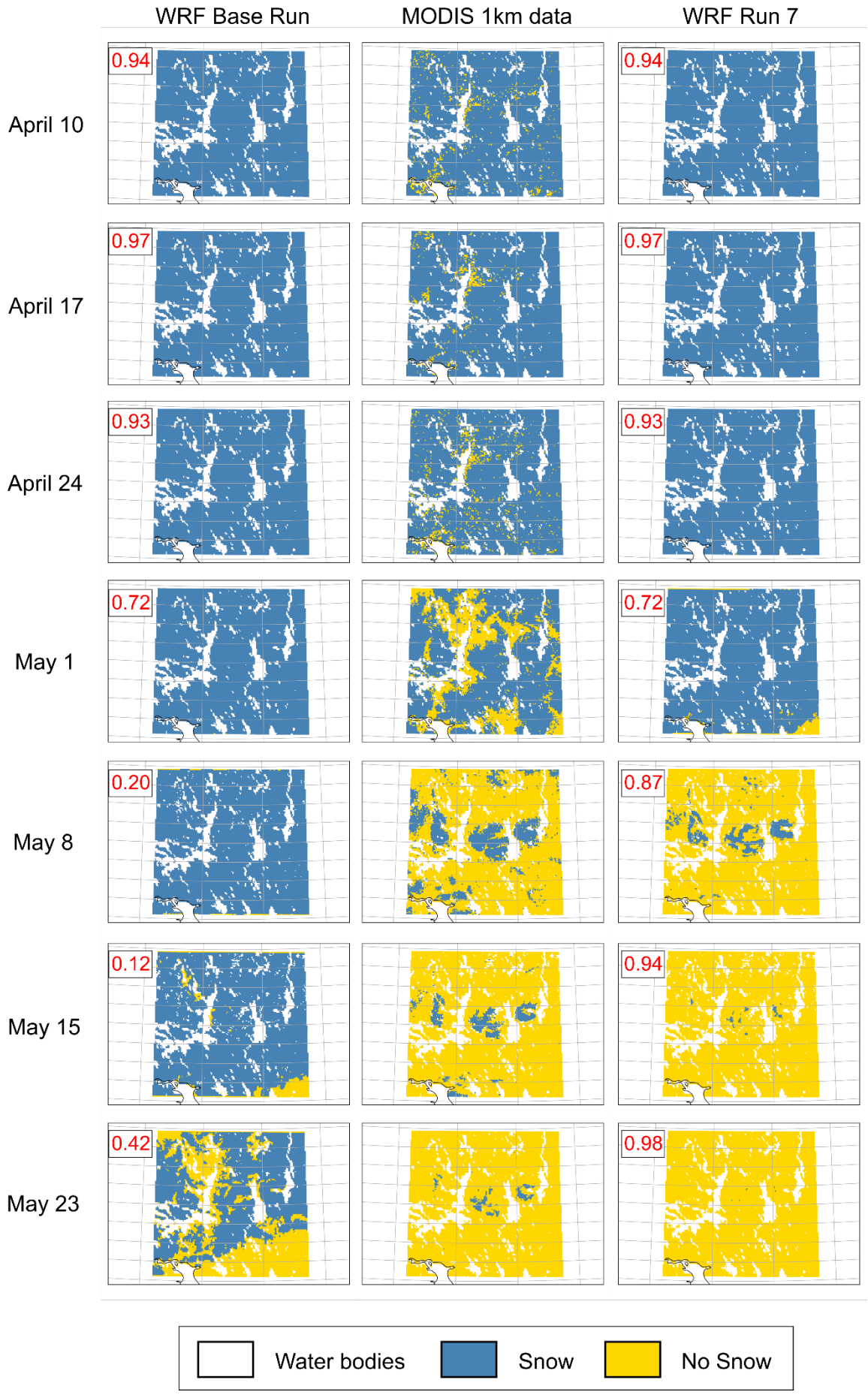

310 **Figure 5.2: Spatial distribution of binary snow/no-snow on the ground in the WMR from the Base Run, MODIS binary 1 km data and Run 7. The PC number for each day is given for both runs in red.**

5.2.3.2 Fit with station data

5.2.3.2.1 Temperature data

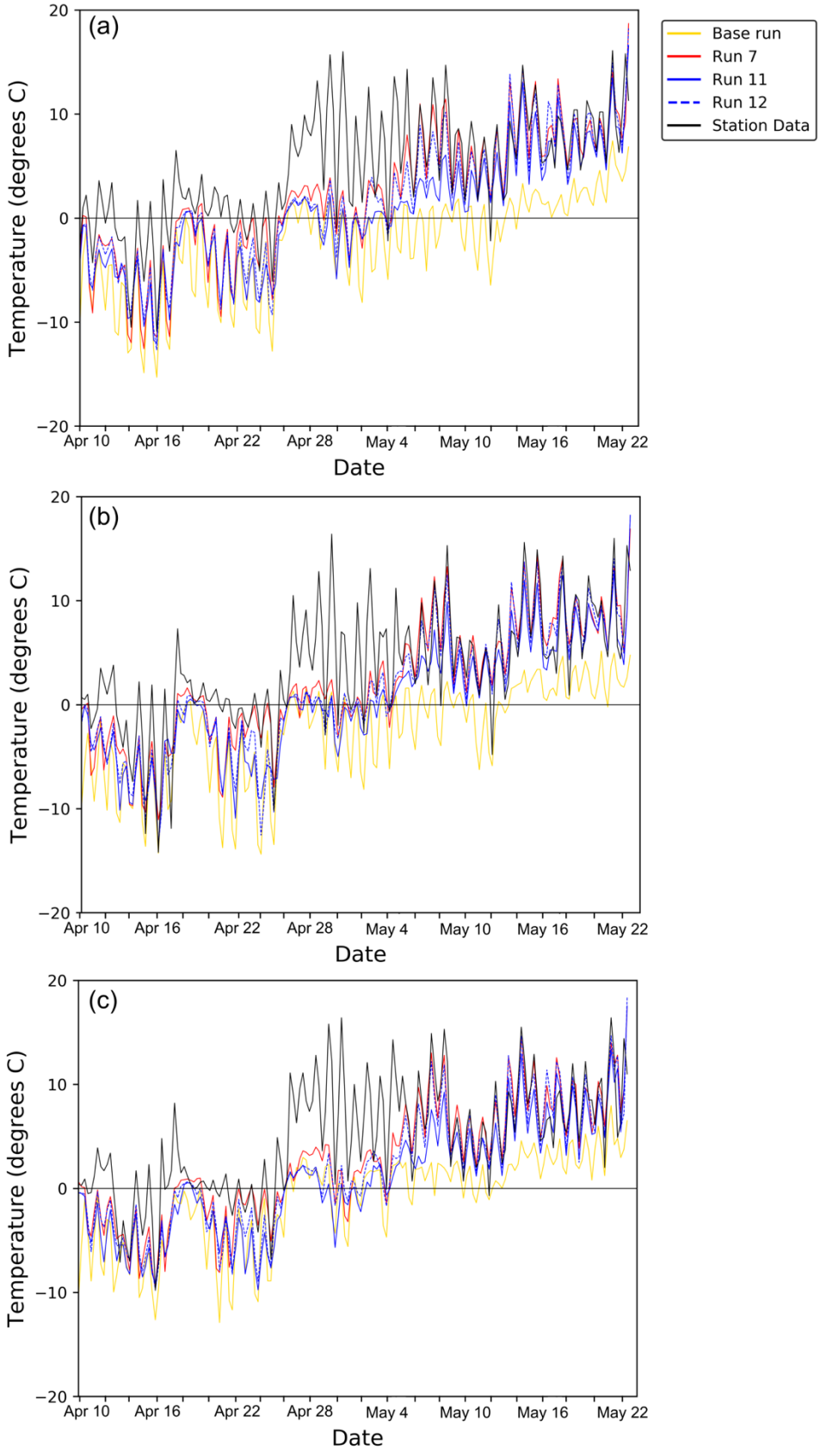

315 **Figure 5.3: 6-hourly surface air temperature from April 10th to May 23rd at (a) Apatity station, (b) Lovozero station and (c) Monchegorsk station. Data are from four WRF runs (Base Run, Run 7, Run 11 and Run 12) as well as from measurements at the stations.**

Model performance was also tested using point measurements. In this section, I look at the performance of three of the best model parameterisations (7, 11 and 12) as well as the Base Run in their representation of surface air temperature (SAT) at the three Khibiny stations. Figure 5.3 shows the 6-hourly station data and the WRF outputs at the Apatity, Lovozero and Monchegorsk stations between April 10th and May 23rd.

In the first part of the simulation period, from April 10th to May 7th, all WRF runs underestimate SAT, but overall reproduce the shape of the SAT time series effectively. The only instances in which the Base Run does the best job at reproducing observed SAT are for anomalously low values, such as on the night of May 11th. Overall, of the WRF outputs represented in Figure 5.3, Run 7 underestimates the SAT the least. The WRF runs struggle the most to reproduce the large jump in SAT, which is seen between April 25th and May 4th. In the second part of the simulation, from May 7th onwards, there is a huge improvement in the SAT representation in the outputs from runs 7, 11 and 12. These fit the station data much more closely and Run 7 seems to give the best fit. In this second part, the Base Run continues to consistently model SAT much too low.

	Base	7	11	12
Slope	0.72	0.94	0.81	0.90
RMSE	7.71	4.35	5.51	4.65

Table 5.7: Result of statistical analysis and RMSE study for the SAT outputs of each run compared to station data. All relationships were significant.

To further test the skill of WRF at modelling SAT, diagnostic statistical analyses were undertaken on the model outputs, comparing these to measured temperatures, and these results are presented in Table 5.7. Overall the Base Run has the slope furthest from 1 and the highest RMSE. Run 7 has the slope closest to 1 and also the lowest RMSE, thus it does best at modelling SAT. Run 12 has the second closest slope to 1 and the second to lowest RMSE. Run 12 thus appears to be the second-best model parameterisation in terms of temperature modelling.

5.2.3.2.2 Snow depth

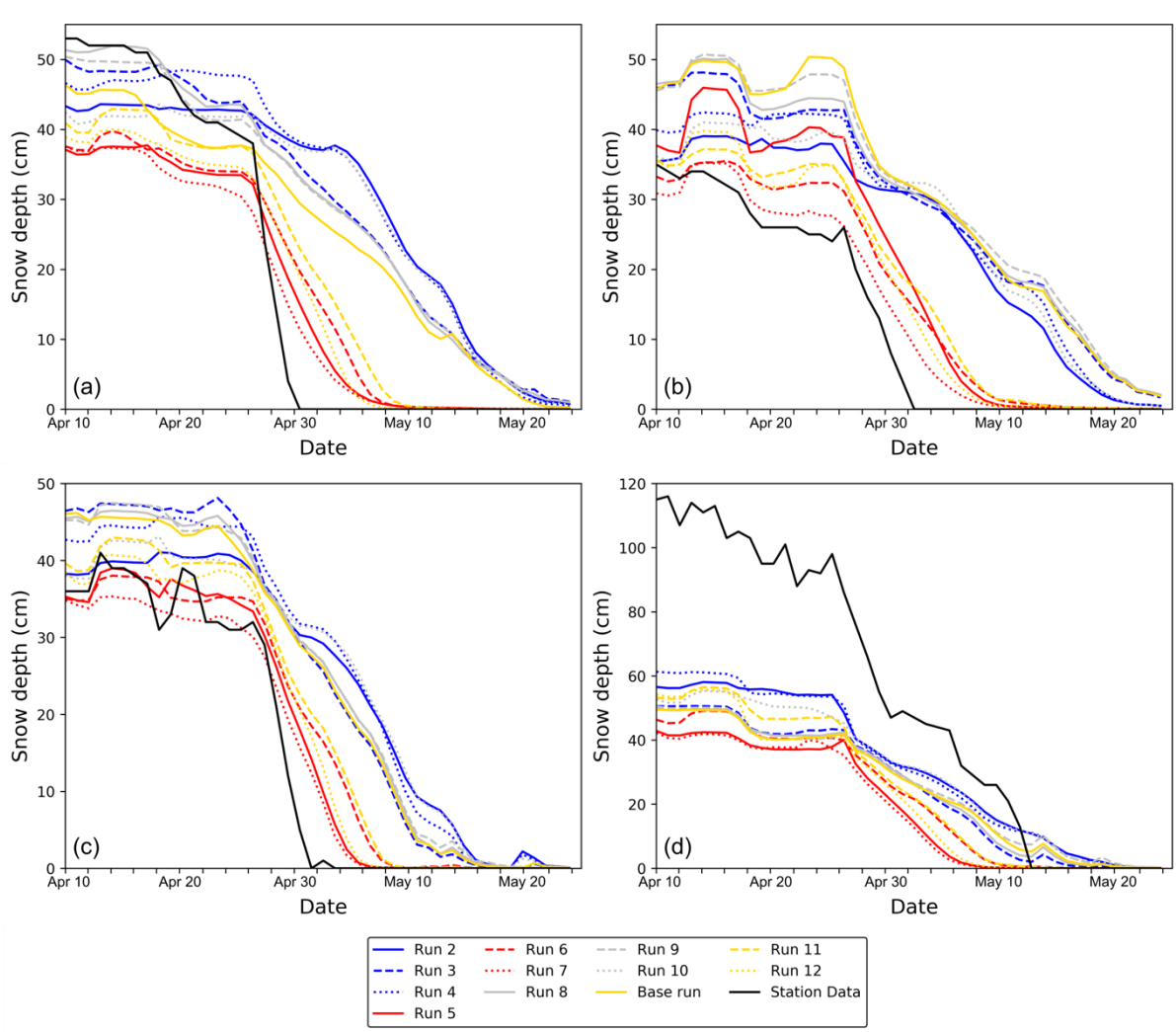

Figure 5.4: Daily snow depth from April 10th to May 23rd at (a) Apatity station, (b) Lovozero station, (c) Monchegorsk station and (d) MSU Khibiny stations. Data are from all WRF sensitivity runs as well as from ground measurements at the stations.

Figure 5.4 shows the snow depth simulated in the 12 sensitivity runs compared to those recorded at the four stations used in this analysis. The results show clumping of the output curves into two groups. The base run along with runs 2, 3, 4, 8, 9 and 10 all model similarly high snow depths with slow melt rates. Runs 5, 6,7, 11 and 12 model lower snow depths, with earlier melt onset and faster melt rates. This clumping of results suggests that the radiation scheme which separates these two groups (see Table 5.2) makes the biggest difference in the skill of the model at simulating snow depth and snow melt rate.

The ability of WRF to model snow depth accurately varies considerably depending on the station. For Apatity station (Fig. 5.4a), Run 7 represents the shape of the snow depth curve the best; it models snow melt best. However, it fails to reproduce the high snow depths early on in the simulation period. Run 8 models the early high snow depths the best at this station; however, it fails to reproduce the early melting of the snow pack. At the Lovozero and Monchegorsk stations (see Fig. 5.4b and 5.4c), WRF is able to reproduce snow depth relatively well. At Lovozero station, Run 7 is closest for almost the entire simulation period, modelling the higher snow depths well and modelling the melting of the snow pack with only a slight delay. At Monchegorsk station, for the period from April 10th until April

23rd, runs 5 and 6 best reproduce the average snow depth. However, all runs fail to reproduce the large variations in snow depth. This is not surprising as the station data is a point measurement and the WRF output is a 1 km square average. From April 23rd onwards, Run 7 best models the snow depth at this station by both matching the values very well between April 23rd and April 29th, and then modelling the snow melt from April 29th with only a small delay. Run 7 models temperature best (see Sect 5.2.3.2.1), thus it is not surprising that it models snow best. The delay in the onset of melting and the lower melt rate modelled at Apatity, Lovozero and Monchegorsk can be partly explained by the delay in the model outputs to reproduce the sudden jump in temperatures that was observed in late April (see Figure 5.3).

Finally, at MSU station, the snow depth outputs do not match ground values (Fig. 5.4d). Runs 5 and 7 have the worse snow depth simulations at this station. WRF is unable to represent the high snow depths there and thus snow depth over the entire simulation period, in all runs, is inaccurate at this station. A test was undertaken to find whether this is caused by an altitude mismatch between the station and the pixel in the model at that latitude/longitude and whether one of the adjacent 8 pixels would represent snow depth better for the MSU station. I found that the original pixel corresponding to the MSU station has the smallest difference in altitude with the real MSU station altitude (18 m). Thus, no adjacent pixels would better represent the altitude of the station. The large underprediction of snow depth is probably partly explained by the fact that a point measurement within a mountain range will be less representative of its 1 km pixel, compared to stations in plains for example. This could also be a result of orographic bias which usually sees predicted snowfall less than measured values (Leung and Qian, 2003). In any case, it is impossible to choose an optimal parameterisation for this station.

Overall, run 7 does not perform ideally when it comes to modelling snow depth. For the three lower altitude stations investigated, it does not match the maximum snow depth well and does not model the melt onset as well as other runs. It does, however, simulate snow melt-out best and, along with run 5, it simulates the closest melt rate at these stations.

5.2.3.3 Optimised model parameterisation

The physics parameterisation from run 7 has been shown to be consistently best for modelling binary snow cover, snow cover extent, temperature and snow depth across the Khibiny Region. Thus, the following setup is used for all following WRF modelling: the microphysics scheme used is Morrison 2-mom (Hong and Pan, 1996); the PBL and surface layer schemes are YSU (Hong et al., 2006); the radiation scheme is RRTMG (Iacono et al., 2008); the cumulus scheme is Kain-Fritsch (Kain, 2004); and 30 atmospheric vertical levels are used.

The PBL, surface layer and cumulus schemes are the same as in the base run. The two schemes responsible for the improved results are the microphysics and the radiation schemes. The microphysics scheme used in run 7, Morrison 2-mom (Morrison double-moment scheme; Morrison et al., 2009), is a double-moment scheme which represents "ice, snow, rain and graupel for cloud-resolving simulations" (Run and Case, 2015, pp5-4). This scheme was added to WRF more recently than the other two microphysics schemes tested. These are: the simple and single-moment WSM3 (WRF Single-Moment

3-class) with snow and graupel at mesoscale levels, and the Thomson single-moment scheme with "ice, snow and graupel processes suitable for high-resolution modelling" (Run and Case, 2015, pp5-3). Double-moment schemes have been shown to better simulate ice-crystal aggregation (Molthan and Colle, 2012). The main difference between single- and double-moment schemes is that multi-moment water microphysics schemes are able to simulate the development of cloud water particles as well as their interactions, growth and precipitation. Hence the main difference between the microphysics schemes of run 7 and the other run is in the specialisation of the multi-moment Morrison 2-mom in cloud-resolving simulations. The radiation scheme (representing both the longwave and shortwave radiation) which returns the best results is the RRTMG scheme (Iacono et al., 2008). This scheme is an updated version of the RRTM (Rapid Radiative Transfer Model; Dudhia, 1989) scheme and the main improvement is in the representation of subgrid-scale cloud variability (Iacono et al., 2008). One important difference between RRTMG and the other tested radiation scheme, the New Goddard scheme, is the trace gas content. RRTMG includes a high content of CO_2 (379.10^{-6}) compared to New Goddard (337.10^{-6}). In summary, the main reasons for the success of the parameterisation of run 7 are its improved representation of cloud processes (in both the microphysics and radiation schemes) and its higher, more representative CO_2 content.

The other schemes unchanged between the base run and run 7 are:

- The surface layer scheme (MM5 similarity): "based on Monin-Obukhov with Carslon-Boland viscous sub-layer and standard similarity functions from look-up tables" (Run and Case, 2015, pp11).
- PBL (Yonsei University scheme): "non-local-K scheme with explicit entrainment layer and parabolic K profile in unstable mixed layer" (Run and Case, 2015, pp14).
- Cumulus Kain-Fritsch scheme: "Deep and shallow convection sub-grid scheme using a mass flux approach with downdrafts and CAPE removal time scale" (Run and Case, 2015, pp17).

5.2.3.4 Nudging

The results of sensitivity testing of nudging for the inner domain are shown in Table 5.7. Spectral nudging was tested only for the optimised physics parameterisation in order to reduce modelling time. For this short simulation period, nudging makes very little difference in the statistical evaluation scores, with no difference in the PC numbers of the two runs. Nudging should increase model accuracy over long simulations (Heikkilä et al, 2011; Radu et al., 2008), and this test on a short simulation was designed only to check that it would not dramatically decrease the accuracy of WRF. The results indicate that spectral nudging can be used in our simulations.

In addition to the validation of the WRF outputs from the 1 km inner domain, a test of the accuracy of WRF over the 15 km domain (D2) was also undertaken. The statistical evaluation scores described in section 5.2.2.6 were applied to the outputs of Run 7 and for nudged Run 7 (Table 5.8). This was done in order to gain an idea of the accuracy of WRF at this resolution, in preparation for Chapter

6. Overall, the statistical evaluation scores are much lower for the 15 km domain. The overall accuracy of the model, represented by the PC number, is lower by almost 20 %. This is unsurprising as regional climate models have been demonstrated to be more effective when run at higher resolution (e.g. Heikkilä et al., 2011). Further validation of 15 km resolution runs is undertaken in the following section using long-term model outputs, which will be directly used in Chapter 6.

	Optimal model parameterisation - Run 7 Not Nudged	Optimal model parameterisation - Run 7 Nudged
BIAS	1.107	1.117
FAR	0.145	0.148
POFD	0.201	0.208
POD	0.947	0.951
KSS	0.746	0.744
PC	0.881	0.881

Table 5.7: Statistical evaluation scores for Run 7 for both non-nudged and nudged settings over D4.

The impact of spectral nudging was also assessed for D2 and it is confirmed that, for short simulations, spectral nudging has no strong impact on outputs. Indeed, nudging makes very little difference in all statistical scores (Table 5.8) and the difference in the PC number in this case is less than 2 %.

	Optimal model parameterisation - Run 7 15 km Not Nudged	Optimal model parameterisation - Run 7 15 km Nudged
BIAS	0.452	0.415
FAR	0.135	0.129
POFD	0.075	0.066
POD	0.391	0.362
KSS	0.316	0.296
PC	0.630	0.618

Table 5.8: Statistical evaluation scores for Run 7 for both non-nudged and nudged settings over D2.

5.3 WRF long-run validation

5.3.1 Objectives

In this section, decade-long historical WRF model runs are validated against observations. The objective of the validation analysis was to gain an understanding of how well WRF models the basic parameters controlling snow cover over a historical period. This section enables an assessment of the difference in

the accuracy of runs forced by different data (see Section 5.2.2.4) as well as to test the spatial variability of WRF accuracy. Gaining a better understanding of biases in WRF is crucial to interpreting outputs and coming to conclusions about future climate, needed for the next chapter in this thesis (Chapter 6).

5.3.2 Validation experiment set-up

5.3.2.1 Domain and resolution selection

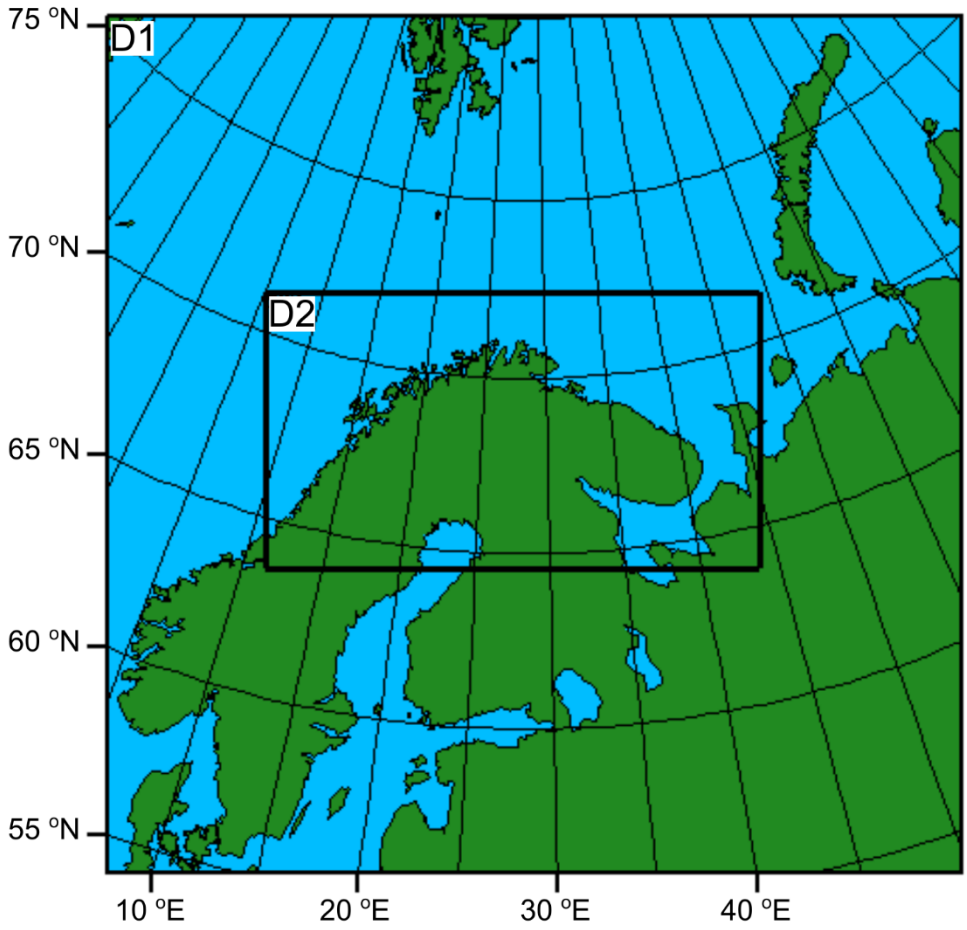

Figure 5.6: Nested domain setup of the long-runs study. Domain 1, the parent domain, makes up the entire figure and has a resolution of 45 km. The nested domain D2 has a resolution of 15 km.

The model was set up with two domains, an outer domain at a 45 km resolution and an inner, higher-resolution, domain (Fig. 5.6). Leung and Qian (2003) studied the impacts of model resolution on precipitation and snowpack simulations in RCM nesting studies over regions of complex terrain. These authors found that, though orographic bias may still affect high-resolution projections, using higher spatial resolution usually results in an improved precipitation and snowpack simulation. Higher spatial resolution, through its association with an improved representation of elevation, usually leads to a better modelling of temperature. This was demonstrated for the WRF model specifically by Heikkilä et al. (2011). The authors showed in their downscaling study of ERA-40 using WRF that a resolution of 10 km showed much smaller biases in modelled temperature, precipitation and wind, than at 30 km resolution. Thus, in this project the inner domain spatial resolution was lowered as much as possible

whilst keeping the model run-time low. This was necessary as I wanted to maximise the number of models used to force WRF (see Section 5.3.2.3) and emission scenarios for the future runs used in the following analysis (see Chapter 6). I followed the advice of the WRF developers and used the recommended 1/3 resolution ratio and restricted the model to two domains in order to keep run-time low. Following these steps, I chose a resolution of 15 km for the inner domain.

I focused the study on Northern Fennoscandia and ensured that the entirety of the Kola Peninsula was included in this domain.

5.3.2.2 Simulation period and model parameterisation

The simulation period was chosen in order to represent the changes to have occurred over a century in northern Fennoscandia. For this purpose, the historical WRF long runs were undertaken for one decade over the end of the 20th century (1990 - 1999). Runs were sent in one-year steps with 9 days spin-up time in order to keep running time minimal and to be able to model multiple years at the same time.

The physics parameterisation optimised in the sensitivity analysis (section 5.2.3.3) and spectral nudging were used for these long runs.

5.3.2.3 Model boundary forcing data

In order to model climate variability, it is best to use a multiple model approach (ENSEMBLES members, 2009). Indeed, multi-model studies enable the reduction of over-confidence which is associated with single-model studies. The ensemble spread will increase, but by doing so, will reduce the ensemble-mean error. In this work, a single RCM (WRF) is used, but this model is forced by multiple datasets. This enables the modelling of a range of different outputs, which mimic the advantages of using multi-model ensembles.

	Frequency			
Variable	Monthly	Daily	6 - hourly	3 - hourly
Soil Moisture Content	x			
Soil Temperature	x			
Sea Surface Temperature		x		
Air Pressure at Sea Level			x	
Specific Humidity			x	x
Air Temperature			x	x
Zonal Wind			x	x
Meridional Wind			x	x

Table 5.9: Range of variables needed as boundary conditions for running WRF.

Three CMIP5 models were chosen as forcing datasets for this project. They were selected based on a number of parameters. Firstly, the CMIP5 data needed to be converted into a format that could be

used as boundary conditions for WRF. Thus, they needed to contain the correct variables needed for running this model (see Table 5.9) over the historical period and over the two RCP scenarios selected for future analysis (see Chapter 6). This removed the option of using the Norwegian CMIP5 model (NorESM1-ME; Bentsen et al., 2012), which would likely have been one of the most accurate over the Northern Fennoscandia region.

Within the models available that suited this selection criteria, those that had been shown to effectively model climate over Northern Fennoscandia were selected. CCSM4 was selected at this stage for being one of the best CMIP5 models for modelling climate over Northern Europe (Perez et al., 2014). Additionally, models that represent the spectrum of climate variability were selected in order to best represent the range of possible precipitation and snow cover changes that may occur over the next century. For this point, the GFDL-CM3 and CNRM-CM5 datasets were selected to represent the higher and lower side of temperature change, respectively. None of the CMIP datasets contained data for February 29th. Leap-year runs forced with the CMIP datasets were performed using a version of WRF which had been recompiled to ignore February 29th.

Finally, data from ERA-I (see Section 5.2.2.4) was used to force a fourth historical WRF run from 1990 to 1999 in order to compare the performance of CMIP-forced WRF to a reanalysis-forced WRF.

5.3.2.3.1 CCSM4 data

Data from version 1 of NCAR's Community Earth System Model (CESM; Hurrell et al., 2013) were used. Perez et al. (2014) tested three aspects of CMIP5 GCMs: their ability to reproduce synoptic situations, their ability to reproduce the historical inter-annual variability and the consistency of GCM experiments in the 21st century projections. They demonstrated that CCSM4 is one of the best models in all three of these tests. Additionally, the CCSM4 data had already been prepared to force WRF and could be readily downloaded. The data were downloaded from the NCAR online Research Data Archive available at https://rda.ucar.edu/datasets/ds316.1/. This dataset consists of bias-corrected CMIP5 CESM data which has been processed into WRF-compatible format (Bruyère et al., 2015). These data are available at 6-hourly intervals, have a horizontal resolution of one degree and have been interpolated to 26 pressure levels. This dataset has been bias corrected by Bruyère et al. (2015) following the methods described in Bruyère et al. (2014) by using ERA-I data for the 1981 to 2005 interval.

5.3.2.3.2 GFDL-CM3 data

Data from the latest coupled climate model from the Geophysical Fluid Dynamics Laboratory (GFDL; Donner et al., 2011) was used. GFDL-CM3 was selected for its good precipitation estimates and slightly high temperature projections for the end of the century. It has been used, for example by Lader et al. (2017), because of the fact that Arctic warming and sea-ice loss are occurring more rapidly in this model than in most CMIP5 simulations, which makes it a good model to obtain a "worst-case-scenario"

estimate. In their work, Lader et al. (2017) did a bias adjustment of the GFDL-CM3 model using ERA-I reanalysis data. Indeed, they found that ERA-I consistently has a lower RMSE than GFDL-CM3 in terms of statistical distribution of variables compared to observations. In this work, bias correction was not undertaken as a result of the time limitations of the project (see Section 5.5). Therefore it is necessary to discuss the performance of this model. Donner et al., (2011) found that annual mean precipitation is generally well modelled by GFDL-CM3 when compared to a large observation dataset (GPCP; Adler et al., 2003). This version of the model has an improved representation of Arctic sea-ice concentration compared to its predecessor, GFDL-CM2 (Griffies et al., 2011). Johanessen et al. (2004) demonstrated that arctic temperature projections are highly impacted by the skill of sea-ice simulations. Thus, improvements in the representation of Arctic sea-ice should improve Arctic temperature outputs also. GFDL-CM3 has been shown to be one of the top-performing CMIP5 models in terms of summer sea ice concentration estimates when compared to passive microwave data (Laliberté et al., 2016). CM3 is also an improvement on CM2 in terms of sea-level pressure (SLP). However, there is still a slight positive bias in SLP over Northern Fennoscandia. This bias is lower on the western side of the region and increases further east over the northern part of the Kola Peninsula (Figure 12 in Griffies et al., 2011). Additionally, at high latitudes, the magnitudes of temperature anomalies are larger in the model outputs than in the observations (Donner et al., 2011). At atmospheric pressure levels lower than 5 – 10 hPa, temperatures modelled by GFDL-CM3 are generally higher than reanalysis data (ERA-40) in the polar regions.

5.3.2.3.3 CNRM-CM5 data

The third CMIP5 model used for forcing data in this project was CNRM-CM5, developed by the Centre National de Recherches Météorologiques (CNRM) as described in Voldoire et al. (2013). CNRM-CM5 was chosen for this project as it has successfully been used in snow studies (e.g. Derksen et al., 2012; Lehtonen et al., 2016) and is on the colder CMIP5 spectrum, thus will help represent the range of potential future climate variability well when used in combination with CCSM4 and GFDL-CM3. As with GFDL-CM3, this model was not bias-corrected before its use in this project. It is thus important to note that, though this model is an improvement on its previous version, it still has significant biases in many regions, including over Northern Fennoscandia. Voldoire et al. (2013) found a slight negative bias in precipitation over the Norwegian mountains in DJF when compared to observational data (GPCP; Adler et al., 2003). In Räisänen and Ylhäisi (2015), CNRM-CM5 is the only model that disagrees with all 31 other CMIP5 models by not predicting an increase in annual mean precipitation in the Northern Europe Land Area between 1981 and 2010. A positive bias in SLP over Northern Fennoscandia was demonstrated in both winter and summer (Brands et al., 2013; Voldoire et al., 2013). CNRM-CM5 has a negative bias in near-surface temperature over Northern Fennoscandia, with a lower bias in summer than in winter. In summer, the cold bias over the region of interest is strongest over the Scandinavian Mountains (Brands et al., 2013).

5.3.2.4 Validation datasets

Daily SAT and precipitation data from ten stations were used in the validation (see Table 5.10). These have been selected for their distribution across the entire Northern Fennoscandian domain (see Fig. 5.7). They represent a range of different altitudes and include stations on the coast and inland.

Number	Station Name	Latitude (°N)	Longitude (°E)	Altitude (m)
1	Abisko	68.36	18.82	394
2	Andøya	69.31	16.13	13
3	Kandalaksha	67.13	32.43	26
4	Krasnoscel'e	67.35	37.05	155
5	Kvikkjokk-Årrenjarka	66.89	18.02	315
6	Murmansk	69.84	21.89	51
7	Nordstraum i Kvaenangen	69.84	21.89	6
8	Šihččajávri	68.76	23.53	384
9	Sodankylä ARC	67.37	26.63	179
10	Vardø Radio	70.37	31.10	15

Table 5.10: Details of the stations used in the validation experiment as ground truth.

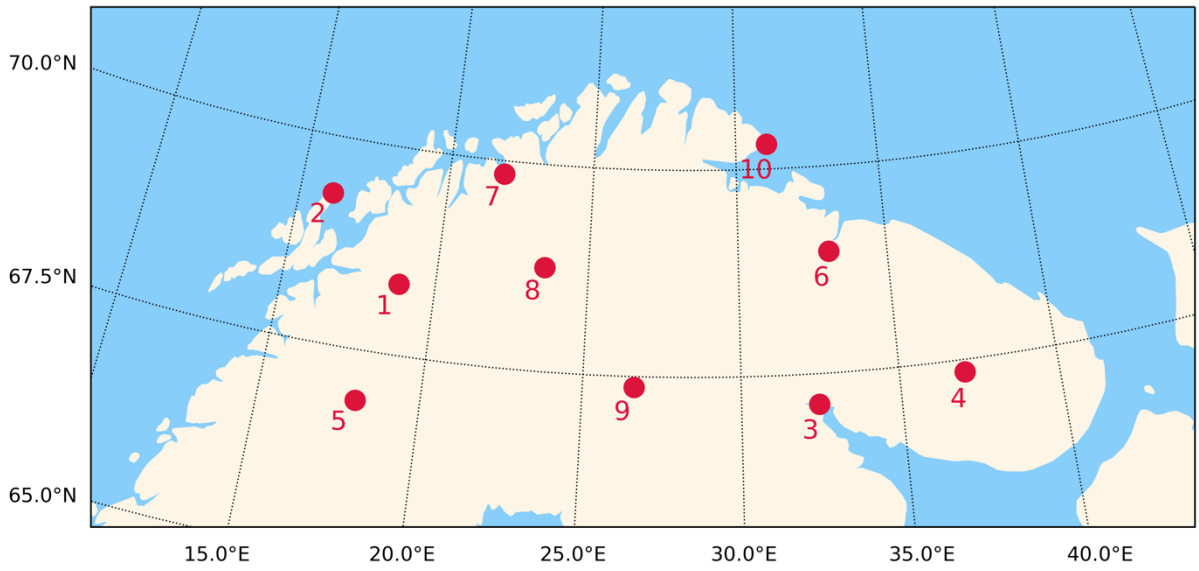

Figure 5.7: Location of the ten stations used in the validation analysis.

5.3.3 Results

5.3.3.1 SAT validation

Box plots showing the spread of mean SAT over the 10 years between 1990 and 1999 as recorded at the stations and as modelled by WRF are shown in Figure 5.8. The plots show the distribution of yearly and seasonal mean SAT and enable an assessment of the skills of WRF in reproducing SAT and a

comparison of the effectiveness of the four different forcing datasets (CCSM4, CNRM-CM5, GFDL-CM3 and ERA-I).

At all stations and for all forcing data, WRF does an excellent job at modelling mean SAT and SAT variability (Fig. 5.8). There is a small cold bias in the WRF model outputs, wherein WRF very slightly underestimates the mean yearly and seasonal SAT at almost all stations. The mean bias in the yearly mean temperature outputs of the CCSM4, CNRM, GFDL and ERA runs is -1.89 °C, and -2.68 °C when excluding the previously bias-corrected CCSM4 outputs. Indeed, the outputs of WRF forced by the CCSM4 data are the closest to the observation data. Thus the CCSM4 runs are the best in terms of SAT modelling. ERA-I-forced WRF is the least accurate in terms of mean SAT modelling, though not by much. The CNRM-CM5 and ERA-I runs consistently underestimate SAT in the spring. In autumn however, both CCSM4 and CNRM-CM5 give good SAT estimates but GFDL-CM3 and ERA-I slightly underestimate the SAT. Overall, the best estimates are made in summer; this is most likely due to the lower variability of SAT in this season.

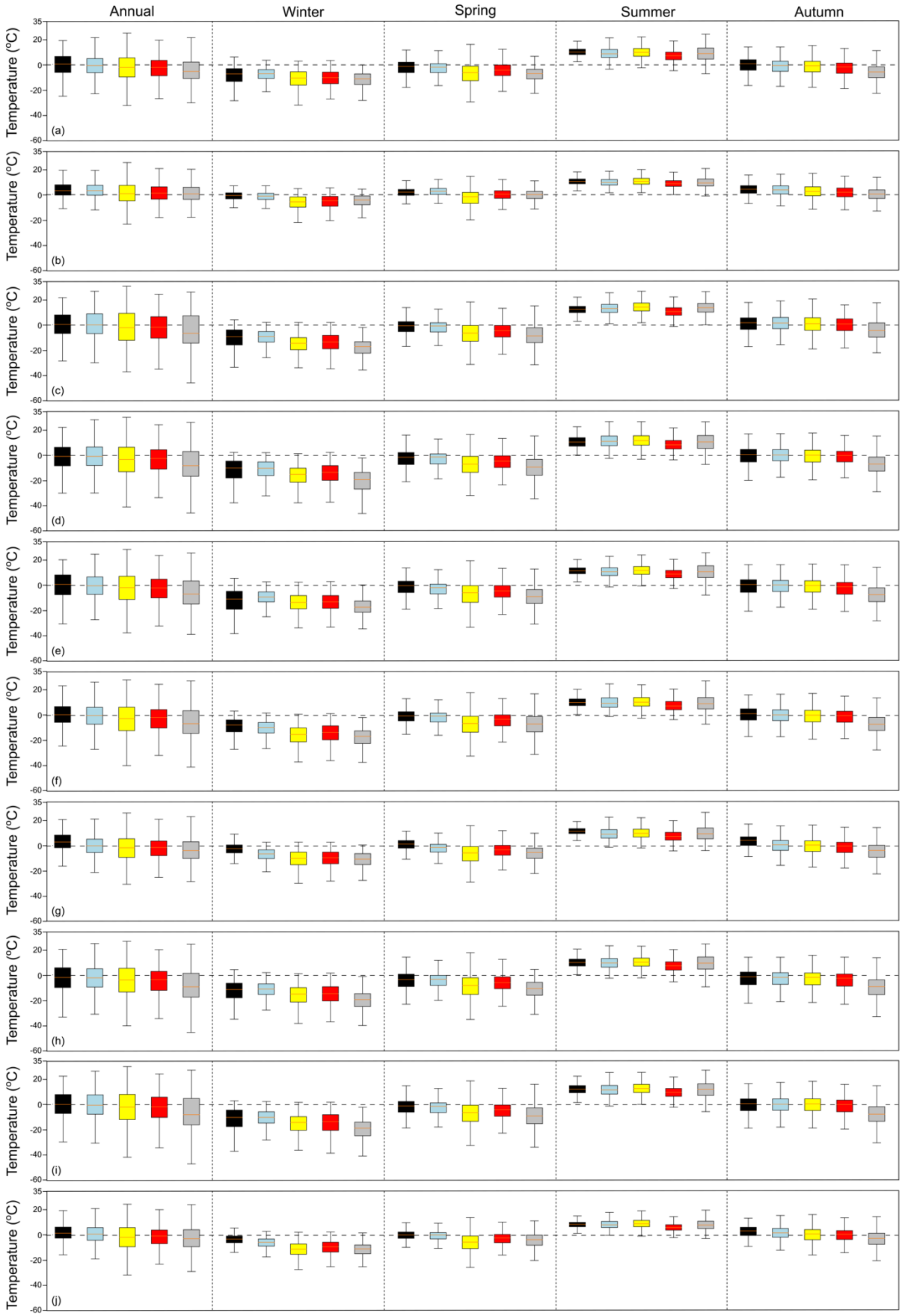

Figure 5.8: Mean SAT at (a) Abisko, (b) Andøya, (c) Kandalaksha, (d) Krasnoscel'e, (e) Kvikkjokk-Årrenjarka, (f) Murmansk, (g) Nordstraum i Kvænangen, (h) Šihččajávri, (i) Sodankylä ARC and (j) Vardø Radio, for station data (black) and WRF forced by CCSM4 (blue), CNRM-CM5 (yellow), GFDL-CM3 (red) and ERA (grey) data. The box represents the upper and lower quartiles, with the mean value shown as an orange horizontal line, and the whiskers the range of data.

5.3.3.2 Precipitation validation

Figure 5.9 shows the spread of total yearly and seasonal precipitation over the 10 years between 1990 and 1999 from observational data and WRF model outputs. These plots enable the assessment of the precipitation modelling skills of WRF which are crucial for snow modelling and the comparison of the effectiveness of the four different forcing datasets (CCSM4, CNRM-CM5, GFDL-CM3 and ERA). WRF precipitation modelling is much less accurate than its temperature modelling (Fig.5.8). As a result, a stronger emphasis is given to the precipitation validation and more effort is undertaken to understand which precipitation aspects are most affected.

At all stations but Andøya (#2, Fig. 5.7), the precipitation is overestimated. This overestimate can be quite large with, for example, the total yearly precipitation modelled at Nordstraum i Kvænangen (#7) in the CCSM4 run being almost three times higher than that recorded in the station data. The large error at this station is explained in part by the mismatch in altitude of the WRF grid cell compared to that of the station measurements. In WRF, the Nordstraum i Kvænangen grid cell is at 396 m altitude, as opposed to the 6 m altitude of the Nordstraum i Kvænangen station. This station is at very low altitude, just by the sea but is surrounded by high topography. Thus the station measurements are not an accurate representation of the entire 15 km grid cell. The error in WRF is thus possibly not as high as it seems were it to be compared to higher altitude observations. Precipitation at Andøya is strongly underestimated and also has the highest RMSE (see Table 5.11 to 5.14). This is also probably primarily a result of the location of this station (Fig. 5.7). As this station is on a very narrow piece of coast, its orography is more imprecise. The WRF grid cell on which the Andøya station lies is at 66 m altitude as opposed to the 13 m station altitude. While this difference is not as great as for Nordstraum i Kvænangen, it probably still has a significant effect on the WRF precipitation estimate.

There is a clear seasonality in the precipitation errors (Fig 5.9). For most stations, the difference between the modelled and the observed total precipitation is highest in summer. Indeed, in this season, WRF greatly overestimates the total precipitation at all stations but Andøya, similar to the annual data At most stations, the second highest seasonal difference is in autumn, and winter and spring have the lowest errors. This is encouraging for my studies of snow cover in Chapter 6, wherein seasons where solid precipitation is likely to be the prevailing form of precipitation have the lower modelling errors. Additionally, it is important to note that spring precipitation is more reliable than autumn precipitation. Indeed, this means that snow cover start projections will be less reliable than snow cover end projections. When looking at seasonal differences, once again, Andøya is the station that fits least well with the other stations. Indeed, not only does this station have the lowest error in summer precipitation, both the mean summer total precipitation and its variability are well modelled. Additionally, the highest difference between the modelled and observed precipitation at this station are in autumn and winter.

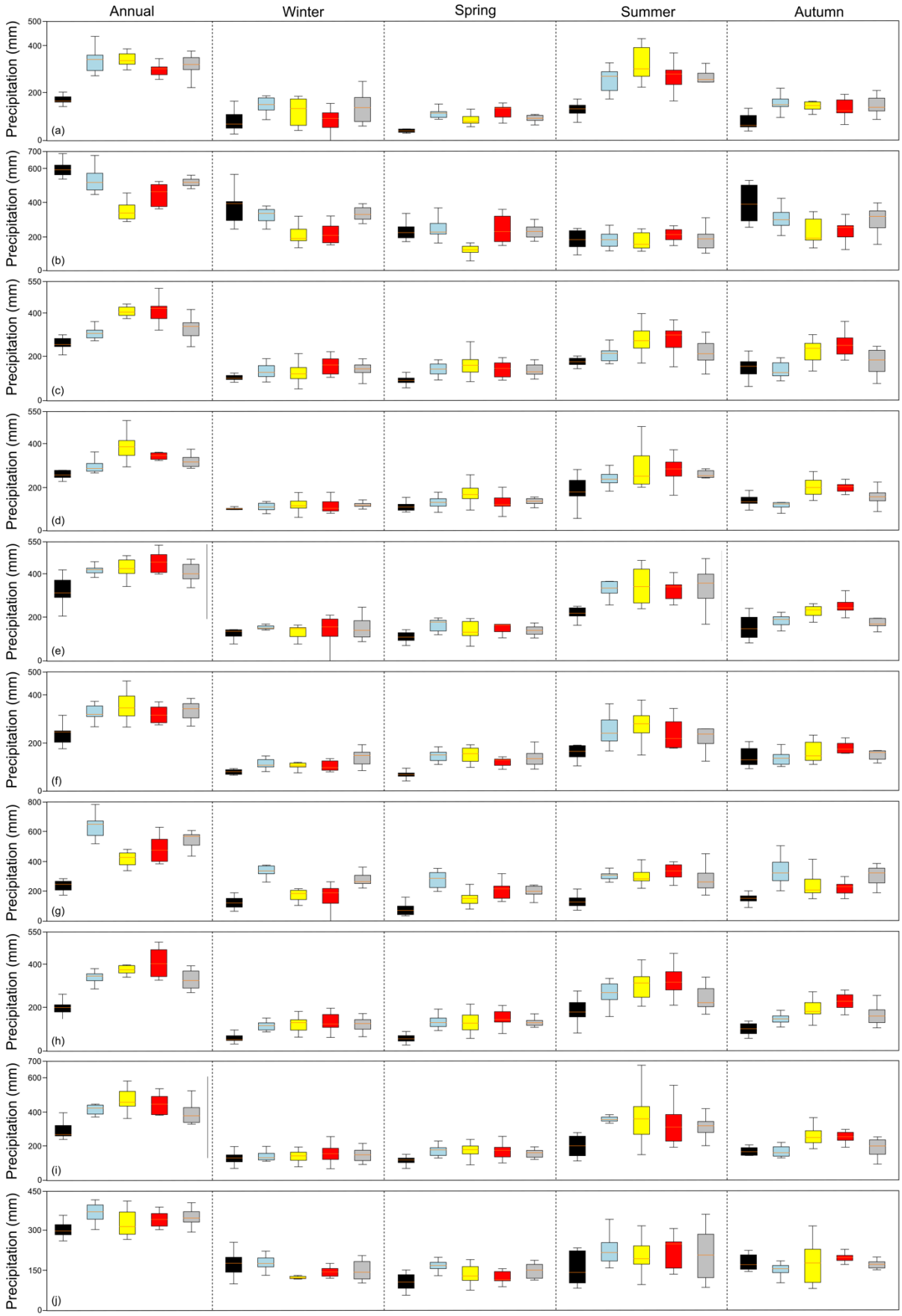

Figure 5.9: Total precipitation at (a) Abisko, (b) Andøya, (c) Kandalaksha, (d) Krasnoscel'e, (e) Kvikkjokk-Årrenjarka, (f) Murmansk, (g) Nordstraum i Kvænangen, (h) Šihččajávri, (i) Sodankylä ARC and (j) Vardø Radio, for station data (black) and WRF forced by CCSM4 (blue), CNRM-CM5 (yellow), GFDL-CM3 (red) and ERA (grey) data. The box and whiskers are as in Fig. 5.8.

Tables 5.12 to 5.14 provide details about the RMSE for all stations in different precipitation bins. Across all precipitation values, CCSM4 and GFDL-CM3 have the same RMSE (RMSE = 5.05 mm) and this value is lower than that of the CNRM-CM5 runs (RMSE = 5.45 mm). CNRM-CM5 is thus the least accurate CMIP-forced model run for precipitation estimates. The difference in overall RMSE comes from the low precipitation bin. Indeed, the RMSE for the CNRM-CM5 run in the 0 – 5 mm precipitation bin is 0.40 to 0.41 mm higher (~ 10 %) than for the CCSM4 and GFDL-CM3 runs. This bin makes up 90.3 % of the precipitation values and thus a higher error here has a large impact on the overall RMSE.

	All PPN values	0-5 mm	5-10 mm	10-15 mm	15-20 mm	20+ mm
Abisko	4.45	3.93	5.82	10.27	14.64	26.02
Andøya	6.94	4.76	6.26	9.76	14.69	28.63
Kandalaksha	4.37	3.51	6.28	10.85	15.42	22.81
Krasnoscel'e	4.33	3.37	6.06	10.56	15.98	23.66
Kvikkjokk-Årrenjarka	5.76	4.82	6.35	10.50	15.22	22.63
Murmansk	4.27	3.52	6.28	10.81	14.95	22.98
Nordstraum i Kvænangen	6.26	5.98	6.45	9.98	14.50	22.04
Šihččajávri	4.23	3.65	6.09	10.56	14.66	22.57
Sodankylä ARC	5.11	4.21	6.59	10.51	15.55	26.32
Vardø Radio	4.73	3.75	5.81	10.88	15.37	24.17
All Stations	5.05	4.15	6.20	10.47	15.10	24.18

Table 5.11: RMSE of precipitation (PPN; mm) in five precipitation bins and for all precipitation values at all 10 stations for CCSM4-forced WRF.

	All PPN values	0-5 mm	5-10 mm	10-15 mm	15-20 mm	20+ mm
Abisko	4.54	4.07	5.83	10.69	15.19	23.70
Andøya	7.04	4.43	6.41	11.18	15.42	29.53
Kandalaksha	5.37	4.74	7.03	10.40	16.83	21.49
Krasnoscel'e	5.42	4.68	7.22	11.15	15.04	24.59
Kvikkjokk-Årrenjarka	5.98	5.09	6.38	10.71	15.87	22.10
Murmansk	4.88	4.21	7.59	10.49	15.95	21.67
Nordstraum i Kvænangen	5.25	4.81	6.29	9.94	14.88	22.23
Šihččajávri	4.93	4.39	6.88	10.16	16.38	23.95
Sodankylä ARC	5.66	4.92	6.24	10.85	15.45	26.82
Vardø Radio	5.13	4.20	6.48	11.35	15.54	23.91
All Stations	5.42	4.55	6.63	10.69	15.65	24.00

Table 5.12: RMSE of precipitation (mm) in five precipitation bins and for all precipitation values at all 10 stations for CNRM-forced WRF.

	All PPN values	0-5 mm	5-10 mm	10-15 mm	15-20 mm	20+ mm
Abisko	4.13	3.57	5.45	10.83	14.90	24.96
Andøya	6.80	4.24	6.12	10.48	14.89	29.53
Kandalaksha	5.04	4.44	6.36	10.75	14.87	20.93
Krasnoscel'e	4.78	3.74	7.84	10.78	15.74	24.26
Kvikkjokk-Årrenjarka	5.87	5.03	6.14	10.55	15.36	20.95
Murmansk	4.22	3.47	6.22	11.72	14.90	21.46
Nordstraum i Kvænangen	5.48	5.09	6.23	9.82	14.69	22.98
Šihččajávri	4.64	4.13	6.05	10.25	16.13	22.54
Sodankylä ARC	4.89	4.01	6.14	10.33	14.43	25.91
Vardø Radio	4.62	3.65	5.87	10.24	14.58	24.07
All Stations	5.05	4.14	6.24	10.57	15.05	23.76

Table 5.13: RMSE of precipitation (mm) in five precipitation bins and for all precipitation values at all 10 stations for GFDL-forced WRF.

Overall, WRF models low precipitation days (0 – 5 mm) well. The mean difference between the modelled and observed values are ~4 mm for all forcing datasets (Fig. 5.10; Tables 5.11 to 5.13). CMIP-forced WRF is not as successful at modelling higher precipitations events. Indeed, all three CMIP-forced runs show a high under-prediction of precipitation for the high-precipitation bins (Fig. 5.10). On average, all three CMIP-forced runs under-estimate precipitation by over 20 mm for precipitation days of 20 mm or more, but do generally model low precipitation on those days. This matches results from validation studies of the CMIP5 models themselves. Donner et al. (2011), for example, find that the most intense precipitation (0.2 %) occurs less often in the atmospheric component of the GFDL-CM3 historical runs.

ERA-I-forced WRF runs do the best at modelling higher-precipitation events (Fig. 5.10). The largest error in the ERA-I run for high-precipitation events is the same as those from the other three models (e.g. approximately –20 mm for 15 – 20 mm precipitation). However, ERA-I successfully modelled some of the higher, observed, precipitation values as is demonstrated by the positive whisker on the box plots. The mean difference is also much closer to zero for the four higher-precipitation boxplots (5 – 10, 10 – 15, 15 – 20, and 20 + mm plots).

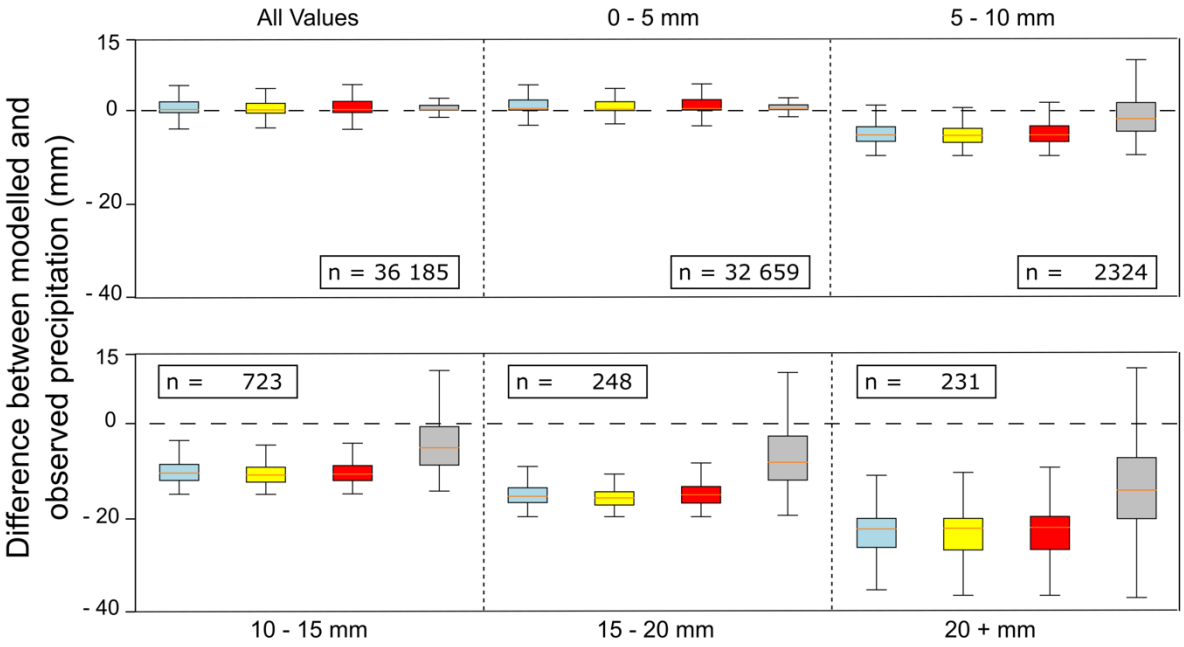

Figure 5.10: Difference between the modelled and observed precipitation for all values, and for five precipitation bins (0 – 5 mm, 5 – 10 mm, 10 – 15 mm, 15 – 20 mm and over 20 mm). The number of days associated with each precipitation bin is given on each plot. The box and whiskers are as in Fig. 5.8.

5.4 Discussion

5.4.1 Limitations of sensitivity study

Three potential sources of error in the sensitivity study and validation exercise are discussed in this section. Firstly, there is uncertainty in the sensitivity study undertaken in this chapter as a result of the limitations of using MODIS as ground truth. This is a result of the Khibiny region being partly under boreal forest which limits the skills of VNIR remote sensing datasets, such as MODIS. However, previous work in this thesis demonstrates the skill of MODIS snow retrievals over the Khibiny region. In chapter 3, MODIS was demonstrated to be a reliable dataset over the Khibiny Mountains specifically with RMSEs lower than 10 %. And in Chapter 4, MODIS was shown to accurately represent trends in snow cover in the WMR, which is reliant on MODIS retrieving accurate snow data. It is important to be aware that models are also limited in their skill at modelling snow cover under boreal forests (Essery et al., 2009; Rutter et al., 2009). This obviously adds uncertainty to the model outputs over the Khibiny Mountains, but both a sensitivity study and a straightforward validation exercise are undertaken in this chapter to demonstrate the skill of the WRF model over the region of interest.

Secondly, the use of binary snow/no-snow pixels in this analysis is a source of uncertainty. Selkowitz et al. (2014) demonstrated that in mountainous environments, 67 to 100 % of all 500 m pixels investigated were mixed (snow and no-snow). Thus, using the binary classification for snow in pixels of 500 m (MODIS) or more (WRF 1 km resolution) has limitations. Selkowitz et al. (2014) emphasised that this is of particular importance when an accurate representation of the spatial distribution of snow cover is needed, which is the case in the sensitivity study. This issue is overcome here by basing the binary classification on fractional snow cover datasets. Both the MODIS data and the model outputs are

originally composed of fractional snow, and the same cap (50 %) is used to convert these into binary pixels.

Finally, related to the previous issue described, there are inherent issues in comparing point measurements to spatial fields (e.g. Painter et al., 2016; Wang et al., 2014). Indeed, points are usually not representative of their surroundings, especially in the case of snow in mountains which is characterised by very high spatial varaibility (e.g. Immerzeel et al., 2009; Scherrer et al., 2013). If only point-to-pixel comparison was used in this sensitivity study (section 5.2.3.2), run 7 would not have been identified as the best parameterisation, and a sub-optimal parameterisation would have been selected. The uncertainty of using point-to-pixel comparisons in the sensitivity study was thus considered in the choice of methodology for this study and MODIS was used as a more representative ground truth over a resolution much closer to that of the model. The issue of point-to-pixel cannot always be avoided however, as is shown in section 5.3.3 of this chapter. The 15 km resolution, long-run, outputs were compared to observations at ten stations (point measurements). This discrepancy in resolution leads to a level of uncertainty in the results, with some of the coastal model outputs not matching coastal stations well (e.g. Andøya and Nordstraum i Kvænangen). These are discussed in a case-by-case basis in the results to address this issue.

5.4.2 Optimised parameterisation choice

In this section, the skill of the optimised model parameterisation is discussed. In the comparison of the model outputs and the MODIS data, the base run parameterisation models a slow snow-melt, close to that observed in the MODIS dataset. The optimal model parameterisation models a faster reduction in snow extent than observed. Run 7 thus is not the best parameterisation for melt-rate modelling. It does, however, model the timing of the end of the snow cover season much more accurately. The end of the snow season in the base run is much too late. Run 7 also demonstrates variable skill when it comes to modelling snow depth, often not modelling maximum depth as well as other parameterisations. However, it does simulate snow melt-out best, i.e. it reaches snow depths of 0 cm most accurately when compared to the point data. Therefore, in both of these validation exercises (MODIS data and station depth data) run 7 demonstrates the greatest skill in modelling the end of the snow cover. This is one of the most important variables for the analysis undertaken in this dissertation. Bokhorst et al. (2016) identified gaps in the study of Arctic snow cover and emphasised the need to improve the understanding of the detailed timing of the snow cover season, including snow melt-out. In this thesis, I aim to address this knowledge gap and, in Chapter 6, there is a large focus on the WRF-modelled timing of the snow cover season (including its end) by the end of the 21st century. Thus, run 7 proves itself the most optimal parameter based, not only on the indices, but also based on its skill in modelling snow melt-out. As described in section 5.2.3.3, the main reasons for the success of the parameterisation of run 7 are its improved representation of cloud processes (in both the microphysics and radiation schemes) and its higher, more representative CO2 content.

5.4.3 Model precipitation skill

In this chapter, it is demonstrated that high precipitation is modelled less accurately than low precipitation. This matches results from validation studies of the CMIP5 models themselves. Donner et al. (2011), for example, found that the most intense precipitation (0.2 %) occurs less often in the atmospheric component of the GFDL-CM3 historical runs. This is an important conclusion from this analysis, as modelling very high precipitation events is crucial to the study of extreme events. Climate extremes are the focus of an increasing number of publications. This is a consequence of the negative impacts of extreme events and their likely increase in frequency with climate change (e.g. Lader et al., 2017). Extreme precipitation and extreme snowfall events can have significant impacts on human activity and the natural environment in Northern Fennoscandia (e.g. Callaghan et al., 2010). Extreme precipitation events have negative impacts on both wildlife and vegetation. Indeed, extreme precipitation has been associated with increases in mortality of lemmings (Callaghan et al., 2013), reindeer (Hansen et al., 2014) and birds (Lamarre et al., 2018) for example. Concerning vegetation, heavy liquid and solid precipitation can flatten grasslands and cause the breaking of trees through loading respectively (Bjerke et al., 2014). Extreme precipitation also impacts human activity in Northern Fennoscandia through its role in triggering nature hazards, such as avalanches, landslides and floods (Jedicke et al., 2008, Dyrrdal et al., 2012). Additionally, extreme precipitation has been demonstrated to have negative impacts on infrastructure, damaging bridges in Sweden (Beylich and Sandberg, 2005, Callaghan et al 2010) and electrical equipment in ports in Artic Russia. For these reasons, extreme precipitation events have been identified as a key challenge for economic development in the Russian Arctic (Khlebnikova et al., 2018, Zolotokrylin et al., 2018). It is therefore crucial to be able to model extreme precipitation events with confidence. The results of the validation exercise presented in this chapter indicate that further work is needed to improve extreme precipitation modelling in WRF using CMIP5 forcing data over Northern Fennoscandia.

5.5 Conclusions

Twelve different model parameterisations were tested in WRF by modelling climate at 1 km resolution over my six-week long 2016 field season. The outputs from these runs were tested by comparing them to remote sensing and field data using statistical evaluation scores; the model set-up was optimised. With this optimal set-up, WRF outputs were shown to be reliable for both temperature and snow modelling. This model is thus appropriate for the modelling work undertaken in Chapter 6.

- With the optimised model parameterisation, WRF has low bias (1.107, close to 1), high Probability of Detection of snow (0.947), a low Probability of Over Detection (0.201) and an overall excellent Proportion Correct score (0.881) compared to the other tested physics parameterisations.

- WRF's skill at reproducing snow extent over the WMR was tested. Though the base run parameterisation models a slow snow-melt, close to that observed in the MODIS dataset, the timing of this melt was very late. The optimal model parameterisation, although modelling a faster reduction in snow extent than observed, modelled the timing of the end of the snow cover season much more accurately. Thus, improved representation of cloud subgrid variability and higher CO_2 concentration both contribute to increased skill in modelling snow melt-out.
- The WRF runs have a delay (~ 8 days) in modelling the sudden jump in temperature that occurred in late April. Before the increase in temperature in the station data and after the jump in temperature in the model outputs, the WRF model does a good job at modelling SAT variability over the field season.
- For the stations situated on the plains, WRF does a good job at modelling early-season snow depth, but the start of the melting of the snow season is a little late and the melt rates are slightly slower than those observed. Within the mountains, WRF considerably underestimates the early-season snow depth, though a significant part of this error is probably a result of the mismatch of scales.
- The effects of spectral nudging were tested and were found not to have a strong negative impact on the model outputs.

Output from three CMIP5 model historical runs and the ERA-I reanalysis were used as lateral boundary conditions for forcing WRF over Northern Fennoscandia using the optimal model parameterisation, with CCSM4, CNRM-CM5, GFDL-CM3 and ERA-I forcing data. These historical WRF runs were validated by comparing the outputs to observations from ten meteorological stations.

- WRF forced by any of the three CMIP models or by ERA-I data does an excellent job at modelling SAT over the 1990 – 1999 interval at all ten stations used for the validation.
- Out of the four historical runs, CCSM4-forced WRF does the best at modelling SAT. The original CMIP5 dataset had been bias adjusted before being used to force WRF, thus this result is not surprising.
- At all but one station, ERA-I- and CMIP-forced WRF overestimate total precipitation.
- All models do better at modelling low precipitation than high precipitation events.
- ERA-I-forced WRF is more effective than the other models at modelling high-precipitation events, with an RMSE of 14.4 mm compared to a CMIP5 'ensemble' mean RMSE of 24.0 mm for 20 + mm precipitation events.
- The lowest precipitation bin (0-5 mm) makes up 90.3 % of the precipitation values at the ten stations studied and thus even low errors in this bin have a large impact on the overall RMSE.
- CNRM-CM5 has the highest RMSE for all precipitation amounts. Thus, in terms of precipitation, for this region, CNRM-forced WRF is the least reliable model analysed.

5.6 Fit within thesis

After showing the low uncertainty and thus reliability of the MODIS dataset in chapters 3 and 4, MODIS was used as ground truth in the sensitivity analysis of WRF in this chapter. The optimal model parameterisation for snow modelling was determined over the WMR and WRF outputs using this parameterisation were validated over Northern Fennoscandia. WRF was thus shown to be reliable for modelling temperature, precipitation and snow projections over Northern Fennoscandia. This is crucial for chapter 6 in which century-scale projections of temperature, precipitation, snowfall and snow cover changes are undertaken.

5.7 References

Adler, R.F., Huffman, G.J., Chang, A., Ferraro, R., Xie, P.P., Janowiak, J., Rudolf, B., Schneider, U., Curtis, S., Bolvin, D. and Gruber, A., 2003. The version-2 global precipitation climatology project (GPCP) monthly precipitation analysis (1979–present). Journal of hydrometeorology, 4(6), pp.1147-1167. https://doi.org/10.1175/1525-7541(2003)004<1147:TVGPCP>2.0.CO;2

Alexandru, A., De Elia, R., Laprise, R., Separovic, L. and Biner, S., 2009. Sensitivity study of regional climate model simulations to large-scale nudging parameters. Monthly Weather Review, 137(5), pp.1666-1686. https://doi.org/10.1175/2008MWR2620.1

Barstad, I., Sorteberg, A., Flatøy, F. and Déqué, M., 2009. Precipitation, temperature and wind in Norway: dynamical downscaling of ERA40. Climate Dynamics, 33(6), pp.769-776. https://doi.org/10.1007/s00382-008-0476-5

Bentsen, M., Bethke, I., Debernard, J.B., Iversen, T., Kirkevåg, A., Seland, Ø., Drange, H., Roelandt, C., Seierstad, I.A., Hoose, C. and Kristjánsson, J.E., 2012. The Norwegian earth system model, NorESM1-M-Part 1: Description and basic evaluation. Geoscientific Model Development Discussions, 5, pp.2843-2931. https://doi.org/10.5194/gmd-6-687-2013

Beylich, A.A. and Sandberg, O., 2005. Geomorphic effects of the extreme rainfall event of 20–21 July, 2004 in the Latnjavagge catchment, northern Swedish Lapland. Geografiska Annaler: Series A, Physical Geography, 87(3), pp.409-419. https://doi.org/10.1111/j.0435-3676.2005.00267.x

Bieniek, P.A., Bhatt, U.S., Walsh, J.E., Rupp, T.S., Zhang, J., Krieger, J.R. and Lader, R., 2016. Dynamical downscaling of ERA-Interim temperature and precipitation for Alaska. Journal of Applied Meteorology and Climatology, 55(3), pp.635-654. https://doi.org/10.1175/JAMC-D-15-0153.1

Bjerke, J.W., Karlsen, S.R., Høgda, K.A., Malnes, E., Jepsen, J.U., Lovibond, S., Vikhamar-Schuler, D. and Tømmervik, H., 2014. Record-low primary productivity and high plant damage in the Nordic Arctic Region in 2012 caused by multiple weather events and pest outbreaks. Environmental Research Letters, 9(8), p.084006. https://doi.org/10.1088/1748-9326/9/8/084006

Bokhorst, S., Pedersen, S.H., Brucker, L., Anisimov, O., Bjerke, J.W., Brown, R.D., Ehrich, D., Essery, R.L., Heilig, A., Ingvander, S. and Johansson, C., 2016. Changing Arctic snow cover: A review of recent developments and assessment of future needs for observations, modelling, and impacts. Ambio, 45(5), pp.516-537. https://doi.org/10.1007/s13280-016-0770-0

Brands, S., Herrera, S., Fernández, J. and Gutiérrez, J.M., 2013. How well do CMIP5 Earth System Models simulate present climate conditions in Europe and Africa?. Climate dynamics, 41(3-4), pp.803-817. https://doi.org/10.1007/s00382-013-1742-8

Bruyère, C.L., Done, J.M., Holland, G.J. and Fredrick, S., 2014. Bias corrections of global models for regional climate simulations of high-impact weather. Climate dynamics, 43(7-8), pp.1847-1856. https://doi.org/10.1007/s00382-013-2011-6

Bruyère, L., Monaghan, J., Steinhoff, F. and Yates, D., 2015. Bias-corrected CMIP5 CESM data in WRF/MPAS intermediate file format. https://doi.org/10.5065/D6445JJ7

Callaghan, T.V., Bergholm, F., Christensen, T.R., Jonasson, C., Kokfelt, U. and Johansson, M., 2010. A new climate era in the sub-Arctic: Accelerating climate changes and multiple impacts. Geophysical Research Letters, 37(14). https://doi.org/10.1029/2009GL042064

Callaghan, T.V., Jonasson, C., Thierfelder, T., Yang, Z., Hedenås, H., Johansson, M., Molau, U., Van Bogaert, R., Michelsen, A., Olofsson, J. and Gwynn-Jones, D., 2013. Ecosystem change and stability over multiple decades in the Swedish subarctic: complex processes and multiple drivers. Philosophical Transactions of the Royal Society B: Biological Sciences, 368(1624), p.20120488. https://doi.org/10.1098/rstb.2012.0488

Chou, M.D. and Suarez, M.J., 1999. A solar radiation parameterization (CLIRAD-SW) for atmospheric studies. NASA Tech. Memo, 10460, p.48.

Dee, D.P., Uppala, S.M., Simmons, A.J., Berrisford, P., Poli, P., Kobayashi, S., Andrae, U., Balmaseda, M.A., Balsamo, G., Bauer, D.P. and Bechtold, P., 2011. The ERA-Interim reanalysis: Configuration and performance of the data assimilation system. Quarterly Journal of the royal meteorological society, 137(656), pp.553-597. https://doi.org/10.1002/qj.828

Derksen, C., Walker, A. and Goodison, B., 2003. A comparison of 18 winter seasons of in situ and passive microwave-derived snow water equivalent estimates in Western Canada. Remote Sensing of Environment, 88(3), pp.271-282. https://doi.org/10.1016/j.rse.2003.07.003

Donner, L.J., Wyman, B.L., Hemler, R.S., Horowitz, L.W., Ming, Y., Zhao, M., Golaz, J.C., Ginoux, P., Lin, S.J., Schwarzkopf, M.D. and Austin, J., 2011. The dynamical core, physical parameterizations, and basic simulation characteristics of the atmospheric component AM3 of the GFDL global coupled model CM3. Journal of Climate, 24(13), pp.3484-3519. https://doi.org/10.1175/2011JCLI3955.1

Dudhia, J., 1989. Numerical study of convection observed during the winter monsoon experiment using a mesoscale two-dimensional model. Journal of the atmospheric sciences, 46(20), pp.3077-3107. https://doi.org/10.1175/1520-0469(1989)046<3077:NSOCOD>2.0.CO;2

Dyrrdal, A.V., Isaksen, K., Hygen, H.O. and Meyer, N.K., 2012. Changes in meteorological variables that can trigger natural hazards in Norway. Climate Research, 55(2), pp.153-165. https://doi.org/10.3354/cr01125

ENSEMBLES members (2009) Climate change and its impacts at seasonal, decadal and centennial timescales. Summary of research and results from the ENSEMBLES project. Available at http://ensembles-eu.metoffice.com/docs/Ensembles_final_report_ Nov09.pdf

Essery, R., Rutter, N., Pomeroy, J., Baxter, R., Stähli, M., Gustafsson, D., Barr, A., Bartlett, P. and Elder, K., 2009. SNOWMIP2: An evaluation of forest snow process simulations. Bulletin of the American Meteorological Society, 90(8), pp.1120-1136. https://doi.org/10.1175/2009BAMS2629.1

Gao, Y., Fu, J.S., Drake, J.B., Liu, Y. and Lamarque, J.F., 2012. Projected changes of extreme weather events in the eastern United States based on a high resolution climate modeling system. Environmental Research Letters, 7(4), p.044025. https://doi.org/10.1088/1748-9326/7/4/044025

Gao, Y., Xu, J. and Chen, D., 2015. Evaluation of WRF mesoscale climate simulations over the Tibetan Plateau during 1979–2011. Journal of Climate, 28(7), pp.2823-2841. https://doi.org/10.1175/JCLI-D-14-00300.1

Giorgi, F., Shields Brodeur, C. and Bates, G.T., 1994. Regional climate change scenarios over the United States produced with a nested regional climate model. Journal of Climate, 7(3), pp.375-399. https://doi.org/10.1175/1520-0442(1994)007<0375:RCCSOT>2.0.CO;2

Grell, G.A. and Dévényi, D., 2002. A generalized approach to parameterizing convection combining ensemble and data assimilation techniques. Geophysical Research Letters, 29(14), pp.38-1. https://doi.org/10.1029/2002GL015311

Griffies, S.M., Winton, M., Donner, L.J., Horowitz, L.W., Downes, S.M., Farneti, R., Gnanadesikan, A., Hurlin, W.J., Lee, H.C., Liang, Z. and Palter, J.B., 2011. The GFDL CM3 coupled climate model: characteristics of the ocean and sea ice simulations. Journal of Climate, 24(13), pp.3520-3544. https://doi.org/10.1175/2011JCLI3964.1

Hall, D.K., Riggs, G.A., Salomonson, V.V., DiGirolamo, N.E. and Bayr, K.J., 2002. MODIS snow-cover products. Remote sensing of Environment, 83(1-2), pp.181-194. https://doi.org/10.1016/S0034-4257(02)00095-0

Hansen, B.B., Isaksen, K., Benestad, R.E., Kohler, J., Pedersen, Å.Ø., Loe, L.E., Coulson, S.J., Larsen, J.O. and Varpe, Ø., 2014. Warmer and wetter winters: characteristics and implications of an extreme weather event in the High Arctic. Environmental Research Letters, 9(11), p.114021. https://doi.org/10.1088/1748-9326/9/11/114021

Heikkilä, U., Sandvik, A. and Sorteberg, A., 2011. Dynamical downscaling of ERA-40 in complex terrain using the WRF regional climate model. *Climate dynamics*, *37*(7-8), pp.1551-1564. https://doi.org/10.1007/s00382-010-0928-6

Hong, S.Y., Dudhia, J. and Chen, S.H., 2004. A revised approach to ice microphysical processes for the bulk parameterization of clouds and precipitation. Monthly Weather Review, 132(1), pp.103-120. https://doi.org/10.1175/1520-0493(2004)132<0103:ARATIM>2.0.CO;2

Hong, S.Y., Noh, Y. and Dudhia, J., 2006. A new vertical diffusion package with an explicit treatment of entrainment processes. Monthly weather review, 134(9), pp.2318-2341. https://doi.org/10.1175/MWR3199.1

Hurrell, J.W., Holland, M.M., Gent, P.R., Ghan, S., Kay, J.E., Kushner, P.J., Lamarque, J.F., Large, W.G., Lawrence, D., Lindsay, K. and Lipscomb, W.H., 2013. The community earth system model: a framework for collaborative research. Bulletin of the American Meteorological Society, 94(9), pp.1339-1360. https://doi.org/10.1175/BAMS-D-12-00121.1

Iacono, M.J., Delamere, J.S., Mlawer, E.J., Shephard, M.W., Clough, S.A. and Collins, W.D., 2008. Radiative forcing by long-lived greenhouse gases: Calculations with the AER radiative transfer models. Journal of Geophysical Research: Atmospheres, 113(D13). https://doi.org/10.1029/2008JD009944

Immerzeel, W.W., Droogers, P., De Jong, S.M. and Bierkens, M.F.P., 2009. Large-scale monitoring of snow cover and runoff simulation in Himalayan river basins using remote sensing. Remote sensing of Environment, 113(1), pp.40-49. https://doi.org/10.1016/j.rse.2008.08.010

Jaedicke, C., Solheim, A., Blikra, L.H., Stalsberg, K., Sorteberg, A., Aaheim, A., Kronholm, K., Vikhamar-Schuler, D., Isaksen, K., Sletten, K. and Kristensen, K., 2008. Spatial and temporal variations of Norwegian geohazards in a changing climate, the GeoExtreme Project. Natural Hazards and Earth System Sciences, 8(4), pp.893-904. https://doi.org/10.5194/nhess-8-893-2008

Janjić, Z.I., 1994. The step-mountain eta coordinate model: Further developments of the convection, viscous sublayer, and turbulence closure schemes. Monthly Weather Review, 122(5), pp.927-945. https://doi.org/10.1175/1520-0493(1994)122<0927:TSMECM>2.0.CO;2

Janjić, Z.I., 2000. Comments on "Development and evaluation of a convection scheme for use in climate models". Journal of the Atmospheric Sciences, 57(21), pp.3686-3686. https://doi.org/10.1175/1520-0469(2000)057<3686:CODAEO>2.0.CO;2

Johannessen, O.M., Bengtsson, L., Miles, M.W., Kuzmina, S.I., Semenov, V.A., Alekseev, G.V., Nagurnyi, A.P., Zakharov, V.F., Bobylev, L.P., Pettersson, L.H. and Hasselmann, K., 2004. Arctic climate change: observed and modelled temperature and sea-ice variability. Tellus A: Dynamic Meteorology and Oceanography, 56(4), pp.328-341. https://doi.org/10.3402/tellusa.v56i4.14418

Kain, J.S., 2004. The Kain–Fritsch convective parameterization: an update. Journal of Applied Meteorology, 43, pp.170-181.https://doi.org/10.1175/1520-0450(2004)043<0170:TKCPAU>2.0.CO;2

Khlebnikova, E.I., Kattsov, V.M., Pikaleva, A.A. and Shkolnik, I.M., 2018. Assessment of Climate Change Impacts on the Economic Development of the Russian Arctic in the 21st Century. Russian Meteorology and Hydrology, 43(6), pp.347-356. https://doi.org/10.3103/S1068373918060018

Lader, R., Walsh, J.E., Bhatt, U.S. and Bieniek, P.A., 2017. Projections of twenty-first-century climate extremes for alaska via dynamical downscaling and quantile mapping. Journal of Applied Meteorology and Climatology, 56(9), pp.2393-2409. https://doi.org/10.1175/JAMC-D-16-0415.1

Laliberté, F., Howell, S.E.L. and Kushner, P.J., 2016. Regional variability of a projected sea ice-free Arctic during the summer months. Geophysical Research Letters, 43(1), pp.256-263. https://doi.org/10.1002/2015GL066855

Lamarre, V., Legagneux, P., Franke, A., Casajus, N., Currie, D.C., Berteaux, D. and Bêty, J., 2018. Precipitation and ectoparasitism reduce reproductive success in an arctic-nesting top-predator. Scientific reports, 8(1), p.8530. https://doi.org/10.1038/s41598-018-26131-y

Lehtonen, I., Kamarainen, M., Gregow, H., Venalainen, A. and Peltola, H., 2016. Heavy snow loads in Finnish forests respond regionally asymmetrically to projected climate change. Natural Hazards and Earth System Sciences (Online), 16(10). https://doi.org/10.5194/nhess-16-2259-2016

Leung, L.R. and Qian, Y., 2003. The sensitivity of precipitation and snowpack simulations to model resolution via nesting in regions of complex terrain. Journal of Hydrometeorology, 4(6), pp.1025-1043. https://doi.org/10.1175/1525-7541(2003)004<1025:TSOPAS>2.0.CO;2

Liston, G.E., 1999. Interrelationships among snow distribution, snowmelt, and snow cover depletion: Implications for atmospheric, hydrologic, and ecologic modeling. Journal of applied meteorology, 38(10), pp.1474-1487. https://doi.org/10.1175/1520-0450(1999)038<1474:IASDSA>2.0.CO;2

Liu, F., Krieger, J.R. and Zhang, J., 2014. Toward producing the Chukchi–Beaufort High-Resolution Atmospheric Reanalysis (CBHAR) via the WRFDA data assimilation system. Monthly Weather Review, 142(2), pp.788-805. https://doi.org/10.1175/MWR-D-13-00063.1

Marshall, G.J., Kivinen, S., Jylhä, K., Vignols, R.M. and Rees, W.G., 2018. The accuracy of climate variability and trends across Arctic Fennoscandia in four reanalyses. International Journal of Climatology. https://doi.org/10.1002/joc.5541

Maussion, F., Scherer, D., Finkelnburg, R., Richters, J., Yang, W. and Yao, T., 2011. WRF simulation of a precipitation event over the Tibetan Plateau, China-an assessment using remote sensing and ground observations. Hydrology and Earth System Sciences, 15(6), p.1795. https://doi.org/10.5194/hess-15-1795-2011

Miguez-Macho, G., Stenchikov, G.L. and Robock, A., 2005. Regional climate simulations over North America: Interaction of local processes with improved large-scale flow. Journal of climate, 18(8), pp.1227-1246. https://doi.org/10.1175/JCLI3369.1

Molthan, A.L. and Colle, B.A., 2012. Comparisons of single-and double-moment microphysics schemes in the simulation of a synoptic-scale snowfall event. Monthly Weather Review, 140(9), pp.2982-3002. https://doi.org/10.1175/MWR-D-11-00292.1

Morrison, H., Thompson, G. and Tatarskii, V., 2009. Impact of cloud microphysics on the development of trailing stratiform precipitation in a simulated squall line: Comparison of one-and two-moment schemes. Monthly weather review, 137(3), pp.991-1007. https://doi.org/10.1175/2008MWR2556.1

Painter, T.H., Berisford, D.F., Boardman, J.W., Bormann, K.J., Deems, J.S., Gehrke, F., Hedrick, A., Joyce, M., Laidlaw, R., Marks, D. and Mattmann, C., 2016. The Airborne Snow Observatory: Fusion of scanning lidar, imaging spectrometer, and physically-based modeling for mapping snow water equivalent and snow albedo. Remote Sensing of Environment, 184, pp.139-152. https://doi.org/10.1016/j.rse.2016.06.018

Perez, J., Menendez, M., Mendez, F.J. and Losada, I.J., 2014. Evaluating the performance of CMIP3 and CMIP5 global climate models over the north-east Atlantic region. Climate dynamics, 43(9-10), pp.2663-2680. https://doi.org/10.1007/s00382-014-2078-8

Radu, R., Déqué, M. and Somot, S., 2008. Spectral nudging in a spectral regional climate model. Tellus A: Dynamic Meteorology and Oceanography, 60(5), pp.898-910. https://doi.org/10.1111/j.1600-0870.2008.00341.x

Räisänen, J. and Ylhäisi, J.S., 2015. CO 2-induced climate change in northern Europe: CMIP2 versus CMIP3 versus CMIP5. Climate Dynamics, 45(7-8), pp.1877-1897. https://doi.org/10.1007/s00382-014-2440-x

Rakesh, V., Singh, R., Pal, P.K. and Joshi, P.C., 2007. Sensitivity of mesoscale model forecast during a satellite launch to different cumulus parameterization schemes in MM5. In Atmospheric and Oceanic (pp. 1617-1637). Birkhäuser Basel. https://doi.org/10.1007/978-3-7643-8493-7_10

Rittger, K., Painter, T.H. and Dozier, J., 2013. Assessment of methods for mapping snow cover from MODIS. Advances in Water Resources, 51, pp.367-380. https://doi.org/10.1016/j.advwatres.2012.03.002

Run, R. and Case, R.D.T., 2015. User's Guide for the NMM Core of the Weather Research and Forecast (WRF) Modeling System Version 3.

Rutter, N., Essery, R., Pomeroy, J., Altimir, N., Andreadis, K., Baker, I., Barr, A., Bartlett, P., Boone, A., Deng, H. and Douville, H., 2009. Evaluation of forest snow processes models (SnowMIP2). Journal of Geophysical Research: Atmospheres, 114(D6). https://doi.org/10.1029/2008JD011063

Scherrer, S.C., Wüthrich, C., Croci-Maspoli, M., Weingartner, R. and Appenzeller, C., 2013. Snow variability in the Swiss Alps 1864–2009. International journal of climatology, 33(15), pp.3162-3173. https://doi.org/10.1002/joc.3653

Selkowitz, D., Forster, R. and Caldwell, M., 2014. Prevalence of Pure Versus Mixed Snow Cover Pixels across Spatial Resolutions in Alpine Environments. Remote Sensing, 6(12), pp.12478-12508. https://doi.org/10.3390/rs61212478

Shrestha, M., Wang, L., Koike, T., Xue, Y. and Hirabayashi, Y., 2010. Improving the snow physics of WEB-DHM and its point evaluation at the SnowMIP sites. Hydrology and Earth System Sciences, 14(12), pp.2577-2594. https://doi.org/10.5194/hess-14-2577-2010

Shrestha, M., Wang, L., Koike, T., Xue, Y. and Hirabayashi, Y., 2012. Modeling the spatial distribution of snow cover in the Dudhkoshi region of the Nepal Himalayas. *Journal of Hydrometeorology*, *13*(1), pp.204-222. https://doi.org/10.1175/JHM-D-10-05027.1

Skamarock, W. C., J. B. Klemp, J. Dudhia, D. O. Gill, D. M. Barker, M. G Duda, X.-Y. Huang, W. Wang, and J. G. Powers, 2008. A Description of the Advanced Research WRF Version 3. NCAR Tech. Note NCAR/TN-475+STR, 113 pp. https://doi.org/10.5065/D68S4MVH

Soares, P.M., Cardoso, R.M., Miranda, P.M., de Medeiros, J., Belo-Pereira, M. and Espirito-Santo, F., 2012. WRF high resolution dynamical downscaling of ERA-Interim for Portugal. Climate Dynamics, 39(9-10), pp.2497-2522. https://doi.org/10.1007/s00382-012-1315-2

Tang, J., Niu, X., Wang, S., Gao, H., Wang, X. and Wu, J., 2016. Statistical downscaling and dynamical downscaling of regional climate in China: Present climate evaluations and future climate projections. Journal of Geophysical Research: Atmospheres, 121(5), pp.2110-2129. https://doi.org/10.1002/2015JD023977

Thompson, G., Field, P.R., Rasmussen, R.M. and Hall, W.D., 2008. Explicit forecasts of winter precipitation using an improved bulk microphysics scheme. Part II: Implementation of a new snow parameterization. Monthly Weather Review, 136(12), pp.5095-5115. https://doi.org/10.1175/2008MWR2387.1

Voldoire, A., Sanchez-Gomez, E., y Mélia, D.S., Decharme, B., Cassou, C., Sénési, S., Valcke, S., Beau, I., Alias, A., Chevallier, M. and Déqué, M., 2013. The CNRM-CM5. 1 global climate model: description and basic evaluation. Climate Dynamics, 40(9-10), pp.2091-2121. https://doi.org/10.1007/s00382-011-1259-y

Waldron, K.M., Paegle, J. and Horel, J.D., 1996. Sensitivity of a spectrally filtered and nudged limited-area model to outer model options. Monthly weather review, 124(3), pp.529-547. https://doi.org/10.1175/1520-0493(1996)124<0529:SOASFA>2.0.CO;2

Wang, L., Koike, T., Yang, K., Jackson, T.J., Bindlish, R. and Yang, D., 2009. Development of a distributed biosphere hydrological model and its evaluation with the Southern Great Plains Experiments (SGP97 and SGP99). Journal of Geophysical Research: Atmospheres, 114(D8). https://doi.org/10.1029/2008JD010800

Wang, Z., Schaaf, C.B., Strahler, A.H., Chopping, M.J., Román, M.O., Shuai, Y., Woodcock, C.E., Hollinger, D.Y. and Fitzjarrald, D.R., 2014. Evaluation of MODIS albedo product (MCD43A) over grassland, agriculture and forest surface types during dormant and snow-covered periods. Remote Sensing of Environment, 140, pp.60-77. https://doi.org/10.1016/j.rse.2013.08.025

Woodcock, F., 1976. The evaluation of yes/no forecasts for scientific and administrative purposes. Monthly Weather Review, 104(10), pp.1209-1214. https://doi.org/10.1175/1520-0493(1976)104<1209:TEOYFF>2.0.CO;2

Yang, M.J. and Tung, Q.C., 2003. Evaluation of rainfall forecasts over Taiwan by four cumulus parameterization schemes. Journal of the Meteorological Society of Japan. Ser. II, 81(5), pp.1163-1183. https://doi.org/10.2151/jmsj.81.1163

Zängl, G., 2007. To what extent does increased model resolution improve simulated precipitation fields? A case study of two north-Alpine heavy-rainfall events. Meteorologische Zeitschrift, 16(5), pp.571-580. https://doi.org/10.1127/0941-2948/2007/0237

Zolotokrylin, A.N., Vinogradova, V.V., Titkova, T.B., Cherenkova, E.A., Bokuchava, D.D., Sokolov, I.A., Vinogradov, A.V. and Babina, E.D., 2018, January. Impact of climate changes on population vital activities in Russia in the early 21st century. In IOP Conference Series: Earth and Environmental Science (Vol. 107, No. 1, p. 012045). IOP Publishing. https://doi.org/10.1088/1755-1315/107/1/012045

Chapter 6
Snow cover predictions for the end of the 21st century

In this chapter, changes in climate over Northern Fennoscandia are studied using future (2090 - 2099) WRF runs, forced using three different CMIP5 models and in two emission scenarios. I focus on studying changes in snowfall and snow cover over the region, looking at the timing and duration of the snow cover season in detail.

6.1 Introduction

Modelling future changes in regional snow is important because of the key role of snow in the Earth's changing climate system and its direct impact on both the natural and human environment. This can only be done in a context of modelling future climate. The Intergovernmental Panel on Climate Change (IPCC), an international scientific collaboration, makes extensive predictions of future climate and, as such, is a key institution in future climate modelling. The IPCC has organised the Coupled Model Intercomparison Project (CMIP), a crucial foundation in modern climate science. CMIP coordinates the design and distribution of past, current and future global climate model simulations (Eyring et al., 2016). In this thesis, I use CMIP5, which is the most recent CMIP ensemble as CMIP6 data is not yet widely available. Overall, the CMIP5 models have been shown to outperform the earlier CMIP3 models when compared to observations in the recent past: CMIP5 had fewer models with large cold temperature biases or high snow cover biases compared to CMIP3 (Fletcher et al., 2015) and Arctic sea-ice trends over the satellite era (1979 - 2011) were more consistent with observations in CMIP5 than CMIP3 (Stroeve et al., 2012). A detailed validation of the three specific CMIP5 models used is given in Chapter 5 and demonstrates the reliability of CMIP5 outputs when downscaled using WRF.

However, there are still limitations in the use of CMIP5. For example, Bruitel-Vuilmet et al. (2013) modelled Northern Hemisphere snow cover extent and found that the CMIP5 models underestimate the significant decrease in spring snow cover extent over 1979 - 2005. Additionally, despite an improvement in the model outputs, most CMIP5 models still underestimate trends in Arctic sea-ice over 1979 - 2011 compared to observed values (Stroeve et al., 2012). Cattiaux et al. (2013) assessed the present-day biases in temperatures in CMIP5 under the RCP 8.5 scenario over Europe. They found that the CMIP5 models exhibit a cold bias in winter and found that this bias is especially marked in north-eastern Europe, including over Northern Fennoscandia.

The origin of the uncertainty in the CMIP5 model projections is threefold. It is a result of inter-model spread, natural variability and the choice of emission scenario (Hawkins and Sutton, 2009; Overland et al., 2011). Inter-model spread is, itself, due to the different parameterisations of physical processes in the various models. Internal variability is a result of the Earth's climate and its chaotic nature, which leads to different model outputs for similar initial conditions (Overland et al., 2014).

Finally, the uncertainty in emission scenario results from the existence of a range of different outcomes of how the future may evolve, based on future socioeconomic, technological, energy, land use and greenhouse gas emission changes (Overland et al., 2014).

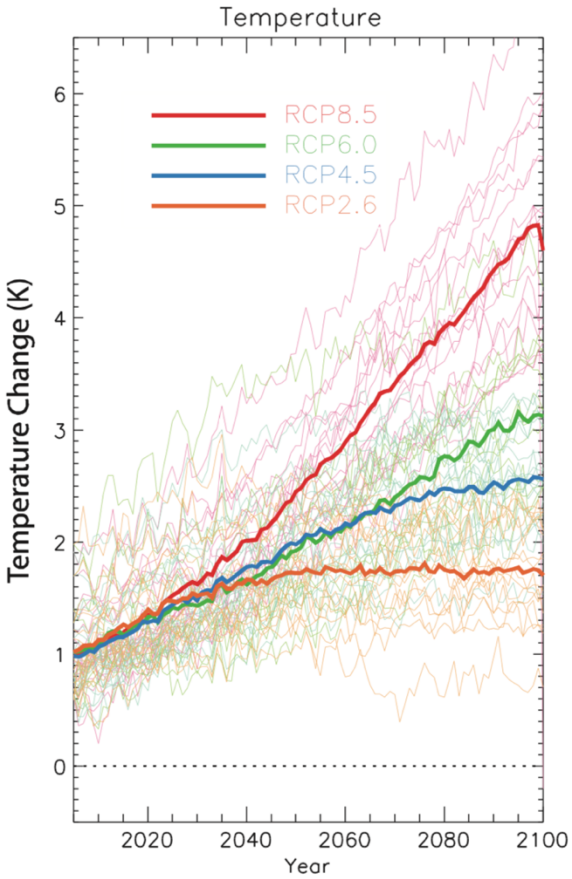

Figure 6.1: The globally averaged surface temperature change since preindustrial times; individual lines are individual CMIP5 model projections and thick lines are the multimodel mean, from Forster et al. (2013).

Overall, the importance of internal variability is higher for near-term projections and increases at smaller spatial scales (Hawkins and Sutton, 2009). For long-term projections, like in this project, the two main sources of uncertainty are the inter-model spread and emission scenario choice. It is thus important to use a range of different CMIP5 models and emission scenarios. The inter-model spread, as well as the uncertainty stemming from emission scenario choice, can be seen in Figure 6.1. This figure from Forster et al. (2013) shows the range of temperature change projections from the different CMIP5 models as well as the different means in the four RCP scenarios. This spread is also seen in other parameters such as precipitation, sea level pressure etc. This shows that the different CMIP5 models simulate very different results and so will predict very different future trends in various climate parameters. However, this inter-model spread does not make the various CMIP5 models any less reliable. Knutti and Sedláček (2013) emphasized that progress in climate modelling is not necessarily limited to narrowing inter-model uncertainties. Indeed, an improvement in climate models does not necessarily imply an increased convergence between different models. However, as the representation of climate processes in the models becomes more detailed, so does the confidence in their projections.

The CMIP5 ensemble has been used in many studies to model future climate over the next century. The future of Arctic amplification (more pronounced warming between 67.5 N° to 90°N

relative to the global mean) has been studied many times and CMIP5 outputs demonstrate a seasonal aspect of this amplified warming (e.g. Lu and Cai, 2009; Kumar et al., 2010). Future Arctic amplification (2081 - 2100 compared to 1986 - 2005) was projected to be highest in early winter (November to December) with a mean warming of the Arctic region four times greater than the global mean in the CMIP5 ensemble in RCP 4.5 (Collins et al., 2013). Using the CMIP5 multi-mean ensemble, Overland et al. (2014) predict an Arctic-wide increase in mean surface temperature of +3 (/ +5) °C in spring and +7 (/ +13) °C in autumn in RCP 4.5 (/RCP 8.5). Finally, Cattiaux et al. (2013) found in an analysis of daily temperature extremes over Europe that temperature variability is projected to decrease in winter and slightly increase in summer by the end of the 21st century.

Regarding snow cover specifically, there is a relative lack of literature investigating future changes in snow cover over the Arctic by the end of the century. Both CMIP3 (Roesch, 2006; Brown and Mote, 2009) and CMIP5 (Brutel-Vuilmet et al., 2013) model outputs project a widespread reduction in the snow cover extent, especially in spring, by the end of the 21st century. These changes in snow cover extent are coherent across all CMIP5 models, though there is considerable inter-model spread (Collins et al., 2013). CMIP5 models are General Circulation Models (GCMs) and, as such, climate projections using these models are made at large scales (~ 100 - 200 km grid-cells). In this thesis, I focus on future changes in regional snow over northern Fennoscandia and a higher spatial resolution is required. Thus, using a Regional Climate Model (RCM) is vital at this stage in order to better understand the impact that climate change will have at a local scale. As in Chapter 5, the Weather Research and Forecasting model (WRF) is used to downscale CMIP5 data, in order to make end-of-century projections in northern Fennoscandian snow cover.

In this chapter, the methods used in the downscaling of CMIP5 data using WRF are given in section 6.2. The experimental set-up is detailed, and data analysis methods are provided. In sections 6.3 and 6.4, the results are given and discussed. Finally, the conclusions of this work are summarized in section 6.5.

6.2 Methods

6.2.1 Experiment design

6.2.1.1 Model setup

The Weather Research and Forecasting model (WRF; Skamarock et al., 2005) was used to downscale CMIP5 data over Northern Fennoscandia in order to produce high-resolution projections over this region. The WRF model was set up in the same manner as in Chapter 5 section 5.3, including the same physics and domain setup. The higher resolution domain is thus at 15 km resolution. Six future model runs were performed. These were run over one decade at the end of the 21st century (2090 - 2099). Runs were performed in one-year increments with 9 days of spin-up, starting on December 23rd at 00:00:00 of the previous year and running until January 1st at 00:00:00 of the following year.

6.2.1.2 Emission scenarios

In order to run climate models over future time periods, it is necessary to use initial and boundary forcing data, which must make assumptions about the future greenhouse gas conditions of the planet. The IPCC (2014) defines four Representative Concentration Pathways (RCP), which represent four possible futures in which different greenhouse gas concentrations are reached. I decided to focus on two RCP scenarios for the future runs. The aim was to establish a realistic spread of results for end-of-21st-century conditions so the RCP 2.6 scenario was discarded as it is highly unlikely that emissions will be reduced to this level over the next few decades. RCP 4.5 was selected as the lowest emission scenario. This is supported by the Paris agreement signed internationally in 2016, in which countries agreed to aim for a target of 1.5 degree warming. RCP 4.5 sees a mean temperature increase of 1.8 °C for the 1981 to 2100 interval, with a likely range of 1.1 to 2.6 °C (IPCC, 2013). The second RCP scenario selected for this study is RCP 8.5 which is the "business as usual" scenario. This scenario will likely result in a global increase in mean surface temperature of 3.7 °C, with a likely range of 2.6 to 4.8 °C, for 2081 - 2100 relative to 1986 - 2005 (IPCC, 2013).

6.2.1.3 Forcing data

The same three CMIP5 models described in Chapter 5 were used to force WRF over the last decade of the 21st century. These are CCSM4 from version 1 of the National Center for Atmospheric Research (NCAR) Community Earth System Model (CESM; Hurrell et al., 2013), CNRM-CM5 developed by the Centre National de Recherches Météorologiques (CNRM; Voldoire et al., 2013) and GFDL-CM3 from the latest coupled climate model from the Geophysical Fluid Dynamics Laboratory (GFDL; Donner et al., 2011).

6.2.1.4 WRF output variables

The different WRF output variables used in this chapter are presented in Table 6.1.

Parameter	WRF name	Unit
Temperature at 2 m (SAT)	T2	K
Convective liquid precipitation	RAINC	$kg.m^{-2}.s^{-1}$
Non-convective liquid precipitation	RAINNC	$kg.m^{-2}.s^{-1}$
Total precipitation	RAINC + RAINNC	$kg.m^{-2}.s^{-1}$
Convective snowfall	SNOWC	$kg.m^{-2}.s^{-1}$
Non-convective snowfall	SNOWNC	$kg.m^{-2}.s^{-1}$
Total snowfall	SNOWC + SNOWNC	$kg.m^{-2}.s^{-1}$
Snow depth	SNOWH	m

Table 6.1: WRF output variables used in the analysis with their WRF names and units.

6.2.1.5 Stations

Stations are used in this chapter as locations of interest to compare model outputs in detail (see Table 6.2). A smaller selection of stations is used in this chapter compared to the previous chapter, as the majority of the analysis is undertaken using the WRF data across the entire Northern Fennoscandia region. Three stations were chosen to cover the latitude and longitude of the region as well as possible (Fig. 6.2), as well as encompass a range of altitudes.

Number	Station Name	Latitude (°N)	Longitude (°E)	Altitude (m)
1	Abisko	68.36	18.82	394
2	Kandalaksha	67.13	32.43	26
3	Vardø Radio	70.37	31.10	15

Table 6.2: Details of the stations used in the validation experiment as ground truth.

Figure 6.2: Map showing the location of the stations used in this analysis.

6.2.2 Decadal changes in climate

In this chapter, century-scale changes in climate over Northern Fennoscandia are investigated. The historical runs used in this analysis as those performed in Chapter 5, described in section 5.3.2.2. These were run for one decade between 1990 and 1999, using CCSM4, CNRM-CM5 and GFDL-CM3 as forcing data. It has been shown that key aspects of snow cover respond to both temperature and precipitation (solid and liquid), with snow cover duration, snow cover extent and snow water equivalent for example (Brown and Mote, 2009). Therefore, changes in surface air temperature (SAT), precipitation and snowfall are investigated in this chapter. Changes in mean SAT, total precipitation and total snowfall are calculated by taking the decadal mean or total for each individual run and subtracting the historical runs from the future runs. These changes are analysed for the entire year (annual) as well as in the four

seasons: spring (March, April and May), summer (June, July and August), autumn (September, October and November) and winter (December, January and February:). Differences between the 1990 - 1999 and 2090 - 2099 decades are calculated using a t-test, defined as significant at $p < 0.05$ with these areas indicated on the difference or change plots.

6.2.3 Extracting snow cover season dates

A similar method to that described in Chapter 4 was implemented here to extract snow cover start (SCS), snow cover end (SCE) and snow cover duration (SCD). The method described in Chapter 4, itself based on Malnes et al. (2016), was modified to fit the different dataset used in this analysis.

The SCS is defined here as the first of ten consecutive days with at least 1 cm snow cover. The snow cover end (SCE) is defined as the first snow-free day when the snow depth value falls below 1 cm more than 10 days in a row. A cap of 1 cm was used, as with the station data in Chapter 4, as an intermediate value between 0 cm used by Dietz et al (2012) and 2 cm used by Malnes et al. (2016). Unlike when using MODIS data, the same number of days was used to define the SCS and SCE because of there being no limitation in retrieval resulting from cloud cover. Similarly, lack of sunlight at higher latitudes resulting from polar night, and very low solar zenith angles associated with low daylight hours, were no longer a hindrance to the dataset. These points meant that with a visible and near infra-red dataset, the dates of SCS and SCE had to be limited to not overlap with the polar night (Chapter 4 Section 3.2.2). In this study, which uses model outputs instead of remote sensing data, any dates could be found to be the SCS or SCE. As a result of the range in latitude and topography over the study area, the earliest possible SCS date and the latest SCE date were selected experimentally, by running multiple tests and finding the best time of year to set as the start and end of possible snow cover seasons. August 15th was selected as the date that matched best with results for an earliest possible SCS date, and thus August 14th of the following year was selected as the last possible SCE date.

6.3 Results and discussion

6.3.1 Mean surface air temperature

The changes in annual mean SAT between the future (2090 - 2099) and historical (1990 - 1999) projections are given in figure 6.3 for the six future runs forced by three CMIP5 models and in two RCP scenarios. Figures 6.4 to 6.7 give these changes in decadal mean values for the individual seasons.

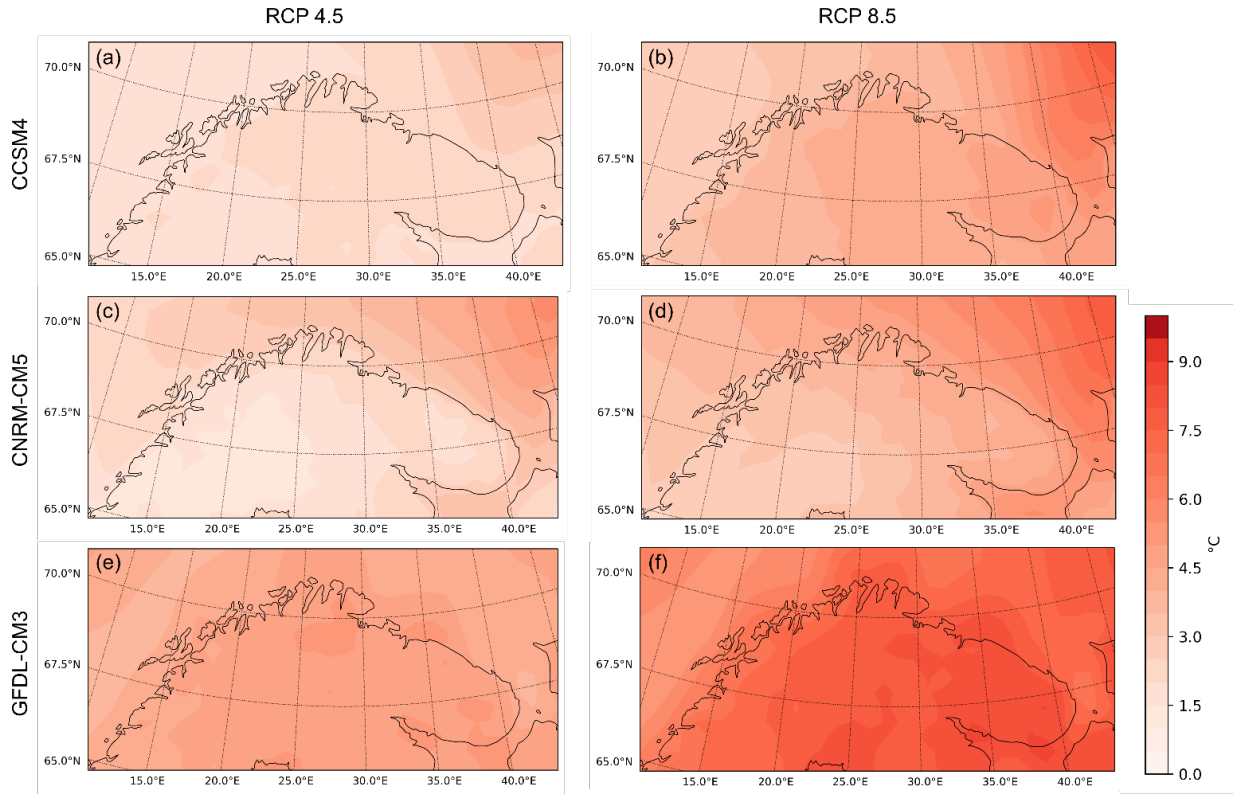

Figure 6.3: Projected change in mean annual SAT over Northern Fennoscandia in RCP 4.5 (left) and RCP 8.5 (right). Model outputs from the three CMIP5 models are shown. All areas are statistically significant.

For all forcing models and in both emission scenarios, WRF predicts an increase in annual mean SAT over the entirety of Northern Fennoscandia in 2090 - 2099 compared to 1990 - 1999 (Fig 6.3). Mean annual SAT changes in all models and emission scenarios are statistically significant. The minimum projected SAT increase is found in the CNRN-CM5-forced run over the south-western part of the domain and is +1.5 °C (Fig 6.3c). The largest annual mean SAT increase is simulated by the GFDL-CM3 RCP 8.5 run over the Kola Peninsula and is of 9 °C (Fig 6.3f). For all models and seasons, the increase in mean SAT is greater in RCP 8.5 than in RCP 4.5. The difference between the two emission scenarios is greatest in the GFDL-forced runs.

Model run	RCP 4.5	RCP 8.5
CCSM4	+ 2.6 °C	+ 4.9 °C
CNRM-CM5	+ 3.1 °C	+ 5.2 °C
GFDL-CM3	+ 5.0 °C	+ 7.8 °C
'Ensemble' mean	+ 3.6 °C	+ 6.0 °C

Table 6.3 Mean annual SAT increase over the entire domain in all model projections.

The mean annual SAT change over the entire domain is shown in Table 6.3 for all model runs. The mean increase ranges between 2.6 and 5.0 °C in RCP 4.5 and between 4.9 and 7.8 °C in RCP 8.5. These values can be compared to the global mean annual SAT increase modelled by the CMIP5 ensemble, as published in the IPCC reports (IPCC, 2013). These predict a global increase of 1.1 to 2.6

°C in RCP 4.5 and of 2.6 to 4.8 °C in RCP 8.5. The results of my model runs clearly demonstrate Arctic Amplification with the 'ensemble' mean value over Northern Fennoscandia (3.6 °C) being double the global ensemble mean (1.8 °C) in RCP 4.5, and nearly 40 % greater in RCP 8.5 (domain: 6.0 °C; global: 3.7 °C).

The mean annual SAT change projected over Northern Fennoscandia is very similar in the CCSM4 and CNRM-CM5 runs, and is much higher in both emission scenarios in the GFDL-CM3 runs. This results in a small overlap between the two emission scenarios in the distribution of mean temperature increase. Indeed, the SAT rise projected in GFDL-CM3 RCP 4.5 (+ 5.0 °C) is greater than that projected in CCSM4 RCP 8.5 (+ 4.9 °C). Additionally, model spread is greater in RCP 8.5 (2.9 °C) than in RCP 4.5 (2.4 °C). The difference between the 'ensemble' mean values is of 2.4 °C, which is the same (RCP 4.5) or less (RCP 8.5) than the model spread. Thus, even with an ensemble of only three models, the model uncertainty contributes the greatest uncertainty in these projections as expected by Hawkins and Suttons (2009).

GFDL-CM3 models the greatest SAT increases over land in all seasons. The highest seasonal SAT increase occurs in winter with a warming up to 9.5 °C over a majority of the Kola Peninsula and the coastal regions around the Gulf of Bothnia, and greater than 9.5 °C over the small part of Arkhangelsk Oblast included in the south-east of the domain. In both emission scenarios, CCSM4 and CNRM-CM5 runs both predict the largest mean annual SAT increase (+4 to 8 °C) over the Barents Sea in the north-eastern corner of the domain. The large increase in SAT predicted over this north-eastern region is probably explained by a sudden decrease in sea-ice. Indeed, this warming originates from changes in SAT in spring (Fig. 6.4) and winter (Fig. 6.7), which fits sea-ice melting timelines and is consistent with Johannessen et al.'s (2004) finding that large Arctic warming events are often associated with sea-ice variability.

In all models and scenarios except for GFDL-CM3 RCP 4.5, the greatest annual mean SAT increases over land are over the Kola Peninsula. The largest SAT change since 1990 - 1999 over the Kola Peninsula is +2.5 °C, +3.0 °C, +5.5 °C in RCP 4.5 and +5.5 °C, +5.5 °C, +9.0 °C in RCP 8.5, for the CCSM4, CNRM-CM5 and GFDL-CM3 models, respectively. In CCSM4 RCP 4.5, the largest land SAT increase covers almost the entirety of the eastern half of Northern Fennoscandia and in GFDL-CM3 RCP 8.5, the largest increase over land is also over the coastal region surrounding the Gulf of Bothnia.

The majority of the outputs of mean seasonal SAT change are statistically significant, and project an increase in SAT by the end of the 21st century (Fig. 6.4 to 6.7). The CNRM-CM5 runs have the most areas of statistically insignificant change, comprising a low increase in SAT (up to +1.5 °C) over the region surrounding the coast along the Gulf of Bothnia in spring of both emission scenarios (Fig. 6.4c and 6.4d), a small increase over the southern half of the Scandinavian Mountains in summer RCP 4.5 (Fig. 6.5c) and finally low change (including a decrease in SAT by up to -1 °C) over all land in winter RCP 4.5 (Fig 6.7c). This statistically insignificant decrease in SAT is the only negative SAT change projected across all models, emission scenarios and seasons. Thus the models are consistent with

regard to significant changes in mean SAT on a seasonal and annual basis. These projected changes in SAT are likely to affect snowfall and Northern Fennoscandian snow cover, as discussed in in Sections 6.3.3 to 6.3.5.

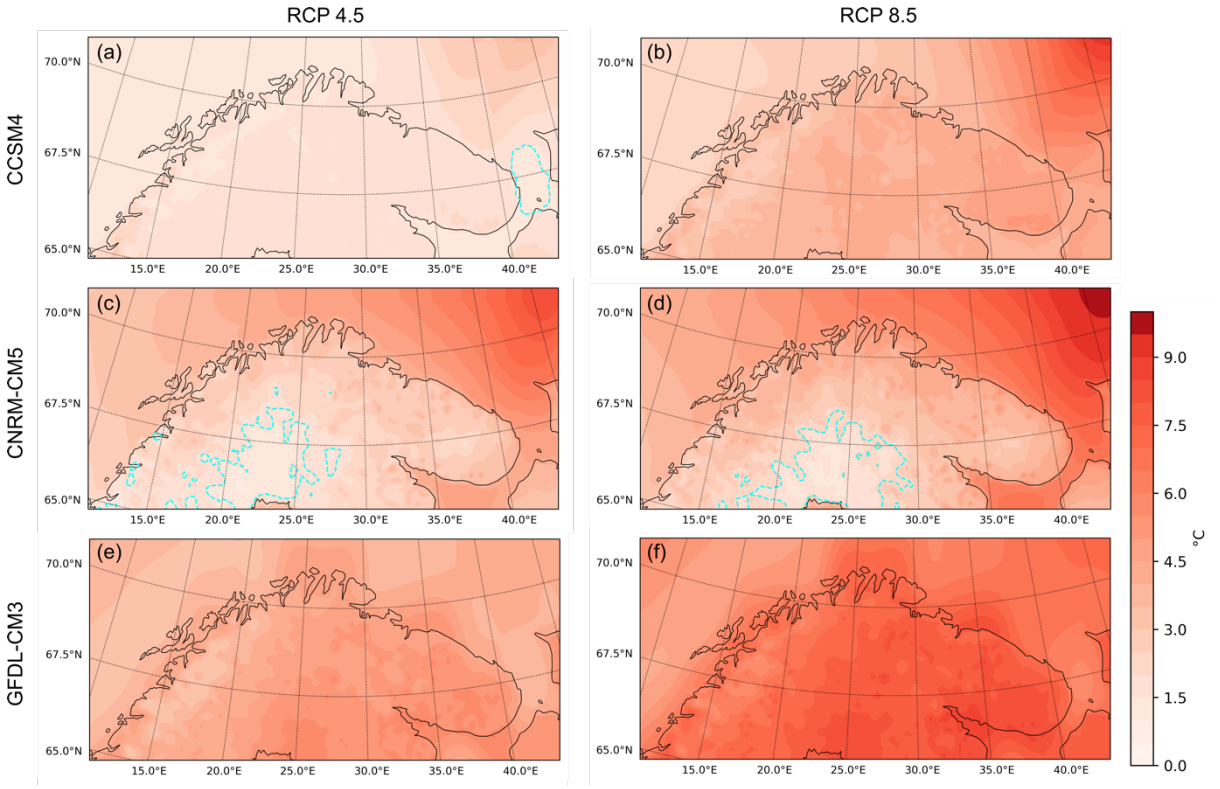

Figure 6.4: Projected change in mean SAT over Northern Fennoscandia in RCP 4.5 and RCP 8.5 in spring. Model outputs from the three CMIP5 models are shown. All areas but those enclosed in cyan dashed lines are statistically significant.

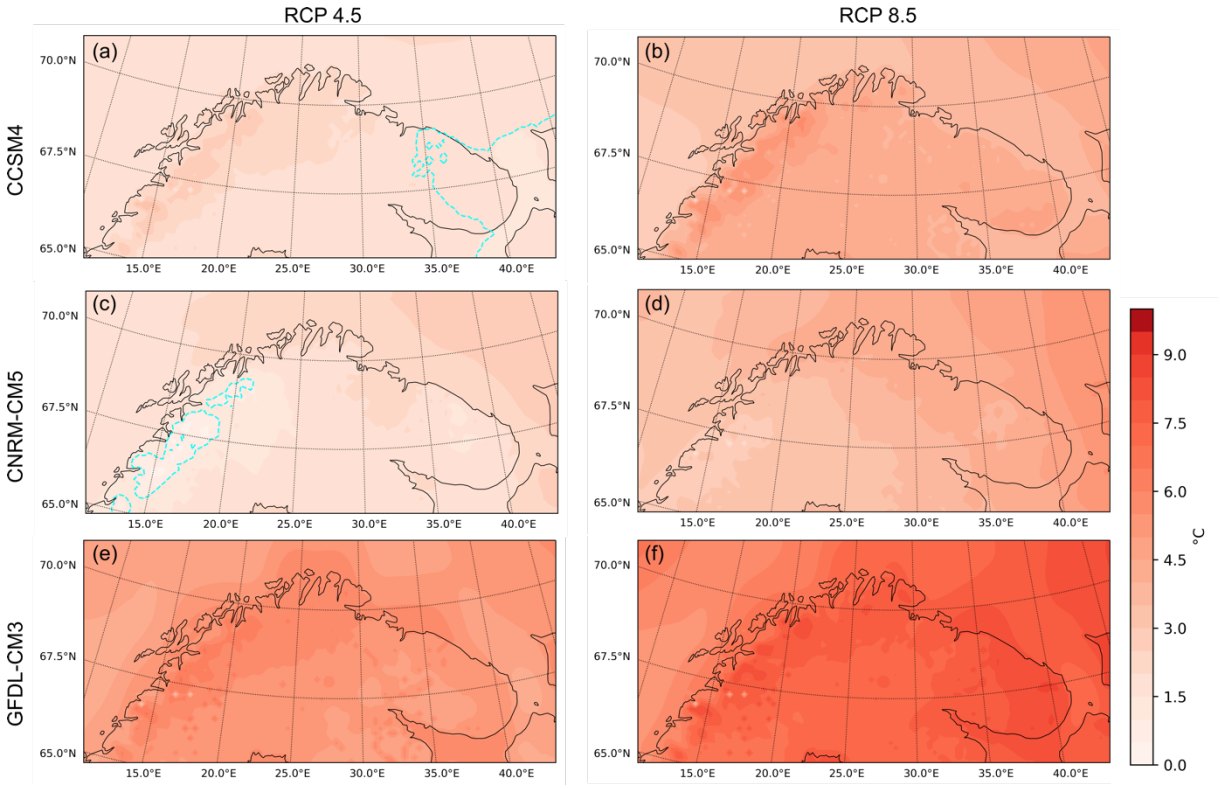

Figure 6.5: Projected change in mean SAT over Northern Fennoscandia in RCP 4.5 and RCP 8.5 in summer. Model outputs from the three CMIP5 models are shown. All areas but those enclosed in cyan dashed lines are statistically significant.

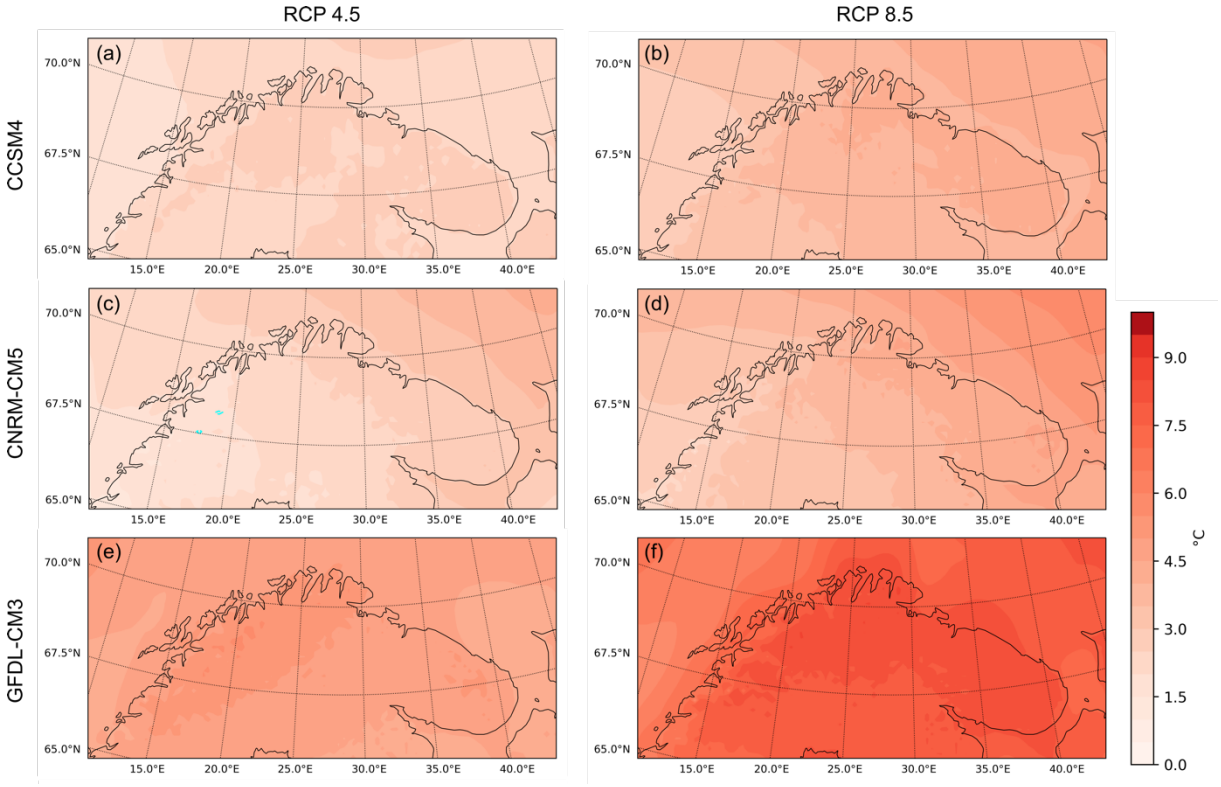

Figure 6.6: Projected change in mean SAT over Northern Fennoscandia in RCP 4.5 and RCP 8.5 in autumn. Model outputs from the three CMIP5 models are shown. All areas but those enclosed in cyan dashed lines are statistically significant.

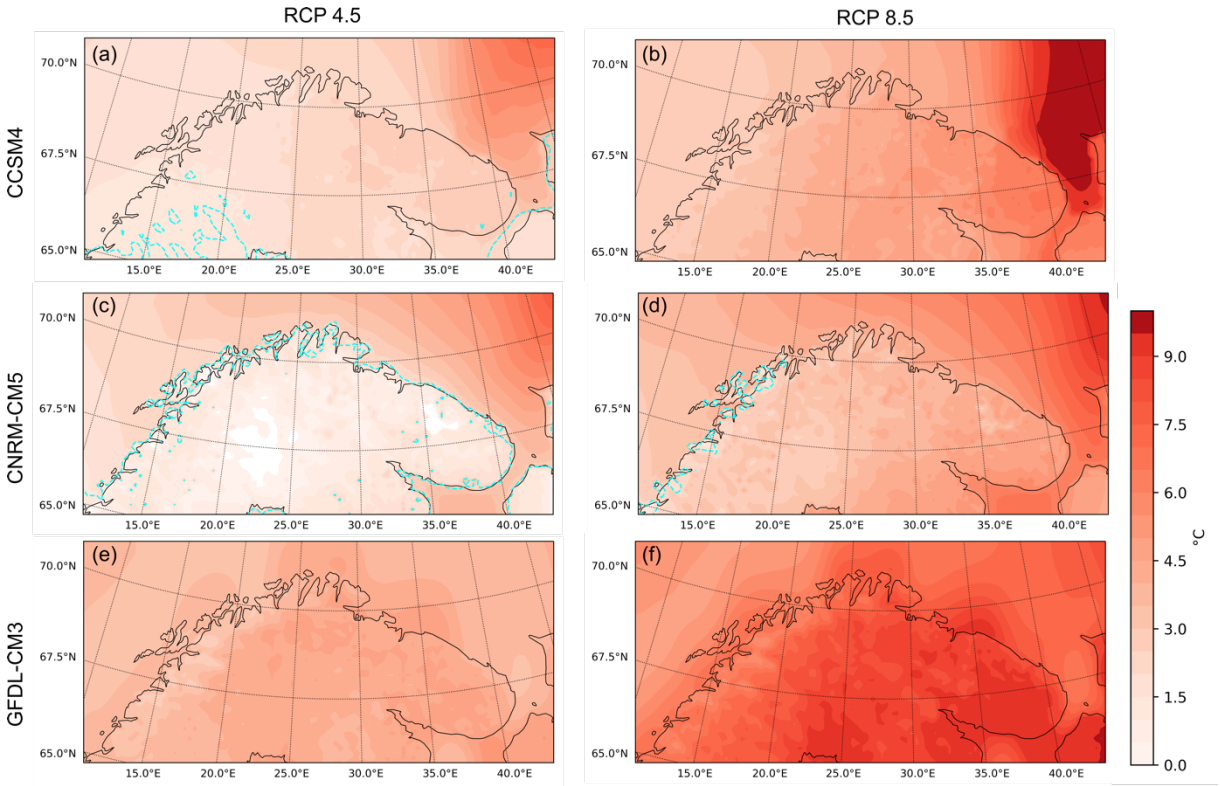

Figure 6.7: Projected change in mean SAT over Northern Fennoscandia in RCP 4.5 and RCP 8.5 in winter. Model outputs from the three CMIP5 models are shown. All areas but those enclosed in cyan dashed lines are statistically significant.

6.3.2 Total precipitation

The changes in annual total precipitation between the future (2090 - 2099) and historical (1990 - 1999) runs are given in figure 6.8, similar to figure 6.3. Figures 6.9 to 6.12 show these changes in total precipitation for individual seasons. It must be noted that there is a linear artefact on the western edge of the domain in the CNRM-CM5 annual and seasonal outputs. This does not negatively impact my results as this effect persists for only a few 10s of kilometres at the very edge of the domain.

Model run	RCP 4.5	RCP 8.5
CCSM4	+ 53 mm	+ 139 mm
CNRM-CM5	- 100 mm	- 49 mm
GFDL-CM3	+ 68 mm	+ 234 mm
'Ensemble' mean	+ 7 mm	+ 108 mm
'Ensemble' RMSE	76 mm	118 mm

Table 6.4 Mean annual precipitation change over the entire domain in all model projections.

Table 6.4 shows the projected mean annual precipitation change over the entire domain for all three CMIP5 models used to force WRF. There is very high inter-model variability between the outputs using the three different models (Fig. 6.8) as represented by the high "ensemble' RMSEs in Table 6.4. CNRM-CM5 stands out for projecting an overall decrease in precipitation over Northern Fennoscandia in both emission scenarios, though it does model increased total precipitation over the western part of the study region: up to +200 mm in RCP 4.5 and +300 mm in RCP 8.5 over the coast. CCSM4 and GFDL-CM3 both project an increase in precipitation by the end of the next century in both emission scenarios. The mean annual precipitation change over the entire domain is very similar for both CMIP5 models in RCP 4.5, but they show very different magnitudes of change in RCP 8.5 with GFDL-CM3 having almost 100 mm more mean annual precipitation over the entire domain than CCSM4 (Table 6.4). CNRM-CM5 is the only model which depicts a decrease in mean annual precipitation by the end of the 21st century. This decrease is lower in 8.5 than in 4.5 however; thus, all CMIP5 models show a wetter projection in RCP 8.5 than in RCP 4.5.

Overall, the projected changes in mean total precipitation have a considerably lower proportion of statistically significant change compared to the projected changes in mean SAT (Fig. 6.8). In all model runs, the eastern region, particularly over the Barents Sea, is projected to undergo a statistically significant change in precipitation by the end of the 21st century. This statistically significant region reaches the Kola Peninsula in four of the six future runs. In the GFDL-CM3 RCP 4.5 run, the northern part of the Kola Peninsula is projected to undergo a significant increase in total annual precipitation reaching +200 mm. In GFDL-CM3 RCP 8.5, the majority of the outputs over Northern Fennoscandia indicate a statistically significant change, including an increase of up to +300 mm over the Kola Peninsula. CNRM-CM5 reveals a strong, statistically significant, decrease (–100 to –300 mm) in

precipitation over the Kola Peninsula in the lower emission scenario (Fig. 6.8c). In the higher emission scenario, the eastern half of the Kola Peninsula undergoes a decrease in total precipitation (–50 to –200 mm; not statistically significant). However, the western side sees a slight, statistically significant, increase in precipitation reaching +100 mm (Fig 6.8d). Only very small statistically significant areas of low increase in precipitation are seen in the two CCSM4 runs (Fig. 6.8a and 6.8b). Thus, future changes in total precipitation in the Kola Peninsula are highly emission-dependent and different GCM models give very different projections.

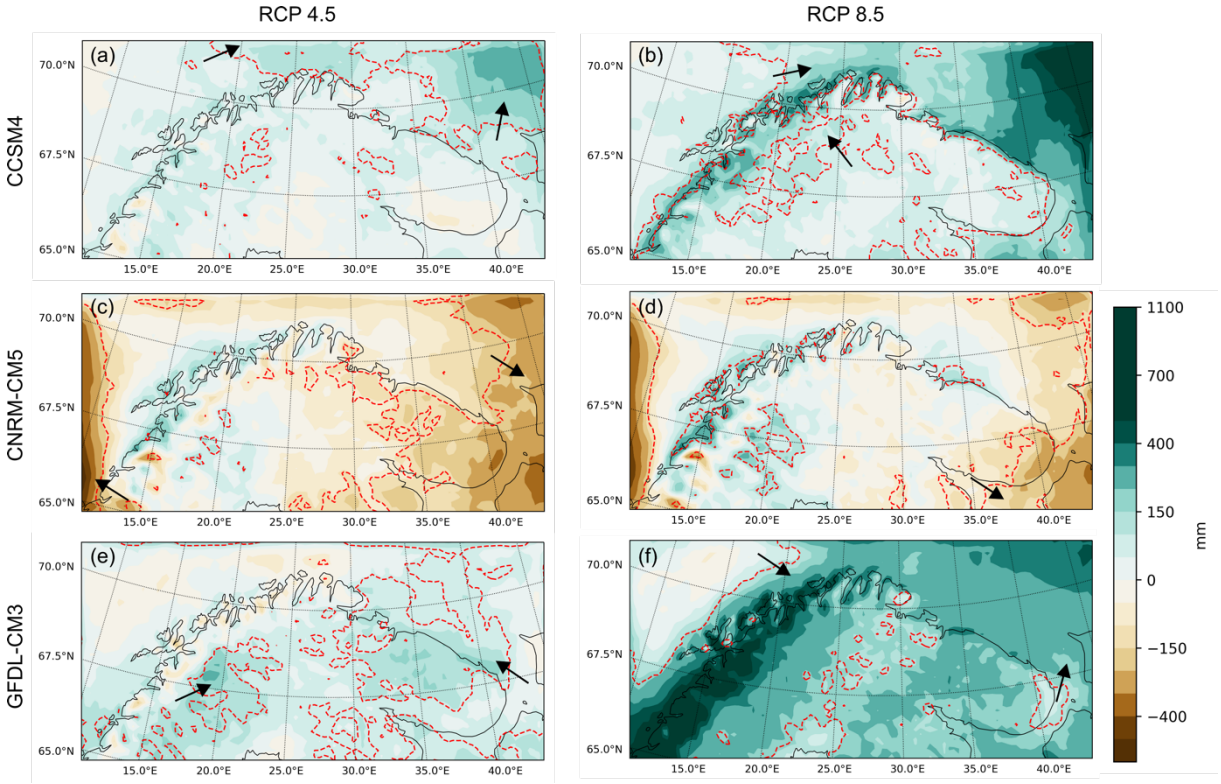

Figure 6.8: Projected change in total annual precipitation over Northern Fennoscandia in RCP 4.5 and RCP 8.5. Model outputs from the three CMIP5 models are shown. Red dashed lines enclose or exclude statistically significant areas – significant side marked by arrowhead.

The largest magnitude changes in the two emission scenarios are in the outputs of different GCM models. In RCP 4.5, the largest magnitude changes are in CNRM-CM5 over the eastern Kola Peninsula, where precipitation is projected to decrease by up to –300 mm (Fig. 6.8c). Whereas in RCP 8.5, the largest magnitude changes are in both the CCSM4 (Fig. 6.8b) and GFDL-CM3 (Fig. 6.8f) where the increase in precipitation reaches values up to +1100 mm over the Barents Sea (see Fig. 6.3) and the Scandinavian Mountains, respectively. These high magnitude changes are statistically significant in all three CMIP5 models.

Scenario choice makes the largest difference in the GFDL-CM3 runs where the western coastal zone goes from undergoing a (statistically insignificant) reduction in precipitation up to –200 mm in RCP 4.5 (Fig. 6.8e) to undergoing the strongest (and statistically significant) increase in total annual precipitation of the entire region in RCP 8.5, reaching values as high as +1100 mm (Fig. 6.8f).

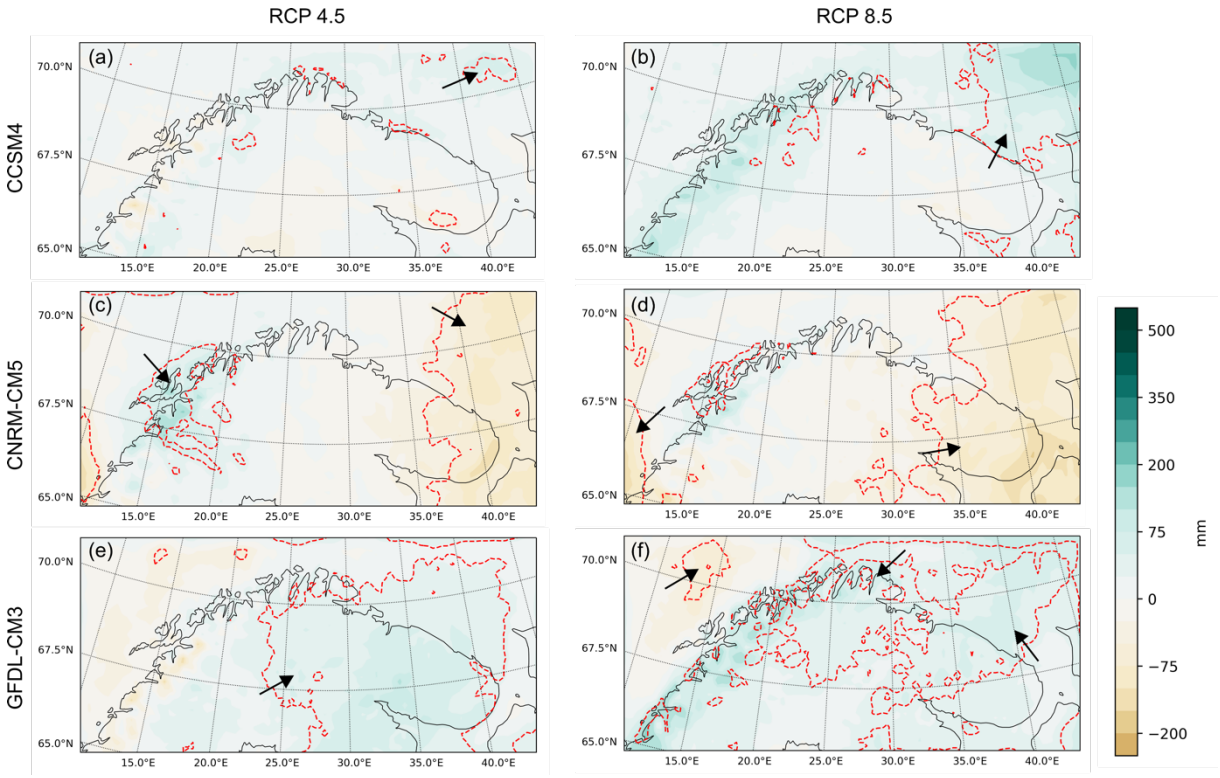

Figure 6.9: Projected change in total precipitation over Northern Fennoscandia in RCP 4.5 and RCP 8.5 in spring. Model outputs from the three CMIP5 models are shown. Red dashed lines enclose or exclude statistically significant areas – significant side marked by arrowhead.

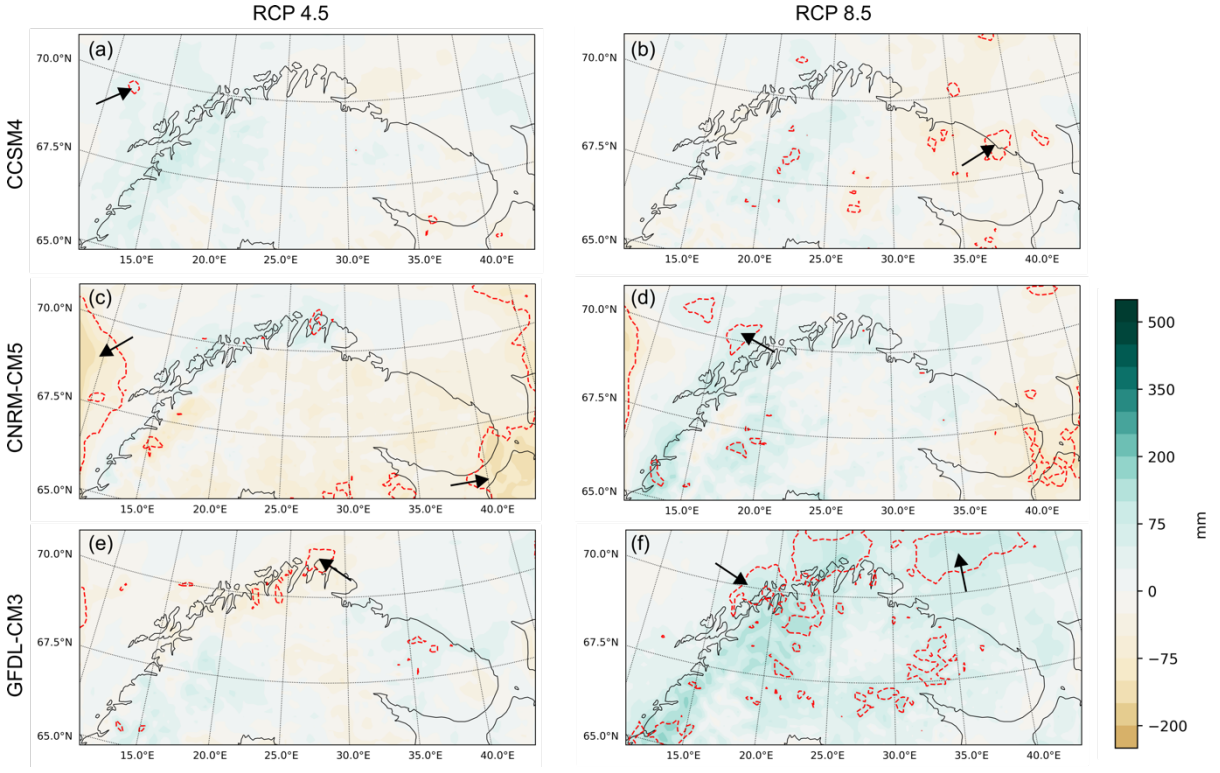

Figure 6.10: Projected change in total precipitation over Northern Fennoscandia in RCP 4.5 and RCP 8.5 in summer. Model outputs from the three CMIP5 models are shown. Red dashed lines enclose or exclude statistically significant areas – significant side marked by arrowhead.

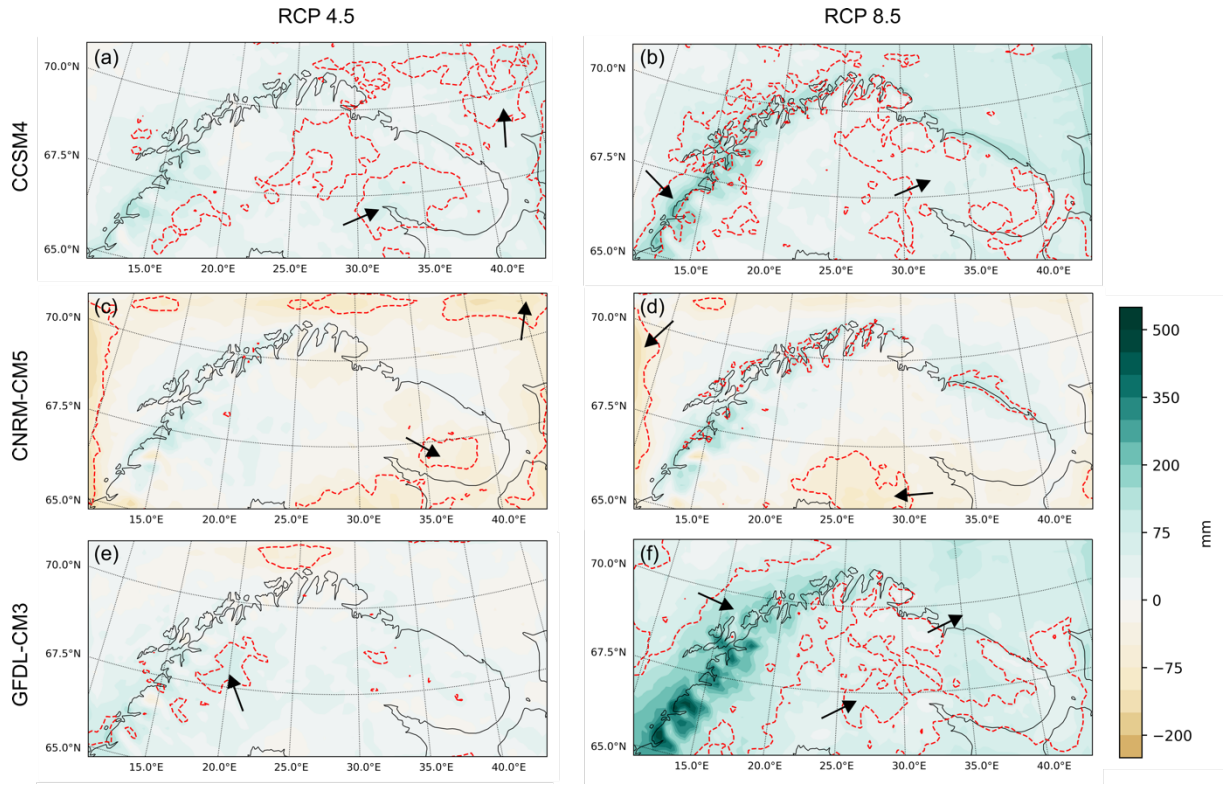

Figure 6.11: Projected change in total precipitation over Northern Fennoscandia in RCP 4.5 and RCP 8.5 in autumn. Model outputs from the three CMIP5 models are shown. Red dashed lines enclose or exclude statistically significant areas – significant side marked by arrowhead.

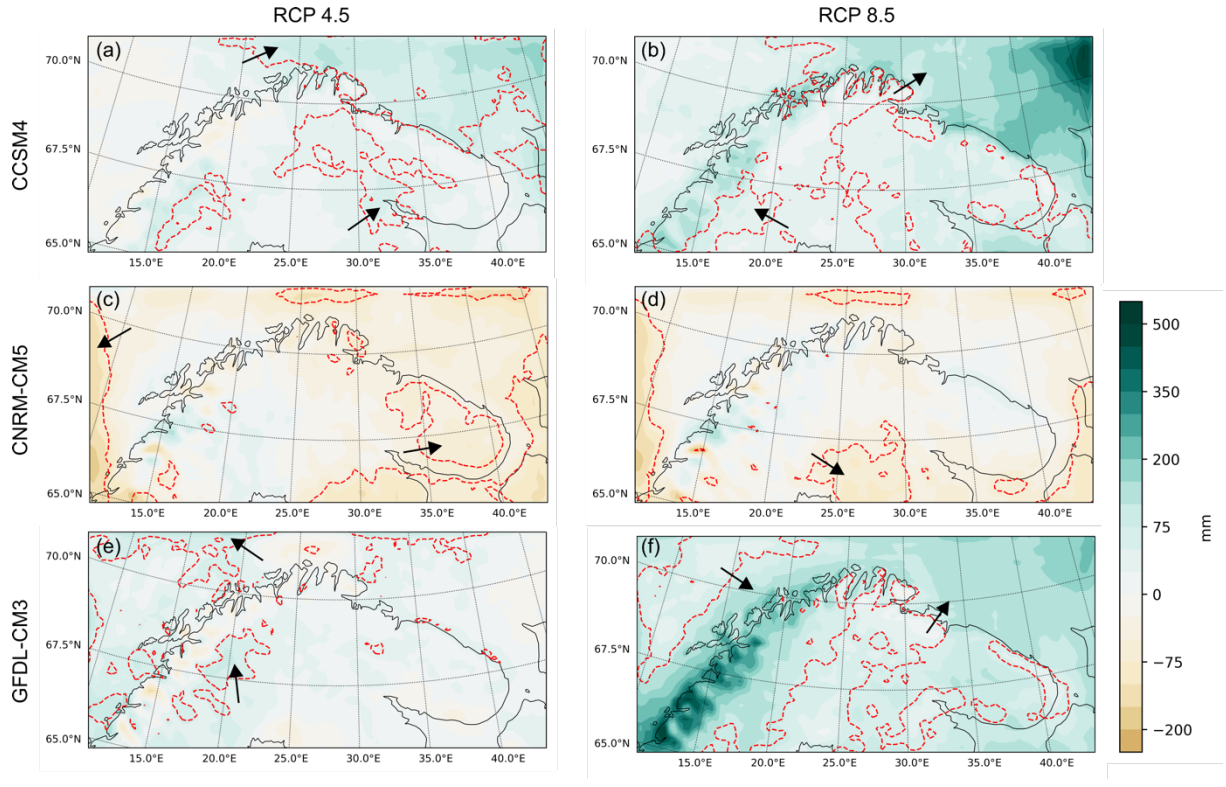

Figure 6.12: Projected change in total precipitation over Northern Fennoscandia in RCP 4.5 and RCP 8.5 in winter. Model outputs from the three CMIP5 models are shown. Red dashed lines enclose or exclude statistically significant areas – significant side marked by arrowhead.

Figures 6.9 to 6.12 show the projected change in mean precipitation in all four seasons. The lowest changes in precipitation in all forcing models occur in spring (Fig. 6.9) and in summer (Fig. 6.10), with the majority of changes being between –100 and +100 mm. The majority of the statistically

significant changes in spring occur over the east of the region. The projected change in summer total precipitation in RCP 8.5 is very similar between CCSM4 and CNRM, with small total precipitation increases over the western and central land and with a slight decrease in precipitation covering the eastern part of the study region. However, these changes are mostly statistically insignificant. GFDL-CM3 shows a spatially consistent increase in precipitation over the entirety of the region, with statistically significant changes projected over the east.

All RCP 8.5 WRF runs have an increase in precipitation over the western coast of Northern Fennoscandia in autumn (Fig. 6.11). However, this west-coast increase is only statistically significant in the GFDL-CM3 RCP 8.5 run. The GFDL-CM3 run has by far the greatest increase, up to +500 mm, compared to +150 mm in the CNRM-CM5 output.

The inter-model spread is most striking in winter (Fig. 6.12), where the CCSM4 and GFDL-CM3 models indicate an increase in total precipitation across most of the domain whereas CNRM-CM5 has a decrease in precipitation over all but a small region of north-western Fennoscandia. In winter, there is a statistically significant increase in total precipitation in the north-eastern corner of the domain, over the Barents Sea, in the CCSM4 (in RCP 4.5 and 8.5) and GFDL-CM3 (in RCP 8.5) outputs (Fig. 6.12). This is possibly linked to the large SAT increases projected over this region (Fig. 6.7). In the CNRM-CM5 runs, only a few areas are projected to undergo significant change, including the majority of the Kola Peninsula in RCP 4.5 (Fig, 6.12c). Finally, annually and in all seasons but summer, the emission scenario makes very little difference to the projected changes in total precipitation from CNRM-CM5.

6.3.3 Total snowfall

The changes in annual total snowfall between the future (2090 - 2099) and historical (1990 - 1999) model projections are given in figure 6.12 for the six future runs forced by three CMIP5 models and in two RCP scenarios. Figures 6.13 to 6.16 give these changes in total snowfall for individual seasons.

Model run	RCP 4.5	RCP 8.5
CCSM4	- 59 mm	- 94 mm
CNRM-CM5	- 124 mm	- 143 mm
GFDL-CM3	- 119 mm	- 179 mm
'Ensemble' mean	- 101 mm	- 139 mm

Table 6.5 Mean annual snowfall change over the entire domain in all model projections.

The inter-model spread is smaller in the snowfall projections compared to total precipitation changes. There is good agreement between the three sets of future projections forced by the three CMIP5 models. Table 6.5 shows the mean annual snowfall change over the entire domain for all models. All three models agree on an overall decrease in annual total snowfall over Northern Fennoscandia. Indeed, all models project a mean annual decrease in snowfall by the end of the century with an 'ensemble'

mean of –101 mm in RCP 4.5 and –139 mm in RCP 8.5. However, there is some inter-model spread in the magnitude of snowfall decrease. CCSM4 reveals a lower decrease in snowfall, projecting a decrease more than 50 % lower than the other two models (Table 6.5). Both CNRM-CM5 and GFDL-CM3 agree well on the magnitude of decrease.

This agreement between models is also seen regionally (Fig. 6.13), with the greatest projected decrease being over the Scandinavian Mountains (–400 to –1100 mm maximum decrease) closely followed by the decrease in snowfall over the Barents Sea (–200 to –500 mm maximum decrease). GFDL-CM3 has a third area of high decrease in precipitation, over the coastal region surrounding the Gulf of Bothnia, where decreases of up to –400 mm are projected in RCP 8.5. All these areas of strong decrease are statistically significant. Across all models, emissions scenarios and in most seasons (spring, autumn and winter), the region to the east of the Scandinavian Mountains (15 to 25 °E and 65 to 69 °N) is projected to undergo statistically insignificant change. The main difference between the models is in this region: a statistically insignificant increase in snowfall in region is shown by CNRM-CM5 in both emission scenarios, while other models have low decreases in snowfall there.

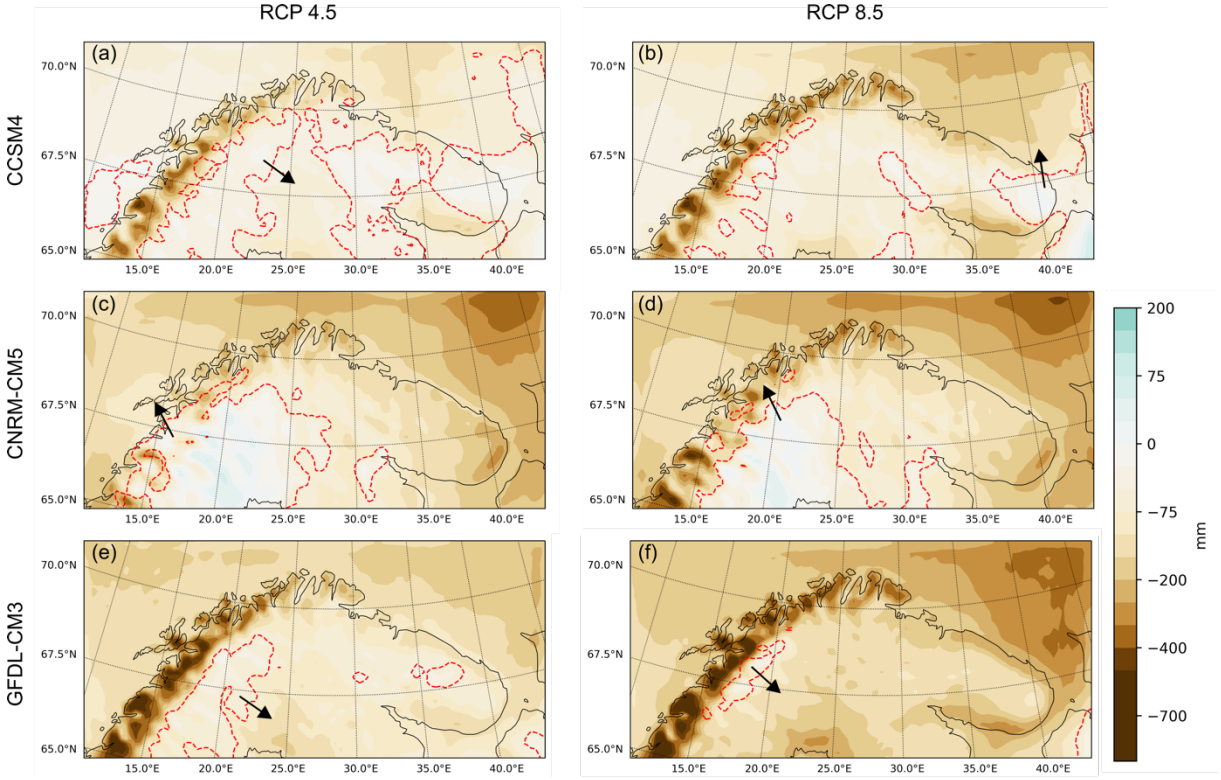

Figure 6.13: Projected change in total annual snowfall over Northern Fennoscandia in RCP 4.5 and RCP 8.5. Model outputs from the three CMIP5 models are shown. Red dashed lines enclose or exclude statistically significant areas – significant side marked by arrowhead.

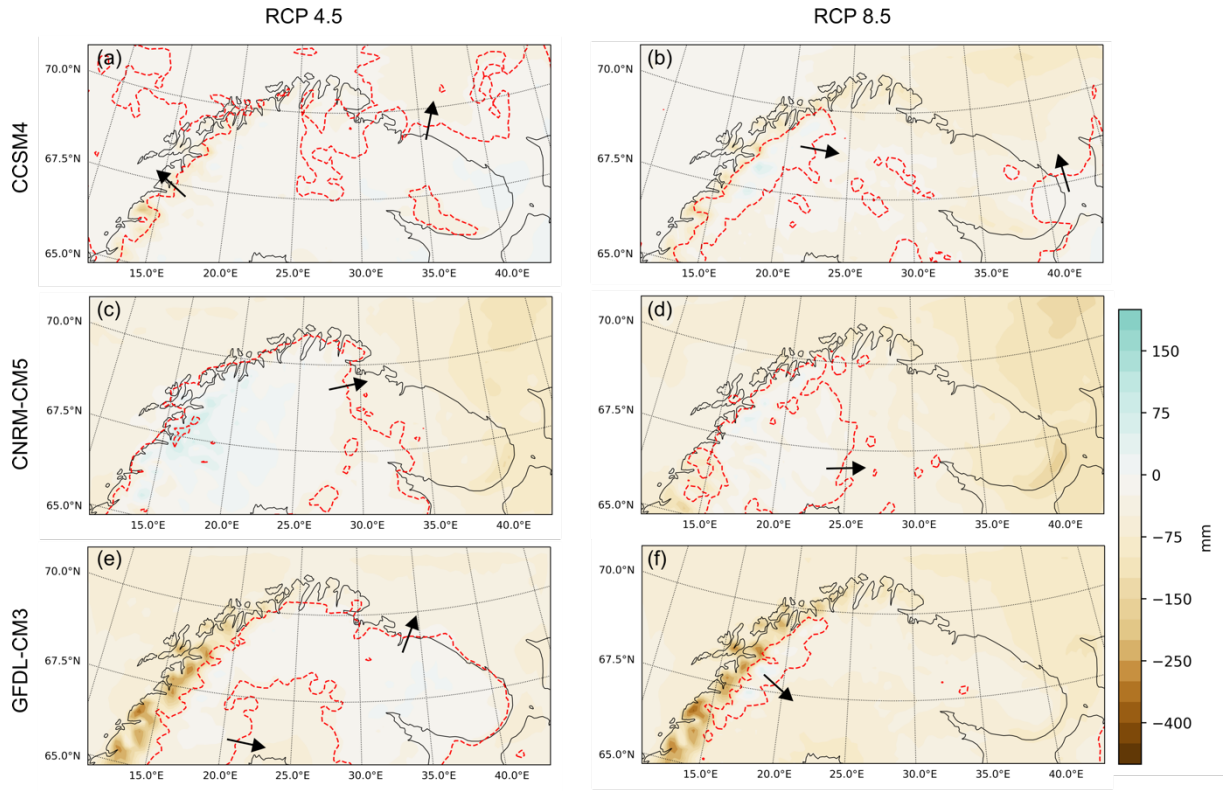

Figure 6.14: Projected change in total snowfall over Northern Fennoscandia in RCP 4.5 and RCP 8.5 in spring. Model outputs from the three CMIP5 models are shown. Red dashed lines enclose or exclude statistically significant areas – significant side marked by arrowhead.

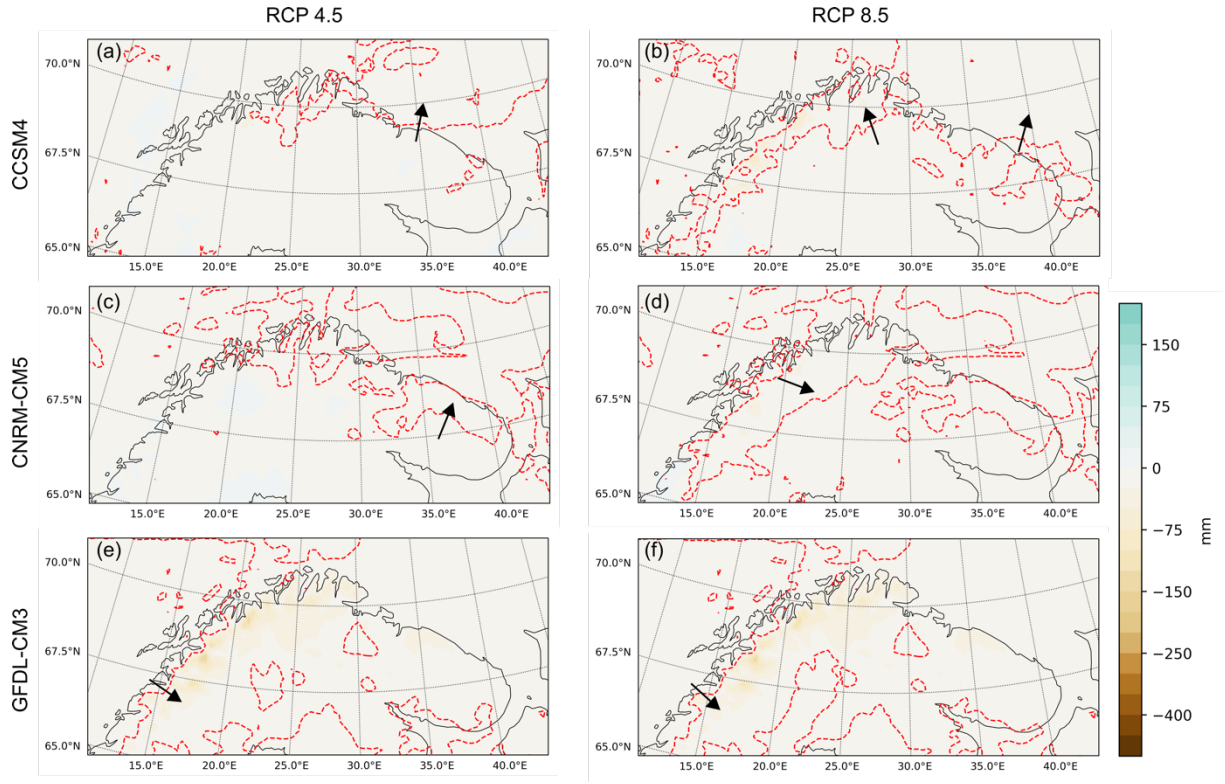

Figure 6.15: Projected change in total snowfall over Northern Fennoscandia in RCP 4.5 and RCP 8.5 in summer. Model outputs from the three CMIP5 models are shown. Red dashed lines enclose or exclude statistically significant areas – significant side marked by arrowhead.

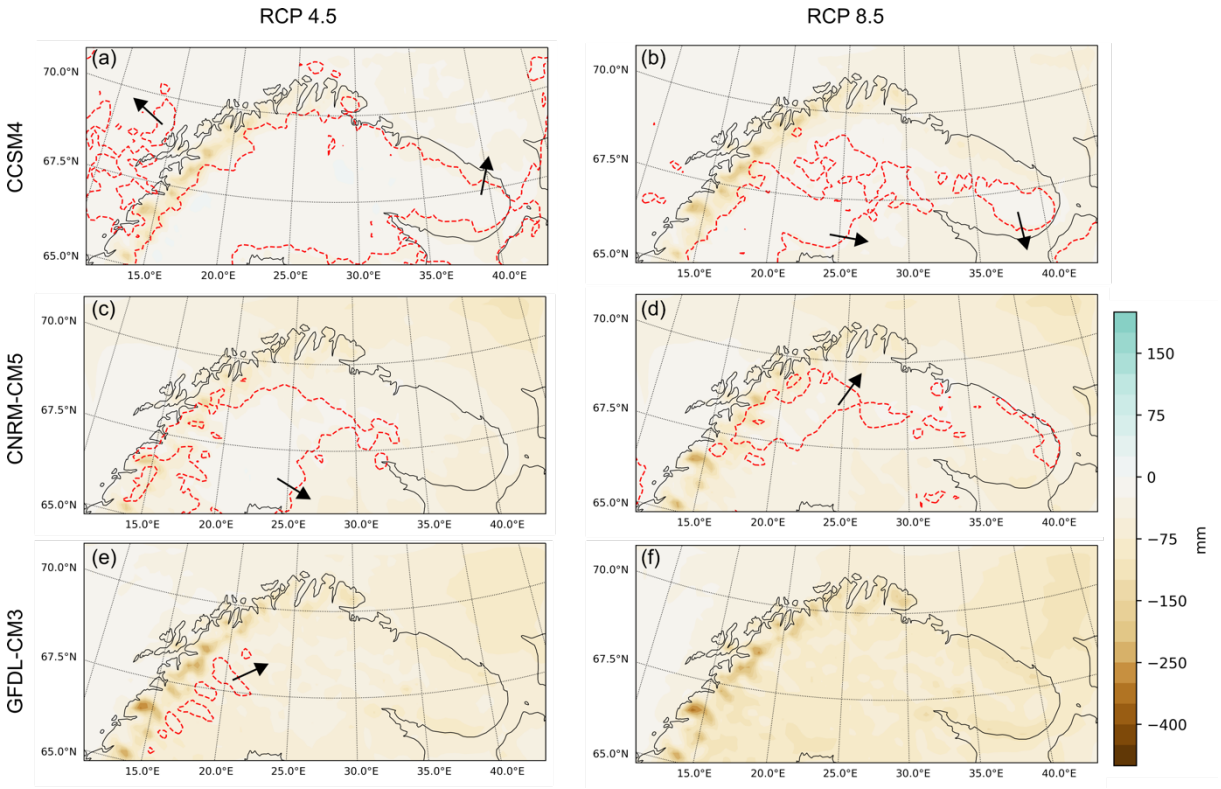

Figure 6.16: Projected change in total snowfall over Northern Fennoscandia in RCP 4.5 and RCP 8.5 in autumn. Model outputs from the three CMIP5 models are shown. Red dashed lines enclose or exclude statistically significant areas – significant side marked by arrowhead.

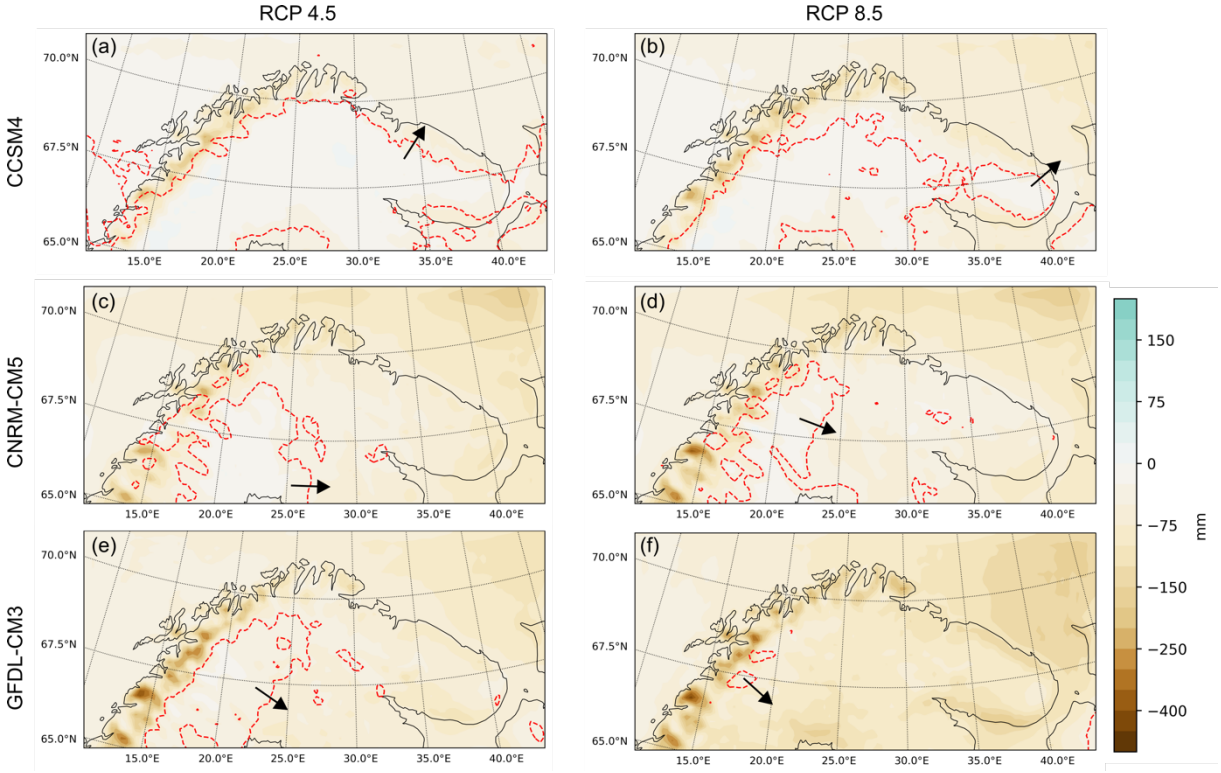

Figure 6.17: Projected change in total snowfall over Northern Fennoscandia in RCP 4.5 and RCP 8.5 in winter. Model outputs from the three CMIP5 models are shown. Red dashed lines enclose or exclude statistically significant areas – significant side marked by arrowhead.

Spring has the largest inter-model spread in the projected change in total snowfall (Fig. 6.14). Indeed, CCSM4 reveals very low changes in total snowfall with a maximum of –200 to +25 mm in RCP 4.5 and of –150 to +75 mm in RCP 8.5. CNRM-CM5 has a similar range of total snowfall (–150 to +75

mm in RCP 4.5), but the increases in total snowfall cover a much wider area of the Scandinavian Mountains than in CCSM4. Finally, GFDL-CM3 demonstrates a large decrease in total snowfall over the entire western coast of Norway, with values reaching –350 mm, and a low increase in snowfall over the eastern half of the domain. Therefore, the CNRM-CM5 and GFDL-CM3 RCP 4.5 projections are near-opposite. However, the projected increase in the CNRM-CM5 run is not statistically significant.

As expected, very little change in total snowfall occurs over the summer season, as a result of there being very little solid precipitation in summer in the first place. In CCSM4, there is a very low decrease in snowfall over the Scandinavian Mountains, which is projected at a slightly higher degree in the GFDL-CM3 RCP 4.5 and RCP 8.5 outputs. This decrease over the Scandinavian Mountains is statistically significant. Conversely, CNRM-CM5, shows a very small snowfall increase (up to 25 mm) over the northern part of the Scandinavian Mountains and around the Gulf of Bothnia coast in RCP 4.5: however, neither of these changes are statistically significant.

The change in total snowfall projected in the six model outputs is very similar in both autumn and winter. In both these seasons, a statistically significant decrease in total snowfall is projected over the entirety of northern Fennoscandia except in very small areas in the CCSM4 outputs. All models agree that the largest change in total snowfall will take place over the Scandinavian Mountains. GFDL-CM3, has the largest projected change in total snowfall in autumn and winter, and also has the largest areas of statistically significant change, with the entire region undergoing statistically significant change in autumn in RCP 8.5 (Fig. 6.16f).

6.3.4 Solid precipitation percentage

Figures 6.18 to 6.20 show the proportion of solid precipitation modelled at three stations in all seasons in the WRF runs forced by the three CMIP5 models. All figures show the solid precipitation proportion in the historical, RCP 4.5 and RCP 8.5 runs side-by-side, in order to permit straightforward comparisons.

A slight increase in solid precipitation is projected in summer at Abisko station in the RCP 4.5 CNRM-CM5 run (Fig. 6.18). However, in all other models and emission scenarios, a decrease in the percentage of solid precipitation is indicated by the end of the 21st century in all seasons. With one exception (Fig. 6.18a, annual), this decrease in solid precipitation is greater in RCP 8.5 than RCP 4.5. This is consistent with SAT predictions in these two emission scenarios. High emissions result in higher SATs (see Section 6.3.1) and thus a higher proportion of liquid precipitation. Annually, the range of decrease in the proportion of precipitation falling as snowfall for the three stations is 8 - 41 % in RCP 4.5 and 16 - 73 % in RCP 8.5, for all three models. At all stations, GFDL-CM3 projects the largest decrease in solid precipitation, with a mean annual decrease greater than 25 % (26 - 41 %) in RCP 4.5 and greater than 50 % (53 - 73 %) in RCP 8.5. Figures 6.18 to 6.20 suggest a greater decrease in the coastal north of the region compared to the coastal west and inland areas (see Figure 6.3). No such clear conclusions can be drawn about the relative decreases between the east and west of Northern Fennoscandia, due to the greater inter-model spread.

Summer has the highest decrease in solid precipitation as a proportion of the total, with close to 100 % decrease in all models and all stations (except at Abisko station, RCP 4.5, CNRM-CM5). At Vardø Radio, summer solid precipitation is projected to decrease by 100 % and so disappear entirely in all future model runs. When excluding summer, the highest decrease in solid precipitation occurs in autumn, closely followed by spring. At all three stations, the lowest decrease is in winter. In the CNRM-CM5 outputs, the difference in the percentage of winter solid precipitation between RCP 4.5 and 8.5 is quite low. The station with the highest winter decrease in solid precipitation is Vardø Radio in the north where both CCSM4 and GFDL-CM3 project a decrease of more than 50 % in RCP 8.5.

Thus, despite large increases in total precipitation predicted at Abisko in all but the CNRM-CM5 RCP 4.5 outputs and at Kandalaksha and Vardø Radio in the CCSM4 and GFDL-CM3 runs (see Fig. 6.8), the proportion of solid precipitation at these stations is projected to greatly decrease in all the model runs.

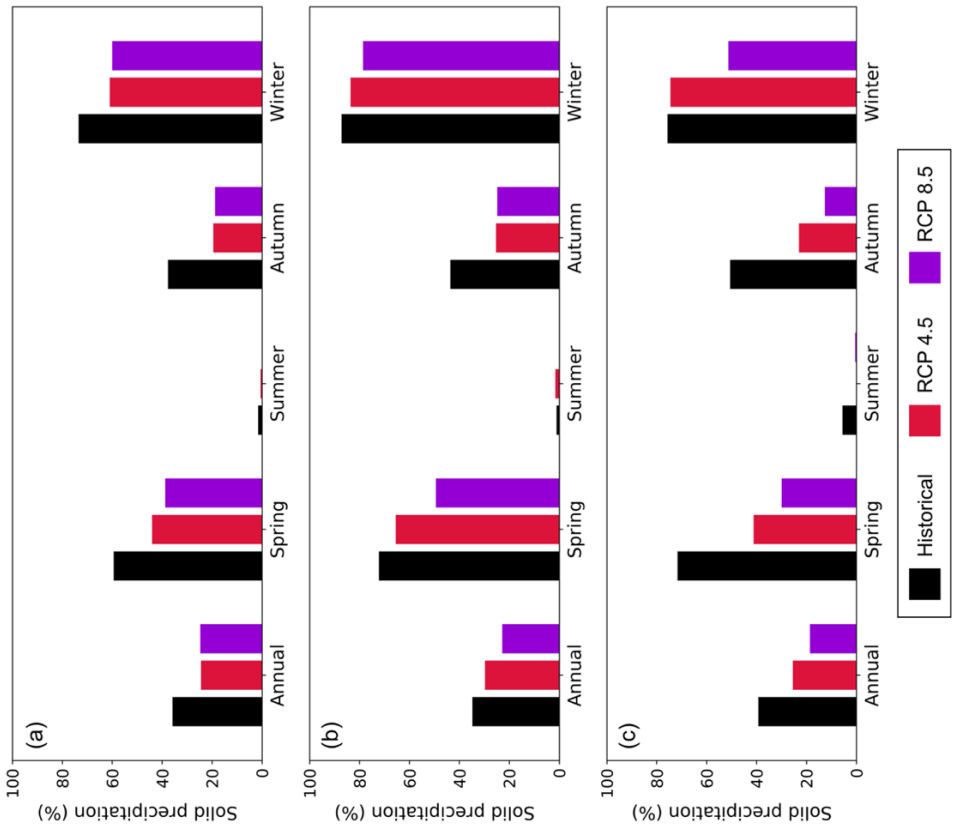

Figure 6.18: Abisko station percent of solid precipitation annually and across all seasons in (a) CCSM4, (b) CNRM-CM5 and (c) GFDL-CM3.

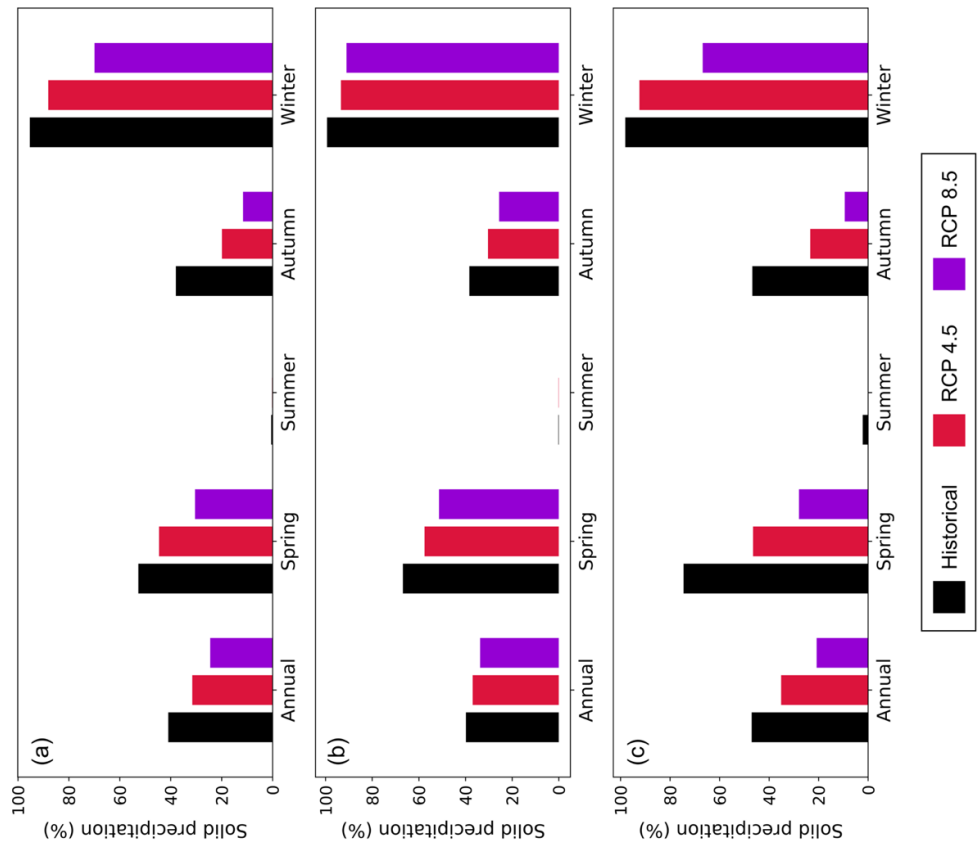

Figure 6.19: Kandalaksha station percent of solid precipitation annually and across all seasons in (a) CCSM4, (b) CNRM-CM5 and (c) GFDL-CM3.

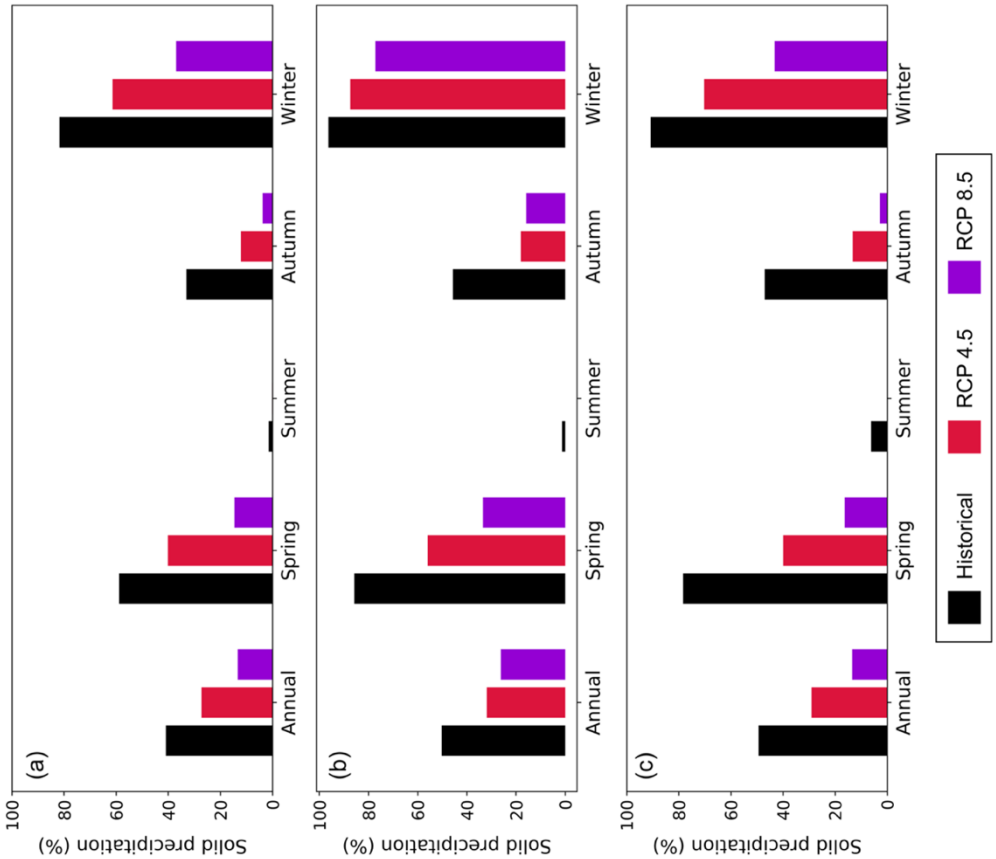

Figure 6.20: Vardø Radio station percent of solid precipitation annually and across all seasons in (a) CCSM4, (b) CNRM-CM5 and (c) GFDL-CM3.

6.3.5 Mean SCS, SCE and SCD change

6.3.5.1 Snow cover start

Figure 6.21 shows the difference in mean SCS between the future and historical runs. In both emission scenarios and for all three CMIP5 models, the WRF outputs indicate a delay in the start of the snow season across the entire Northern Fennoscandian region. There are no areas with an increasingly early SCS.

The modelled delay in the SCS is very similar in the CCSM4 and the CNRM outputs. In RCP 4.5, all delay is between 0 and 30 days in these two model projections (Fig. 6.21a and 6.21c). The main difference between the two models is over the central Kola Peninsula where CNRM projects a 30-day delay in the SCS and CCSM4 projects a delay of less than 10 days over this same area. In the future projections, the delay in the start of the snow cover season increases with increased emissions. In both CCSM4 and CNRM, the SCS in the RCP 8.5 run is only slightly more delayed than in RCP 4.5, with approximately one to two week's difference between the two.

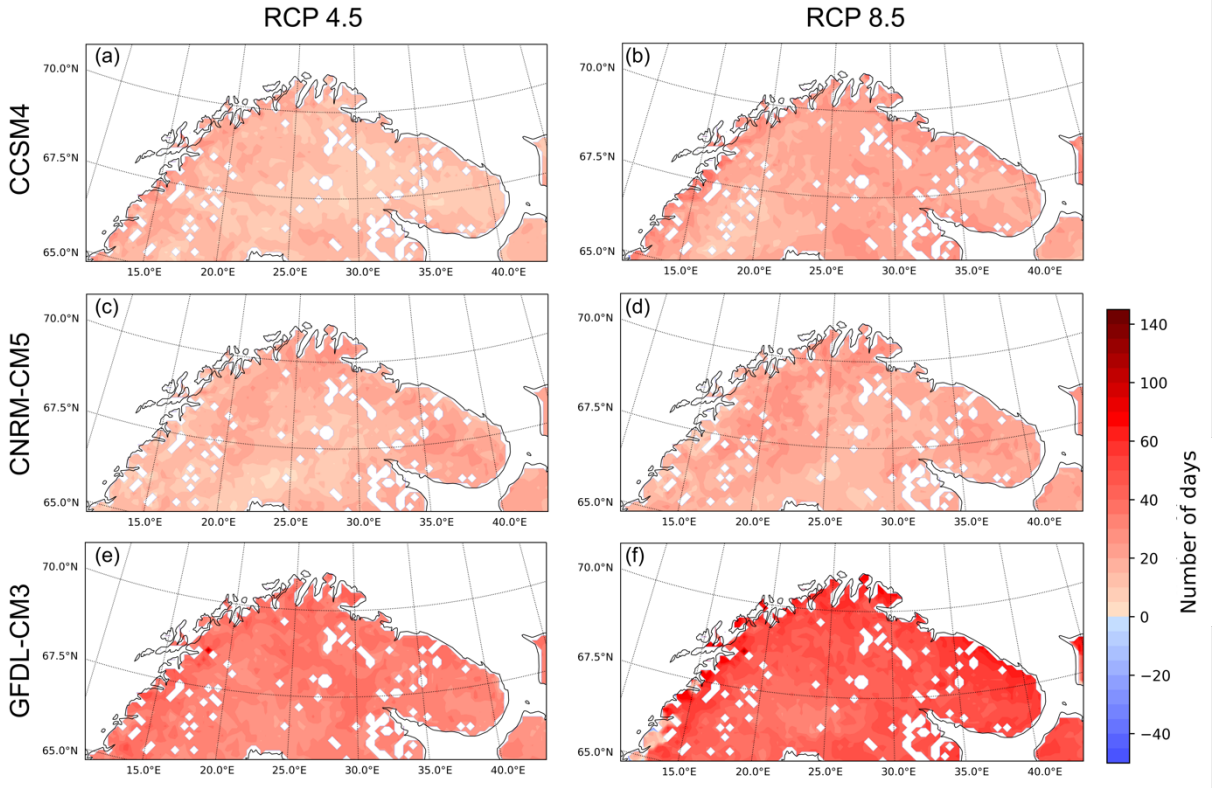

Figure 6.21: Difference in mean snow cover start between RCP 4.5 and historical runs for (a) CCSM4, (c) CNRM-CM5 and (e) GFDL-CM3, and between RCP 8.5 and historical runs for (b) CCSM4, (d) CNRM-CM5 and (f) GFDL-CM3. White data gaps on land are water bodies.

The largest projected change is observed in the GFDL-CM3 model. This is unsurprising as the GFDL-CM3 projections have the largest change in mean SAT and snowfall in autumn and winter (Figs. 6.6, 6.7, 6.16 and 6.17). In RCP 4.5, the delay in the SCS is projected to be between 20 and 40 days across Northern Fennoscandia. In RCP 8.5, the delay in the start of the snow season is between 35 to 70 days across the majority of the study region, with the larger changes projected to occur in the coastal areas. One point over the Scandinavian Mountains is projected to undergo a much larger delay in SCS

than the rest of the study region. This delay is of 90 and 100 days in RCP 4.5 and RCP 8.5 respectively and is over the only permanent snow cover zone identified in the WRF GFDL historical run.

6.3.5.2 Snow cover end

Figure 6.22 shows the difference in mean SCE between the future and historical runs. Little change in future SCE dates is indicated by the CNRM-CM5 projections (Fig. 6.22c and 6.22d). Indeed, the projected SCE change over Northern Fennoscandia is between -5 to +10 days in RCP 4.5 and between -10 and +5 days in RCP 8.5, with the majority of values being constrained between -5 and +5 in both emission scenarios. This fits with previous findings from these projections, in which only small changes in SAT over land are shown in spring and summer (Fig. 6.4 and 6.5). It is worth noting, however, that the majority of the region is projected to undergo a positive SCE change (a later end to the snow season) in RCP 4.5 and a negative change (an earlier end to the snow season) in RCP 8.5.

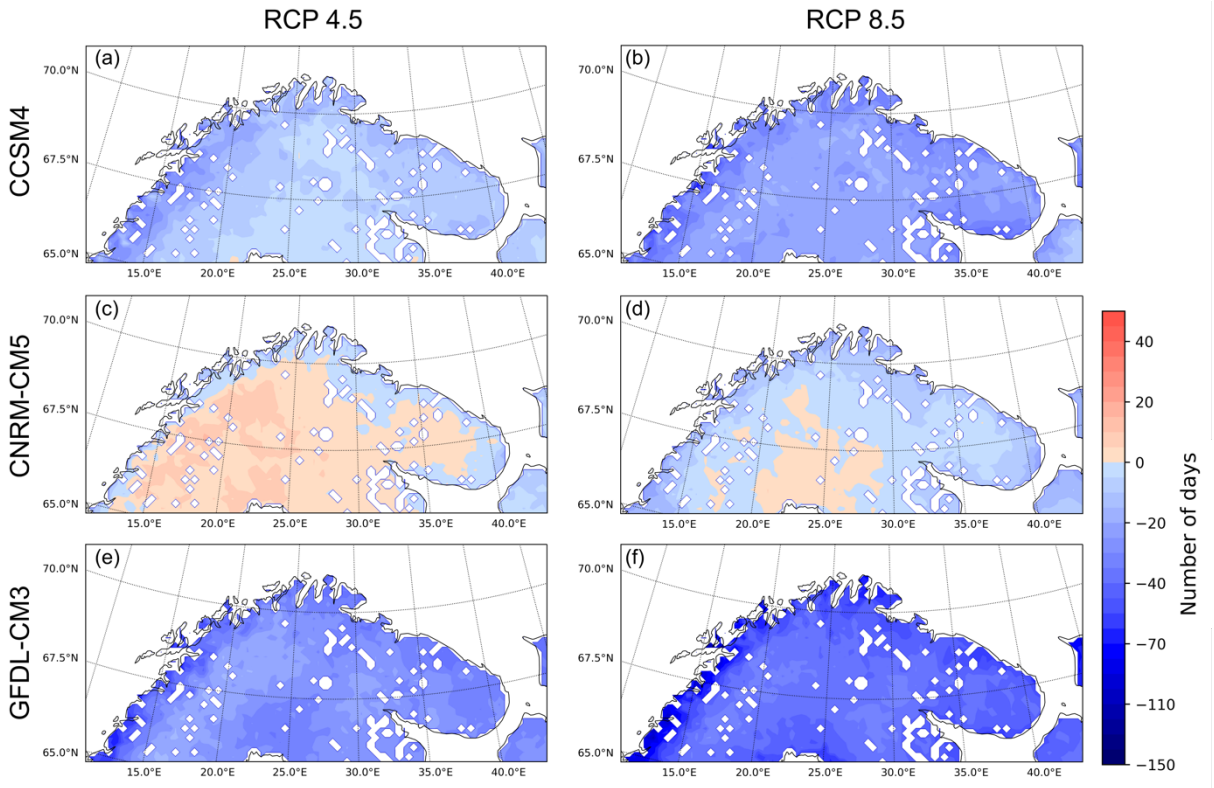

Figure 6.22: Difference in mean snow cover end between RCP 4.5 and historical runs for (a) CCSM4, (c) CNRM-CM5 and (e) GFDL-CM3, and between RCP 8.5 and historical runs for (b) CCSM4, (d) CNRM-CM5 and (f) GFDL-CM3. White data gaps on land are water bodies.

An increasingly early end to the snow cover season is revealed in both the CCSM4 and GFDL-CM3 projections. In RCP 4.5, CCSM4 shows low changes (-5 to -10 days) in mean SCE over the majority of the region (Fig. 6.22a). Larger changes are projected on the west coast of the region and over the Scandinavian Mountains reaching -25 days there. CCSM4 sees an overall larger change in mean SCE in RCP 8.5 over the plains. Indeed, the SCE becomes increasingly earlier over the majority of the centre of Northern Fennoscandia, with SCE dates earlier by 10 to 15 days in RCP 8.5 compared to 4.5.

The mean SCE change over the western coast and the Scandinavian Mountains in CCSM4 is more similar in both RCP 4.5 and RCP 8.5, though the SCE is slightly earlier in the higher emission scenario.

The changes in SCE in the GFDL-CM3 future projections are the greatest of all three CMIP5 forcing models (Fig. 6.22e and 6.22f). In both emission scenarios, GFDL-CM3 outputs project an earlier end of the snow season. In RCP 4.5, the majority of Northern Fennoscandia is projected to see a SCE 20 (over the Scandinavian Mountains) to 35 (around the Gulf of Bothnia) days earlier than over the historical period. A difference as high as 60 days is projected over a very small area: the edge of the western coast. In the RCP 8.5 GFDL-CM3 projections, there is a more extreme advance in the SCE over the entirety of Northern Fennoscandia compared to RCP 4.5, which includes a greater advance in the SCE over the western part of the region, in contrast to the CCSM4 RCP 8.5 projection. The advance in the SCE over the west coast is between 55 and 90 days; this is the largest projected change in SCE in all runs. The SCE advance over the rest of the region is greater in RCP 8.5 compared to 4.5 by 10 to 20 days. The lowest change in SCE projected in the "business-as-usual" scenario is 35 days.

6.3.5.3 Snow cover duration

Figure 6.23 shows the difference in mean SCD between the future and historical runs. All CMIP5 models agree that in both emission scenarios mean SCD will be lower over 2090 to 2099 than it was between 1990 and 1999. Only a very small area is projected to have a longer SCD in CNRM RCP 4.5 and this increase is of less than 5 days (see Fig 6.23c). All CMIP5 forcing models agree that the higher the emissions over the next century, the larger the negative impact on the duration of the snow cover season.

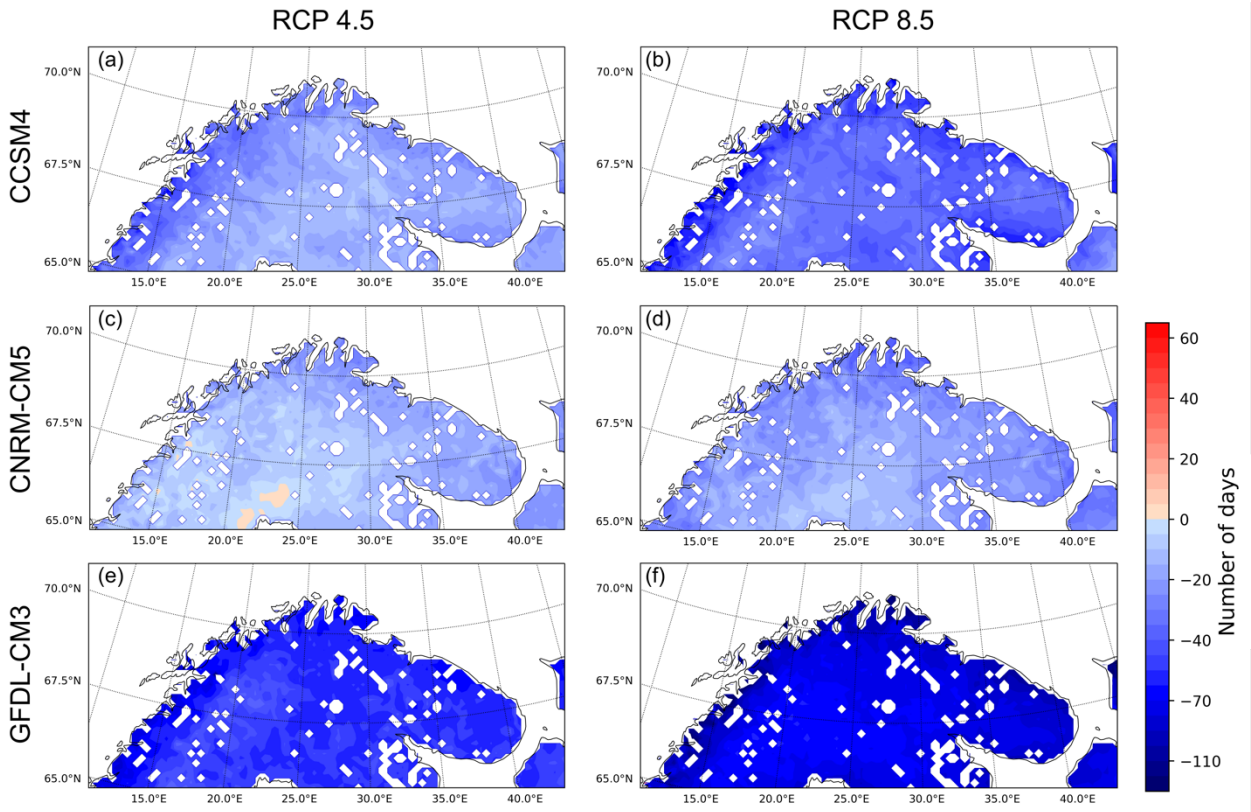

Figure 6.23: Difference in mean snow cover duration between RCP 4.5 and historical runs for (a) CCSM4, (c) CNRM-CM5 and (e) GFDL-CM3, and between RCP 8.5 and historical runs for (b) CCSM4, (d) CNRM-CM5 and (f) GFDL-CM3. White data gaps on land are water bodies.

Table 6.6 shows the mean difference in SCD over the entire region of Northern Fennoscandia projected in the different WRF runs. Though the CMIP5 models agree on the direction of change, the magnitude of decrease in SCD is subject to important inter-model spread. GFDL-CM3 projects the greatest decrease in the SCD with a 50-day decrease and 74-day decrease projected on average in RCP 4.5 and RCP 8.5 respectively. These projections are much higher than those of the CCSM4 and CNRM runs. CCSM4 models a decrease almost twice as great as those projected by CNRM, and GFDL projects changes more than four times greater than that of CNRM in RCP 4.5 and more than three times greater than of CNRM in RCP 8.5.

Model run	RCP 4.5	RCP 8.5
CCSM4	- 21 days	- 36 days
CNRM-CM5	- 12 days	- 20 days
GFDL-CM3	- 50 days	- 74 days
'Ensemble' mean	- 28 days	- 43 days

Table 6.6 Mean difference in SCD between future and historical runs over the entire domain.

This inter-model spread is also found in the maximum decrease in SCD projected over the Northern Fennoscandian region. CNRM-CM5 projects a maximum difference in SCD of 30 and 40 days for the lower and higher emission scenarios respectively; CCSM4 models a maximum change in SCD of 45 and 70 days in RCP 4.5 and 8.5 respectively; the GFDL outputs see a maximum difference in SCD of 80 and 110 days in RCP 4.5 and 8.5 respectively.

6.4 Discussion

In this section, the previously described results are revisited, with a focus on the causes for these changes and what this means for the future of snow cover in a warming world. It is not straightforward to determine causes of changes in snow cover characteristics. In fact, Bulygina et al. (2011) found that, in Northern Eurasia, nonlinearity is a key feature of changes of the thermal and hydrological regimes over the past century. They explain that snow cover characteristics also change nonlinearly as they are a product of multiple climate factors that simultaneously affect them. However, it is possible to look at these various climate factors for some explanation for changes in snow.

In this chapter, both changes in temperature and precipitation are considered. There is a clear directional change for temperature: for all forcing models and in both emission scenarios, WRF projects an increase in annual mean SAT over the entirety of Northern Fennoscandia in the 2090 - 2099 interval compared to 1990 - 1999. Contrastingly, there is very high inter-model variability in the total precipitation change projections. CNRM-CM5 reveals an overall decrease in precipitation over Northern Fennoscandia, while CCSM4 and GFDL-CM3 both have an increase in precipitation by the end of the next century but with different magnitudes of change. CNRM-CM5, however, was found to have the highest RMSE for modelling precipitation in Chapter 5 and was originally selected for being a slight

outlier CMIP5 model. For example, Voldoire et al. (2013) found a slight negative bias in precipitation over the Norwegian mountains for CNRM-CM5 outputs when compared to observational data. A study published in 2014 made projections of future changes in annual mean temperature and total annual precipitation over Europe, including Northern Fennoscandia for 2071 - 2100 compared to 1971 - 2000 (Jacob et al., 2014). Though they did not make any projections of future changes in snowfall or snow cover, it is useful to compare their findings regarding temperature and precipitation as they used more models (seven RCMs and five GCMs). Jacob et al. (2014) found that in RCP 8.5, the majority of Northern Scandinavia will be exposed to a warming greater than 4.5 °C compared to 1971 - 2000, which would be avoided in RCP4.5. The authors also found changes in total annual precipitation across Europe. The ensemble-mean projects a statistically significant increase in Northern Europe of up to about 25 %. Dankers et al. (2005) also found that by the end of the century, mean annual precipitation in Northern Fennoscandia is expected to increase, by 10 to 40 %. As results from these studies point towards a significant increase in precipitation over Northern Europe (including Northern Fennoscandia) by the end of the 21st century, this reaffirms the that CNRM is an outlier CMIP5 model, and that an overall increase in precipitation by the end of the 21st century is most likely.

However, despite this projected increase in precipitation a considerable decrease in snowfall is found in all model runs. This counter-intuitive change is not the only one associated with future changes in snow in a warming world. Mussleman et al. (2017) investigated spring snow melt in the western USA. They found that slower snow melt will occur in a warmer climate. This is due to the reduction of spring snow cover extent, resulting in less snow being exposed to sufficiently high energy fluxes to drive moderate to high snow melt rates. Thus, counter-intuitive changes may be a defining characteristic of the future of snow cover in a warming world. The large, projected decreases in snowfall in spite of considerable increases in precipitation are explained by the shift from solid to liquid precipitation, likely caused by the projected increases in mean temperature in all seasons (e.g. Ye et al., 2008; Mudryk et al., 2017), suggesting that increased temperature outcompetes increased precipitation. Indeed, for all stations investigated and, in all models and emission scenarios except for the summer season in CNRM-CM5 RCP 4.5, a decrease in the percentage of solid precipitation (up to 100 % in summer) is projected to occur by the end of the 21st century in all seasons. Understanding the likelihood and degree of such shifts from solid to liquid precipitation is key in snow studies due to the importance of rain-on-snow events. Indeed, rain-on-snow events have been shown to lead to accelerated snow metamorphism, increased runoff in heavy rain and increased snow melt (Singh et al., 1997). Following rain-on-snow events, snow cover is slightly reduced in forested areas and a more significant reduction occurs in open areas, though in both cases rain-on-snow events increase snow melt (Marks et al., 2001). Increasing liquid precipitation over solid precipitation would thus potentially lead to increasing snow melt and, as a result, a decrease in SCD.

Future snow cover timing, including SCS, SCE and SCD, are analysed in this chapter and a decrease in SCD is indeed projected. All CMIP5 models agree that in both emission scenarios mean SCD will be lower over 2090 to 2099 than it was between 1990 and 1999. All CMIP5 forcing models

agree that the higher the emissions over the next century, the larger the negative impact on the duration of the snow cover season. The ensemble mean SCD change is of -28 days and -43 days in RCP 4.5 and RCP 8.5 respectively. This matches the overall large projected increase in temperature, associated decrease in snowfall and likely increases in rain-on-snow events. In both emission scenarios and for all three CMIP5 models, the WRF outputs indicate a delay in the start of the snow season across the entire Northern Fennoscandian region. The largest projected change in SCS is observed in the GFDL-CM3 model. This is unsurprising as the GFDL-CM3 model projections have the largest increase in mean SAT in autumn and winter. An increasingly early end to the snow cover season is revealed in the CCSM4 projections, GFDL-CM3 projections, and in the majority of the region in CNRM-CM5 RCP 8.5. This projected earlier SCE matches results from Mussleman et al. (2017) who found that there is a tendency towards earlier melt for all melt rate categories and snowpacks in a warming world. Understanding future changes to the end of the snow season is important in terms of understanding future water supply. Barnett et al. (2005) demonstrated that an earlier end to the snow season, regardless of whether it is associated with changes in precipitation, will lead to a shift in peak river runoff to winter and early spring, away from summer and autumn when water demand is highest. These conclusions are relevant to Northern Fennoscandia, as all areas investigated in this chapter, including the Scandinavian Mountains, are projected to see earlier SCE in the majority of the model runs. The snow cover season ending consistently earlier in a warming world is of great concern at a global level, as more than half of the world's drinking water is provided by rivers (Barnett et al., 2005), which are sensitive to changes in snow melt.

In summary, the results of this chapter communicate a message of increased temperature outcompeting increased precipitation (for some models), leading to large decreases in snowfall causing decreased snow cover duration. Importantly, in the lower emission scenario changes in temperature, precipitation and snowfall are less, and snow cover is least impacted compared to the higher emission scenario. Therefore, aiming to reduce greenhouse gas emissions is still crucial to reducing the negative impacts of a warming world on Arctic snow cover.

6.5 Conclusions

Across all aspects of future climate investigated in this chapter, it is clear that the CMIP5 forcing model makes a huge difference in the projections: inter-model spread is the largest uncertainty in my results. Nevertheless, some interesting conclusions can be extracted from the results of this analysis.

Relating to changes in climate over Northern Fennoscandia:

- For all forcing models and in both emission scenarios, WRF projects an increase in annual mean SAT over the entirety of Northern Fennoscandia in the 2090 - 2099 interval compared to 1990 - 1999. Model results clearly indicate Arctic Amplification over Northern Fennoscandia with the 'ensemble' mean SAT increase over the domain (3.6 °C) being double the global ensemble

mean (1.8 °C; IPCC, 2013) in RCP 4.5, and nearly 40 % greater in RCP 8.5 (domain: 6.0 °C; global: 3.7 °C).

- There is very high inter-model variability in the total precipitation change projections. CNRM-CM5 reveals an overall decrease in precipitation over Northern Fennoscandia, while CCSM4 and GFDL-CM3 both have an increase in precipitation by the end of the next century but with very different magnitudes of change. This is unsurprising as CNRM-CM5 was selected as an outlier in the CMIP5 models. The lowest changes in precipitation in all forcing models occur in spring and in summer.
- The inter-model spread in the snowfall projections is small when compared to total precipitation changes. All three model projections agree on an overall decrease in annual total snowfall over Northern Fennoscandia, with the greatest decrease over the Scandinavian Mountains closely followed by the decrease in snowfall over the Barents Sea.
- Except for the summer season in CNRM-CM5 RCP 4.5, in all models and emission scenarios, a decrease in the percentage of solid precipitation (up to 100 % in summer) is projected to occur by the end of the 21st century in all seasons. Additionally, RCP 8.5 consistently sees a higher decrease in solid precipitation (16 - 73 % annual decrease) than RCP 4.5 at all stations (8 – 41 % annual decrease), and for all models and seasons.
- Finally, despite the large increases in total precipitation projected over the majority of Fennoscandia in both the CCSM4 and GFDL-CM3 output, both models indicate a significant contemporaneous decrease in total annual snowfall in both emission scenarios.

Relating to changes in the timing of the snow cover season:

- The start of the snow cover season is delayed in future projections and is increasingly delayed with greater greenhouse gas concentrations. Little to no change in future in SCE is shown in the CNRM-CM5 model outputs while an increasingly early end to the snow cover season is shown in both CCSM4 and GFDL-CM3 projections.
- All CMIP5 models agree that in both emission scenarios mean SCD will be lower over 2090 to 2099 than it was between 1990 and 1999. All CMIP5 forcing models agree that the higher the emissions over the next century, the larger the negative impact on the duration of the snow cover season. The ensemble mean SCD change is of -28 days and -43 days in RCP 4.5 and RCP 8.5 respectively.

In summary, large changes in climate and, especially, snow cover are projected to occur in Northern Fennoscandia by the end of the 21st century in both a mitigation and a 'business-as-usual' scenario. Importantly, in the lower emission scenario changes in SAT, precipitation and snowfall are less, and snow cover is least impacted. Thus, aiming to reduce greenhouse gas emissions is still crucial to reducing the anthropogenic impact on Arctic snow cover.

6.6 References

Barnett, T.P., Adam, J.C. and Lettenmaier, D.P., 2005. Potential impacts of a warming climate on water availability in snow-dominated regions. Nature, 438(7066), p.303. https://doi.org/10.1038/nature04141

Brands, S., Herrera, S., Fernández, J. and Gutiérrez, J.M., 2013. How well do CMIP5 Earth System Models simulate present climate conditions in Europe and Africa?. Climate dynamics, 41(3-4), pp.803-817. https://doi.org/10.1007/s00382-013-1742-8

Brown, R.D. and Mote, P.W., 2009. The response of Northern Hemisphere snow cover to a changing climate. Journal of Climate, 22(8), pp.2124-2145. https://doi.org/10.1175/2008JCLI2665.1

Brutel-Vuilmet, C., Ménégoz, M. and Krinner, G., 2013. An analysis of present and future seasonal northern hemisphere land snow cover simulated by CMIP5 coupled climate models. Cryosphere, 7(1). https://doi.org/10.5194/tc-7-67-2013

Bruyère, C.L., Done, J.M., Holland, G.J. and Fredrick, S., 2014. Bias corrections of global models for regional climate simulations of high-impact weather. Climate dynamics, 43(7-8), pp.1847-1856. https://doi.org/10.1007/s00382-013-2011-6

Bruyère, C.L., Monaghan, A.J., Steinhoff, D.F. and Yates, D., 2015. Bias-Corrected CMIP5 CESM Data in WRF/MPAS Intermediate File. https://doi.org/10.5065/D6445JJ7

Bulygina, O.N., Groisman, P.Y., Razuvaev, V.N. and Korshunova, N.N., 2011. Changes in snow cover characteristics over Northern Eurasia since 1966. Environmental Research Letters, 6(4), p.045204.

Cattiaux, J., Douville, H. and Peings, Y., 2013. European temperatures in CMIP5: origins of present-day biases and future uncertainties. Climate dynamics, 41(11-12), pp.2889-2907. https://doi.org/10.1007/s00382-013-1731-y

Collins, M., R. Knutti, J. Arblaster, J.-L. Dufresne, T. Fichefet, P. Friedlingstein, X. Gao, W.J. Gutowski, T. Johns, G. Krinner, M. Shongwe, C. Tebaldi, A.J. Weaver and M. Wehner, 2013: Long-term Climate Change: Projections, Commitments and Irreversibility. In: Climate Change 2013: The Physical Science Basis. Contribution of Working Group I to the Fifth Assessment Report of the Intergovernmental Panel on Climate Change [Stocker, T.F., D. Qin, G.-K. Plattner, M. Tignor, S.K. Allen, J. Boschung, A. Nauels, Y. Xia, V. Bex and P.M. Midgley (eds.)]. Cambridge University Press, Cambridge, United Kingdom and New York, NY, USA.

Dankers, R. and Christensen, O.B., 2005. Climate change impact on snow coverage, evaporation and river discharge in the sub-arctic Tana Basin, Northern Fennoscandia. Climatic Change, 69(2-3), pp.367-392. https://doi.org/10.1007/s10584-005-2533-y

Derksen, C. and Brown, R., 2012. Spring snow cover extent reductions in the 2008–2012 period exceeding climate model projections. Geophysical Research Letters, 39(19). https://doi.org/10.1029/2012GL053387

Dietz, A.J., Wohner, C. and Kuenzer, C., 2012. European snow cover characteristics between 2000 and 2011 derived from improved MODIS daily snow cover products. Remote Sensing, 4(8), pp.2432-2454. https://doi.org/10.3390/rs4082432

Donner, L.J., Wyman, B.L., Hemler, R.S., Horowitz, L.W., Ming, Y., Zhao, M., Golaz, J.C., Ginoux, P., Lin, S.J., Schwarzkopf, M.D. and Austin, J., 2011. The dynamical core, physical parameterizations, and basic simulation characteristics of the atmospheric component AM3 of the GFDL global coupled model CM3. Journal of Climate, 24(13), pp.3484-3519. https://doi.org/10.1175/2011JCLI3955.1

Eyring, V., Bony, S., Meehl, G.A., Senior, C.A., Stevens, B., Stouffer, R.J. and Taylor, K.E., 2016. Overview of the Coupled Model Intercomparison Project Phase 6 (CMIP6) experimental design and organization. Geoscientific Model Development (Online), 9(LLNL-JRNL-736881). https://doi.org/10.5194/gmd-9-1937-2016

Fletcher, C.G., Thackeray, C.W. and Burgers, T.M., 2015. Evaluating biases in simulated snow albedo feedback in two generations of climate models. Journal of Geophysical Research: Atmospheres, 120(1), pp.12-26. https://doi.org/10.1002/2014JD022546

Forster, P.M., Andrews, T., Good, P., Gregory, J.M., Jackson, L.S. and Zelinka, M., 2013. Evaluating adjusted forcing and model spread for historical and future scenarios in the CMIP5 generation of climate models. Journal of Geophysical Research: Atmospheres, 118(3), pp.1139-1150. https://doi.org/10.1002/jgrd.50174

Griffies, S.M., Winton, M., Donner, L.J., Horowitz, L.W., Downes, S.M., Farneti, R., Gnanadesikan, A., Hurlin, W.J., Lee, H.C., Liang, Z. and Palter, J.B., 2011. The GFDL CM3 coupled climate model: characteristics of the ocean and sea ice simulations. Journal of Climate, 24(13), pp.3520-3544. https://doi.org/10.1175/2011JCLI3964.1

Hawkins, E. and Sutton, R., 2009. The potential to narrow uncertainty in regional climate predictions. Bulletin of the American Meteorological Society, 90(8), pp.1095-1108. https://doi.org/10.1175/2009BAMS2607.1

Heikkilä, U., Sandvik, A. and Sorteberg, A., 2011. Dynamical downscaling of ERA-40 in complex terrain using the WRF regional climate model. Climate dynamics, 37(7-8), pp.1551-1564. https://doi.org/10.1007/s00382-010-0928-6

Hurrell, J.W., Holland, M.M., Gent, P.R., Ghan, S., Kay, J.E., Kushner, P.J., Lamarque, J.F., Large, W.G., Lawrence, D., Lindsay, K. and Lipscomb, W.H., 2013. The community earth system model: a framework for collaborative research. Bulletin of the American Meteorological Society, 94(9), pp.1339-1360. https://doi.org/10.1175/BAMS-D-12-00121.1

IPCC, 2013: Summary for Policymakers. In: Climate Change 2013: The Physical Science Basis. Contribution of Working Group I to the Fifth Assessment Report of the Intergovernmental Panel on Climate Change [Stocker, T.F., D. Qin, G.-K. Plattner, M. Tignor, S.K. Allen, J. Boschung, A. Nauels, Y. Xia, V. Bex and P.M. Midgley (eds.)]. Cambridge University Press, Cambridge, United Kingdom and New York, NY, USA.

Jacob, D., Petersen, J., Eggert, B., Alias, A., Christensen, O.B., Bouwer, L.M., Braun, A., Colette, A., Déqué, M., Georgievski, G. and Georgopoulou, E., 2014. EURO-CORDEX: new high-resolution climate change projections for European impact research. Regional environmental change, 14(2), pp.563-578. https://doi.org/10.1007/s10113-013-0499-2

Johannessen, O.M., Bengtsson, L., Miles, M.W., Kuzmina, S.I., Semenov, V.A., Alekseev, G.V., Nagurnyi, A.P., Zakharov, V.F., Bobylev, L.P., Pettersson, L.H. and Hasselmann, K., 2004. Arctic climate change: observed and modelled temperature and sea-ice variability. Tellus A: Dynamic Meteorology and Oceanography, 56(4), pp.328-341. https://doi.org/10.3402/tellusa.v56i4.14418

Knutti, R. and Sedláček, J., 2013. Robustness and uncertainties in the new CMIP5 climate model projections. Nature Climate Change, 3(4), p.369. https://doi.org/10.1038/nclimate1716

Kumar, A., Perlwitz, J., Eischeid, J., Quan, X., Xu, T., Zhang, T., Hoerling, M., Jha, B. and Wang, W., 2010. Contribution of sea ice loss to Arctic amplification. Geophysical Research Letters, 37(21). https://doi.org/10.1029/2010GL045022

Lehtonen, I., Kamarainen, M., Gregow, H., Venalainen, A. and Peltola, H., 2016. Heavy snow loads in Finnish forests respond regionally asymmetrically to projected climate change. Natural Hazards and Earth System Sciences (Online), 16(10). https://doi.org/10.5194/nhess-16-2259-2016

Lu, J. and Cai, M., 2009. Seasonality of polar surface warming amplification in climate simulations. Geophysical Research Letters, 36(16). https://doi.org/10.1029/2009GL040133

Malnes, E., Karlsen, S.R., Johansen, B., Bjerke, J.W. and Tømmervik, H., 2016. Snow season variability in a boreal-Arctic transition area monitored by MODIS data. Environmental Research Letters, 11(12), p.125005, https://doi.org/10.1088/1748-9326/11/12/125005

Marks, D., Link, T., Winstral, A. and Garen, D., 2001. Simulating snowmelt processes during rain-on-snow over a semi-arid mountain basin. Annals of Glaciology, 32, pp.195-202. https://doi.org/10.3189/172756401781819751

Mudryk, L.R., Kushner, P.J., Derksen, C. and Thackeray, C., 2017. Snow cover response to temperature in observational and climate model ensembles. Geophysical Research Letters, 44(2), pp.919-926. https://doi.org/10.1002/2016GL071789

Musselman, K.N., Clark, M.P., Liu, C., Ikeda, K. and Rasmussen, R., 2017. Slower snowmelt in a warmer world. Nature Climate Change, 7(3), p.214. https://doi.org/10.1038/nclimate3225

Overland, J.E., Wang, M., Bond, N.A., Walsh, J.E., Kattsov, V.M. and Chapman, W.L., 2011. Considerations in the selection of global climate models for regional climate projections: The Arctic as a case study. Journal of Climate, 24(6), pp.1583-1597. https://doi.org/10.1175/2010JCLI3462.1

Overland, J.E., Wang, M., Walsh, J.E. and Stroeve, J.C., 2014. Future Arctic climate changes: Adaptation and mitigation time scales. Earth's Future, 2(2), pp.68-74. https://doi.org/10.1002/2013EF000162

Perez, J., Menendez, M., Mendez, F.J. and Losada, I.J., 2014. Evaluating the performance of CMIP3 and CMIP5 global climate models over the north-east Atlantic region. Climate dynamics, 43(9-10), pp.2663-2680. https://doi.org/10.1007/s00382-014-2078-8

Radu, R., Déqué, M. and Somot, S., 2008. Spectral nudging in a spectral regional climate model. Tellus A: Dynamic Meteorology and Oceanography, 60(5), pp.898-910. https://doi.org/10.1111/j.1600-0870.2008.00341.x

Räisänen, J. and Ylhäisi, J.S., 2015. CO2-induced climate change in northern Europe: CMIP2 versus CMIP3 versus CMIP5. Climate Dynamics, 45(7-8), pp.1877-1897. https://doi.org/10.1007/s00382-014-2440-x

Roesch, A., 2006. Evaluation of surface albedo and snow cover in AR4 coupled climate models. Journal of Geophysical Research: Atmospheres, 111(D15). https://doi.org/10.1029/2005JD006473

Sillmann, J., Kharin, V.V., Zhang, X., Zwiers, F.W. and Bronaugh, D., 2013. Climate extremes indices in the CMIP5 multimodel ensemble: Part 1. Model evaluation in the present climate. Journal of Geophysical Research: Atmospheres, 118(4), pp.1716-1733. https://doi.org/10.1002/jgrd.50203

Singh, P., Spitzbart, G., Hübl, H. and Weinmeister, H.W., 1997. Hydrological response of snowpack under rain-on-snow events: a field study. Journal of Hydrology, 202(1-4), pp.1-20. https://doi.org/10.1016/S0022-1694(97)00004-8

Skamarock, W.C., Klemp, J.B., Dudhia, J., Gill, D.O., Barker, D.M., Wang, W. and Powers, J.G., 2005. A description of the advanced research WRF version 2 (No. NCAR/TN-468+ STR). National Center For Atmospheric Research Boulder Co Mesoscale and Microscale Meteorology Div.

Stroeve, J.C., Kattsov, V., Barrett, A., Serreze, M., Pavlova, T., Holland, M. and Meier, W.N., 2012. Trends in Arctic sea ice extent from CMIP5, CMIP3 and observations. Geophysical Research Letters, 39(16). https://doi.org/10.1029/2012GL052676

Voldoire, A., Sanchez-Gomez, E., y Mélia, D.S., Decharme, B., Cassou, C., Sénési, S., Valcke, S., Beau, I., Alias, A., Chevallier, M. and Déqué, M., 2013. The CNRM-CM5. 1 global climate model: description and basic evaluation. Climate Dynamics, 40(9-10), pp.2091-2121. https://doi.org/10.1007/s00382-011-1259-y

Yan, M., Wang, B. and Liu, J., 2016. Global monsoon change during the Last Glacial Maximum: a multi-model study. Climate Dynamics, 47(1-2), pp.359-374. https://doi.org/10.1007/s00382-015-2841-5

Ye, H., Yang, D. and Robinson, D., 2008. Winter rain on snow and its association with air temperature in northern Eurasia. Hydrological Processes: An International Journal, 22(15), pp.2728-2736. https://doi.org/10.1002/hyp.7094

Chapter 7
Conclusions

7.1 Introduction

In this dissertation, I have studied Arctic to sub-Arctic snow in Northern Fennoscandia by using a combination of field measurements, station data, remote sensing data and regional climate model outputs. The overarching aim of my dissertation was to answer the following two research questions:

1. What are the uncertainties in remote sensing and climate modelling datasets used in snow studies?
2. How has snow cover been changing since the 1960s, and how will it change over the next century, at a regional level over Northern Fennoscandia?

7.2 Summary of answers to research questions

7.2.1 Question 1: Uncertainties in remote sensing and climate model datasets

The first aspect of my dissertation was assessing the accuracy of the datasets I used to study snow, namely the Moderate Resolution Imaging Spectroradiometer (MODIS) remote sensing product and the Weather Research and Forecasting (WRF) regional climate model. Assessing the uncertainty of these datasets was crucial due to the difficulties of retrieving snow data from remote sensing and modelling snow in boreal forest environments. The evaluation of the MODIS dataset was twofold. MODIS was directly ground truthed using field data (Chapter 3) and the processed version of this remote sensing data was also evaluated by comparing its predictions to those of meteorological stations in the western mountain regions (WMR; Chapter 4).

A combined ground truthing of both MODIS snow products, albedo and Normalised Difference Snow Index (NDSI; used as fractional snow), was undertaken using data collected in the Khibiny Mountains over two field seasons. The MODIS ground truthing effort was a success despite the cloud cover limiting the number of pixels that could be ground truthed. Overall 62 and 43 albedo measurements were used from the Aqua and Terra snow datasets respectively. The overall RMSE (root mean square error) for both MODIS instruments was found to be less than 10 % (8.1 % and 8.9 % RMSE for Aqua and Terra respectively). This is a low error and is of the same order of magnitude as RMSEs found in MODIS ground truthing studies undertaken over homogenous pixels (Stroeve et al., 2013).

For the evaluation of the processed MODIS dataset, I compared the MODIS-derived timing of the snow cover season and snow trends to those recorded at local stations. The average differences between the snow cover start (SCS) and snow cover end (SCE) dates derived from the station data and

the processed MODIS dataset are 8.6 and 10.4 days, respectively, both relatively low errors. I also found that for 85.8 % of pixels investigated (SCS and SCE combined) the deviation in the MODIS-derived dates is less than 20 days which is an improvement on previous studies of this kind (Dietz et al., 2012). I also demonstrated that it is possible to extract realistic trends from the processed MODIS dataset. MODIS-extracted trends were shown to be identical to observed trends in that MODIS was able to identify the only statistically significant trend while not giving spuriously significant trends elsewhere. Thus, MODIS was shown to be a highly reliable snow dataset for the WMR of Northern Fennoscandia.

The skill of the WRF regional climate model at modelling snow and temperature was tested in Chapter 5. First a sensitivity analysis was undertaken, testing twelve different physics setups in order to find the best setup of the model for snow studies over the WMR. This sensitivity test of WRF was done at very high resolution (1 km) over my six-week long 2016 field season. The outputs from these runs were tested by comparing them to remote sensing and field data using statistical evaluation scores. WRF outputs using the best setup found were shown to be reliable for both temperature and snow modelling, with a high overall Proportion Correct score (88.1 %) for its representation of snow on the ground. WRF was also shown to have a high Probability of Detection of snow (94.7 %) and low Probability of Over Detection of snow (20.1 %). One of the main issues with the WRF modelling of snow was over mountains, where WRF considerably underestimated the early-season snow depth. At the low-elevation stations, WRF modelled snow depth and melt rates well. Overall, the WRF model does an excellent job at modelling the variability of the temperature over the field season. Finally, the effects of spectral nudging were tested and were found not to have a strong negative impact on the model outputs. Spectral nudging was then used in the decadal WRF runs later in the dissertation.

In addition to a WRF sensitivity test, a validation of WRF historical outputs over Northern Fennoscandia was undertaken. The validated runs were forced by three CMIP5 models (CCSM4, CNRM-CM5 and GFDL-CM3) and one reanalysis (ERA-I) in order to test the CMIP5-forced WRF skill relative to a reanalysis dataset shown to be very reliable over Northern Fennoscandia (e.g. Marshall et al., 2018). Observations from ten meteorological stations were used as truth in this validation study. Overall, this validation confirmed the findings of the sensitivity study, in that WRF modelled temperature very well, and was less accurate at modelling precipitation. WRF forced by all three CMIP models and ERA-I data does an excellent job at modelling temperature and out of the four historical runs, CCSM4-forced WRF does the best at modelling temperature. The original CMIP5 dataset had been bias adjusted before being used to force WRF, thus this result is not surprising. At all but one station, ERA-I- and CMIP-forced WRF overestimate total precipitation. In all runs, WRF models low precipitation better than high precipitation events. ERA-I-forced WRF was shown to be more effective than CMIP5-forced WRF at modelling high-precipitation events. However, the lowest precipitation bin (0-5 mm) makes up 90.3 % of the precipitation values at the 10 stations studied and thus higher errors in the high-precipitation events have less of an impact on the overall RMSE. CNRM-CM5 was shown to be the least reliable model in terms of precipitation. Overall, WRF was demonstrated to model snow,

temperature and precipitation well, thus showing that WRF is reliable for the modelling work undertaken in Chapter 6. It is nevertheless useful to bear in mind the higher error in the precipitation projections when considering those results.

7.2.2 Question 2: Past and Future snow cover changes in Northern Fennoscandia

The second question addressed in this dissertation can be divided into two sections: past and future changes. In this dissertation, I used a combination of field, station and remote sensing data to study past and recent snow in the Khibiny Mountains and the broader WMR, as defined in Chapter 4. Results from my field seasons in the Khibiny Mountains indicate that inter-annual variability is high in the region in terms of temperature, wind and snow. Station snow depth data and MODIS NDSI data were converted into SCS and SCE dates and from these snow cover duration (SCD) was calculated.

Although for some areas and some years, the start and end of the snow season could not be detected due to long overcast periods, the MODIS post-processing reduced the number of missing pixels by more than half. Both high inter-annual variability and spatial variability were identified in the long-term snow cover trends in the WMR of the Kola Peninsula. Between 2000 and 2016, the end of the snow cover season has become increasingly later in the plains of the WMR, but there is not such a clear trend in SCE in the higher altitude (> 400 m above sea level) areas. However, overall, the snow cover duration has been decreasing at higher altitudes and increasing at lower altitudes between these dates. Contrastingly, a uniform, statistically significant, regional decrease in the duration of the snow cover season has occurred between 1992 and 2016 across the lower altitudes of the western Murmansk Region. Snow depth was also found to be highly spatially variable and the difference in maximum yearly snow depth was found to be over 50 cm between two stations only 2 km apart at very similar altitudes in valleys within the Khibiny Mountains (PABGI Khibiny and MSU Khibiny). These differences in snow depth as well as some of the trends in the snow cover season are probably explained by a combination of changes in air temperature, wind and, potentially, atmospheric patterns over the WMR (Farlaz, 2004).

The second part of this research question concerns future changes in snow. In order to make predictions of future snow over Northern Fennoscandia, a regional climate model, WRF, was used to downscale three CMIP5 models (CCSM4, CNRM-CM5 and GFDL-CM3). Predictions were made for two RCP scenarios: a mitigation scenario (RCP 4.5) and a "business-as-usual" scenario (RCP 8.5). Future runs were made for the 2090 to 2099 interval and WRF runs were also performed over a historical period (1990 - 1999) to enable a comparison between past and future climate. As predicted by Hawkins and Sutton (2009) and by Overland et al. (2014), inter-model spread had a large impact on my results. Nevertheless, some interesting conclusions were extracted from the results of this analysis.

Both total snowfall and the fraction of solid to liquid precipitation are projected to change by the end of the 21st century. The inter-model spread is smaller in the snowfall predictions compared to the total precipitation changes. All three CMIP5 models agree on an overall decrease in total annual

snowfall over Northern Fennoscandia, with the greatest decrease occurring over the Scandinavian Mountains and over the Barents Sea. With the exception of the summer season in CNRM-CM5 RCP 4.5, in all models and emission scenarios, a decrease in the percentage of solid precipitation is predicted by the end of the 21st century in all seasons. RCP 8.5 consistently sees a higher decrease in solid precipitation than RCP 4.5 at all stations, and for all models and seasons. The large decreases projected in the percentage of solid precipitation explain the decreases in total annual snowfall modelled despite the large increases in total precipitation modelled over a majority of Fennoscandia in both the CCSM4 and GFDL-CM3 outputs.

The future runs also project changes in the timing and duration of the snow cover season. The start of the snow cover season is modelled to be later between 2090 - 2099 compared to 1990 - 1999. Importantly, SCS is increasingly delayed with increasing greenhouse gas concentrations. Little to no change in future in SCE is predicted in the CNRM model runs, but both other models (CCSM4 and GFDL) predict an increasingly early end to the snow cover season by the end of the century. Finally, all CMIP5 models agree that in both emission scenarios mean SCD will be lower over 2090 to 2099 than it was between 1990 and 1999. All CMIP5 forcing models agree that the higher the emissions over the next century, the larger the negative impact on the duration of the snow cover season. The ensemble mean SCD change is of -28 days and -43 days in RCP 4.5 and RCP 8.5 respectively.

To summarise, snow cover duration and depth have been undergoing changes over the past few decades in the WMR and large changes in both climate and snow cover are expected to occur in Northern Fennoscandia by the end of the 21st century in both a mitigation and a 'business-as-usual' scenario.

7.3 Summary of novel work

7.3.1 Novel outputs

The main novel outputs of the work done in this dissertation are summarised in the following points:

1. Ground truthed MODIS snow products for the first time over the Khibiny Mountains in Arctic Russia.
2. Focused on a new area (WMR) in Northern Fennoscandia to study past changes in snow.
3. Used remote sensing for high resolution study of timing of snow cover, including start, end and duration, for the first time over the WMR.
4. Experimentally determined the optimal model parameterisation for WRF over the WMR which includes the double-moment Morrison et al. (2009) microphysics scheme and the Iacono et al. (2008) radiation scheme which improves the representation of subgrid-scale cloud variability.
5. Validated CMIP5-forced WRF across Northern Fennoscandia for the first time.
6. Made regional, high-resolution predictions of climate (temperature and precipitation) and snow (snowfall, timing and duration of the snow cover season) using WRF over the entirety of

Northern Fennoscandia. This is the first time such snow predictions have been performed in this region.

7. Created two new datasets: 17-years of combined Aqua and Terra MODIS data processed to remove as much cloud cover as possible over the WMR and nine decades of model runs can now be used for further study by my team with three decadal historical runs (1990 - 1999) and six future decadal runs (2090 - 2099) covering two RCP scenarios (RCP 4.5 and 8.5) and three CMIP5 models.

7.3.2 Results relevant to debates in the literature

Some of my results are pertinent to some debates in the literature. In Chapter 3, I demonstrate that MODIS retrievals are accurate up to SZA of just below 70 º supporting work done by Stroeve et al. (2013) which demonstrated inaccuracies in the conclusions of Wang and Zender (2010). The literature also contains disagreements regarding the impacts of liquid water on albedo retrievals. Wang and Zender (2010) argued that MODIS retrievals are less accurate for wet snow and Painter et al. (2009), contrastingly, explained that MODIS retrievals are not affected by the presence in liquid water in the snow surface. My results in Chapter 3 support neither of these findings. Indeed, I found that as snow wetness increases, MODIS errors decrease, though it is possible that MODIS retrieval date is an insufficient proxy for snow wetness.

Finally, my results in Chapter 4 have reconciled seemingly contradictory findings concerning the length of the snow-free season in the Kola Peninsula (Bulygina et al, 2009; Kozlov and Berlina, 2002). Extracting the trends in the snow cover duration at Kandalaksha station over comparable timescales to these two studies demonstrates that the contrasting conclusions of these previous studies can be explained by the different time periods analysed. Kandalaksha station shows a statistically significant lengthening of the snow cover season in the 1936 to 1998 interval of 4.5 days/decade, thus a decrease of the length of summer similar to Kozlov and Berlina (2002). However, in the 1966 to 2007 interval, a shortening of the snow cover season of 1.9 days/decade is found, though it is not statistically significant. This trend supports the conclusions of Bulygina et al. (2009).

7.4 Future direction

Overall, there is much potential to expand on the work done in this dissertation. Firstly, there is potential for further work to enhance the existing datasets created in this study. The principal example of this is the possibility of further analysis on the rich modelling dataset described in Chapter 6. Investigating changes in atmospheric circulation patterns could help explain the changes in climate and snow described in this chapter. Another potential direction of study would be to analyse climate extremes, such as the frequency of extreme precipitation and extreme snowfall events, which can have significant impacts on human activity and the natural environment in Northern Fennoscandia (e.g. Callaghan et al., 2010).

The second type of further work would be to improve the datasets obtained in the field, both in terms of increasing the amount of data and the quality of the data used. It would be useful to undertake another field season in the Khibiny Mountains in order to collect additional data: collecting more albedo point measurements for validation would likely improve the significance of my conclusions in Chapter 3. In addition to this, measurements of snow wetness over the entire melting season would be useful to test my conclusions regarding the impact of snow wetness on MODIS retrievals. A second example of greater data improving results would be to increase the interval of time of analysis of the past changes in snow using MODIS data (Chapter 4). Indeed, as of 2019, a 20-year MODIS dataset is available. A study of trends in snow cover over this longer period would be a more robust analysis (Bormann et al., 2018).

To improve the quality of the results, two different sets of data used could be refined. First, with more time and resources, an error analysis could be undertaken on field measurements by completing another field season with an emphasis on spatial variability of albedo at a sub-500 m scale. By doing this, it would be possible to add an interval of variability in the observations used as ground truth in the validation of the MODIS snow data, and thus make the ground truthing more precise (Chapter 3). Another step to increase the reliability of results would be to bias-correct the CNRM- and GFDL-forced WRF precipitation (Chapter 5). This would improve results in terms of reliability of future projections and would make comparisons between the outputs of these two models to the already bias-corrected CCSM4 outputs more straightforward. Bias correction can be done by using station data as ground truth and spatially nudging the WRF outputs in the direction of the known regional precipitation.

Finally, in addition to further analysis on pre-existing datasets and additions and improvements to the datasets used, spatial extrapolation of some of the work undertaken would be valuable. Indeed, the work done in Chapter 4 could be expanded to a wider area. In this chapter, the study area was small, as I was studying regional changes at a very high resolution. With more time, this analysis could be performed on the entirety of Northern Fennoscandia whilst keeping the high resolution. This would provide high-resolution information on the recent changes in the timing and duration of the snow cover season over Northern Fennoscandia.

7.5 Overview

In conclusion, I believe the research described in this dissertation was successful for two reasons. Firstly, this dissertation contributes novel science, including the creation of two new datasets: a processed 17-year MODIS dataset with reduced cloud cover over the WMR and nine decades of climate model outputs over Northern Fennoscandia. Secondly, the overarching aims of my dissertation were met and I was able to answer my two main research questions, as described above. The remote sensing dataset used proved to be highly reliable to study snow in the WMR. And by undertaking a sensitivity analysis of WRF, an optimised model parameterisation was used which showed excellent

skill in modelling temperature over Northern Fennoscandia and good skill as modelling precipitation, both key parameters in the modelling of snow. Using these datasets, snow cover was shown to have changed over the past few decades over the WMR, with a decrease in SCD in the low elevations between 1992 and 2016 and an increase there between 2000 and 2016. Regarding the future of snow cover over Northern Fennoscandia, despite high inter-model spread in the results, large changes in climate and snow cover are expected to occur in Northern Fennoscandia by the end of the 21st century in both a mitigation and a 'business-as-usual' scenario. Importantly, changes in temperature, precipitation and snowfall are all higher, and snow cover is most impacted, in the higher emission scenario. RCP 8.5 consistently sees a higher decrease in solid precipitation than RCP 4.5 at all stations, and for all models and seasons, for example. Thus, aiming to reduce greenhouse gas emissions is still crucial to reducing anthropogenic impact on Northern Fennoscandian snow.

7.6 References

Bokhorst, S., Pedersen, S.H., Brucker, L., Anisimov, O., Bjerke, J.W., Brown, R.D., Ehrich, D., Essery, R.L., Heilig, A., Ingvander, S. and Johansson, C., 2016. Changing Arctic snow cover: A review of recent developments and assessment of future needs for observations, modelling, and impacts. Ambio, 45(5), pp.516-537. https://doi.org/10.1007/s13280-016-0770-0

Bormann, K.J., Brown, R.D., Derksen, C. and Painter, T.H., 2018. Estimating snow-cover trends from space. Nature Climate Change, 8(11), p.924. https://doi.org/10.1038/s41558-018-0318-3

Bulygina, O.N., Razuvaev, V.N. and Korshunova, N.N., 2009. Changes in snow cover over Northern Eurasia in the last few decades. Environmental Research Letters, 4(4), p.045026, https://doi.org/10.1088/1748-9326/4/4/045026

Callaghan, T.V., Bergholm, F., Christensen, T.R., Jonasson, C., Kokfelt, U. and Johansson, M., 2010. A new climate era in the sub-Arctic: Accelerating climate changes and multiple impacts. Geophysical Research Letters, 37(14). https://doi.org/10.1029/2009GL042064

Dietz, A.J., Wohner, C. and Kuenzer, C., 2012. European snow cover characteristics between 2000 and 2011 derived from improved MODIS daily snow cover products. Remote Sensing, 4(8), pp.2432-2454, https://doi.org/10.3390/rs4082432.

Falarz, M., 2004. Variability and trends in the duration and depth of snow cover in Poland in the 20th century. International Journal of Climatology: A Journal of the Royal Meteorological Society, 24(13), pp.1713-1727. https://doi.org/10.1002/joc.1093

Hawkins, E. and Sutton, R., 2009. The potential to narrow uncertainty in regional climate predictions. Bulletin of the American Meteorological Society, 90(8), pp.1095-1108.

Iacono, M.J., Delamere, J.S., Mlawer, E.J., Shephard, M.W., Clough, S.A. and Collins, W.D., 2008. Radiative forcing by long-lived greenhouse gases: Calculations with the AER radiative transfer models. Journal of Geophysical Research: Atmospheres, 113(D13). https://doi.org/10.1029/2008JD009944

Kozlov, M.V. and Berlina, N.G., 2002. Decline in length of the summer season on the Kola Peninsula, Russia. Climatic Change, 54(4), pp.387-398, https://doi.org/10.1023/A:1016175101383

Marshall, G.J., Vignols, R.M. and Rees, W.G., 2016. Climate change in the Kola Peninsula, Arctic Russia, during the last 50 years from meteorological observations. Journal of Climate, 29(18), pp.6823-6840. https://doi.org/10.1175/JCLI-D-16-0179.1

Marshall, G.J., Kivinen, S., Jylhä, K., Vignols, R.M. and Rees, W.G., 2018. The accuracy of climate variability and trends across Arctic Fennoscandia in four reanalyses. International Journal of Climatology, 38(10), pp.3878-3895. https://doi.org/10.1002/joc.5541

Morrison, H., Thompson, G. and Tatarskii, V., 2009. Impact of cloud microphysics on the development of trailing stratiform precipitation in a simulated squall line: Comparison of one-and two-moment schemes. Monthly weather review, 137(3), pp.991-1007. https://doi.org/10.1175/2008MWR2556.1

Overland, J.E., Wang, M., Walsh, J.E. and Stroeve, J.C., 2014. Future Arctic climate changes: Adaptation and mitigation time scales. Earth's Future, 2(2), pp.68-74.

Painter, T.H., Rittger, K., McKenzie, C., Slaughter, P., Davis, R.E. and Dozier, J., 2009. Retrieval of subpixel snow covered area, grain size, and albedo from MODIS. Remote Sensing of Environment, 113(4), pp.868-879.

Stroeve, J., Box, J.E., Wang, Z., Schaaf, C. and Barrett, A., 2013. Re-evaluation of MODIS MCD43 Greenland albedo accuracy and trends. Remote sensing of environment, 138, pp.199-214. https://doi.org/10.1016/j.rse.2013.07.023

Wang, X. and Zender, C.S., 2010. MODIS snow albedo bias at high solar zenith angles relative to theory and to in situ observations in Greenland. Remote Sensing of Environment, 114(3), pp.563-575.